The Effect of Specimen Size on the Mechanical Response of Laminated Composite Coupons Loaded in Tension and Flexure

by

David P. Johnson

Dissertation submitted to the Faculty of the
Virginia Polytechnic Institute and State University
in partial fulfillment of the requirements for the degree of

DOCTOR OF PHILOSOPHY
in
Engineering Mechanics

APPROVED:

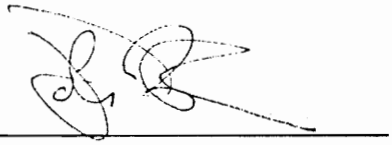

John Morton, Chairman

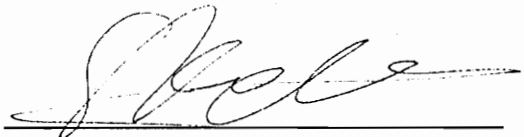

Sotiris Kellas, Co-Chairman

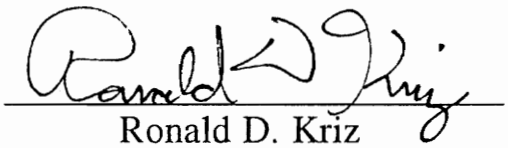

Ronald D. Kriz

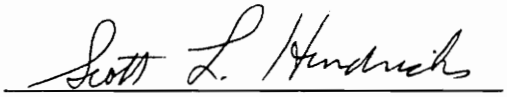

Scott L. Hendricks

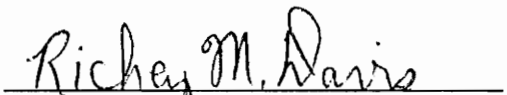

Richey M. Davis

April, 1994
Blacksburg, Virginia

The Effect of Specimen Size on the Mechanical Response of Laminated Composite Coupons Loaded in Tension and Flexure

by:

David P. Johnson

Chairman: John Morton
Department: Engineering Mechanics

(ABSTRACT)

The effect of specimen size on the uniaxial tensile stress/strain response of sublaminate-level scaled composite specimens, and the four point flexure load/deflection response of ply- and sublaminate-level scaled composite specimens was investigated.

Three laminates were studied in the tensile program, namely $[+30/-30/90_2]_{ns}$, $[+45/-45/0/90]_{ns}$ and $[90/0/90/0]_{ns}$, where n = 1, 2, 3, 4. Two material systems were used, namely AS4/3502 graphite/epoxy and APC-2 graphite/PEEK, to investigate the relative effect of resin toughness.

Three laminates were also studied in the flexure program. The baseline lay-ups were $[\pm 45/0/90]_{2ns}$, $[0/90/0/90]_{2ns}$ and $[\pm 45/\pm 45]_{2ns}$, where n = 1, 2, 4. Ply- and sublaminate-level scaling were used to increase specimen thickness. All flexure specimens were of AS4/3502 graphite/epoxy.

Enhanced X-ray radiography and edge photomicroscopy were used to examine damage development in specimens loaded to various fractions of their ultimate stress. This non-destructive examination was coupled with observations of critical events in the stress/strain response to try to correlate scaling effects with the damage development in the specimens.

Analytical and numerical methods were employed in order to understand the stresses driving certain damage modes observed. 2-D and 3-D finite element models were used to find delamination stresses in an undamaged laminate, and an approximate elasticity approach was used to find stresses due to cracks in the 90° plies.

It was found that the tensile strength of the $[+30/-30/90_2]_{ns}$ and $[+45/-45/0/90]_{ns}$ laminates generally increased as n increased. This effect was more pronounced for the matrix-dominated $[+30/-30/90_2]_{ns}$. Both the $[+30/-30/90_2]_{ns}$ and the quasi-isotropic $[+45/-45/0/90]_{ns}$ laminates seemed to be approaching a maximum strength, beyond which the strength scaling either stops, or is reversed. As n increased from 1 to 4, these two laminates exhibited a delay in the onset of certain damage mechanisms, such as delamination and transverse matrix cracking.

The $[90/0/90/0]_{ns}$ laminates showed no tensile stress/strain response scaling effects, although the stress at which first ply failure occurred was found to increase as n increased.

$[\pm 45/0/90]_{2ns}$ and $[\pm 45/\pm 45]_{2ns}$ flexure specimens showed no strength scaling effects when sublaminate-level scaling was used, but significant decreases in strength were found when specimen size was increased using ply-level scaling. $[0/90/0/90]_{2ns}$ specimens showed no global load/deflection scaling effects.

ACKNOWLEDGEMENTS

I am indebted to my doctoral advisor Prof. John Morton, and to Dr. Sotitis Kellas, my doctoral committee co-chair for their invaluable help, encouragement and support. I am also very grateful to the other members of my doctoral committee, including the late Prof. Wayne W. Stinchcomb, Prof. Scott L. Hendricks (thanks for all the wood too), Prof. Ronald D. Kriz, and Prof. Richey M. Davis, for their help and advice.

For their friendship, as well as technical expertise, I would like to thank my present and former co-workers Dr. Ming-Yi Tsai, Dr. Henjen Ho, Dr. Todd Wieland, Dr. Publio Pintado, Dr. Kuen Tat Teh, Dr. Yanhong Zhang, Harry Budiman, Enrst Lutz, Alan Nettles, André Lavoie, Robert Bennett, and Diane Peters.

Most of all, I thank my wife Jann for her continued support and love, as well as her willingness to remain in poverty for so long. It's been a long two years for her. Her chosen occupation of household engineer has been invaluable to the education and well-being of our children, Emily, Peter, and Laura. Also, without help from my parents, Prof. D. Lynn and Mrs. R. LaRae P. Johnson, and Jann's parents, Mr. Clarence "Mac" McAlister and Mrs. Deanna E. B. Murdock, this work would not have been possible.

Support from NASA Langley Research Center's Landing and Impact Dynamics Branch under contract NAS1-18471-40, and the National Science Foundation's Science and Technology Center for High Performance Polymeric Adhesives and Composites at Virginia Tech under contract DMR#912004 is gratefully acknowledged.

LIST OF TABLES

LIST OF FIGURES

TABLE OF CONTENTS

1. INTRODUCTION

In order for advanced composite materials to be more widely used for structural applications, it is necessary to understand the nature of changes in mechanical behavior as composite laminates are scaled in size. In order to reduce development costs, full scale structures are typically designed using small scale coupon and/or scale model testing. These results must then be used to predict the behavior of the full scale part. It is necessary, therefore, to know if composite materials show any "scaling effect" or "size effect," which can be defined as any deviation in the mechanical response of a material from some accepted law of mechanics. As an example, it is well known that brittle materials, such as glass, show a significant decrease in ultimate tensile stress (strength) as the size of the specimen is increased [1].

Several researchers [2-7] have found that brittle matrix composite materials also exhibit scaling effects in tensile strength, as well as damage initiation and damage development. Depending on the laminate stacking sequence, type of loading, method of increasing the thickness, etc., these scaling effects may be more or less pronounced. Hence, there exists a need to understand the damage processes and other factors that alter a material's response

with size, so that data obtained from small scale (model) specimens can be used in the design of full scale structures.

Because fiber diameter and interface/interphase geometry cannot be scaled, two practices of scaling the thickness of a laminated composite coupon have been used [4]. Ply-level scaling increases the thickness of each ply by placing laminae of the same orientation adjacent to each other, thus "blocking" the plies. This is done in order to satisfy, as closely as possible, the requirements of similitude when scaling the laminate thickness. Sublaminate-level scaling increases the laminate thickness by repeating a basic sublaminate. Figure 1.1 illustrates the difference between ply-level scaling and sublaminate-level thickness scaling.

According to Classical Lamination Theory (CLT) and ply failure criteria that have been used previously [8], uniaxial tensile stiffness and strength should be independent of size, regardless of the method of scaling. Kellas and Morton [6] have shown that for ply-level scaled coupons loaded in tension, the initial laminate stiffness is indeed independent of size. However, these same specimens do not exhibit identical load/displacement response in that the initiation and development of damage can vary greatly with size. Their findings show a marked decrease in strength when plies are blocked together to create a geometrically scaled laminate.

Kellas and Morton [4] also studied the ±45° specimen in both ply-level and sublaminate-level scaling. They found that while the ply-level scaled specimens showed a significant decrease in scaled strength, in agreement with their earlier work, sublaminate-level scaled specimens showed a marked increase in scaled strength and strain to failure.

With the desire to understand more about scaling effects in laminated composites, it was determined to continue with the work started by Kellas and Morton. The study presented herein describes two different experimental programs. The first (as a continuation of Kellas

and Morton's [6] ply-level tensile scaling work) investigates scaling effects found in tensile specimens scaled at the sublaminate level. The second experimental program is a study of the response of scaled coupons loaded in flexure. In order to move from tensile properties to an eventual investigation of compressive properties, it was decided to load specimens in flexure, which involves a combination of tensile and compressive loading. Four point flexure loading was chosen in order to minimize the influence of shear stresses on the response.

CLT and simple beam theory indicate that the bending stiffnesses, as defined by Whitney [9], of ply-level scaled specimens of a given laminate stacking sequence should be independent of size. Bending stiffnesses of sublaminate-level scaled coupons may increase or decrease in larger scaled specimens, depending on the stacking sequence (Figure 1.2).

Four stacking sequences were used previously by Kellas and Morton [4, 6]. These included a delamination-type stacking sequence similar to that used by previous investigators (e.g. [10]), a quasi-isotropic stacking sequence, a crossply stacking sequence, and a ±45° stacking sequence.

Enhanced radiography and optical microscopy were used to evaluate damage processes and modes of failure. Characteristic response curves for the different sizes were normalized and compared for each laminate stacking sequence, and observed damage processes were correlated with specific features on the stress/strain curves.

Finite element analysis and an approximate elasticity solution were employed to find interlaminar stresses leading to ply delamination under tensile loading.

2. EXPERIMENTAL PROCEDURE

The material for most of the specimens was AS4/3502 graphite/epoxy. In addition, tensile coupons were machined from two panels of APC-2 graphite/PEEK to determine if matrix toughness affected the tensile response of the specimens.

2.1 Lay-ups

Since this work builds on past research, the stacking sequences were chosen in order to compare the results obtained with the previous results.

2.1.1 Tension

The stacking sequences for the three sublaminate-scaled laminates were as follows:

$[+30/-30/90_2]_{ns}$ denoted Lay-up ***A***,

$[+45/-45/0/90]_{ns}$ denoted Lay-up ***B***,

$[90/0/90/0]_{ns}$ denoted Lay-up ***C***,

where n = 1, 2, 3 or 4.

APC-2 panels were of Lay-up ***B***, where n = 1 and 4.

The APC-2 panels were chosen to be of Lay-up ***B*** since quasi-isotropic lay-ups have a wide range of application in industry and research. Lay-up ***C*** was chosen with 90° plies (instead of 0° plies) on the outer surfaces in order to eliminate the need for end tabs. Abrasive cloth was used between the jaws of the testing machine and the specimen to improve gripping.

2.1.2 Flexure

The stacking sequences for the three sublaminate- and ply-level scaled laminates were as follows:

$[+45/-45/0/90]_{2ns}$ and
$[+45_n/-45_n/0_n/90_n]_{2s}$ denoted Lay-up ***B***,

$[90/0/90/0]_{2ns}$ and
$[0_n/90_n/0_n/90_n]_{2s}$ denoted Lay-up ***C***,

$[+45/-45/+45/-45]_{2ns}$ and
$[+45_n/-45_n/+45_n/-45_n]_{2s}$ denoted Lay-up ***D***,

where n = 1, 2 or 4.

2.2 Specimen Preparation

All AS4/3502 panels were fabricated from unidirectional prepreg and cured in an autoclave following the manufacturers recommended curing cycle. Following fabrication, each panel was C-scanned to assess quality. The two APC-2 panels used in the tensile work were fabricated and C-scanned by ICI*. All coupons were cut using a water-cooled diamond saw, and stored at nominal room conditions.

* Imperial Chemical Industries Plc.

2.2.1 Tension

Although only the 2/4 scale specimens conform with the size restrictions set by ASTM, the ASTM D 3039 tensile test was used as a guideline for all testing.

After all tensile specimens were tested, it was deemed necessary to fabricate a second set of 8- and 16-ply panels. Since all of the original prepreg had been used, these panels were made from a different batch of AS4/3502 material. Therefore, when discussing the 8- and 16-ply tensile specimens, the terms "batch *I*" and "batch *II*" will refer to the original and subsequent material batches, respectively. Batch *I* specimens were used for comparison of stress/strain response, while batch *II* specimens were used to assess damage onset and development in the tensile work only.

The in-plane dimensions of the tensile specimens were chosen to be $(12.5)n$ mm x $(125)n$ mm where n = 1, 2, 3 or 4. These sizes are denoted by lower case letters ***a***, ***b***, ***c*** and ***d***, corresponding to 1/4, 2/4, 3/4 and 4/4 scale, respectively.

The notation used to identify a given tensile specimen type has 3 characters: the first being an upper case letter referring to the stacking sequence, the second being a lower case letter referring to the in-plane dimensions, and the third being a number corresponding to the number of plies in the specimen. As an example, an ***Aa-8*** specimen would be one of Lay-up ***A***, in-plane dimensions 12.5 x 125 mm, and having 8 plies.

Tensile specimen sizes were scaled in three ways to study different effects. These are denoted as:

- 1-D scaling — in-plane dimensions remain constant, while thickness is scaled
- 2-D scaling — in-plane dimensions are scaled, while thickness remains constant
- 3-D scaling — in-plane dimensions and thickness are scaled together

The differences between 1-, 2- and 3-D scaling are illustrated in Figure 2.1. Tables 2.1 and 2.2 represent the test matrices for the AS4/3502 and APC-2 specimens studied. Moving horizontally, vertically or diagonally along the table corresponds to 1-, 2- or 3-D scaling, respectively.

2.2.2 Flexure

The in-plane dimensions of the flexure specimens were chosen to be (12.5)n mm x (75)n mm where n = 1, 2 or 4. These sizes are denoted by lower case letters ***a***, ***b*** and ***d*** , corresponding to 1/4, 2/4 and 4/4 scale, respectively. Only 3-D scaled (Figure 2.1) specimens were tested.

The notation used to identify a given flexure specimen type has 2 or 3 characters, depending on the size: the first being an upper case letter referring to the stacking sequence, the second being a lower case letter referring to the specimen size, and the third (sizes ***b*** and ***d*** only) being a character (s or p) corresponding to sublaminate- or ply-level scaling, respectively. As an example, a ***Ba*** specimen would be one of Lay-up ***B*** and in-plane dimensions 12.5 x 75 mm, whereas a ***Bdp*** specimen would be one of Lay-up ***B***, in-plane dimensions 50 x 300 mm, and having blocked plies (ply-level scaling).

2.3 Mechanical Testing

For each specimen size and laminate stacking sequence, at least five coupons were tested to failure. Typical load/deflection response was then examined, and points of interest were identified. The remaining specimens of each type were then loaded to different proof loads, corresponding to these points of interest. These pre-loaded specimens were then removed from the testing machine and examined for damage using non-destructive techniques.

2.3.1 Tension

Load was recorded directly from the testing machine, and longitudinal strain was recorded using extensometers with both scaled and unscaled gage lengths. The crosshead speed was varied with the specimen gage length to yield a uniform 2.8 % strain/min. for all specimens.

2.3.2 Flexure

Load and crosshead displacement were recorded directly from the testing machine, and the specimen top and bottom longitudinal strains were recorded using longitudinal foil-type strain gages. The crosshead speed was varied with the specimen gage length to yield nominally equivalent strain rates.

2.4 Damage Evaluation

Pre-loaded specimens were examined using two non-destructive techniques. These were penetrant-enhanced X-ray radiography, and optical microscopy.

2.4.1 X-ray Radiography

Pre-loaded specimens were soaked in an X-ray-opaque zinc iodide dye penetrant solution, and washed. With the specimens placed directly on the film, contact exposures were then made to yield radiographs of the damage in each preloaded specimen.

Some of the specimens were reloaded after the X-ray process; therefore, it was assumed that the zinc iodide solution had negligible effect on the behavior of the composite material. Reloading was performed as quickly after penetrant soaking as practically possible in order to minimize any adverse effects.

2.4.2 Optical Microscopy

After loading, the edges of the specimens were polished using 1 μm aluminum oxide powder. The specimen edges were then examined and photographed using an optical microscope. These micrographs were used to locate the plies in which damage occurred. Damage sites seen on the radiographs could then be directly compared with optical micrographs of the same region of the specimen edge in order to better characterize the damage. This yielded the ability to develop a 3-D understanding of the damage in the specimens.

2.5 Apparatus

2.5.1 Damage Evaluation

All radiographs were made using Kodak Industrex M X-ray film and a Faxitron Series 43805N X-ray cabinet. Prints of the negatives were made on Kodak Ploycontrast F paper. Micrographs of specimen edges were taken using a Nikon UM-2 OPTIPHOT microscope and Polaroid type 55 90x120 mm positive/negative film.

2.5.2 Data Acquisition

Load and strain information for the batch *I* tensile specimens was logged using an IBM PC based data acquisition package (hardware and software) with 8 bit resolution. Load, strain and displacement information for batch *II* and APC-2 tensile specimens, and for all flexure specimens was logged using Apple Macintosh based data acquisition hardware and software with 12 bit resolution.

2.5.3 Tension

Load Frames

All of the batch *I* specimens were loaded on a 260 kN (60 kip) MTS servo-hydraulic testing machine equipped with hydraulic grips. Batch *II* specimens were loaded on a 45 kN (10 kip) Instron screw driven testing machine equipped with mechanical wedge-action grips.

Extensometers

AS4/3502 batch *II* and APC-2 specimens were fitted with an MTS 25 mm gage length extensometer. Batch *I* specimens were fitted with an MTS 25 mm gage length extensometer, and/or with one of four custom-built extensometers. These extensometers, shown in Figure 2.2, were designed with 37.5, 75, 112.5 and 150 mm gage lengths for size ***a***, ***b***, ***c*** and ***d*** specimens, respectively. Some of the smaller specimens (sizes ***a*** and ***b***) were fitted with the MTS extensometer, and the remaining were fitted with the custom extensometer. The larger specimens (sizes ***c*** and ***d***) accommodated both custom and MTS extensometers on the same specimen.

2.5.4 Flexure

Load Frame

All flexure specimens were loaded on a 45 kN (10 kip) Instron screw driven testing machine, with 0.0 - 10.0 V analog output.

Fixture

A four point flexure was designed and built for the tests. The fixture allowed geometric scaling of the moment arms, roller diameters, etc. by employing scaled brackets that could

be fixed to the base and top plates. Specimens were loaded in flexure by a applying tensile load to the top plate. See Figure 2.3.

Strain Gages

All specimens were gaged top and bottom with Micro-Measurements EA-06-125BZ-350 type strain gages from Measurements Group, Inc. to measure longitudinal strain. Micro-Measurements type 2210 signal conditioners/amplifiers were used to provide 0.0 - 10.0 V analog output.

3. METHODS OF ANALYSIS

3.1 Tension

In order to better understand the response of the scaled specimens, numerical and analytical methods were employed. Edge effect stresses through the thickness of undamaged laminates were found using the finite element method. These stresses were needed in order to understand failure modes, particularly delamination, observed in Lay-ups ***A*** and ***B***. An approximate elasticity approach was used to find stresses around a crack in a 90° ply.

3.1.1 Finite Element Analysis

Tensile through-the-thickness edge stresses appeared to be responsible for delamination in Lay-ups ***A*** and ***B***. Therefore, both 3-D and 2-D generalized plane strain finite element models were generated in order to find the stress distributions through the thickness of the laminate caused by edge effects. Both models were 16-ply ($n=2$) laminates. Both Lay-ups ***A*** and ***B*** were modeled. Figures 3.1 and 3.2, respectively, show the meshes used for 3-D and generalized plane strain models. The generalized plane strain model was a more highly refined model, with eight elements through each ply, compared to only four elements through each ply in the 3-D model. Both meshes were generated using PATRAN by PDA

Engineering, and the finite element analysis was run using ABAQUS, on an IBM RISC/6000 work station. The difference between cure and service temperatures was assumed to be -140°C.

Generalized Plane Strain Model

The generalized plane strain model assumed that the plies were all orthotropic, neglecting the presence of shear/extension coupling, but the stress of interest, namely the through-the-thickness stress σ_z (see Figure 3.1), depended only on the Poisson's ratio mismatch (the 3-D model was used to verify this assumption). Using symmetry arguments, only one quarter of the cross-section of the laminate (the y-z plane) was modeled. Six-node quadrilateral elements, and five-node triangle elements were used, where the last two nodes in each case specified the extensional strain in the x-direction, and angles of rotation about the y- and z-axes. The model was given a 0.1% strain in the x-direction (see Figure 3.2), and zero rotation about the y- and z-axes in order to simulate a simple tensile test.

3-D Model

The 3-D model was used to provide a rough check on the generalized plane strain model used to find σ_z. Because of the size of the problem, only a relatively course mesh was used. Because the 3-D model incorporated off-axis plies, and the resultant shear/extension coupling, no symmetry about the z-axis existed and one half of the laminate was the simplest model that could be used. Eight node brick elements, and 6 node wedge elements were used throughout. Figure 3.2 shows the boundary conditions used.

3.1.2 Analytical Model

The finite element model used could only predict the stresses of undamaged specimens. Since the actual specimens contained 90° ply cracks before delamination occurred, some method of incorporating stresses generated by the presence of cracks was needed.

An approximate elasticity approach was implemented. The method used herein is a modification of an approach developed by Vasiliev [11]. His model is a four-ply symmetric $[0°/90°]_S$ lay-up containing a crack in the central block of two plies (Figure 3.3). All plies were of the same thickness. Figure 3.4 shows the more general laminate used in the present development. The three dimensions h_i in Figure 3.4 are of arbitrary thickness, and symmetry about the midplane is not required. The model assumes that layers 1 and 3 (see Figure 3.4) are homogeneous, orthotropic plies. Of course, the stresses in these layers will be incorrect, but the stresses in layer 2 are those of interest, and will be correct. The properties of layers 1 and 3 can be found using lamination theory, and the properties of layer 2 are the properties of a 90° ply. Neglecting Poisson effects, we begin with equilibrium,

$$\begin{aligned} \frac{\partial \sigma_x}{\partial x} + \frac{\partial \tau_{xz}}{\partial z} &= 0 , \\ \frac{\partial \sigma_z}{\partial z} + \frac{\partial \tau_{xz}}{\partial x} &= 0 , \end{aligned} \tag{3.1}$$

where

$$\sigma_x = E_x \frac{\partial u}{\partial x} , \; \sigma_z = E_z \frac{\partial w}{\partial z} , \; \tau_{xz} = G_{xz}\left(\frac{\partial u}{\partial z} + \frac{\partial w}{\partial x}\right). \tag{3.2}$$

It is known that at the crack surface (x=0), $\sigma_x^{(2)} = \tau_{xz}^{(2)} = 0$. In addition, as $x \rightarrow \infty$, $\sigma_x^{(2)} \rightarrow \sigma_o^{(2)}$, where $\sigma_o^{(2)}$ is the far field stress in layer 2. Therefore, the stresses in the x-direction can be thought of as a combination of a penetrating and a boundary solution. The approximating assumption is that the boundary solution depends only on x, as follows:

$$\sigma_x^{(1)} = \sigma_o^{(1)} + \sigma_1(x)\,,$$
$$\sigma_x^{(2)} = \sigma_o^{(2)} + \sigma_2(x)\,, \qquad (3.3)$$
$$\sigma_x^{(3)} = \sigma_o^{(3)} + \sigma_3(x)\,,$$

where $\sigma_i(x)$ are stresses (functions of x only) in each layer caused by the crack, and

$$\sigma_o^{(1)} = E_1\,\varepsilon_o\,,\ \sigma_o^{(2)} = E_2\,\varepsilon_o\,,\ \sigma_o^{(3)} = E_3\,\varepsilon_o\,. \qquad (3.4)$$

In Equations 3.4,

$$\varepsilon_o = P/(h_1E_1+h_2E_2+h_3E_3)\,, \qquad (3.5)$$

where P is the applied load in the x-direction. By integrating the first equilibrium equation for layer 1, and taking into account the boundary condition at $z = h_1+h_2+h_3$, it can be shown that

$$\tau_{xz}^{(1)} = (h_1+h_2+h_3-z)\,\sigma_1'\,. \qquad (3.6)$$

Integrating of the second equilibrium equation for layer 1, and taking into account the homogeneous boundary condition at $z = h_1+h_2+h_3$ (top surface), leads to

$$\sigma_z^{(1)} = \frac{1}{2}\,(z-h_1-h_2-h_3)^2\,\sigma_1''\,. \qquad (3.7)$$

Doing the same for layer 3 with homogeneous boundary conditions at $z = 0$ (bottom surface) it can be shown that

$$\tau_{xz}^{(3)} = -z\,\sigma_3'\,, \qquad (3.8)$$

and

$$\sigma_z^{(3)} = \frac{1}{2}\,z^2\,\sigma_3''. \qquad (3.9)$$

Continuing with layer 2, and (using the functions of integration) matching the boundary conditions in layers 1, 2 and 3 at $z = h_1$ and $z = h_1+h_2$, it can be shown that all stresses can be written in terms of σ_2 and its derivatives, as follows.

$$\begin{aligned} \sigma_x^{(1)} &= \sigma_o^{(1)} + H_1\, \sigma_2(x)\,, \\ \tau_{xz}^{(1)} &= H_1\, (h_1 + h_2 + h_3 - z)\, \sigma_2'(x)\,, \\ \sigma_z^{(1)} &= \frac{1}{2} H_1\, (z - h_1 - h_2 - h_3)^2\, \sigma_2''(x)\,, \end{aligned} \tag{3.10}$$

$$\begin{aligned} \sigma_x^{(2)} &= \sigma_o^{(2)} + \sigma_2(x)\,, \\ \tau_{xz}^{(2)} &= [h_3\, (1 - H_2) - z]\, \sigma_2'(x)\,, \\ \sigma_z^{(2)} &= [-\frac{1}{2} z^2 + h_3\, (1 - H_2)\, z + \frac{1}{2} h_3^2\, (3H_2 - 1)]\, \sigma_2''(x)\,, \end{aligned} \tag{3.11}$$

$$\begin{aligned} \sigma_x^{(3)} &= \sigma_o^{(3)} + H_2\, \sigma_2(x)\,, \\ \tau_{xz}^{(3)} &= -H_2\, z\, \sigma_2'(x)\,, \\ \sigma_z^{(3)} &= \frac{1}{2} H_2\, z^2\, \sigma_2''(x)\,. \end{aligned} \tag{3.12}$$

where

$$H_1 = \frac{h_2}{h_1} \frac{(h_2-h_3)}{(h_1-2h_2+h_3)}\,,\; H_2 = \frac{h_2}{h_3} \frac{(h_2-h_1)}{(h_1-2h_2+h_3)}\,. \tag{3.13}$$

In the process of finding these expressions for the stresses, relationships are found expressing σ_1 and σ_3 in terms of σ_2, as follows.

$$\sigma_1 = H_1\, \sigma_2\,,\; \sigma_3 = H_2\, \sigma_2. \tag{3.14}$$

The appendix contains a detailed development of the above equations. Now the w displacement can be solved for by using the second of Equations 3.2, and satisfying compatibility of displacements using functions of integration. With the third of Equations 3.2, the u displacement can be found. It was noted that the first of Equations 3.2 cannot be satisfied exactly. This is in reality a compatibility equation in strains that can be solved

approximately using the principle of minimization of strain energy. The strain energy can be written

$$U = \frac{1}{2}\int\int\left(\frac{\sigma_x^2}{E_x} + \frac{\sigma_z^2}{E_z} + \frac{\tau_{xz}^2}{G_{xz}}\right) dz\, dx, \tag{3.15}$$

and substituting in the expressions for stresses, can be simplified to the form

$$U = \int F\,(\sigma_2,\ \sigma_2',\ \sigma_2'')dx. \tag{3.16}$$

The Euler Equation,

$$\frac{\partial F}{\partial \sigma_2} - \frac{d}{dx}\left(\frac{\partial F}{\partial \sigma_2'}\right) + \frac{d^2}{dx^2}\left(\frac{\partial F}{\partial \sigma_2''}\right) = 0, \tag{3.17}$$

then yields the characteristic equation

$$\begin{aligned}\left(\frac{h_1^5 H_1^2}{10 E_z^{(1)}} + \frac{h_2^5}{10 E_z^{(2)}} + \frac{h_2^4 H_2 h_3}{2 E_z^{(2)}} - \frac{h_2^3 H_2 h_3^2}{3 E_z^{(2)}} + \frac{2 h_2^3 H_2^2 h_3^2}{3 E_z^{(2)}} - \frac{h_2^2 H_2 h_3^3}{E_z^{(2)}} + \frac{h_2 H_2^2 h_3^4}{2 E_z^{(2)}} + \frac{H_2^2 h_3^5}{10 E_z^{(3)}}\right)\sigma_2'''' \\ + \left(\frac{2 h_1^3 H_1^2}{3 G_{xz}^{(1)}} + \frac{2 h_2^3}{3 G_{xz}^{(2)}} + \frac{2 h_2^2 H_2 h_3}{G_{xz}^{(2)}} + \frac{2 h_2 H_2^2 h_3^2}{G_{xz}^{(2)}} + \frac{2 H_2^2 h_3^3}{3 G_{xz}^{(3)}}\right)\sigma_2'' \\ + \left(\frac{2 h_1 H_1\left[H_1 + \sigma_o^{(1)}\right]}{E_x^{(1)}} + \frac{2 h_2\left[1 + \sigma_o^{(2)}\right]}{E_x^{(2)}} + \frac{2 H_2 h_3\left[H_2 + \sigma_o^{(3)}\right]}{E_x^{(3)}}\right)\sigma_2 = 0.\end{aligned} \tag{3.18}$$

The solution to any homogeneous, linear, ordinary differential equation with constant coefficients of the form

$$A\ \sigma_2'''' + B\ \sigma_2'' + C\ \sigma_2 = 0 \tag{3.19}$$

can be written as

$$\sigma_2 = C_1\, e^{r_1 x} + C_2\, e^{r_2 x} + C_3\, e^{r_3 x} + C_4\, e^{r_4 x}, \tag{3.20}$$

where $r_{1,2,3,4}$ are the roots of the equation

$$A r^4 + B r^2 + C = 0. \tag{3.21}$$

If the roots are distinct and real, two will be positive, and two negative. One of the conditions of a boundary-type solution is that it decays to zero as x goes to infinity. Therefore, the coefficients $C_{1,2}$ of the two positive roots must be zero.

If the roots are complex, the solution can be rewritten as

$$\sigma_2 = e^{\alpha x}\left(C_1 \sin \beta x + C_2 \cos \beta x\right) + e^{-\alpha x}\left(C_3 \sin \beta x + C_4 \cos \beta x\right). \tag{3.22}$$

Again, the solution must decay to zero as x goes to infinity, so the coefficients $C_{1,2}$ must be zero. The other two coefficients $C_{3,4}$ can be found by substituting Equation 20 or 22 into Equations 11, and using the boundary conditions at the crack.

3.2 *Flexure*

In a uniaxial tensile test, if the material properties of the specimen remain linear to failure, the stress/strain response will also be linear. With laminated composite materials, the stress/strain response tends to be quite linear until damage begins to propagate in the specimen. Hence, the observation of the specimen's response, and in particular, noting the onset and magnitude of non-linearities present, yields certain information about the initiation and propagation of damage in the specimen.

It would be hoped that a similar technique could be employed with the flexure specimens. However, because of the geometry of the test fixture, and the fact that the deflections are too large for the application of small deflection beam theory, the load/deflection response for even linear elastic materials is non-linear throughout the response. In order to provide a means whereby the experimental response could be accurately compared with the case of

linear material properties, the response of the specimen in the fixture was modeled numerically.

3.2.1 Numerical Model

The model used the non-linear bending simple beam equation, and the geometry of the test fixture and specimen.

$$\frac{d^2z}{dx^2} = \frac{M}{EI}\left(1 + \left(\frac{dz}{dx}\right)^2\right)^{\frac{3}{2}} \tag{3.1}$$

The computer code employed a fourth-order Runga-Kutta routine to reduce the second-order differential equation to a first-order equation, and then used Euler's method to solve the remaining equation for the shape of the beam. The beam was discretized, and the geometry of the specimen and fixture were used to calculate bending moments applied as a function of position along the beam.

In the absence of friction at the rollers, the load was always applied normal to the surface of the specimen. The typical linear friction model could then be employed to calculate frictional forces, assuming some friction coefficient. The vertical component of the load, crosshead displacement, top and bottom surface strains, etc. could then be output for comparison with the experimental data. The specimen surface strains were calculated using both the bending moment strains, and the extensional strains arising from axial loading of the specimen.

4. RESULTS (TENSION)

The general trends in sublaminate-scaled tensile specimens were to enhance properties such as strength, strain to failure, etc. with increased specimen size. However, scaling effects were present in varying degrees in the different stacking sequences studied. Results for the AS4/3502 and APC-2 composites will be discussed separately.

4.1 Stress/strain Response

All strain measurements were taken using extensometers. Initially, difficulties were encountered with the APC-2 specimens. These specimens had smooth, hard surfaces that did not allow the knife edges of the extensometer sufficient friction to resist slipping. This problem was overcome by lightly abrading the surface of the specimens, which provided sufficient friction to avoid slipping.

Tables 4.1-4.4 summarize the initial laminate stiffness of Lay-ups ***A***, ***B*** and ***C***. Figure 4.1 shows the initial modulus for the 3-D scaled specimens of each laminate plotted versus specimen size. Initial laminate stiffness was found by dividing the load by the cross sectional area of the specimen to yield the average laminate stress, and using a linear regression fit of the stress/strain response between 0 and 0.2% strain. All stress/strain curves exhibited linear response in this region. As indicated in Figure 4.1, there is some slight

variation of the stiffness for different sized specimens. This makes direct comparison between stress/strain curves of different specimens more difficult. Hence, a normalization with respect to volume fraction was deemed useful.

In the process of curing, some variations in panel thickness are inevitable, but the load carrying capacity of the specimen should depend only on the number of plies (and hence, fibers) in a given orientation. Changes in thickness only represent slight differences in volume fraction, or the amount of polymer matrix material surrounding the fibers. Thus, two crossply specimens of the same material, stacking sequence, and width, will carry the same load, even if they have slightly different thicknesses because of curing effects. The number of 0° fibers in each specimen is the same, and the load carrying capacity will be the same. If the actual thickness were used, as above (Figure 4.1), one would conclude that the specimens had slightly different stiffnesses. If, however, a nominal thickness (based on the number of plies) were used, both specimens would exhibit the same stiffness, and their stress/strain responses would be directly comparable. Therefore, when stress/strain plots are shown in this work, the stress calculations will be as follows:

$$\sigma_x = \frac{P}{n\, t_o\, w}, \tag{4.1}$$

where P is the load, n is the scaling factor, t_o is the nominal thickness of the n=1 (baseline) specimen, and w is the width of the specimen.

4.1.1 AS4/3502 Specimens

Figures 4.2-4.4 show the typical tensile stress/strain response of 3-D scaled Lay-ups ***A***, ***B*** and ***C***, respectively. The Figures show results from both the 25 mm MTS extensometer, and the custom extensometers. It must be noted that the smaller two specimen sizes (***a*** and ***b***) had only one extensometer mounted on each specimen, whereas the two larger sizes (***c*** and ***d***) had both the MTS and the custom extensometer mounted on the same specimen. As

a result, the stress/strain curves for the ***a-8*** and ***b-16*** specimens come from different specimens in plots (a) and (b) in Figures 4.2-4.4, while the stress/strain curves of the ***c-24*** and ***d-32*** specimens represent the same specimen in both plots.

Each curve represents the response of one coupon from its size and stacking sequence, although the coupon selected was representative of the typical response of all specimens in the group. The repeatability of the response is depicted in the stress/strain curves of Figure 4.5, in which eight specimens of a given stacking sequence are shown.

It was found that the factor that had the greatest influence on the tensile stress/strain response was the scaled thickness. Figures 4.6 and 4.7 show stress/strain responses for 1-D and 2-D scaled specimens of Lay-ups ***A*** and ***B***, respectively. Note that scaling the in-plane dimensions alone (2-D) yields virtually identical response, but that scaling the thickness alone (1-D) produces a change in both the non-linear behavior and the strength, similar to the response exhibited by 3-D scaled specimens.

One of the features of the stress/strain plots of Lay-ups ***A*** and ***B*** (shown in Figures 4.2 and 4.3) was the point at which the response deviated from linearity, which will be referred to as the "non-linear knee." Unlike Lay-ups ***A*** and ***B***, the response of Lay-up ***C*** specimens was typically linear to failure, as shown in Figure 4.4. Tables 4.5 and 4.6 summarize the non-linear knee stresses for all sizes of Lay-up ***A*** and AS4/3502 Lay-up ***B*** specimens, and Figure 4.8 shows the effect of specimen size upon the knee stress, for 3-D scaled specimens. The values in the figure are normalized with respect to the size ***a*** specimens for purposes of comparison. The knee stress increases with increased specimen size.

Lay-up A [30/-30/90/90]ns

Note from Figure 4.2 that the stress/strain responses of the all Lay-up ***A*** specimens are very similar in shape. Note also that the differences in the stress/strain responses of these specimens follow a definite trend. Upon inspection of individual stress/strain curves from each size of specimen, it was determined that the non-linear knee stress was higher for larger specimens (Table 4.5). Also the failure stress and strain are greater for larger specimens. All specimens deviated significantly from linearity before final failure. However, despite the non-linear response, the stress/strain curves of all sizes virtually coincide until approximately 90% of the failure load of each specimen, when even more severe non-linear effects take place.

Lay-up B [45/-45/0/90]ns

The response of Lay-up ***B*** specimens showed a different kind of trend with increased size. Not only did the non-linear knee stress and failure stress increase, but the specimens showed stress/strain responses that changed in character with increased specimen size. Note in Figure 4.3 that whereas 8-ply specimens demonstrated pronounced non-linearities, larger specimens tended toward linearity.

Lay-up C [90/0/90/0]ns

From Figure 4.4, it can be seen that Lay-up ***C*** specimens exhibited a response that was linear to failure, and independent of scaled size. The responses of all sizes were virtually identical, including the failure strength and strain.

4.1.2 APC-2 Specimens [45/-45/0/90]ns

All APC-2 specimens were of the quasi-isotropic Lay-up ***B***. Figure 4.9 shows the stress/strain response curves of several specimens cut from the same 8-ply panel. Some were size ***a-8*** and some were size ***b-8***, but as noted before with respect to the AS4/3502 specimens, scaling the in-plane dimensions while leaving the thickness constant (2-D) produced virtually no size effect. Figure 4.10 shows a schematic of the panel from which the specimens were cut, with the specimens numbered as shown. The relatively large amount of scatter observed in Figure 4.9 can be directly correlated to the location on the panel from which the specimen was cut. Those specimens cut from regions near the edge of the panel exhibited moduli of approximately 80% and strengths of about 85% of values for specimens cut from the center of the panel.

Figure 4.11 shows the initial modulus and ultimate strength as functions of position in the panel. It is shown that the variation in properties is much less for specimens cut from the interior of the panel, compared to specimens cut from the edges. Therefore, throughout this report, values discussed for comparison of APC-2 specimens will be for specimens from within the center portion of the panel.

Figure 4.12 shows the typical stress/strain response from the two geometrically scaled APC-2 specimen sizes. The responses are nearly linear, although a slight deviation from the original slope of the response can be detected. It is significant to note that no scaling effects are present. This is true also of APC-2 specimens that were scaled in the 1- and 2-D regimes. The response is independent of specimen thickness and in-plane dimensions.

4.2 Damage Processes

4.2.1 AS4/3502 Specimens

The investigation of damage processes was performed on batch *II* specimens. Figure 4.13 shows the stress/strain response of two ***Ba-8*** specimens. One is a batch *I* specimen and the other is a batch *II* specimen. Note that although the non-linear knee occurs at different stresses, the main features of the stress/strain plots are similar for both specimens. Therefore, it is expected that the general correlation between damage and stress/strain response observed in the batch *II* specimens will be similar to that of the batch *I* specimens.

One purpose of the damage investigation was to pinpoint the first ply failure for each type and size of laminate. Because there was no identifiable event on the stress/strain response corresponding to this first ply failure, this was accomplished by loading a specimen until the first audible crack was heard, and then unloading and examining the specimen. It was found that there was a one-to-one correlation between the number of cracks heard while loading a specimen, and the number of cracks observed in the subsequent radiographs of that specimen. However, only one specimen per Lay-up/size group was used to find the first ply failure. Therefore, although the data may be used to observe general trends, more tests would be needed to accurately determine an average first ply failure stress. Tables 4.7 - 4.9 and Figure 4.14 show the resulting normalized first ply failure stresses for the 3-D geometrically scaled specimens for Lay-ups ***A***, ***B*** and ***C***.

A second goal of the damage evaluation was to characterize the types of failure mechanisms present in each of the different laminate stacking sequences. In order to do so, several specimens of each size and stacking sequence were tested to destruction. After observing the stress/strain behavior of each laminate type, points of interest, such as deviation from

linearity or abrupt changes in slope, were identified for investigation. Some of the remaining specimens were then loaded to stresses corresponding to these points of interest, and unloaded. Non-destructive techniques were then used to observe the damage in these pre-loaded specimens in order to sequentially record the damage processes of each type of laminate.

Lay-up A [30/-30/90/90]ns

Figure 4.15 shows the typical stress/strain response of the ***Aa-8*** specimens. Included are micrographs and radiographs that document the damage associated with various features on the stress/ strain curves. It can be seen that first ply failure occurred within the linear region of the response (point ***A*** in Figure 4.15). In the 16-ply and larger specimens, first ply failure was in one of the outer blocks of 90° plies, not in the center block of four 90° plies.

At progressively higher loads, the transverse crack density continued to increase, with most of the cracks in the larger specimens concentrated in the outer 90° plies, and the stress/strain response started to deviate from linearity.

As loading increased, the crack density remained relatively uniform throughout the gage section. From Figure 4.15 it can be seen that at a certain point, areas of higher transverse crack density developed. It was observed that the areas of higher crack density were associated with regions where cracks had formed in the -30° plies adjacent to the 90° plies (point ***B*** in Figure 4.15). This is most obvious in the small region of delamination. However, when examined microscopically, it was found that other regions of high crack density also contained -30° cracks. Crossman and Wang [12] have also noted such behavior in a similar lay-up.

At some higher load, the -30° edge crack began to propagate along the 30°/-30° interface, and eventually the crack propagated through the +30° ply to the surface of the specimen, or to the next 90° ply if it was not a surface +30° ply. Subsequently, an area of delamination formed at the outermost 90°/-30° interfaces (point ***C*** in Figure 4.15). Even though the stress/strain response was already non-linear as a result of the 90° cracks, a knee was present in the stress/strain response due to a reduction in stiffness as delamination initiated (point ***C*** in Figure 4.15). The knee corresponded to the point at which the delamination initiated, and the stiffness dropped appreciably.

Although there were cracks at +30°/-30° and 90°/-30° interfaces throughout the thickness in all specimen sizes, the areas where these crack systems connected to form distinct delaminations were always confined to the outermost 90°/-30° interfaces in the ***Ab-16*** and larger specimens, as seen in Figure 4.16.

It was observed from failed ***Aa-8*** specimens that before this localized delamination could grow to form a general edge delamination, global failure of the laminate occurred. Larger specimens, however, showed delaminations along a greater length of the specimen edge, to the point that the ***Ad-32*** specimens had delaminations formed in the outer 90°/30° interfaces along almost their entire length prior to global failure.

It was observed that in thicker specimens, the transverse cracks in the outermost 90° plies tended to be at some angle as viewed from the edge, as seen in Figure 4.17, indicating the presence of some edge-effect interlaminar shearing stresses in addition to the normal stresses. These cracks twisted as they propagated through the width, so that on opposite edges of the specimen, they were angled in opposing direction. Figure 4.18 shows the failure modes of the 3-D scaled specimens.

Lay-up B [45/-45/0/90]ns

Figure 4.19 shows a typical stress/strain response of an AS4/3502 ***Ba-8*** specimen, as well as micrographs and radiographs that document associated damage. It can be seen that first ply failure occurred within the linear region of the stress/strain curve (point ***A*** in Figure 4.19). Thicker Lay-up ***B*** specimens failed first in the central block of 90° plies. As the transverse matrix cracks continued to increase in number, most cracks in the thicker specimens were located in the central block of 90° plies, rather than the outer 90° plies. There was also a slight deviation from linearity following point ***A*** in the stress/strain curve as transverse cracking continued. This non-linearity due to cracking in the 90° plies alone becomes more pronounced, and of longer duration in the larger specimens.

At approximately 335 MPa, a distinct knee occurred (point ***B*** in Figure 4.19). Upon examination of a coupon loaded to this point, it was determined that a small thumbnail shaped delamination had started at one of the edges of the specimen at the -45°/90° interfaces (see radiograph ***B*** in Figure 4.19). The delamination switched interfaces periodically as shown in Figure 4.19, and did not occur at both interfaces simultaneously. In thicker Lay-up ***B*** specimens, this "delamination knee" occurred further into the non-linear response. In other words, the non-linearity due to 90° cracking continued for a longer period before delamination onset. Tables 4.10 and 4.11 show the average strain and stress, respectively, at the onset of delamination. Figure 4.20 shows the 3-D scaled delamination knee stress.

As this small delamination grew, and others like it formed, the stiffness continued to change. Some 8-ply specimens showed another knee in the stress/strain plot, seen as point ***C*** in Figure 4.19. This was the point at which the localized regions of delamination connected to form a general edge delamination. As the now general delamination continued to propagate widthwise, the stiffness was further reduced. In the 8-ply specimens, the edge

delaminations propagated through the width until the coupon was almost completely divided into two separate sublaminates of stacking sequence $[\pm 45/0]_T$ with blocks of 90° plies at intervals adhering to the 0° plies.

Larger specimens experienced delamination only at the central 90°/0° interfaces, and the degree to which delamination propagated was significantly reduced. While delaminations in the 8-ply specimens propagated to the middle of the coupon, delaminations in larger specimens were confined to a few millimeters in from the edge (Figure 4.21). Just before global failure, matrix cracks occurred in the +45° and -45° plies. Figure 4.22 shows the typical failure modes of the 3-D scaled specimens.

Lay-up C [90/0/90/0]ns

First ply failure occurred as transverse matrix cracks, always in the surface 90° plies. As loading continued, cracks formed throughout all 90° plies, with the characteristic crack density increasing. However, no other damage modes were observed. Finally, fiber fracture caused global failure of the specimens. Figure 4.23 shows the typical failure modes of the 3-D scaled specimens.

4.2.2 APC-2 Specimens [45/-45/0/90]ns

Recall that results discussed will be for APC-2 specimens cut well away from the edges of the panel. This minimized the variation of properties related to the specimen's position within the panel.

The APC-2 Lay-up ***B*** specimens failed in a manner unlike the AS4/3502 Lay-up ***B*** specimens. From the radiographs it was observed that the first ply failure was by transverse matrix cracking in the 90° plies. These cracks typically did not run through the width of the specimen, as cracks did in the AS4/3502 specimens. Upon examination of the specimen

edges under an optical microscope, no delamination could be found. In fact, the only damage that could be seen under the microscope was the presence of the cracks in the 90° plies.

4.3 Ultimate Stress and Strain

Tables 4.12-4.15 summarize the ultimate stress measured for each specimen size for Lay-ups ***A***, ***B*** and ***C***. Recall that when moving along the diagonal from size ***a-8*** to size ***d-32***, all dimensions are scaled geometrically (3-D). When moving down or across the table, the in-plane dimensions (2-D) or the thickness dimensions (1-D) are scaled, respectively. Normalized ultimate stress results from the 3-D scaled specimens of Lay-ups ***A***, ***B***, and ***C*** are plotted versus size in Figure 4.24.

Tables 4.16-4.19 summarize the effect of specimen size upon failure strain for Lay-ups ***A***, ***B*** and ***C***, respectively. Figure 4.25 shows the normalized failure strain for the 3-D scaling of each laminate plotted with specimen size.

4.3.1 AS4/3502 Specimens

Lay-up A [30/-30/90/90]ns

Lay-up ***A*** showed a pronounced increase in strength with size for the 3-D scaled specimens. Also note that the strength appears to level off as the specimen size is increased. The strength seems to be approaching a maximum strength, beyond which increased size would either have no effect, or could perhaps lead to a strength decrease. Strain to failure follows the same increasing trend with increased specimen size.

Lay-up B [45/-45/0/90]ns

AS4/3502 Lay-up ***B*** specimens followed a similar trend in strength as Lay-up ***A*** specimens did, but the effect was not as pronounced. In fact, the three larger sizes seem to have es-

sentially the same strength, with only the 8-ply specimen showing a lower ultimate stress. In all cases, however, the strain to failure was essentially constant as the presence of 0° fibers tends to control the failure of the specimen.

Lay-up C [90/0/90/0]ns

Lay-up ***C*** specimens showed no significant scaling effect in ultimate stress or strain. Again, this is due to the presence of 0° fibers, which control the failure.

4.3.2 APC-2 Specimens [45/-45/0/90]ns

Like the Lay-up ***C*** specimens, APC-2 Lay-up ***B*** specimens showed no trend of strength change with increased size (see Tables 4.14 and 4.15). However, APC-2 Lay-up ***B*** specimens had an average strength and strain to failure of nearly 10% greater than the largest AS4/3502 Lay-up ***B*** specimens, even though the same fiber is employed in each material. Note from Tables 4.2 and 4.3 that the average stiffnesses are the same for both laminates, indicating that the fiber volume fractions are not significantly different.

4.4 Finite Element Model

The finite element model was used in order to determine the interlaminar tensile stresses. It was hoped that this would lead to an understanding of why Lay-up ***A*** specimens always delaminated at the outermost -30°/90° interfaces, whereas the Lay-up ***B*** specimens always delaminated at the central 0°/90° interfaces. Figure 4.26 shows σ_z as a function of position through the thickness for the $n = 2$ case for both Lay-ups ***A*** and ***B***. Note that tensile edge stresses are maximum in the outer 90° plies for both lay-ups. However, the difference between primary and secondary peaks is much larger for Lay-up ***A*** than for Lay-up ***B***. Ratios of secondary to primary peaks were 59.6% for Lay-up ***A*** vs. 85.3% for Lay-up ***B***.

4.5 Analytical Model

Figure 4.27 shows typical stresses in the 90° ply in the vicinity of a single crack. The axial stress σ_x must be zero at the free surface, after which it builds to the value of the far field stress in that layer. The shear stress τ_{xy} also must be zero at the crack surface. It increases to a maximum value, and then must decay to zero as x goes to infinity. The through-the-thickness stress σ_z has its maximum value at the crack surface, passes through zero into compression, and decays back to zero.

4.5.1 Lay-up A [30/-30/90/90]ns

For comparison with the finite element model, the $n = 2$ case was used to calculate stresses. Table 4.20 gives σ_z predicted by the model for Lay-ups ***A*** and ***B*** at the outer 90° plies, and the central 90° plies. In addition, Table 4.20 gives σ_z for the finite element calculations at locations of maximum stress in the central and outer 90° plies. Note that s_z at the outer 90° plies in Lay-up ***A*** specimens was significantly higher than σ_z at the central 90° block, adding to the stresses calculated in the finite element analysis. Hence, the combination of the finite element and the analytical models still predicts that Lay-up ***A*** specimens will de-laminate at the outer 90° block, as observed in experiment.

4.5.2 Lay-up B [45/-45/0/90]ns

From Table 4.20 note that the opposite trend is predicted by the analytical model for Lay-up ***B*** specimens. Through-the-thickness stress σ_z for a single crack is greater at the central block of 90° plies by about 6%. However, this is not enough to compensate for the finite element results. When σ_z from the finite element model is added to σ_z for the analytical model with a single crack, the combination still predicts delamination failure in the outer 90° ply. However, in the actual specimens, there are multiple cracks. As mentioned earlier,

cracks in the central 90° block are significantly more closely spaced, with an average spacing of about 0.2 mm between cracks. This is close enough for tensile σ_z stresses from adjacent cracks to interact, adding to the tensile σ_z stresses. Just prior to delamination, crack spacing in the outer 90° ply was on the order of 0.5 mm, which does not allow interaction of tensile σ_z stresses from adjacent cracks (see Figure 4.28).

5. RESULTS (FLEXURE)

All strain measurements were taken using longitudinal strain gages on the top and bottom of the specimens. Load and crosshead displacement were measured directly from the testing machine.

The spans between inner and outer rollers on the fixture were scaled at $25n$ mm and $55n$ mm respectively, and the span to depth ratio used was nominally 30.

Due to the nature of laminated composite materials, some bend/twist coupling exists in Layups ***B*** and ***D***. This coupling is most pronounced in the baseline/ply-level scaled specimens, where the coupling terms are about 16% and 19% of the bending stiffness terms for ***Ba*** and ***Da*** specimens, respectively, and less pronounced with increased sublaminate-level scaled size. Coupling terms are 4% and 5% of the bending stiffnesses in ***Bds*** and ***Dds*** specimens, respectively.

5.1 Verification of Numerical Model

The numerical model required a knowledge of the frictional forces imparted to the specimen through interaction with the fixture's rollers, which were equipped with ball bearings in order to minimize the effect. The frictional forces were found by applying a known vertical

load to the top plate of the fixture, and measuring the force required to move the specimen laterally in the fixture. Because of the ball bearings, no specimen/roller slippage occurred. Rather, rolling friction in the bearings was responsible for the forces. It was found that the load/roller force relationship was linear, and that the effective coefficient of friction at each bearing was 0.014. The effect on the load/deflection response was so minimal in comparison with the frictionless case that it did not effect the analysis.

The numerical simulation was checked against three isotropic materials in order to validate the predictions obtained. Uniaxial tensile tests were performed first on steel, aluminum and polymethylmethacrylate (PMMA) specimens in order to obtain Young's Modulus *E*. This stiffness, and the specimen and fixture geometry were entered as the only inputs for the program, and predicted load/deflection plots were produced. Flexure tests were then performed on the same specimens. Figures 5.1-5.3 show the resulting predictions and experimental results. Excellent agreement was obtained for the portions of the response before plastic yielding occurred in each case. Having validated that the shape of the predicted load/deflection curves was accurate, a method of comparing experimental load/deflection plots with the non-linear load/deflection predictions for linear elastic material behavior was then available.

5.2 Load/Deflection Response

Because the responses of different sizes of flexure specimens cannot be directly compared, some method of normalization was needed. A natural way to do this would be to simply remove any geometrically-dependent terms. This can be accomplished by considering the strain at the specimen surface according to simple beam theory.

$$\varepsilon = \frac{P\ L\ c}{E_b\ I} \tag{5.1}$$

The length L, the half thickness c, and the second moment of area I are scaled as follows:

$$\begin{aligned} L &= n\,L^*, \\ c &= n\,c^*, \\ I &= n^4\,I^*, \end{aligned} \tag{5.2}$$

where L^*, c^* and I^* are the dimensions of the baseline specimens, and n = 1,2,4. Recognizing that the scaled deflection will be

$$\delta = n\,\delta^*, \tag{5.3}$$

and substituting Equations 5.2 into Equation 5.1 yields

$$\begin{aligned} \varepsilon &= \frac{P\,L^*\,c^*}{n^2\,E_b\,I^*}, \text{ and} \\ \delta^* &= \frac{\delta}{n}. \end{aligned} \tag{5.4}$$

These equations give the correct order of the scaling factor n to be used in the normalization process. In addition, since the bending stiffness of each size of sublaminate-level scaled specimen will vary according to CLT (Figure 1.2), the bending stiffness E_b was used in the normalization process. Hence the equations used were simply

$$\begin{aligned} \Pi &= \frac{P}{n^2\,E_b}, \text{ and} \\ \Delta &= \frac{\delta}{n}. \end{aligned} \tag{5.5}$$

This normalization collapses the elastic responses of all geometrically scaled specimens onto the same curve, so that differences in response with scaled size can be readily compared. Because the first of Equations 5.5 is based on the elastic surface strain of the beam, any value of Π (within the linear elastic properties range) represents a specific value of surface strain regardless of scaled specimen size. This is also true of Δ.

Figures 5.4-5.6 show the normalized ply-level and sublaminate-level scaled responses of Lay-ups ***B***, ***C*** and ***D***. Note that even though the material properties were assumed to remain linear, the load/deflection response predicted was non-linear. The initial stiffening of the response comes about as a result of changing geometry. As the specimen begins to deflect, and the contact point between the rollers and the specimen begins to move inward. The moment arm thus becomes smaller, and it takes a higher load to apply a given moment (Figure 5.7). Subsequent softening of the response occurs after the specimen has deflected significantly. This is because the testing machine can only measure the vertical component of the load. Since the load is applied at some angle (ideally normal) to the surface of the specimen, there is a portion of the applied load not being measured by the testing machine (Figure 5.8). Hence, as deflection continues, a given measured load will apply a somewhat higher moment, depending on the angle of contact at the roller.

Given these considerations, the response is in reality a structural response, not a material response. However, with the aid of the numerical solution, deviation from linear material properties can still be detected. This point of deviation from linear properties should lend clues to the failure processes in the composite laminate.

Tables 5.1-5.3 present the bending stiffness, ultimate load and ultimate deflection of each lay-up, and Figures 5.9-5.17 show the normalized values of stiffness, strength and ultimate deflection for each lay-up. These are values extracted from the load/deflection plots of each specimen type, and are averages of several specimens each.

Note in Figures 5.12-5.17 that the ply-level scaled specimens show a pronounced reduction in strength as the size of the specimen increases. Flaggs and Kural [18] used an energy based method to model the damage in $[0°/90°_n]_S$ laminates. Kellas and Morton used the same model to predict reductions in strength as ply-level scaled composites were increased

in size. They showed that Flaggs and Kural's equation could be reduced to Equation 5.6 in the case of ply-level scaled specimens, where $\sigma^{cr\cdot}$ is the critical strain at which damage is propagated, and n is the scaling parameter. The subscripts $_p$ and $_m$ refer to prototype and model sizes, respectively.

$$\frac{\sigma_p^{cr\cdot}}{\sigma_m^{cr\cdot}} = \frac{1}{\sqrt{n}} \tag{5.6}$$

Hence, when strength or damage results are presented in the following sections, they will be plotted against Equation 5.6 for comparison to the ply-level scaled specimens only. It was previously noted that the equation used by Flaggs and Kural yielded no predicted scale effect in sublaminate-level scaled specimens.

All specimens of each lay-up showed some deviation from uniform linear properties. This behavior was most pronounced in the Lay-up ***D*** specimens, but even in Lay-up ***C*** specimens, some deviation was present in the load/deflection response. Tables 5.4-5.5 give the loads and deflections at which this deviation occurred, and Figures 5.18-5.23 show the normalized loads and deflections at deviation for each lay-up.

5.2.1 Lay-up B [45/-45/0/90]ns and [45n/-45n/0n/90n]s

Figure 5.4 shows the ply- and sublaminate-level scaled flexure responses of Lay-up ***B***. They are normalized with respect to the geometry and stiffness of the specimen (Equation 5.5), so if there were no scaling effect, all responses would be identical. Note that the results of the numerical model assuming linear material properties is plotted with the results for comparison. Deviation from this prediction would indicate a deviation of the beam from linear elastic response, and thus indicate that some damage in the specimen or other effect is taking place.

From the results of Kellas and Morton [6], it was expected that a reduction in strength would result from the practice of ply-level scaling Lay-up ***B*** specimens. This is indeed the case with the ply-level scaled flexure response.

However, there is no corresponding increase in scaled strength when sublaminate-level scaling is employed. In the tensile portion of this work, it was observed that sublaminate-level scaled specimens of a stacking sequence similar to Lay-up ***B*** exhibited a marked increase in strength with size when loaded in uniaxial tension. This is not the case with the flexure specimens of this class. In fact, there was a significant decrease in failure strain as the coupon size was increased using sublaminate-level scaling.

Note that all responses except the n=4 case in ply-level scaling (***Bdp***) follow the same load/deflection response, but fail at various locations along that response. The ***Bdp*** specimens deviate significantly from that response before failure, indicating perhaps that there is some different failure mechanism at work in this case.

Tables 5.1-5.3 give the bending stiffnesses and failure loads and deflections for each specimen size, and scaling method. Figures 5.9, 5.12 and 5.15 depict the bending stiffnesses and normalized failure loads and deflections, respectively.

5.2.2 Lay-up C [0/90/0/90]ns and [0n/90n/0n/90n]s

Figure 5.5 shows the normalized ply- and sublaminate-level scaled flexure responses of Lay-up ***C***. The load/deflection curves of these specimens remain identical to the linear prediction throughout most of the response. Based upon the tensile results of Kellas and Morton [6] and the tensile portion of this work, this would be expected since the only damage modes present in the tensile Lay-up ***C*** specimens was transverse cracking in the 90° plies.

However, there is a pronounced difference in the ultimate load and deflection with scaled size. This constitutes a departure from trends observed under tensile loading.

Note that the load/deflection response typically shows an initial failure, at which the load drops to about 70-80% of its previous value, followed by additional elastic response of reduced modulus. A second failure of the specimen is accompanied by an even greater drop in load. Notice also that in the case of the ply-level scaled specimens, the secondary elastic responses seem to coincide with one another.

The secondary failure was associated with tensile fiber fracture. It was observed that the first drop in load was associated with delamination and buckling of the outer compressive ply (or plies) between the two inner rollers, as depicted in the box in Figure 5.5. Plotted in the figure, for comparison purposes, is the numerical prediction of the response where the outer compressive plies of a ply-level scaled specimen have been discounted.

Tables 5.1-5.3 give the bending stiffnesses and failure loads and deflections for each specimen size, and scaling method. Figures 5.10, 5.13 and 5.16 depict the bending stiffnesses and normalized failure loads and deflections, respectively.

5.2.3 Lay-up D [45/-45/45/-45]ns and [45n/-45n/45n/-45n]s

Figure 5.6 shows the normalized ply- and sublaminate-level scaled flexure responses of Lay-up ***D***. These specimens never suffered a catastrophic failure, as the other lay-ups did. Loading could have continued beyond that shown. The tests were stopped after a maximum load was reached, and the load began to fall. For the purposes of comparison later, the point at which the maximum load occurred was called the failure load, except for the $n = 4$ ply-level scaled case where the location of the first drop in load was called the failure point.

As expected from previous tensile studies, the ply-level scaled response shows the typical decrease in failure load and deflection. However, the sublaminate-level scaled specimens showed no corresponding increase in failure load. Indeed, their responses were essentially identical until the maximum load was reached. Even the n=2 ply-level scaled case deformed identically to the sublaminate-level scaled specimens for a significant portion of the non-linear response. ***Ddp*** specimens showed a significant departure from the response of all other specimens just prior to 2 mm normalized deflection. With the exception of the n=4 ply-level scaled case, no discontinuities in the load were present.

Tables 5.1-5.3 give the bending stiffnesses and failure loads and deflections for each specimen size, and scaling method. Figures 5.11, 5.14 and 5.17 depict the bending stiffnesses and normalized failure loads and deflections, respectively.

5.3 Strain Response

In addition to monitoring load and deflection, the strains at the top and bottom of the specimen were measured. It can readily be shown, based on simple beam theory, that the surface strain vs. roller displacement response is intrinsically independent of the bending stiffness of the specimen. For a given size specimen, the surface strain vs. roller displacement relationship for the four-point bend fixture employed is as follows:

$$\varepsilon_x = \frac{3\,c}{\ell_o\,(\ell_o + 3\,\ell_i)}\,\delta\,, \tag{5.7}$$

where ε_x is the longitudinal surface strain (top or bottom), c is the half thickness of the specimen, δ is the relative roller displacement, and ℓ_o and ℓ_i are inner and outer roller spans, defined in Figure 5.24. For scaled specimens, both c and the length measurements ℓ_o and ℓ_i, are scaled, leading to a factor of $1/n$ in the coefficient of δ above. This indicates that if $\Delta = \delta/n$ were employed, the response would be independent of size also. This re-

sponse is not dependent on the stiffness, but does assume that the material properties do not vary as a function of position along the beam. Deviation from the predicted strains would therefore not strictly indicate non-linear properties, but rather a change in properties over a portion of the specimen. The strain/deflection response itself will be non-linear, due to the fixture geometry and significant deflections.

Figure 5.25 shows a typical strain vs. scaled roller displacement response, along with the strains predicted by the numerical simulation. Note that the experimental response diverges significantly from that predicted by the model assuming uniform elastic material properties. In addition, the deviation from the prediction is not symmetric, which results in a shift of the neutral axis away from the center of the specimen as the loading proceeds.

Figures 5.26-5.28 show the strain/deflection plots for Lay-ups ***B***, ***C*** and ***D***, along with numerical predictions assuming uniform, linear properties, and negligible friction. These plots consist of five curves each, representing typical load/strain curves for each specimen size and scaling type. By plotting both the average strain $(\varepsilon_x^t + \varepsilon_x^b)/2$, and the deviation from the average strain $(\varepsilon_x^t - \varepsilon_x^b)/2$, it can be seen both how different the top and bottom strains are, and how much the response has diverged from the case of uniform properties.

It was not possible to capture the response all the way to specimen failure, as the strain gages failed before that point. The cause of the gage failures seemed to be surface damage propagating in the specimen, consisting of either transverse cracking of the 45° plies in Lay-up ***B*** and ***D*** specimens, or delamination and buckling of the compressive 0° plies in Lay-up ***C*** specimens.

Both Lay-ups ***B*** and ***D*** showed very consistent strain/deflection plots. Specimens of each size and scaling method displayed virtually identical response. The responses showed the

same initial slope, the same point of deviation from the uniform properties prediction, and continued to coincide in the region of non-uniform properties. Specimens of Lay-up ***C*** showed similar trends. However, the ***Cds*** specimens did not lie on the same curve as the others of its lay-up, with variations in strain ranging as high as 13% for a given value of Δ. This indicates some difference in the way the ***Cds*** coupons responded to load.

However, in all cases, there was a significant shift of the neutral axis of the coupons as load was applied. Although the isotropic materials tested also showed a shift in the neutral axis upon loading, the composite specimens showed a much more pronounced effect. This can be seen in Figure 5.29, which shows the response of a Lay-up ***B*** specimen along with the response of the PMMA isotropic specimen.

Lay-up ***B*** showed the greatest shift in the neutral axis, whereas Lay-ups ***C*** and ***D*** showed similar magnitudes in neutral axis shift. Lay-up ***D*** showed the greatest deviation from the uniform properties prediction. Lay-up ***C*** showed very little deviation from the uniform properties prediction.

5.4 Damage Processes

Deviation in both load/deflection response and deflection/strain response, from predictions based on uniform linear elastic material properties, were expected to be due to the initiation and propagation of damage in the specimens, as was the case in the tensile work. This damage was monitored using non-destructive techniques outlined before, and the point of initiation of various failure modes was compared among different scaled sizes of each specimen type. First ply failure was missed for three specimen types. These were the ***Bds***, ***Cdp*** and ***Ddp*** specimens

Since strain gages were not able to capture the entire response up until failure, Δ was used to define points of initiation of damage. The relationship between Δ and the specimens' surface strains, while not linear, is still unique regardless of specimen size.

Comparison of radiographs, and micrographs taken of polished specimen edges showed that some transply cracks were fine enough that they did not appear on the radiographs. This was not true of the tensile scaling work, where all cracks viewed in the micrographs also appeared on the radiographs.

5.4.1 Lay-up B [45/-45/0/90]ns and [45n/-45n/0n/90n]s

In all sizes, the first damage mode was matrix cracking in the outermost tensile 90° plies while the load/deflection response was still in the range of linear material properties. With continued loading, cracking continued in the outer 90° tensile plies. These 90° cracks were normal to the major axis of the specimen between the inner rollers of the loading fixture, confirming the lack of shear stresses in the gage section of the specimen. Beyond the inner rollers, the cracks were at an oblique angle indicating the presence of shear stresses as, expected based upon beam theory.

Table 5.4 presents the deflection at the onset of cracking in these specimens. Figure 5.30 shows the corresponding normalized deflections corrected for the strains in the 90° ply. In sublaminate-level scaled specimens, the outer 90° ply lay in a relative location that was closer to the surface than the ply-level scaled specimens. Since the strain distribution is linear (valid for small strains, as was the case here), finding the relative strain involved no more than a geometric correction for the ply's relative position in the laminate. This is illustrated in Figure 5.31. Δ^* in Figure 5.30 is simply h*/h Δ, and represents an effective strain in the 90° ply.

From Kellas and Morton [6], and from the tensile part of this work, it was expected that the first ply failure strain of ply-level scaled specimens would decrease, and that the ply failure strain of sublaminate-level scaled specimens would increase, with increased specimen size. This is indeed the case for Lay-up ***B*** specimens.

Damage that occurred in Lay-up ***B*** specimens subsequent to the outer 90° cracking depended on the specimen size and method of scaling employed. Figures 5.32-5.36 show typical load/deflection curves from Lay-up ***B*** specimens, showing damage modes and their occurrences.

Ba Specimens

At some point in the loading of ***a*** size specimens, some of the 90° cracks extend into the adjacent +45° plies. Figure 5.32 depicts the failure process in the ***Ba*** specimens, correlated to a load/deflection plot. These +45° plies were confined to a region within about 1 mm from the specimen edges. Subsequently, delaminations initiated in the outer 90° tensile plies. These delamination cracks tended to follow along the 0°/90° interface, with penetrations into the 90° ply. Final failure was by fiber fracture in the 0° plies.

Bbp Specimens

Damage in the size ***b*** ply-level scaled specimens initiated in much the same manner as the ***Ba*** specimens. Cracking in the outermost 90° tensile plies was followed by propagation of some of the 90° cracks into the adjacent +45° plies (see Figure 5.33). As with the ***Ba*** specimens, the +45° cracks did not propagate through the specimen width, but were confined to the specimen edges.

As loading continued, delamination in the outermost tensile 90° ply initiated and propagated. At some point, cracks in the tensile surface +45° plies propagated across the full

width of the specimen, followed in each instance by a crack (confined to a few mm from the edge) in the adjacent -45° ply. Final failure was by fiber fracture in the 0° plies.

Bdp Specimens

These specimens followed damage modes in the ***Bbp*** specimens with two additions. The cracks in the tensile surface plies propagated into delaminations at the outermost tensile ±45° interface. As the delamination grew (see Figure 5.34), additional cracks occurred in the -45° plies. The second addition is the presence of delaminations at the outermost tensile -45°/0° interface (see Figure 5.34). Note that even though cracks already existed in the -45° plies, the -45° crack that initiated the delamination did not follow any of these. Again, final failure was by fiber fracture on the tensile side.

Bbs Specimens

The size ***b*** sublaminate-level scaled specimens failed in much the same way as the size ***a*** specimens. The only difference was that there were additional 90° plies that could crack before ultimate failure. Figure 5.35 shows the failure process in these specimens.

Bds Specimens

The largest size sublaminate-level specimens experienced 90° tensile cracking, as other sizes did, however, the delamination in the outer 90° ply was delayed considerably. As the loading continued, cracks in the outermost 90° tensile ply continued, followed by cracking in the second and third 90° tensile plies (see Figure 5.36). Not until the load increased to over 90% of the failure load did 90° delaminations appear. No +45° cracks were detected before final failure of the specimen by fiber fracture in the 0° plies.

5.4.2 Lay-up C [0/90/0/90]ns and [0n/90n/0n/90n]s

The first damage mode observed in Lay-up ***C*** specimens was 90° matrix cracking. Table 5.4 gives the deflection of each specimen type and size at the onset of 90° cracking. Figure 5.37 shows the strain-corrected normalized deflections in the outer 90° ply at damage onset. Again, in sublaminate-level scaled specimens, the outer 90° ply lay in a relative location that was closer to the surface than the ply-level scaled specimens, so ratios of relative position were employed to account for the strain in the desired ply for a given normalized displacement Δ (similar to Figure 5.31). Although the initiation of damage in the size ***c*** ply-level specimens was not captured, it can nevertheless be seen that both the sublaminate-level and ply-level scaling methods leads to a decrease in the initiation of 90° cracking.

The material properties of the specimens remained linear until damage began to propagate in the 90° plies. Cracking continued as load was increased, and in larger sublaminate-level specimens, 90° cracks occurred several plies deep in the tensile portion of the specimen. As a result, the response began to deviate from linearity.

Lay-up ***C*** specimens showed signs of local crushing on the tensile side under the outer rollers of the fixture, and on the compressive side under the inner rollers. As mentioned before, ultimate tensile-side failure of the specimens was preceded by buckling and delamination of the compressive surface 0° plies between the inner two fixture rollers, causing a significant drop in load. Figure 5.5 shows the load/deflection response of the ply-level scaled specimens showing the linear predictions for both an undamaged specimen, and a specimen whose compressive surface ply has failed. This was done by assigning the outer compressive 0° ply zero stiffness in a lamination theory calculation, and finding the reduction in bending stiffness. Note that after the drop in load associated with the buckling of the

compressive plies, the load/deflection responses of these specimens coincide with the linear prediction using properties that simulate buckled surface plies.

After this drop in load associated with buckling of the compressive surface plies, the specimens continued to take load. Final failure was by fiber fracture at the tensile surface.

5.4.3 Lay-up D [45/-45/45/-45]ns and [45n/-45n/45n/-45n]s

In all cases, first ply failure was experienced as a single crack in the tensile surface +45° ply. Table 5.4 gives the deflection at the onset of damage. Since it was the surface ply in all cases, no correction was needed in order to compare normalized failure deflections, as in the other two lay-ups. Figure 5.38 gives the normalized damage onset deflections.

While Lay-ups ***B*** and ***C*** both showed linear material response until damage onset, Lay-up ***D*** specimens deviated dramatically from the linear prediction before any damage (except in the ***Ddp*** specimens) could be detected by microscope or X-ray. Specimens loaded well into the non-linear region of the load/deflection response sustained permanent deformation upon unloading, but still did not show any signs of matrix cracks. All specimens, except the ***Ddp*** specimens, underwent basically the same damage development, although the ***Dbp*** specimens underwent each damage mode earlier in its response. ***Ddp*** specimens delaminated at the outermost ±45° interface just prior to 2 mm normalized deflection. This is the reason that the response diverges from the response of the other specimens in Figure 5.6.

Figure 5.39 shows the type of damage sustained by the Lay-up ***D*** specimens. The first damage that could be detected was a matrix crack in the tensile surface +45° ply. This was followed by a short crack running along the ±45° interface that then turned and ran through the -45° ply. The delamination then began to grow along the outer ±45° interface, with cracks in the adjacent -45° ply forming as the crack extended. Subsequently, cracks began

to form in deeper and deeper ±45° plies. The specimens never failed catastrophically, but kept deforming and cracking in successively deeper ±45° plies. At very high levels of displacement, the cracking went beyond the midplane of the specimens and into the plies below. One 16-ply specimen that was loaded until it physically popped out of the fixture contained damage down to the 11^{th} ply.

One difference between the ply-level scaled specimens and the sublaminate-level specimens was that the ply-level specimens tended to form larger areas of delamination (Figure 5.40) that ran across the width of the specimen, whereas the sublaminate-level specimens formed delaminations that were confined to the edges of the specimen.

5.5 Ultimate Load and Deflection

Tables 5.2 and 5.3 present the ultimate load and deflection for the scaled flexure specimens. From the tensile portion of this work, and previous research done by Kellas and Morton [6], it was expected that those specimens failing in tension would follow the trends of ply- and sublaminate-level scaling. That is, ply-level specimens would show a decrease in normalized ultimate load and deflection, and the sublaminate-level coupons would exhibit an increase in ultimate load and deflection. While the ply-level specimens followed the trend, the sublaminate-level specimens did not.

5.5.1 Lay-up B [45/-45/0/90]ns and [45n/-45n/0n/90n]s

Lay-up ***B*** specimens were the only ones where the ply that was critical to failure (in this case, the outermost 0° ply) was not a surface ply. This means that the results for ultimate load/deflection have to be corrected for the strains present in the 0° ply. Again, as in section 5.4.1, a simple geometric correction that accounts for the relative position of the 0° plies in the laminate was used. Figures 5.12 and 5.15 show the strain-corrected scaled normalized

ultimate load and deflections. The ply-level scaled specimens showed a marked decrease in ultimate load and deflection, while the sublaminate-level specimens showed no signs of any scaling effect.

5.5.2 Lay-up C [0/90/0/90]ns and [0n/90n/0n/90n]s

Figures 5.13 and 5.16 show the scaled ultimate load and deflections for Lay-up ***C*** specimens. Like Lay-up ***B*** specimens, the ply-level scaled specimens showed a marked decrease in ultimate load and deflection, but the sublaminate-level specimens also exhibited a decrease in ultimate load and deflection. However, recall that the failure of these specimens was different than Lay-up ***B*** specimens. The compressive surface plies buckled between the inner rollers of the fixture, causing premature failure in these specimens. Data plotted in Figures 5.13 and 5.16 are for this first drop in load caused by fiber buckling and delamination.

It was decided after most specimens had already been loaded to failure that the crushing of the 0° fibers on the surface of the specimens led to the buckling of the plies. Therefore, two additional ***Ca*** specimens, and one each of ***Cb*** and ***Cd*** specimens were tested using shims between the specimen and rollers, as in Figure 5.41. This padding was sufficient to suppress buckling, and the specimens failed by fiber fracture on the tensile surface. Figure 5.42 shows the load/deflection curve of a ***Ca*** specimen with the shims compared to a typical ***Ca*** curve without the shim material.

0.25 mm paper shims were used on the ***Ca*** specimens. ***Cb*** and ***Cd*** specimens incorporated 3 mm thick polycarbonate shims between the specimen and the rollers, rather than the paper ones. The reason was simply to supply additional assurance that the rollers would not cause fiber damage on the compressive side. No unfailed ***Cdp*** specimen was available. Figure 5.43 shows the scaled load/deflection response of the Lay-up ***C*** specimens using

the shims, and Figure 5.44 presents the ultimate normalized load. Averages for failure load and deflection could not be calculated, as there were not enough specimens tested. Although the ***Ca***, ***Cbp*** and ***Cbs*** specimens cannot be said to be statistically different in their ultimate failure, the ***Cds*** specimen appears to have failed well below the failure load and deflection of the other specimens.

5.5.3 Lay-up D [45/-45/45/-45]ns and [45n/-45n/45n/-45n]s

Lay-up ***D*** specimens did not fail catastrophically. They simply continued to bend. Therefore, the ultimate deflection was taken to be the deflection at which the load peaked. Figures 5.14 and 5.17 show the ultimate load and deflections of scaled specimens. Only the ply-level scaled specimens showed any scale effect in the load/deflection plots, and they suffered dramatic reductions in their ultimate load and deflection.

6. DISCUSSION (TENSION)

It can be seen that, in general, the degree to which strength scaling effects are present in the AS4/3502 specimens depends, at least in part, on the relative amount of 0° fibers present in the lay-up. Although the first ply failure stress of the crossply Lay-up ***C*** specimens increased notably as the scaled size was increased, no dependence of strength on specimen size was manifest because the 90° plies carried only a small portion of the total load. This can be seen by observing the stress/strain plots (Figure 4.4) of the crossply laminates. No notable change in stiffness is associated with failure of the 90° plies, hence the strain energy is being stored almost entirely in the 0° plies.

In Lay-up ***A*** and AS4/3502 Lay-up ***B*** specimens, the non-linear effects were quite pronounced. On the other hand, the Lay-up ***C*** specimens, in which the strain energy was stored almost entirely in the 0° fibers, and APC-2 Lay-up ***B*** specimens, in which matrix damage was vastly reduced, showed no size effects on the stress/strain behavior. This indicates that scaling effects depend upon the strain energy released due to damage processes, and how that energy release changes as the specimens are increased in size. Therefore, the nature of the matrix damage occurring in a given lay-up was observed and insights relative to size effects were sought.

The character of the non-linearities in the stress/strain response proved to be repeatable for specimens of the same size and lay-up. It was interesting, therefore, to note the correlation between certain identifiable features on the stress/strain curves and the damage developing in the coupon at that point.

Also presented is a brief discussion of the strain energy release rate model proposed by O'Brien [10]. Originally, Lay-up ***A*** was chosen for this study to investigate scaling effects in delamination. However, as has been noted previously, the stress/strain response of Lay-up ***A*** specimens was already non-linear before delaminations formed. The delamination model was therefore applied to the quasi-isotropic Lay-up ***B*** specimens.

6.1 Stress/Strain Response

If no scaling effects were present, the stress/strain responses for all sizes of a given laminate would be identical. However, Lay-up ***A*** and AS4/3502 Lay-up ***B*** specimens showed significant scaling effects in stress/strain response. Differences with increased size included variations in strength and strain to failure, location of the non-linear knee and locations of other identifiable features of the stress/strain response.

6.1.1 Lay-up A [30/-30/90/90]ns

Figure 4.2 shows the response of 3-D scaled batch *I* specimens of Lay-up ***A***. The plots indicate a steady increase in ultimate stress, strain to failure and the non-linear knee stress as the size of the specimen increases from n=1 to 4 . They also showed a very regular trend in the change of the stress/strain curves. All curves exhibit the same initial modulus, and although the general shape of the curve is the same for all sizes, the non-linear effects are delayed in the larger specimens. The similarity in stress/strain curve shape indicates that the same type of damage is occurring in the three sizes of specimen, while the delay in non-lin-

earities shows that the initiation and propagation of damage occurs at increasingly higher applied stress and strain levels for the larger specimens.

6.1.2 Lay-up B [45/-45/0/90]ns

Figure 4.3 shows the response of 3-D scaled AS4/3502 Lay-up ***B*** specimens. Again, as the specimen size was increased, the general trend was toward higher ultimate stress and delay in the stress at which non-linearity occurs. 8-ply specimens showed a behavior completely different from the other specimen thicknesses. Note in Figure 4.3 that the three largest specimens were almost linear to failure, whereas the ***Ba-8*** specimens exhibited highly non-linear response. This change in the degree of non-linear effects is related to the manner in which the thickness was increased using sublaminate-level scaling. The technique of repeating sublaminate groups affects the way that damage is propagated in the laminate, specifically with regard to delamination, as will be discussed later. This dependence of the stress/strain response on damage propagation can also be seen by observing the response of the APC-2 Lay-up ***B*** specimens. No delamination, and reduced 90° ply cracking was present in these specimens. As a result, the response was linear to failure, and was independent of the size of the specimen.

Recall also that the response of the APC-2 specimens varied as a function of its position in the panel. Cantwell *et al.* [16] have reported that the properties of APC-2 composites can vary significantly with different cooling rates. Differences in cooling rates lead to variations in the degree of crystalinity in the semi-crystalline PEEK matrix material. In the fabrication process, it is likely that the edges of the panel cooled more quickly than the center. This non-uniform cooling rate would then lead to non-uniformities in the laminate mechanical properties throughout the panel, as was found experimentally.

6.1.3 Lay-up C [90/0/90/0]ns

Like the APC-2 Lay-up ***B*** specimens, Lay-up ***C*** specimens showed no size effects (Figure 4.4). Reasons for this, and the linear stress/strain response will be discussed in the next section.

6.2 Damage Processes

Kellas and Morton [6] observed that for the larger sizes of AS4/3502 ply-level scaled laminates, transverse matrix cracks existed in cut, but unloaded coupons. No such transverse cracks were observed in any of the sublaminate-level scaled specimens. This seems to support their conclusion that ply thickness is an important scaling parameter controlling damage propagation [6]. However, ply thickness alone cannot fully account for scaling phenomena, since it was observed that the first ply failure was delayed in larger sublaminate-scaled specimens. All sublaminate-scaled specimens had the same ply thickness. Kellas and Morton [4, 6] suggested, further, that the manner in which a crack or flaw in a given ply is constrained by neighboring plies may also contribute to scaling effects.

As mentioned before, Flaggs and Kural [18] used an energy based model for the transverse cracking of a 90° ply constrained by 0° plies, from which Equation 5.6 was derived [4]. The model can also be used to yield Equation 6.1 [20], where b^c and E^c are the thickness and stiffness, respectively, of the constraining plies; and t and E_2 are the thickness and stiffness of the 90° plies, respectively. The subscripts $_p$ and $_m$ refer to prototype and model sizes, respectively.

$$\frac{\varepsilon_p^{cr.}}{\varepsilon_m^{cr.}} = \left[\frac{b_p^c E_p^c \left[b_m^c E_m^c + tE_2 \right]}{b_m^c E_m^c \left[b_p^c E_p^c + tE_2 \right]} \right]^{1/4} . \tag{6.1}$$

In order to investigate the cracking of 90° plies in sublaminate-level scaling, Equation 6.1 can be simplified to Equation 6.2, where first ply failure occurs in the linear response range. The constraining plies are all plies in the laminate except the ply under investigation.

$$\frac{\varepsilon_p^{cr.}}{\varepsilon_{8-ply}^{cr.}} = \frac{\sigma_p^{cr.}}{\sigma_{8-ply}^{cr.}} = \left[\frac{1 + \left[\frac{E_2}{6E_{8-ply}^c} \right]}{1 + \left[\frac{E_2}{(8n-2)E_p^c} \right]} \right]^{1/4} . \tag{6.2}$$

Flaggs and Kural [18] used this energy based model to investigate damage in $[0°/90°_n]_s$ laminates, with some success in modeling the reduction (with increased values of n) in the strain at which damage initiated. Kellas and Morton [6] also used the model (Equation 5.6) in order to predict the reduction in strength as ply-level scaled specimens increased in size.

Equation 6.2 predicts the scaling effect in sublaminate-level scaling to be negligible. The maximum value of Equation 6.2, in the case of sublaminate-level scaling, is approached as n goes to infinity. In this case, the denominator goes to unity, and the equation reduces to the numerator, all of whose values are constant with respect to specimen size. With typical values (where $E_2 << E_{8\text{-}ply}$), the numerator is quite close to unity, and hence predicts minimal scaling effect.

However, other fracture mechanics models can be useful for describing the sequence of damage in a laminate. Consider a homogeneous isotropic material under tensile loading. The mode I stress intensity factor, k_1, is given by Equation 6.3, where σ is the applied load, and $F(a/W)$ is a geometric function of a and W called the compliance function.

$$k_1 = F\left(\frac{a}{W}\right) \sigma \sqrt{\pi a} . \tag{6.3}$$

Two cases are presented in Figure 6.1. Case (a) represents an edge crack in a plate. Case (b) represents a central crack in an otherwise identical plate. In both of these cases, the crack half length is a. In the case where a/W tends to zero, it is well known that for cases (a) and (b), respectively,

$$k_1 \approx 1.12\ \sigma\sqrt{\pi a}\ , \text{ and } k_1 = \sigma\sqrt{\pi a}\ . \tag{6.4}$$

This indicates that an edge crack will propagate before a central crack. In a similar manner, all other things being equal, a surface ply of a given orientation will crack before a central block of two plies of the same orientation, as was noted by Kellas and Morton [4].

Finally, Kellas and Morton [6] also noted that for fiber dominated Lay-ups scaled at the ply-level, the ultimate failure mode depended on the size of the specimen. It was found that for the sublaminate-level scaling, this was not the case with Lay-ups ***B*** and ***C***.

6.2.1 Lay-up A [30/-30/90/90]ns

Because there are no 0° plies in the Lay-up ***A*** specimens, the 90° plies contribute significantly to the laminate stiffness. As the 90° plies lost their integrity through increasing transverse cracking, the laminate stiffness changed. To determine how much cracking of the 90° plies could affect the laminate stiffness, CLT was employed to model a damaged laminate. Using a $[+30/-30/90_2]_{ns}$ stacking sequence, the stiffness transverse to the fibers (E_{22}) in the 90° plies was assigned a value of zero, while the other ply stiffnesses remained unchanged. Obviously, this is an extreme case, and in practice, delamination initiated before transverse cracking reached this point. It was found that this led to a 10% reduction in laminate stiffness, thus indicating that transverse cracking in the 90° plies is one factor that contributed to the reduction in laminate stiffness in Lay-up ***A***.

The second factor contributing to the non-linear stress/strain response was the formation of delaminations. In the larger sizes, the delamination always occurred at the outermost -30°/90° interfaces. In effect, the ±30° plies on the outer surfaces of the specimen were lost as the delamination propagated. The ±30° plies on both surfaces, therefore, can be thought of as "weak" plies, since they lose their structural integrity before the other plies in the laminate. This produces a scaling effect, since the relative effect of losing the four surface plies would be diminished as the thickness is scaled, and more ±30° plies are available to carry the load. The **Aa-8** specimens failed shortly after the ±30° plies were delaminated.

This leads to a difference in the way the specimen fails. The delamination of the **Aa-8** specimens allows separation of the coupon without fiber fracture. Larger specimens contained additional ±30° plies, which resulted in the ability to sustain a more extensive delamination lengthwise, but required that fibers fracture in order to break the coupon. Thus, only the larger specimens exhibited fiber fracture in the ultimate failure mode.

Finally, as noted before, the first plies to fail in the Lay-up *A* specimens were always the outermost 90° plies. Since there are no surface 90° plies (which would fail first according to reasoning associated with Equation 6.4), Equation 6.1 leads to the conclusion that the thicker center block plies would fail first. Recall, however, that cracks in the outer 90° plies were at some angle other than perpendicular to the applied loading. Hence, these plies were experiencing some additional stresses other than would be predicted by CLT. These stresses result from interlaminar shear stresses at the free edges, caused by the shear constraint of the adjacent ±30° plies. The surface angle-plies, being less constrained than interior angle-plies, would give rise to higher interlaminar shear stresses at the free edge. It is felt that these additional stresses would account for the location of the first ply failure being in the outermost plies, rather than the central blocked plies, in spite of the fracture mechan-

ics reasoning presented earlier. Recall that these arguments were based on the assumption that all plies were orthotropic in the global reference frame.

6.2.2 Lay-up B [45/-45/0/90]ns

First ply failure in all sizes of Lay-up ***B*** specimens was in the center block of 90° plies, as expected based upon the fracture mechanics arguments presented. The outer 90° plies are separated from the ±45° plies by 0° plies, so they do not see the same shear constraint that caused the Lay-up ***A*** specimens to fail there first.

The effect of the delamination process on the stress/strain curve was to reduce the stiffness of the laminate by decoupling its constituent plies. This reduced stiffness produced higher laminate strains for a given load. Since there are 0° plies present in the laminate, the failure is fiber strain dominated. Note in Figure 4.26 that the average strain to failure of the scaled specimens remains roughly constant. One effect of the delamination, then, is to precipitate early failure of the specimen by decreasing the stiffness, and thereby reducing the average stress required to reach the failure strain of the fibers. The degree to which a specimen delaminates will then determine the extent of the failure stress reduction.

This is an important observation, since the propensity of a sublaminate-scaled Lay-up ***B*** specimen to delaminate is reduced with increased size. The change in the extent of delamination is an unavoidable result of the method employed in scaling the laminate thickness by repeating sublaminate blocks, as will be discussed in the next section.

Another way to change the nature of delamination is to change the toughness of the matrix material. It was anticipated that the higher toughness of PEEK matrix material would significantly reduce the damage propagated in the APC-2 Lay-up ***B*** specimens. Still, upon examination of the radiographs of the APC-2 specimens (see Figure 4.24), there was evi-

dence of cracking in both the 90° plies, and the ±45° plies. In addition, there appeared to be delaminations at the specimen edges, although the regions of delamination lacked the sharp clarity at their boundary that the AS4/3502 delaminations exhibited. However, when the specimen edges were viewed under the microscope, no delaminations were present, and no cracking of the 45° plies was present. Furthermore, the cracking in the 90° plies was not as extensive as appeared in the radiographs. Therefore, some other mechanism was responsible for the observations on the radiographs. Perhaps there was fiber/matrix debonding that allowed the dye penetrant to be absorbed at the fiber/matrix interface, and the images to be recorded. More research is needed to determine the cause of this phenomenon.

The PEEK resin system did prove to render a composite with significantly higher toughness (as compared to the AS4/3502), which yielded much less damage in the Lay-up *B* APC-2 specimens. The lack of delamination, and significantly reduced cracking in the 90° plies produced the linear stress/strain response of the APC-2 specimens, which, because the failure was fiber strain dominated, resulted in a lack of strength scaling effects.

6.2.3 Lay-up C [90/0/90/0]ns

Figure 4.4 shows the typical stress/strain response of the specimens of Lay-up ***C***. The response was nearly linear to failure, and there was no indication of any influence of size on the strength. The first ply failure occurred at a higher stress for the full scale case (Figure 4.14), but this did not affect the global stress/strain response, which is almost entirely controlled by the 0° fibers.

First ply failure occurred in the surface plies, which is consistent with the arguments associated with equations 6.4. The sublaminate-scaled crossply laminates also displayed a local failure across the width of the specimens, as opposed to the longitudinal splitting of the 0° plies noted by Kellas and Morton [6] in similar ply-level scaled specimens.

6.3 *Delamination*

O'Brien [10] has used a fracture mechanics approach to study delamination and has proposed a test specimen for use in determining an effective combined mode fracture toughness G_c. His analysis proposed that G_c is a material property (independent of stacking sequence), which can be determined from the ply properties, and a small number of tests. Once obtained for a given material, G_c can then be used to predict the onset of delamination in other stacking sequences. O'Brien's equation is

$$G_c = \frac{1}{2}\varepsilon_c^2 t\left(E_{Lam} - E^*\right), \tag{6.5}$$

where ε_c is the critical strain at the onset of delamination, t is the thickness of the laminate, E_{Lam} is the stiffness of the undamaged laminate, and E^* is the stiffness of a totally delaminated specimen. As mentioned before, the stress/strain response is elastic in nature. It is assumed that deviation from linearity is simply a reflection of the changing elastic stiffness due to progressive decoupling of the sublaminates produced by the delamination. If the specimen were unloaded at any point along the stress/strain curve, the response would trace a linear path back to zero permanent deformation (Figure 6.2). If then loaded again, the response of the specimen would return along this same linear path of reduced modulus, until the stress/strain reached the point at which damage could again be propagated. As the delamination propagates all the way to the center of the specimen, the decoupling is completed. The slope of the line passing through the origin, and tangent to this final portion of the curve yields E^*.

O'Brien proposed that E^* can also be found using CLT by modeling the delaminated specimen as three separate sublaminates as shown in Figure 6.3, and finding the average stiffness using a rule of mixtures approach [10]. The critical strain ε_c is the strain at which

delamination starts. As noted above, this strain coincides with the first knee in the stress/strain response, and is determined experimentally by testing a small number of delamination specimens.

O'Brien originally proposed a stacking sequence similar to that of Lay-up ***A*** for his delamination studies, namely $[\pm 30/\pm 30/90/\overline{90}]_S$. Because of the additional set of ±30° plies, the interlaminar shear and normal stresses are higher in this laminate than in Lay-up ***A*** in this study, causing his specimens to delaminate more readily. Consequently, O'Brien observed general edge delamination, which was not the case with the ***Aa-8*** and ***Ab-8*** specimens discussed previously.

In a more recent work, O'Brien [13] proposed the use of a $[\pm 35/0/90]_S$ as a standard test specimen. The performance of this Lay-up is quite similar to the quasi-isotropic specimens of Lay-up ***B***. Since the data from the Lay-up ***B*** specimens were available, it was decided that a closer examination of O'Brien's model might prove useful. Figure 6.4 shows a typical ***Ba-8*** stress/strain plot, along with the average experimental values for E_{Lam}, E^* and the critical strain, ε_c.

The ply property data for AS4/3502 graphite/epoxy are given in Table 6.1. Values for both E_{Lam} and E^* measured from the stress/strain curves of the baseline *Ba-8* specimens compared very well with those predicted by CLT. These computed values are also included in Figure 6.4.

After G_c was found using Equation 6.5, ε_c was predicted for the different sizes of Lay-up ***B*** by finding the new E^* for each size, and inverting Equation 6.5 as shown in Equation 6.6.

$$\varepsilon_c = \sqrt{\frac{2\,G_c}{t\left(E_{Lam} - E^*\right)}} \tag{6.6}$$

Figure 6.5 shows the model's predictions of ε_c for the four 3-D scaled Laminate ***B*** sizes, along with the observed experimental data. G_c was found from the ***Ba-8*** specimens, and was then used in the prediction of the other sizes. Although the model predicts ε_c well for the ***Bb-16*** specimens, the prediction is off for the larger sizes. This is because the larger specimens undergo more extensive transverse cracking in the 90° plies prior to delamination. O'Brien's model neglects strain energy released due to transverse cracking, and showed this to be valid [10] for specimens that did not undergo extensive cracking prior to delamination since negligible strain energy is released. This is evidenced by the linear stress/strain response to the point of delamination in Figure 6.6(a). However, because the delamination onset stress for the larger specimens was higher, the transverse cracking could progress to a greater extent before delamination initiated. In fact, the larger specimens underwent non-linearities in their stress/strain response before delamination onset, as seen in Figure 6.6(b).

CLT was used to determine the loss of stiffness due to damage in the 90° plies, as described in section 6.2.1. It was determined that the laminate stiffness could be reduced by 4% if damage was extensive. Figure 6.6(b) shows that indeed the stiffness was reduced, and hence appreciable strain energy was released prior to delamination. Therefore, less energy was available to drive a delamination crack than was predicted by O'Brien's model, and delamination was delayed. It is for this reason that the experimental data do not agree with predictions based on O'Brien's approach.

As mentioned before, as n increased, the extent of delamination of the specimen became less. While the 8-ply specimens delaminated completely before global failure, the larger specimens exhibited reduced levels of delamination. Two of the 32-ply specimens had not developed delaminations along their entire edges before they failed catastrophically. In all

32-ply specimens, the effect of delamination on laminate stiffness was very small, as indicated by CLT where E^* approached E_{Lam}. This indicates that it becomes less energetically favorable for delamination to occur as n increases using sublaminate-level scaling. Hence, the stress/strain response tends toward linearity, as observed experimentally.

6.4 Ultimate Stress and Strain

The main goal of this study was to understand the nature of the changes in the ultimate stress and strain in scaled composite laminates, and to determine the reasons behind these changes. Since the ultimate failure depended on the state of the damage introduced into the specimen, differences in damage processes for the different sizes of specimen were observed.

The data in Tables 4.12-4.15 show that differences in laminate strength due to specimen size were less pronounced in laminates with 0° fibers. This indicates that for sublaminate-level scaling, the size differences are caused by damage states in the angle-ply and 90° laminae. The global response of the laminate is then governed by how the 0° fibers can compensate for the changes brought about by the damage.

As an example, in Lay-up ***C***, size differences in the first ply failure stresses of 90° plies were definitely present, but the global stress/strain responses of scaled Lay-up ***C*** specimens showed no net effect because the load is carried almost exclusively by the 0° plies. Ultimate failure of the laminate is controlled by fiber fractures in the 0° plies which do not appear to be affected by specimen size.

In all cases, the scaled strength seemed to approach some maximum beyond which specimen strength became insensitive to scaled size. In the case where 0° plies made up one quarter of the plies in the laminate, such as the quasi-isotropic Lay-up ***B***, the ultimate

strength of an 8-ply laminate was about 80% the full scale strength, and a 16-ply had essentially reached full scale strength for the lay-up. Hence, for most structural applications, which contain at least 25% 0° fibers, the testing of a 16-ply laminate should yield results close to the limiting value for full scale structures.

In fact, the delamination of a laminate can be reduced or eliminated by reordering the stacking sequence. Herakovich [17] noted that the $[\pm 45/0/90]_{ns}$ laminate is the worst case arrangement of the twelve unique permutations of 8-ply quasi-isotropic stacking sequences. If the stacking sequence were changed to minimize interlaminar stresses, delamination would be suppressed, and the response would be more linear. In this case, the scaling effects would also be minimized.

The reason that the strength of Lay-ups ***A*** and ***B*** reached maximum values as the size of specimens increased lies in the way in which damage occurred in the laminates. When matrix damage was reduced, as in the case of the APC-2 specimens, or when the fibers dominated the response, as in the case of Lay-up ***C***, strength scaling effects were not present.

6.4.1 Lay-up A [30/-30/90/90]ns

In Lay-up ***A*** specimens, significant non-linearity existed in the stress/strain curve before delamination onset. This was because the 90° plies contribute significantly to the laminate stiffness. As the 90° plies failed by transverse cracking, the stiffness of the laminate decreased. It might be expected that the larger specimens would have the same stress/strain response as the smaller specimens, since they have the same relative amount of 90° plies, but the non-linear knee was delayed in the larger specimens. This indicates that damage in the 90° plies was delayed in the larger specimens, due to different ply constraint.

In addition, the surface ±30° plies delaminated in all specimen sizes. In the process of delamination, these surface plies were damaged enough that their contribution as load bearing plies was greatly reduced. The remaining plies, therefore, were forced to share the added load, increasing the stress in these plies. In the case of the ***Aa-8*** specimens, shortly after one of these areas of delamination started, the specimen failed. However, as n was increased, other ±30° plies were able to take up the load, so the specimens could sustain more extensive delamination before global failure. In the case of the ***Ad-32*** specimens, the weak plies constituted a relatively small portion of the total number of plies.

Hence, not only did a larger Lay-up ***A*** specimen require higher stress to propagate damage in the 90° plies, but larger specimens also contained a relatively smaller percentage of weak plies, resulting in a smaller rise in stress in the other plies when the weak plies failed. The combination of these two effects produced a pronounced strength scaling effect.

6.4.2 Lay-up B [45/-45/0/90]ns

As the thickness of an AS4/3502 Lay-up ***B*** specimen is increased using sublaminate-level scaling, the amount of energy released during delamination is decreased. This is predicted by O'Brien's model [9], where E^* approaches E_{Lam} as the stacking sequence is changed from $[\pm 45/0/90]_S$ to $[\pm 45/0/90]_{4S}$.

As delamination developed, there was a progressive decoupling of the lateral constraint imposed by the 90° plies on the $[45/-45/0]_T$ sublaminate blocks. This decoupling due to delamination, which was more pronounced in the smaller specimens, yielded higher strains for a given load. AS4/3502 Lay-up ***B*** specimens, however, showed only a slight increase in strain to failure as the specimen size increases. This is because the strength response was dominated by the fibers in the 0° plies. When the failure strain of the fibers was reached, failure was precipitated. Therefore, if delamination is retarded, the stress/strain response of

the Lay-up ***B*** specimens will be more linear, as was is the case with the larger AS4/3502 specimens and the APC-2 specimens. In this case, the ultimate strength would not be effected by specimen size.

Finally, the results from the APC-2 test program showed that scaling effects can be eliminated altogether by toughening the matrix material. This is because when the matrix material is toughened, transverse cracks in the 90° plies are reduced, and delamination is eliminated. Since the scaling effects are a result of the initiation and growth of damage in the specimen, then retarding the onset of damage by toughening the matrix, should reduce the scaling effect. As mentioned above, the thinner specimens tend to delaminate more readily than the thicker specimens because of the strain energy that is released upon damage. If, as in the case of APC-2, even the small specimens do not delaminate, then no scaling effect is present.

6.4.3 Lay-up C [90/0/90/0]ns

Lay-up ***C*** specimens showed no strength or strain to failure scaling because the load was carried almost exclusively by the 0° plies. Because the 90° plies are so compliant compared to the 0° plies, only very small stress concentrations result from cracks in the 90° plies. There was also no tendency to delaminate, so the stress/strain response was linear to failure. Hence, the 0° plies controlled the response, and no strength scaling effects were observed.

6.5 Finite Element Model

Finite element analysis was used to find the through-the-thickness edge stresses driving delamination. The 2-D model was chosen in order to avoid the large number of degrees of freedom that a full 3-D model would require. Generalized plane strain elements allowed the

modeling of a cross section of the specimen in the y-z plane, as shown in Figure 3.1, with a prescribed strain in the x-direction. Because the model was only 2-D, a relatively high degree of mesh refinement was possible, with eight elements through the thickness of each ply.

In order to use the generalized plane strain model, the angle plies had to be modeled as orthotropic plies with the lamination theory properties of a symmetric $\pm\theta$ laminate. This incorporated the effect of the Poisson's ratio of the angle plies, but did not allow the modeling of shear/extension coupling. However, the shear behavior does not give rise to edge stresses in the z-direction σ_z. Rather, shear coupling produces out-of-plane shear stresses τ_{xz} near the edge. Hence, the generation of σ_z edge stresses is solely a result of mismatches in the effective Poisson's ratio of the different plies, and can be modeled using the generalized plane strain elements.

In order to check this, a more crude 3-D model was used. Only four elements through the ply thickness were used in order to limit the total number of degrees of freedom. Figure 3.2 shows that the two models are in agreement, with the 2-D model showing smoother stress distribution.

Stresses calculated by the model predicted delamination at the outermost 90° plies for both Lay-ups ***A*** and ***B***. However, the difference between peak stress in the outer 90° ply, and the stress in the central 90° plies in Lay-up ***B*** , was much smaller than the same difference in the Lay-up ***A*** specimens. Recall that the Lay-up ***B*** specimens delaminated in the central 90° block, not the outer 90° plies. Therefore, some other stresses must be present in order to cause the delamination at the central block. Recall also that the specimens contained many cracks in the 90° plies, which were not modeled in the finite element model. Through-the-thickness stresses will result from the cracks in 90° plies. Hence, a way to

calculate the stresses due to the presence of a crack was employed. The two mechanisms of producing σ_z are uncoupled, and can be added linearly.

6.6 Analytical Model

The method used models a crack in the middle ply of a 3-ply laminate (see Figure 3.4). All layers are modeled as orthotropic plies, with the crack located in layer 2. The method is an extension of a model by Vasiliev [11], with the added capability of handling cracks in layers that do not lie on the mid-plane of the specimen. This allows finding the stresses due to a crack in the outer 90° plies of the lay-ups in this work.

When modeling the laminates in this study, the model in effect smears the stiffness of some of the plies in the laminate into a single ply with a given "effective" stiffness. Since all angle plies exist in balanced $\pm\theta$ pairs, this is not a bad assumption.

The stresses found in an n=2 Lay-up ***A*** specimen added to the finite element results to predict delamination in the outer 90° plies (Table 4.20), as observed in the experiments. Stresses calculated in an n=2 Lay-up ***B*** specimen showed the reverse trend. The finite element model calculated higher σ_z stresses in the outer 90° plies by about 17%. With the crack present, the analytical model predicted σ_z stresses to be higher in the central 90° plies by about 6% (see Table 4.20). When added together, the stresses in the undamaged finite element model and the cracked analytical model still predicted σ_z stresses to be slightly higher in the outer 90° plies, by about 11%. However, upon examination of the damage in Lay-up ***B*** specimens just prior to delamination onset, it was noted that the crack spacing in the central 90° block was on the order of 0.2 mm, whereas the crack spacing in the outer 90° plies was on the order of 0.5 mm. Note from Figure 4.29 that this allows interaction of adjacent cracks in the central plies, but not in the outer 90° plies. Stresses from neighboring cracks in the central plies could add together to cause σ_z to be higher in these central plies.

7. DISCUSSION (FLEXURE)

When coupons are loaded in flexure, there is a certain amount of anticlastic curvature associated with the bending. If this curvature is restricted by rollers, the response will be slightly stiffer than if the specimen were allowed to bend free of anticlastic curvature constraint. This curvature effect was assumed to be small in the present work.

In general, the ply-level scaled flexure response was as expected from previous research [4, 6], but the sublaminate-level scaled specimens did not follow trends observed in the tensile portion of this work. No increase in specimen strength in Lay-ups ***B*** and ***D*** was noted with increased sublaminate-level scaled size. It is unlikely that the compressive loading of a portion of the specimens was a major contributor to this lack of strength increase, as Lay-ups ***B*** and ***D*** failed in the tensile plies. Lay-up ***C*** specimens did fail by compressive buckling, but as will be discussed in this chapter, using shims between the rollers and the specimens eliminated compressive buckling.

7.1 Numerical Model

The numerical model was compared to three isotropic materials. These were steel, aluminum and polymethylmethacrylate (PMMA). One of the differences between isotropic

materials and composites is that the bending stiffness of a composite laminate depends upon the stacking sequence, and is completely independent of the longitudinal tensile stiffness. The bending stiffness can be predicted by using some theory, such as Classical Lamination Theory, or some higher-order plate theory, but this prediction is only approximate and is limited by the approximations made in developing the theory. By contrast, the bending stiffness of isotropic materials is equivalent to the extensional stiffness, or Young's modulus.

Hence, the extensional stiffness of the three isotropic materials was found, and along with the specimen and fixture geometry was input into the numerical model. Load/deflection plots were generated using the model, and the results agree quite well with the experimental load/deflection plots until plastic yielding occurred (Figures 5.1-5.3).

This model was then used to find the actual bending stiffnesses of the composite laminates. The shape of the curve agreed very well with the composite specimens as well up to a point where the experimental response diverged from the predicted. It was found that in the cases of Lay-ups ***B*** and ***C***, this divergence was directly associated with damage occurring in the specimens. Lay-up ***D*** specimens did not show cracks in individual plies at the point of divergence from the prediction, indicating that some other form of damage, that could not be detected by the methods employed, was present.

In light of the above, it was found that the model provided a convenient way to determine when damage in a specimen became important to the stiffness of that specimen.

7.2 Load/Deflection Response

As discussed in chapter 5, in order to compare the load/deflection responses of different sized specimens, some sort of normalization method was needed. It was decided to use a

normalization based upon the strain at the specimen surface (See Equations 5.5). This method of normalizing the load/deflection response collapses the response of any scaled size of specimen to the same curve, regardless of stiffness.

For ply-level scaling the normalized ultimate load, ultimate deflection, response curve shape, etc., should be identical if no scaling effect is present, as the strains in each ply or block of plies of a given orientation should be the same for any value of Δ. In general, this was not true for the laminates studied. Hence, there is indeed a scaling effect in ply-level scaled specimens, and the general trend is toward degraded properties as more plies are blocked together. Note in Figures 5.12-5.17 that the model used by Kellas and Morton [6] predicted this drop in ultimate load and deflection, although the degree to which the model fits the data depends upon the stacking sequence. Note in particular Figure 5.38, where the buckling failure mode was eliminated from the Lay-up ***C*** specimens. This dependence on stacking sequence is not modeled by Equation 5.6.

The interpretation for sublaminate-level scaling was not as simple. The normalized load/deflection response should have the same shape as the ply-level scaled specimens, but it is not necessarily true that the normalized ultimate load and deflection should be unaffected if no scale effect were present. Depending upon the critical failure mode and the stacking sequence, the mechanics of the problem may still suggest differences in the normalized load/deflection at which failure occurs in sublaminate-level scaled specimens.

7.2.1 Lay-up B [45/-45/0/90]ns and [45n/-45n/0n/90n]s

All but the ***Bdp*** specimens showed very similar normalized load/deflection response, even in the non-linear properties range. This indicates that similar failure processes were taking place. Final failure occurred at different normalized load and deflection levels, but the failure mechanisms that govern loss of stiffness were very similar.

The ***Bdp*** specimens showed severe non-linearities before any of the others showed any signs of damage. This was a combination of two different effects. The first was the fact that larger ply-level scaled specimens show damage at lower strain levels than smaller ones. Hence, damage began to accumulate early in these specimens. Secondly, there was a damage mode in these specimens that did not occur in the other specimens. This damage mode was delamination at the -45°/0° interface (see Figure 5.29). Large portions of the ±45° blocks on the tensile surface simply delaminated and lost their load carrying capacity. Note that in Figure 5.4, the prediction based on the complete loss of these surface ±45° plies is plotted along with the data. The ***Bdp*** specimens were clearly approaching this case, but did not quite reach it before failure of the 0° fibers.

7.2.2 Lay-up C [0/90/0/90]ns and [0n/90n/0n/90n]s

Lay-up ***C*** should show very little or no scaling effect, based on tensile. Figure 5.5 seems to indicate that there was a pronounced scale effect, but recall that the outer compressive 0° plies buckled before failure of the tensile surface 0° plies. Figure 5.37 shows the scaled responses of Lay-up ***C*** specimens when no compressive buckling took place. Unfortunately, there is no ***Cds*** specimen, and only one or two specimens of each of the other sizes were available. Therefore, it is not known if these normalized load/deflection plots are typical, and there is no way of calculating average load and deflection at failure.

It can be seen, however, that there was very little stiffness loss due to cracking in the 90° plies, as most of the strain energy is stored in the 0° plies. This result is similar to that noted in the tensile work.

Buckling was averted by placing compliant shims between the rollers and the specimen, as in Figure 5.35. These shims distributed the load of the rollers to a wider area on the speci-

men, thus avoiding crushing of the 0° surface ply. As crushing was avoided, no buckling occurred.

7.2.3 Lay-up D [45/-45/45/-45]ns and [45n/-45n/45n/-45n]s

Sublaminate-level scaled Lay-up ***D*** specimens showed no scaling effects at all to very high non-linear strain levels. Ply-level scaled specimens followed what would be expected from previous work by Morton and Kellas [6] (Equation 5.6).

Like the ***Bdp*** specimens, the ***Ddp*** specimens showed a departure from the load/deflection response of the other types of specimen. This early departure was due to the comparably more sever delamination of surface ±45° plies, as seen in Figure 5.34. As this severe delimitation propagated, the surface ±45° plies lost their load carrying capacity, and the stiffness changed significantly.

7.3 Strain Response

It is seen in Figures 5.20-5.22 that there are two independent deviations from ideal uniform elastic response of the beam specimens. One effect is that the top and bottom strains did not remain equal in magnitude, opposite in sign, indicated by the fact that the average strain does not remain zero throughout the response. This shift may be due several factors, one of which could include the addition of compressive axial loading of the specimen. Compressive axial loading is indeed present in the gage section due to differences in the horizontal components (*R* in Figure 5.8) of the applied load at the inner and outer rollers. However, using the numerical model, it was found that this axial loading could account for only about 4% of the actual strain deviation observed (see Figure 7.1), indicating that other mechanisms control the effect. A second possible explanation is the shift from linear strain distribution through the thickness. It is well known that as deflections become large, the

strain distribution through the thickness becomes slightly non-linear, which would cause a shift in the neutral axis. However, the deflections at which the deviations occurred in the specimens were still small, starting at about one specimen thickness.

The second variation from ideal elastic response is the deviation of the magnitude of the strains from that predicted by the model. Both using simple beam theory, and the non-linear bending equation in the numerical model of the beam, it was assumed that the material properties remained linear and uniform throughout the beam. Equation 5.6 shows that for small strains, the deflection/strain response is independent of stiffness, as long as the properties remain uniform. Therefore, experimental deviation from the uniform properties prediction, such as is seen in Figures 5.20-5.22, indicates that something has affected some local portion of the specimen (the gage section), which leads to local softening of the beam specimen. The softened structure allows greater strain in the gage section for a given roller displacement, as illustrated in Figure 7.2.

This local stiffness change could be due to two possible effects, namely elastic non-linearities, and specimen damage. Damage tends to reduce the stiffness of a flexure specimen in the local region of the gage section, which would lead to deviation from the uniform properties prediction. This could also lead to a shift in the neutral axis if damage occurs asymmetrically about the specimen mid-plane. As noted before, damage in the specimens observed under the microscope was concentrated in the tensile plies, which would lead to a shift of the neutral axis in the positive z-direction. However, the shifts noted were always in the negative z-direction. In addition, the shifts of neutral axis and deviations from the uniform properties prediction occurred at displacement levels below those at which damage initiated in each specimen type, with the exception of the ply-level scaled specimens, which contained damage in virgin specimens.

Unidirectional composite materials have been shown to exhibit strain hardening properties in tension, and strain softening properties in compression [19]. In the range of strains represented in Figures 5.20-5.22, all laminates have been shown to be linear elastic under tensile loading [4, 6, and chapter 4 herein]. However, in compression, there may be some non-linear material property behavior. Note in Figure 5.19 that the deviation from the prediction is almost entirely in the compressive strain. This was true of both Lay-ups ***B*** and ***C***. Lay-up ***D*** specimens showed deviation from linearity in both tension and compression. In light of the above, it is thought that the shift in neutral axis in Lay-ups ***B*** and ***C*** was a result of local softening caused by the compressive loading of a portion of the laminate before damage initiated.

Recall that each of Figures 5.20-5.22 consists of five typical curves, one for each specimen size and scaling method. With the sole exception of the ***Cds*** specimens, all curves for the same lay-up coincide, indicating that the same amount of local stiffness variation is occurring in each specimen of the same lay-up.

7.4 Damage Processes

Considering the findings of Kellas and Morton [6], it was expected that the ply-level scaled specimens would follow the trend they did. Larger ply-level scaled specimens began the failure process at considerably lower strain levels than their sublaminate-level scaled counterparts.

However, there was no corresponding increase in strain levels needed to initiate damage in the sublaminate-level scaled specimens, as was found in the tensile part of the current work. This may be due to the fact that only a small portion of the coupon actually sees high tensile strains.

7.4.1 Lay-up B [45/-45/0/90]$_{ns}$ and [45$_n$/-45$_n$/0$_n$/90$_n$]$_s$

Unfortunately, the first ply failure was missed in the ***Bds*** specimens. It is therefore not known what the trend in sublaminate-level scaled specimens would be. It would not be conclusive to say that based on the first two sizes, there is an increase in first ply failure strain.

One thing of interest is the change in failure modes present in the two scaling methods. Ply-level scaled specimens had damage in the surface ±45° plies, whereas the baseline and sublaminate-level scaled specimens did not. The ***Bdp*** specimens did not delaminate in the 90° plies, but rather, the delimitation at the outermost ±45° interface propagated. As the delamination grew in size (see X-rays in Figure 5.29), cracks in the -45° plies continued to occur. At some point, the -45° plies began to delaminate from the 0° plies beneath them (Figure 5.29). This released enough strain energy that the delamination in the 90° plies did not initiate.

The sublaminate-level specimens all behaved like the baseline specimens as far as which failure modes were present, with the exception that larger specimens had more 90° layers in tension. These additional plies could then fail by transverse cracking.

7.4.2 Lay-up C [0/90/0/90]$_{ns}$ and [0$_n$/90$_n$/0$_n$/90$_n$]$_s$

Lay-up ***C*** sublaminate-level specimens followed a trend similar to the ply-level scaled specimens, with decreasing strains in the 90° plies at first ply failure. However, this difference in first ply failure strain with increased scaled size had little effect on the ultimate failure of the specimens. The cause of failure in these specimens was compressive buckling of the surface 0° plies. This buckling was precipitated by indentation and damage caused by

the steel rollers that applied the load to the specimens. When a shim was added to eliminate the crushing damage, no buckling was present.

Another way to avoid buckling would be to modify the stacking sequence so that no 0° plies were on the surface. If the baseline stacking sequence had been the 16-ply analog of that used in the tensile work, namely $[90°/0°/90°/0°]_{2s}$, the surface 90° plies would have prevented buckling.

7.4.3 Lay-up D [45/-45/45/-45]ns and [45n/-45n/45n/-45n]s

From Figure 5.6 it can be seen that the load/deflection response of Lay-up ***D*** specimens varies from the linear properties prediction after about 2 mm of normalized deflection Δ. However, the first damage observed by either penetrant-enhanced radiography, or photomicroscopy, did not occur until nearly 4 mm normalized deflection. Yet, specimens loaded into the non-linear range, but below the damage initiation range, showed permanent deformation upon unloading. Therefore, some form of damage that could not be detected by either of the above methods was occurring. This could have been plastic yielding of the matrix, or fiber/matrix debonding among other things.

7.5 Ultimate Load and Deflection

7.5.1 Lay-up B [45/-45/0/90]ns and [45n/-45n/0n/90n]s

The failure of Lay-up ***B*** specimens was governed by failure in the 0° fibers, but these specimens did not contain any 0° surface plies. As discussed above, there is no problem when comparing load/deflection response of ply-level scaled specimens. For a given value of Δ, the strains in the plies of any fiber orientation are the same, and since the failure is controlled by the fiber strain, different sized ply-level specimens should fail at the same value of normalized load or deflection. However, when discussing sublaminate-level scaled

specimens, the strain in the outermost 0° fibers will be different for different sizes. For a given Δ, the surface strains are the same for any size specimen using any scaling method, but the outermost 0° plies are closer to the surface than their counterparts in ply-level scaling (similar to Figure 5.25).

Since the strain at the surface of the specimens is a function of the normalized values of load and deflection (Π and Δ), the strain in the outermost 0° fibers will be simply some ratio multiplied by the surface strain. As the strain distribution is linear, that ratio is simply the ratio of the ply's position with respect to the surface of the specimen, as noted in Figure 5.25. Therefore, the failure loads and deflections presented in Figures 5.12 and 5.15 are corrected using this ratio for the larger sublaminate-level scaled specimens.

These figures show that the sublaminate-level scaled specimens show no scaling effect with respect to ultimate failure. Although this may not appear to be consistent with the tensile work presented earlier, it does show some consistency with those previous findings. The reason the Lay-up ***B*** tensile specimens showed scaling effects is simply the fact that the baseline specimens delaminated much more severely than the other sizes, causing significant loss of stiffness, and therefore reaching the fiber failure strain at a lower stress. When the damage modes between sizes were similar, as in the case of the APC-2 specimens, scaling effects were reduced or eliminated.

Lay-up ***B*** flexure specimens showed the same damage modes in all sublaminate-level scaled sizes, and the stiffness loss was the same for all sizes. Hence, the failure strain of the fibers was reached at the same load level and no scaling effect was present.

Ply-level scaled specimens lost strength as the size was increased, which is consistent with the previous findings of Kellas and Morton [6].

7.5.2 Lay-up C [0/90/0/90]ns and [0n/90n/0n/90n]s

Figures 5.13 and 5.16 show a decrease in strength with increased scaled size using both scaling methods. However, as noted before, these failures were by buckling of the compressive surface 0° plies. When shims were placed between the fixture and the specimens, this buckling phenomenon did not occur. Instead, failure was by tensile fiber fracture. Figure 5.38 shows the normalized ultimate load when the shims were used.

Unfortunately, only one specimen from most specimen types, and no ***Cds*** specimen was available for testing. Hence, no averages could be computed, and it cannot be concluded whether the apparent slight drop in strength of the ply-level scaled coupons is real or not. If the effect is real, it is very slight. This agrees with previous findings showing crossply laminates to be insensitive to scaling effects.

7.5.3 Lay-up D [45/-45/45/-45]ns and [45n/-45n/45n/-45n]s

Further research into the nature of the non-linear behavior of Lay-up ***D*** specimens is needed before specific conclusions can be drawn about its flexural response. If damage is occurring, it is damage unlike that in the other two lay-ups, as it could not be seen as transply cracks or delaminations until well into the non-linear response. In the other two lay-ups, the initiation of damage could be directly correlated to the onset of non-linear behavior.

8. CONCLUSIONS

Because design of large scale structures is often begun by tests on small scale coupons, a study was performed to investigate the effect of specimen size and laminate stacking sequence on the uniaxial tensile and four-point flexure response of carbon fiber composite specimens of four different laminate stacking sequences.

The purpose of the study was to determine any change in the load/deformation response of a given stacking sequence as the size of the specimen was increased. Two methods of increasing the thickness of scaled laminates were used, namely ply-level and sublaminate-level scaling. These methods of scaling thickness are illustrated in Figure 1.1. The tensile program built on work done previously by Kellas and Morton [6] wherein they investigated the ply-level scaling of composites loaded under uniaxial tension. Hence, the tensile work presented herein studied only the sublaminate-level scaling of composites loaded under uniaxial tension. The flexure program investigated both ply- and sublaminate-level scaling of composites under four-point flexure loading.

This work shows unequivocally that there are scaling effects in composite laminates. Although it is understood in the composites community that blocking plies together, the ply-level work presented above points to some important scaling considerations. In addi-

tion, sublaminate-level scaling has been shown to have an effect on certain laminate stacking sequences in brittle matrix composites.

It was found that any effects scaling had on the global load/deformation response of specimens could be linked directly to damage propagation in plies that contributed significantly to the strength or stiffness of a laminate. Because of this, scaling effects were more pronounced in laminates whose response was governed significantly by matrix properties, and less pronounced in fiber dominated Lay-ups. Four major factors were found to govern the extent to which damage propagation effected the stress/strain response of a given coupon. These factors were 1) the laminate stacking sequence, 2) the thickness of the scaled specimen, 3) the toughness of the matrix material, and 4) the method of scaling the specimen thickness.

8.1 Tension

Only sublaminate-level scaling of the thickness was used in the tensile portion of this work because Kellas and Morton [6] have previously reported the ply-level scaling effects observed in the three stacking sequences studied in this work.

The stacking sequences chosen for the program were $[\pm 30/90_2]_{ns}$, $[\pm 45/0/90]_{ns}$ and $[90/0/90/0]_{ns}$. These stacking sequences were designated Lay-ups ***A***, ***B*** and ***C***, respectively. Two material systems were investigated. Most specimens were fabricated of AS4/3502 graphite/epoxy. In addition, two panels of Lay-up ***B*** were fabricated of APC-2 graphite/PEEK to study the effect of matrix toughness on scaled response.

8.1.1 Lay-up A [30/-30/90/90]ns

It was found that Lay-up ***A*** specimens contained "weak" ±30° surface plies. These four plies lost structural integrity before interior ±30° plies because of damage resulting from a delamination propagated always at the outermost -30°/90° interface.

A combination of finite element analysis to model interlaminar edge stresses, and an analytical model used to account for the presence of damage in the form of 90° transply cracks, was used to find the through-the-thickness stresses. It was found that these methods were able to predict that the delimitation would occur in the outermost 90° plies. With the delimitation, the two sets of surface ±30° plies physically separated from the rest of the specimens, and were damaged to the extent that they could no longer carry significant load. Hence, the remaining plies in the laminate were forced carry the added stress. In the case of the ***Aa-8*** specimens, this delamination precipitated global failure, since there were no other plies to take up the load. As the number of plies increased, additional ±30° plies were available to bear the load, and the delamination became less of a controlling factor in the global failure of the specimens. As a result, the strength increased with increasing specimen size, but leveled off at some maximum value as the four surface plies constituted less of the total makeup of the laminate.

8.1.2 Lay-up B [45/-45/0/90]ns

Lay-up ***B*** specimens with the brittle 3502 epoxy-matrix system exhibited delayed first ply failure stresses, decreased tendency toward delamination and more linear stress/strain response for specimens scaled at the sublaminate level. The decrease in extent of delamination was due to the fact that as the thickness was scaled by repeating sublaminates, less strain energy could be released through propagation of a delamination crack.

The analysis techniques described in chapter 3, were used to describe the through-the-thickness stresses in a Lay-up ***B*** specimen containing cracked 90° plies. It was found that with a single crack in each 90° layer, the delimitation was predicted in the outermost 90° plies. However, the experimental results showed that the specimens were significantly more densely cracked in the central 90° block than in the other 90° plies. Just prior to delamination, the central 90° cracks were close enough that tensile through-the-thickness stresses could interact, and their effects be added. With this consideration, delamination would occur in the central 90° block, as was found in experiment.

Delamination of the specimen was the major contributor to the non-linear stress/strain response. Non-linear softening in the response yielded higher strains for a given load. As a result, the failure strain of the 0° fibers was reached at a lower average stress, and premature failure resulted. Scaling effects in the AS4/3502 Lay-up ***B*** specimens could then be considered as artifacts resulting from the manner in which the thickness was scaled. By changing the thickness using sublaminate-level scaling, the propensity to delaminate was changed, and it was the degree to which a specimen delaminated that controlled the tensile response, since more extensive delamination yielded changes in modulus, higher transverse crack densities, and early failure.

In the case of the APC-2 specimens, even the small specimens did not delaminate. Hence, the non-linearities present in the tensile response are virtually eliminated. Where damage is delayed or suppressed, the response is more nearly linear, and strength of the specimen tends to be independent of size. Where damage is allowed to propagate, non-linearities are present in tensile response, and strength is lower.

Therefore, any method used that suppresses delamination would also avoid scaling phenomena. Choosing a stacking sequence that does not delaminate readily, or using a tougher

resin system would be two ways of assuring less scale-dependent results. It was noted that for the $[\pm 45/0/90]_{ns}$ stacking sequence, using PEEK as the matrix material eliminated the scaling effects. Even if an epoxy system were used, switching the quasi-isotropic Lay-up from $[\pm 45/0/90]_{ns}$ to $[90/0/\pm 45]_{ns}$ would suppress delamination in all specimen sizes, and therefore yield more uniform stress/strain response among the scaled sizes.

8.1.3 Lay-up C [90/0/90/0]ns

Postponement of first ply failure with increased specimen size was most pronounced in Lay-up ***C*** specimens, due to differences in the way in which plies are constrained. However, no scaling effects were present in the stress/strain response of these specimens because the 90° plies did not contribute significantly to the load carrying capability of the specimen. Although the 90° plies were damaged extensively during loading, they did not effect the stiffness of the laminate. No other type of damage occurred until global failure of the specimen.

8.2 Flexure

The baseline stacking sequences chosen for the flexure program were $[\pm 45/0/90]_{2s}$, $[0/90/0/90]_{2s}$ and $[\pm 45/\pm 45]_{2s}$. These stacking sequences were designated Lay-ups ***A***, ***B*** and ***C***, respectively. Both ply- and sublaminate-level scaling of the thickness were used. The material system used in the investigation was AS4/3502 graphite/epoxy.

In general, ply-level scaling led to reductions in the strength of the laminates, whereas sublaminate-level scaling did not affect the structural response. Unlike the tensile scaling work, no increases in flexural response properties were found with sublaminate-level scaling.

For comparison of the response curves of specimens of different size, a load and deflection normalization was used. The normalization process collapsed all load/deflection responses onto the same curve. Differences in response between sizes would then indicate that the damage mechanisms were different.

In addition, since the response was non-linear due to fixture and specimen geometry, a numerical model was developed in order to predict the response if properties remained linear elastic. In this manner, deviations from linear material properties could be noted and examined.

8.2.1 Lay-up B [45/-45/0/90]ns and [45n/-45n/0n/90n]s

Lay-up ***B*** specimens showed a reduction in normalized strength, and the normalized load at which damage initiated, with increased size using ply-level scaling. In addition, there was a change in the types of damage the largest size specimen sustained.

Baseline specimens (***Ba***) showed cracks in the outermost 90° ply and in the adjacent +45° ply, as well as edge delaminations in the outermost 90° ply. This was also true of the ***Bbp*** specimens, with the addition of cracks in the surface ±45° plies. However, the ***Bdp*** specimens showed no delamination in the outermost 90° plies. Instead, a delamination developed at the outer ±45° interface, followed by a delamination at the -45°/0° interface. These delaminations grew, and large portions of the tensile surface ±45° plies were simply detached from the specimen before global failure of the specimens by fiber fracture of the tensile 0° plies.

Sublaminate-level scaled specimens showed a decrease in the normalized load and deflection they could sustain (Figure 5.4), but it could not be called a scaling effect. Because the outermost 0° lies relatively closer to the surface in the larger sublaminate-level scaled

specimens (similar to Figure 5.25), the same normalized load or deflection will produce a higher strain in these plies. Figures 5.12 and 5.15 show the failure load and deflection corrected for the strain in the outer 0° plies. No scaling effect is present in sublaminate-level scaled specimens.

8.2.2 Lay-up C [0/90/0/90]ns and [0n/90n/0n/90n]s

Lay-up ***C*** specimens showed no significant scaling effects in either ply- or sublaminate-level scaling. Figure 5.5 indicates an apparent effect, but the specimens failed prematurely due buckling of the compressive surface 0° plies. This buckling was caused by indentation and crushing damage from the rollers on the fixture that introduced the load. When shims were used to prevent local crushing, no buckling took place, and no significant scaling effect was present (Figure 5.38).

8.2.3 Lay-up D [45/-45/45/-45]ns and [45n/-45n/45n/-45n]s

Because Lay-up ***D*** specimens contained no 0° plies, they behaved somewhat differently from the other two lay-ups. Non-linear material properties began quite early in the response, and unlike the other two flexure lay-ups, no damage could be detected associated with the initiation of non-linear material properties. Not until over 3 mm normalized deflection did damage in the form of matrix cracks occur in the specimens (except ***Ddp*** specimens). Further investigation into other possible damage modes would need to be carried out in order to understand the non-linear behavior in these specimens. Two possible explanations may be either plastic deformation in the matrix, or fiber/matrix debonding. Global scaling effects on the load/deformation response were only present in the ply-level scaled specimens. Sublaminate-level scaled specimens showed identical response in all sizes.

9. RECOMMENDATIONS

This research can be expanded by looking more specifically at fiber dominated lay-ups that are practical from a structures point of view. In this work, the most pronounced scaling effects were noted in either non-structural laminates (as in the tensile Lay-up ***A*** specimens, and the flexural Lay-up ***D*** specimens), or in lay-ups that should be avoided in practice (namely the baseline tensile Lay-up ***B***, as edge stresses are very high in this lay-up).

Although fiber dominated lay-ups showed no significant scaling effects (compared to scaling effects in matrix dominated lay-ups) in this work, one must remember that the largest specimens were only four times the size of the smallest. When, for instance, the aircraft industry engages in testing and certifying of materials that will be used in large structures, it is possible that the difference in size between coupons and the full scale parts may be orders of magnitude. If volumetric scaling has even a slight effect on the response of a material, it must be known in order to accurately predict the response of the full scale structure.

In addition, the types of scaling used in this work may not be practical for applications in industry. It may be that a stacking sequence being considered for a full scale structure has no real means of being scaled down using sublaminate groups. The most practical course to follow may be testing of net thickness specimens, in which case it must be known how much scaling of the in-plane dimensions affects the structural response.

REFERENCES

[1] Atkins A. G. and Caddell R. M., "The Laws of Similitude and Crack Propagation," *International Journal of Mechanics Science*, Pergamon Press, Vol. 16, 1974.

[2] Zweben C. "The Effect of Stress Nonuniformity and Size on the Strength of Composite Materials," *Composites Technology Review*, Vol. 3, No. 1, 1981.

[3] Batdorf S. B., "Note on Composite Size Effects," *Journal of Composites Technology & Research*, Vol. 11, No. 1, 1989.

[4] Kellas, S. and Morton J. "Scaling Effects in Angle-ply Laminates," *NASA Contractor Report 4423*, February 1992.

[5] Jackson K. E., "Scaling Effects in the Static and Dynamic Response of Graphite-Epoxy Beam-Columns," Ph.D. Thesis, Engineering Science and Mechanics Dept., Virginia Polytechnic Institute and State University, Blacksburg VA, 1990.

[6] Kellas S. and Morton J., "Strength Scaling in Fiber Composites," *NASA Contractor Report 4335*, November 1990.

[7] Morton J., "Scaling of Impact-Loaded Carbon-Fiber Composites," *AIAA Journal*, vol. 26, no. 8, August 1988.

[8] Jones, Robert M., *Mechanics of Composite Materials*, Hemisphere Publishing Corporation, New York, 1975.

[9] Whitney, J. M., *Structural Analysis of Laminated Anisotropic Plates*, Technomic Publishing Co., Inc., 1987.

[10] O'Brien, T. K., "Characterization of Delamination Onset and Growth in a Composite Laminate," *Damage in Composite Materials, ASTM STP 775*, K. L. Reifsnider, Ed., American Society for Testing and Materials, 1982, pp. 140-167.

[11] Vasiliev, V. V., Dudchenko, A. A. and Elpatievskii, A. N., "On Some Features of Deformation of Orthotropic Glass Plastics in Tension," Mekhanika Polimerov, No. 1, 1970, pp. 144-147.

[12] Crossman, F. W. and Wang, A. S. D., "The Dependence of Transverse Cracking and Delamination on Ply Thickness in Graphite/Epoxy Laminates," *Damage in Composite Materials, ASTM STP 775*, American Society for Testing and Materials, 1982, pp. 118-139.

[13] O'Brien, T. K., "Mixed-Mode Strain-Energy-Release Rate Effects on Edge Delamination of Composites," *Effect of Defects in Composite Materials, ASTM STP 836*, American Society for Testing and Materials, 1984, pp. 125-142.

[14] Hercules, Inc.

[15] Law, G. E., "A Mixed-Mode Fracture Analysis of $[\pm 25/90_n]_S$ Graphite/Epoxy Composite Laminates," *Effect of Defects in Composite Materials, ASTM STP 836*, American Society for Testing and Materials, 1984, pp. 125-142.

[16] Cantwell, W. J., Davies, P. and Kausch, H. H., "The Effect of Cooling Rate on Deformation and Fracture in IM6/PEEK Composites," *Composite Structures*, 14, 1990, pp. 151-171.

[17] Herakovich, C. T., "On the Relationship Between Engineering Properties and Delamination of Composite Materials," *Journal of Composite Materials*, Vol. 15, July 1981, pp. 336-348.

[18] Flaggs, D. L. and Kural, M. H., "Experimental Determination of the In Situ Transverse Lamina Strength in Graphite/Epoxy Laminates," *Journal of Composite Materials*, Vol. 16, 1982, pp. 103-115.

[19] Sensmeier, M. D., Griffin, O. H. and Johnson, E. R., "Static and Dynamic Large Deflection Flexural Response of Graphite-Epoxy Beams," *NASA Contractor Report 4118*, March 1988.

[20] Kellas, S., Johnson, D. P., Morton, J. and Jackson, K. E., "Scaling Effects in Sublaminate-Scaled Composite Laminates," *Proceedings of the 34th Structures, Structural Dynamics, and Materials Conference*, La Jolla, CA, April 1993.

TABLES

Table 2.1 Test matrix for AS4/3502 specimens indicating the specimen dimensions and the nominal thickness for each case. Note that specimens **a8**, **b16**, **c24**, and **d32** are scaled in three dimensions.

	Size Designation			
Size (mm)	**8-ply** (1.0 mm)	**16-ply** (2.0 mm)	**24-ply** (3.0 mm)	**32-ply** (4.0 mm)
a (12.5x125)	**a-8 Baseline**	a-16	a-24	–
b (25x250)	b-8	b-16	–	–
c (37.5x375)	–	–	c-24	–
d (50x500)	–	–	–	d-32

Table 2.2 Test matrix for APC-2 specimens indicating the specimen dimensions and the nominal thickness for each case.

	Size Designation			
Size (mm)	**8-ply** (1.0 mm)	**16-ply** (2.0 mm)	**24-ply** (3.0 mm)	**32-ply** (4.0 mm)
a (12.5x125)	**a-8 Baseline**	–	–	–
b (25x250)	b-8	–	–	b-32
c (37.5x375)	–	–	–	–
d (50x500)	–	–	–	d-32

Table 4.1 Average* stiffness (Lay-up *A*).

Size (mm)	**Stiffness - GPa** (Coefficient of Variation)			
	8 $[\pm 30/90_2]_s$	**16** $[\pm 30/90_2]_{2s}$	**24** $[\pm 30/90_2]_{3s}$	**32** $[\pm 30/90_2]_{4s}$
a (12.5x125)	39.5 (5.52) 42.4 (2.44)[3]	45.8 (1.64)[1,5]	44.1 (2.77)[5]	–
b (25x250)	38.7 (1.36)[4]	42.0 (4.22)[4] 42.5 (2.03)[3,4]	–	–
c (37.5x375)	–	–	46.4 (4.64) 45.8 (1.62)[3,4]	–
d (50x500)	–	–	–	41.6 (3.60) 42.2 (3.91)[2,3]

* average of at least 8 specimens unless otherwise indicated.
1 batch *II* material.
2 different autoclave run.
3 custom extensometer used.
4 average of 4 specimens.
5 average of 5 specimens.

Table 4.2 Average* stiffness (AS4/3502 Lay-up *B*).

Size (mm)	**Stiffness - GPa** (Coefficient of Variation)			
	8 $[\pm 45/0/90]_s$	**16** $[\pm 45/0/90]_{2s}$	**24** $[\pm 45/0/90]_{3s}$	**32** $[\pm 45/0/90]_{4s}$
a (12.5x125)	50.2 (5.73) 50.9 (4.82[3]	56.5 (4.97)[1,5]	49.4 (1.39)[5]	–
b (25x250)	49.4 (4.46)[4]	50.8 (2.48[4] 50.1 (0.64)[3,4]	–	–
c (37.5x375)	–	–	50.3 (2.94) 51.1 (1.91)[3,6]	–
d (50x500)	–	–	–	56.2 (5.36)[5] 54.6 (5.09)[2,3,6]

* average of at least 8 specimens unless otherwise indicated.
1 batch *II* material.
2 different autoclave run.
3 custom extensometer used.
4 average of 4 specimens.
5 average of 5 specimens.
6 average of 6 specimens.

Table 4.3 Average stiffness (APC-2 Lay-up *B*).

Size (mm)	**Stiffness - GPa** (Coefficient of Variation)			
	8 $[\pm 45/0/90]_s$	**16** $[\pm 45/0/90]_{2s}$	**24** $[\pm 45/0/90]_{3s}$	**32** $[\pm 45/0/90]_{4s}$
a (12.5x125)	51.1 (2.61)[2]	–	–	–
b (25x250)	50.6 (2.90)[2]	–	–	50.2 (0.37)[1]
c (37.5x375)	–	–	–	–
d (50x500)	–	–	–	49.1 (1.20)[2]

[1] average of 2 specimens.
[2] average of 5 specimens.

Table 4.4 Average* stiffness (Lay-up *C*).

Size (mm)	**Stiffness - GPa** (Coefficient of Variation)			
	8 $[90/0/90/0]_s$	**16** $[90/0/90/0]_{2s}$	**24** $[90/0/90/0]_{3s}$	**32** $[90/0/90/0]_{4s}$
a (12.5x125)	69.2 (3.83) 73.1 (4.84)[3]	76.5 (4.13)[1,5]	–	–
b (25x250)	68.7 (4.82)[4]	70.8 (2.16)[6] 69.7 (2.88)[3,6]	–	–
c (37.5x375)	–	–	70.8 (3.57) 71.5 (2.90)[3,7]	–
d (50x500)	–	–	–	75.3 (5.87) 73.1 (7.06)[2,3]

* average of at least 8 specimens unless otherwise indicated.
[1] batch *II* material.
[2] different autoclave run.
[3] custom extensometer used.
[4] average of 2 specimens.
[5] average of 3 specimens.
[6] average of 4 specimens.
[7] average of 6 specimens.

Table 4.5 Average* non-linear knee stress (Lay-up *A*).

Size (mm)	**Non-linear Knee Stress - MPa** (Coefficient of Variation)			
	8 $[\pm 30/90_2]_s$	**16** $[\pm 30/90_2]_{2s}$	**24** $[\pm 30/90_2]_{3s}$	**32** $[\pm 30/90_2]_{4s}$
a (12.5x125)	142 (5.80) 144 (5.63)[2]	–	278 (2.92)[5]	–
b (25x250)	154 (7.71)[4]	218 (2.10)[4] 206 (4.00)[2,4]	–	–
c (37.5x375)	–	–	251 (6.90) 228 (0.67)[2,3]	–
d (50x500)	–	–	–	268 (4.90)[1] 258 (7.72)[1,2]

* average of at least 8 specimens unless otherwise indicated.
1 different autoclave run.
2 custom extensometer used.
3 average of 3 specimens.
4 average of 4 specimens.
5 average of 5 specimens.

Table 4.6 Average* non-linear knee stress (AS4/3502 Lay-up *B*).

Size (mm)	**Non-linear Knee Stress - MPa** (Coefficient of Variation)			
	8 $[\pm 45/0/90]_s$	**16** $[\pm 45/0/90]_{2s}$	**24** $[\pm 45/0/90]_{3s}$	**32** $[\pm 45/0/90]_{4s}$
a (12.5x125)	252 (4.26) 244 (3.37)[2]	–	376 (3.19)[3]	–
b (25x250)	243 (3.96)[3]	289 (5.52)[3] 268 (2.20)[2,3]	–	–
c (37.5x375)	–	–	332 (4.63)[5] 335 (4.44)[2,5]	–
d (50x500)	–	–	–	447 (1.92)[1,4] 448 (3.08)[1,2,5]

* average of at least 8 specimens unless otherwise indicated.
1 different autoclave run.
2 custom extensometer used.
3 average of 4 specimens.
4 average of 5 specimens.
5 average of 6 specimens.

Table 4.7 First ply failure (Lay-up *A*).

Size (mm)	First Ply Failure Stress* - MPa			
	8 $[\pm 30/90_2]_s$	**16** $[\pm 30/90_2]_{2s}$	**24** $[\pm 30/90_2]_{3s}$	**32** $[\pm 30/90_2]_{4s}$
a (12.5x125)	170[2]	–	–	–
b (25x250)	–	170[2]	–	–
c (37.5x375)	–	–	175[1]	–
d (50x500)	–	–	–	210[1]

* one specimen.
1 batch *I* material.
2 batch *II* material.

Table 4.8 First ply failure (AS4/3502 Lay-up *B*).

Size (mm)	First Ply Failure Stress* - MPa			
	8 $[\pm 45/0/90]_s$	**16** $[\pm 45/0/90]_{2s}$	**24** $[\pm 45/0/90]_{3s}$	**32** $[\pm 45/0/90]_{4s}$
a (12.5x125)	250[2]	–	–	–
b (25x250)	–	245[2]	–	–
c (37.5x375)	–	–	300[1]	–
d (50x500)	–	–	–	275[1]

* one specimen.
1 batch *I* material.
2 batch *II* material.

Table 4.9 First ply failure (Lay-up *C*).

Size (mm)	First Ply Failure Stress* - MPa			
	8 $[90/0/90/0]_S$	**16** $[90/0/90/0]_{2S}$	**24** $[90/0/90/0]_{3S}$	**32** $[90/0/90/0]_{4S}$
a (12.5x125)	380[2]	–	–	–
b (25x250)	–	440[2]	–	–
c (37.5x375)	–	–	530[1]	–
d (50x500)	–	–	–	575[1]

* one specimen.
1 batch *I* material.
2 batch *II* material.

Table 4.10 Average* delamination knee strain (AS4/3502 Lay-up *B*).

Size (mm)	Delamination Knee Strain - % (Coefficient of Variation)			
	8 $[\pm45/0/90]_S$	**16** $[\pm45/0/90]_{2S}$	**24** $[\pm45/0/90]_{3S}$	**32** $[\pm45/0/90]_{4S}$
a (12.5x125)	0.62 (5.40) 0.61 (4.01)[2]	–	–	–
b (25x250)	–	0.84 (5.23)[3] 0.76 (4.15)[2,3]	–	–
c (37.5x375)	–	–	1.06 (3.61)[5] 1.07 (4.12)[2,5]	–
d (50x500)	–	–	–	1.10 (5.12)[1,4] 1.11 (3.82)[1,2,5]

* average of at least 8 specimens unless otherwise indicated.
1 different autoclave run.
2 custom extensometer used.
3 average of 4 specimens.
4 average of 5 specimens.
5 average of 6 specimens.

Table 4.11 Average* delamination knee stress (AS4/3502 Lay-up *B*).

	Delamination Knee Stress- MPa (Coefficient of Variation)			
Size (mm)	**8** $[\pm45/0/90]_S$	**16** $[\pm45/0/90]_{2S}$	**24** $[\pm45/0/90]_{3S}$	**32** $[\pm45/0/90]_{4S}$
a (12.5x125)	306 (3.26) 295 (3.37)[2]	–	545 (3.19)[3]	–
b (25x250)	298 (3.96)[3]	423 (5.02)[3] 396 (2.20)[2,3]	–	–
c (37.5x375)	–	–	532 (2.63)[5] 536 (4.44)[2,5]	–
d (50x500)	–	–	–	600 (2.92)[1,4] 604 (3.08)[1,2,5]

* average of at least 8 specimens unless otherwise indicated.
1 different autoclave run.
2 custom extensometer used.
3 average of 4 specimens.
4 average of 5 specimens.
5 average of 6 specimens.

Table 4.12 Average* ultimate stress (Lay-up *A*).

	Ultimate Stress - MPa (Coefficient of Variation)			
Size (mm)	**8** $[\pm30/90_2]_S$	**16** $[\pm30/90_2]_{2S}$	**24** $[\pm30/90_2]_{3S}$	**32** $[\pm30/90_2]_{4S}$
a (12.5x125)	262 (2.72)	331 (2.67)[1,4]	368 (1.56)[4]	–
b (25x250)	271 (4.85)[3]	353 (2.67)	–	–
c (37.5x375)	–	–	406 (2.17)	–
d (50x500)	–	–	–	414 (2.64)[2]

* average of at least 8 specimens unless otherwise indicated.
1 batch *II* material.
2 different autoclave run.
3 average of 3 specimens.
4 average of 5 specimens.

Table 4.13 Average* ultimate stress (AS4/3502 Lay-up B).

	Ultimate Stress - MPa (Coefficient of Variation)			
Size (mm)	**8** $[\pm 45/0/90]_s$	**16** $[\pm 45/0/90]_{2s}$	**24** $[\pm 45/0/90]_{3s}$	**32** $[\pm 45/0/90]_{4s}$
a (12.5x125)	548 (4.59)	662 (5.89)[1,4]	612 (10.24)[4]	–
b (25x250)	526 (2.79)[3]	660 (3.28)	–	–
c (37.5x375)	–	–	652 (6.00)	–
d (50x500)	–	–	–	677 (6.78)[2,4]

* average of at least 8 specimens unless otherwise indicated.
1 batch *II* material.
2 different autoclave run.
3 average of 4 specimens.
4 average of 5 specimens.

Table 4.14 Average ultimate stress (APC-2 Lay-up *B*).

	Ultimate Stress - MPa (Coefficient of Variation)			
Size (mm)	**8** $[\pm 45/0/90]_s$	**16** $[\pm 45/0/90]_{2s}$	**24** $[\pm 45/0/90]_{3s}$	**32** $[\pm 45/0/90]_{4s}$
a (12.5x125)	765.7 (6.61)[2]	–	–	–
b (25x250)	752.4 (6.14)[2]	–	–	764.1 (3.73)[1]
c (37.5x375)	–	–	–	–
d (50x500)	–	–	–	745.0 (1.15)[2]

1 average of 2 specimens.
2 average of 5 specimens.

Table 4.15 Average* ultimate stress (Lay-up *C*).

Size (mm)	**Ultimate Stress - MPa** (Coefficient of Variation)			
	8 $[90/0/90/0]_s$	**16** $[90/0/90/0]_{2s}$	**24** $[90/0/90/0]_{3s}$	**32** $[90/0/90/0]_{4s}$
a (12.5x125)	956 (5.92)	1091 (1.97)[1,4]	968 (1.56)[4]	–
b (25x250)	946 (0.12)[3]	951 (5.84)	–	–
c (37.5x375)	–	–	908 (6.32)	–
d (50x500)	–	–	–	971 (8.43)[2]

* average of at least 8 specimens unless otherwise indicated.
1 batch *II* material.
2 different autoclave run.
3 average of 2 specimens.
4 average of 3 specimens.

Table 4.16 Average* strain corresponding to ultimate stress (Lay-up *A*).

Size (mm)	**Ultimate Strain - %** (Coefficient of Variation)			
	8 $[\pm 30/90_2]_s$	**16** $[\pm 30/90_2]_{2s}$	**24** $[\pm 30/90_2]_{3s}$	**32** $[\pm 30/90_2]_{4s}$
a (12.5x125)	0.77 (5.15) 0.77 (4.06)[3]	0.88 (6.53)[1,5]	0.95 (5.10)[5]	–
b (25x250)	0.78 (8.33)[4]	0.90 (3.77)[4] 0.95 (4.88)[3,4]	–	–
c (37.5x375)	–	–	1.10 (6.71) 1.04 (2.79)[3,4]	–
d (50x500)	–	–	–	1.09 (3.12)[2] 1.11 (3.90)[2,3]

* average of at least 8 specimens unless otherwise indicated.
1 batch *II* material.
2 different autoclave run.
3 custom extensometer used.
4 average of 4 specimens.
5 average of 5 specimens.

Table 4.17 Average* strain corresponding to ultimate stress (AS4/3502 Lay-up ***B***).

	Ultimate Strain - % (Coefficient of Variation)			
Size (mm)	**8** $[\pm 45/0/90]_s$	**16** $[\pm 45/0/90]_{2s}$	**24** $[\pm 45/0/90]_{3s}$	**32** $[\pm 45/0/90]_{4s}$
a (12.5x125)	1.23 (2.78) 1.40 (7.79)[3]	1.27 (4.82)[1,5]	1.24 (10.09)[5]	–
b (25x250)	1.18 (14.50)[4]	1.36 (1.04) 1.32 (3.30)[3]	–	–
c (37.5x375)	–	–	1.37 (4.12) 1.40 (3.06)[3]	–
d (50x500)	–	–	–	1.30 (8.91)[2,5] 1.28 (8.00)[2,3,5]

* average of at least 8 specimens unless otherwise indicated.
1 batch *II* material.
2 different autoclave run.
3 custom extensometer used.
4 average of 4 specimens.
5 average of 5 specimens.

Table 4.18 Average strain corresponding to ultimate stress (APC-2 Lay-up *B*).

	Ultimate Strain - % (Coefficient of Variation)			
Size (mm)	**8** $[\pm 45/0/90]_s$	**16** $[\pm 45/0/90]_{2s}$	**24** $[\pm 45/0/90]_{3s}$	**32** $[\pm 45/0/90]_{4s}$
a (12.5x125)	1.55 (7.82)[2]	–	–	–
b (25x250)	1.52 (6.38)[2]	–	–	1.55 (4.56)[1]
c (37.5x375)	–	–	–	–
d (50x500)	–	–	–	1.49 (1.64)[2]

1 average of 2 specimens.
2 average of 5 specimens.

Table 4.19 Average* strain corresponding to ultimate stress (Lay-up *C*).

Size (mm)	Ultimate Strain - % (Coefficient of Variation)			
	8 $[90/0/90/0]_s$	**16** $[90/0/90/0]_{2s}$	**24** $[90/0/90/0]_{3s}$	**32** $[90/0/90/0]_{4s}$
a (12.5x125)	1.29 (6.42) 1.37 (5.39)[3]	1.38 (3.83)[1,5]	–	–
b (25x250)	1.32 (2.13)[4]	1.29 (5.24)[6] 1.31 (4.17)[3,6]	–	–
c (37.5x375)	–	–	1.25 (7.91) 1.31 (3.65)[3,7]	–
d (50x500)	–	–	–	1.28 (5.98)[2] 1.28 (6.71)[2,3]

* average of at least 8 specimens unless otherwise indicated.
1 batch *II* material.
2 different autoclave run.
3 custom extensometer used.
4 average of 2 specimens.
5 average of 3 specimens.
6 average of 4 specimens.
7 average of 6 specimens.

Table 4.20 Through-the-thickness stresses predicted from FEM and analytical models.

	σ_z (MPa)	
	2-D FEM model	**Analytical model**
$[\pm 30/90_2]_{2s}$	183 (outer plies) 109 (central plies)	145 (outer plies) 79.3 (central plies)
$[\pm 45/0/90]_{2s}$	159 (outer plies) 136 (central plies)	54.5 (outer plies) 57.6 (central plies)

Table 5.1 Average* bending stiffness E_b.

Lay-up		Bending Stiffness - GPa (Coefficient of Variation)		
		$n = 1$ (12.5mmx75mm)	$n = 2$ (25mmx150mm)	$n = 4$ (50mmx300mm)
B s	$[45/-45/0/90]_{2ns}$	37.8 (2.24)	46.1 (1.74)	47.7 (1.73)[1]
B p	$[45_n/-45_n/0_n/90_n]_{2s}$		42.5 (1.89)	56.1 (5.14)[1]
C s	$[0/90/0/90]_{2ns}$	71.0 (2.53)	70.3 (1.59)	67.2 (0.47)[2]
C p	$[0_n/90_n/0_n/90_n]_{2s}$		77.2 (1.10)	80.0 (4.40)[2]
D s	$[45/-45/45/-45]_{2ns}$	20.3 (4.34)	19.8 (1.51)	22.2 (1.89)[1]
D p	$[45_n/-45_n/45_n/-45_n]_{2s}$		21.0 (1.35)	20.1 (3.46)[2]

* average of at least 7 specimens unless otherwise indicated.
[1] average of 4 specimens.
[2] average of 5 specimens.

Table 5.2 Average* ultimate load P_u.

Lay-up		Maximum Load - kN (Coefficient of Variation)		
		$n = 1$ (12.5mmx75mm)	$n = 2$ (25mmx150mm)	$n = 4$ (50mmx300mm)
B s	$[45/-45/0/90]_{2ns}$	0.923 (3.50)	3.68 (2.32)[3]	14.9 (5.20)[1]
B p	$[45_n/-45_n/0_n/90_n]_{2s}$		2.79 (3.56)[2]	7.52 (1.39)[2]
vC s	$[0/90/0/90]_{2ns}$	1.37 (3.91)	4.94 (3.24)[3]	19.4 (1.24)[2]
C p	$[0_n/90_n/0_n/90_n]_{2s}$		4.31 (3.22)[3]	14.8 (10.4)[4]
D s	$[45/-45/45/-45]_{2ns}$	0.295 (0.95)	1.29 (1.03)[3]	5.24 (0.42)[1]
D p	$[45_n/-45_n/45_n/-45_n]_{2s}$		1.14 (0.25)[1]	2.85 (2.16)[2]

* average of at least 6 specimens unless otherwise indicated.
[1] average of 2 specimens.
[2] average of 3 specimens.
[3] average of 4 specimens.
[4] average of 5 specimens.

Table 5.3 Average* ultimate deflection δ_u.

Lay-up		Maximum Deflection - mm (Coefficient of Variation)		
		$n = 1$ (12.5mmx75mm)	$n = 2$ (25mmx150mm)	$n = 4$ (50mmx300mm)
B s	$[45/-45/0/90]_{2ns}$	5.89 (4.74)	10.2 (3.17)[3]	18.2 (5.54)[1]
B p	$[45_n/-45_n/0_n/90_n]_{2s}$		8.20 (3.16)[2]	13.4 (5.79)[2]
C s	$[0/90/0/90]_{2ns}$	4.90 (4.66)	8.61 (5.00)[3]	16.4 (2.82)[2]
C p	$[0_n/90_n/0_n/90_n]_{2s}$		6.99 (4.67)[3]	13.2 (8.42)[4]
D s	$[45/-45/45/-45]_{2ns}$	6.91 (3.47)	14.0 (2.20)[3]	27.0 (0.13)[1]
D p	$[45_n/-45_n/45_n/-45_n]_{2s}$		11.3 (1.75)[1]	10.2 (6.56)[2]

* average of at least 6 specimens unless otherwise indicated.
[1] average of 2 specimens.
[2] average of 3 specimens.
[3] average of 4 specimens.
[4] average of 5 specimens.

Table 5.4 Average* load at deviation from linearity P_n.

Lay-up		Non-Linear Load - kN (Coefficient of Variation)		
		$n = 1$ (12.5mmx75mm)	$n = 2$ (25mmx150mm)	$n = 4$ (50mmx300mm)
B s	$[45/-45/0/90]_{2ns}$	0.503 (15.4)	1.93 (8.93)[4]	5.43 (9.60)[2]
B p	$[45_n/-45_n/0_n/90_n]_{2s}$		1.29 (5.86)	4.09 (7.62)[1]
C s	$[0/90/0/90]_{2ns}$	0.934 (14.8)	2.63 (6.74)[4]	9.04 (1.98)[2]
C p	$[0_n/90_n/0_n/90_n]_{2s}$		2.65 (5.28)[4]	9.01 (2.04)[3]
D s	$[45/-45/45/-45]_{2ns}$	0.104 (7.66)	0.460 (3.48)[4]	1.47 (5.88)[2]
D p	$[45_n/-45_n/45_n/-45_n]_{2s}$		0.390 (7.40)	1.24 (6.39)[3]

* average of at least 7 specimens unless otherwise indicated.
[1] average of 3 specimens.
[2] average of 4 specimens.
[3] average of 5 specimens.
[4] average of 6 specimens.

Table 5.5 Average* deflection at deviation from linearity δ_n.

Lay-up		Non-Linear Deflection - mm (Coefficient of Variation)		
		$n = 1$ (12.5mmx75mm)	$n = 2$ (25mmx150mm)	$n = 4$ (50mmx300mm)
B s	$[45/-45/0/90]_{2ns}$	2.87 (15.9)	4.95 (9.29)	6.43 (10.0)[2]
B p	$[45_n/-45_n/0_n/90_n]_{2s}$		3.63 (6.43)	6.15 (7.88)[1]
C s	$[0/90/0/90]_{2ns}$	3.25 (15.3)	4.39 (7.46)	7.54 (0.85)[2]
C p	$[0_n/90_n/0_n/90_n]_{2s}$		4.27 (4.57)	7.39 (7.38)[3]
D s	$[45/-45/45/-45]_{2ns}$	1.35 (8.88)	2.79 (3.76)	4.27 (5.47)[2]
D p	$[45_n/-45_n/45_n/-45_n]_{2s}$		2.39 (8.29)	3.78 (6.48)[3]

* average of at least 7 specimens unless otherwise indicated.
[1] average of 3 specimens.
[2] average of 4 specimens.
[3] average of 5 specimens.

Table 5.6 Damage initiation.

Lay-up		Deflection* at onset of damage - mm		
		$n = 1$ (12.5mmx75mm)	$n = 2$ (25mmx150mm)	$n = 4$ (50mmx300mm)
B s	$[45/-45/0/90]_{2ns}$	2.8	5.1	—
B p	$[45_n/-45_n/0_n/90_n]_{2s}$		4.9	7.2
C s	$[0/90/0/90]_{2ns}$	3.2	5.1	9.4
C p	$[0_n/90_n/0_n/90_n]_{2s}$		5.0	—
D s	$[45/-45/45/-45]_{2ns}$	3.8	7.0	—
D p	$[45_n/-45_n/45_n/-45_n]_{2s}$		6.5	7.6

* one specimen per value.

Table 6.1 Ply properties of AS4/3502 graphite/epoxy.

E_{11}	137.2 GPa
E_{22}	9.86 GPa
G_{12}	4.83 GPa
ν_{12}	0.29

FIGURES

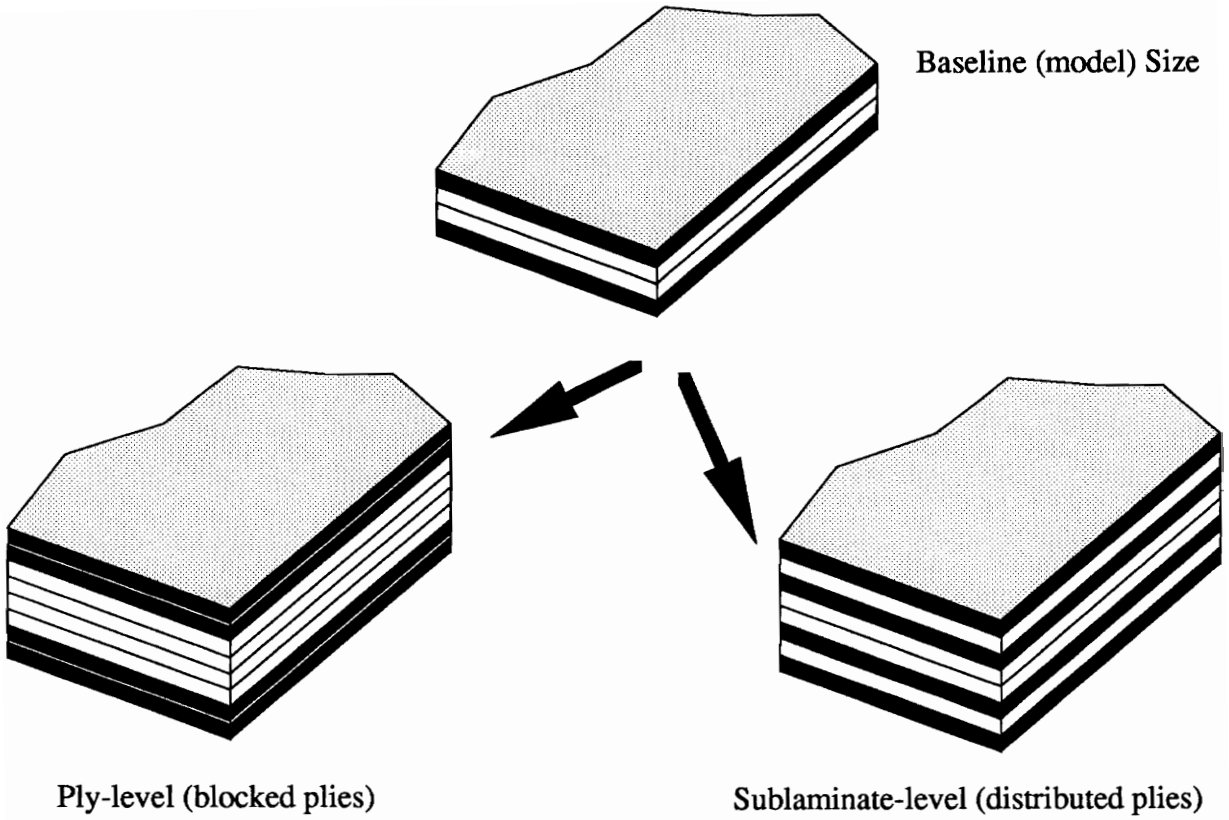

Figure 1.1 Ply-level vs. sublaminate-level thickness scaling.

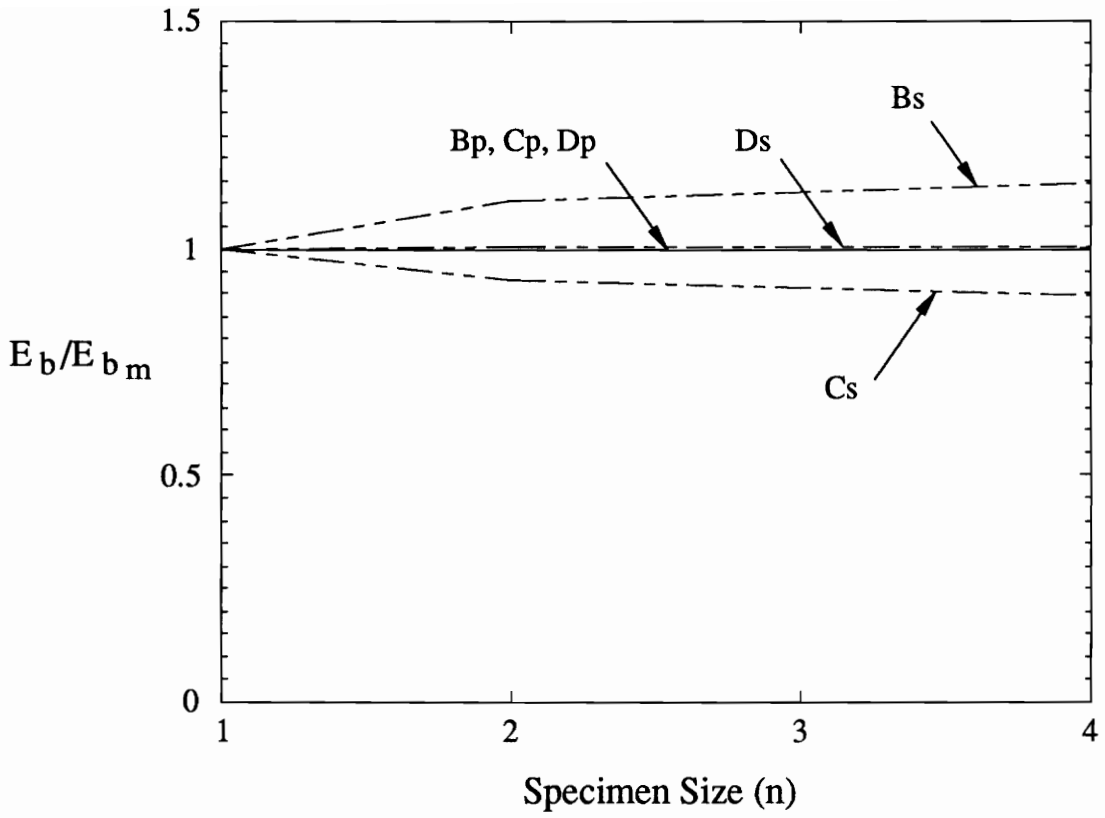

Figure 1.2 Normalized CLT bending stiffnesses of Lay-ups *B* , *C* and *D* in both sublaminate- and ply-level scaling, as functions of specimen size.

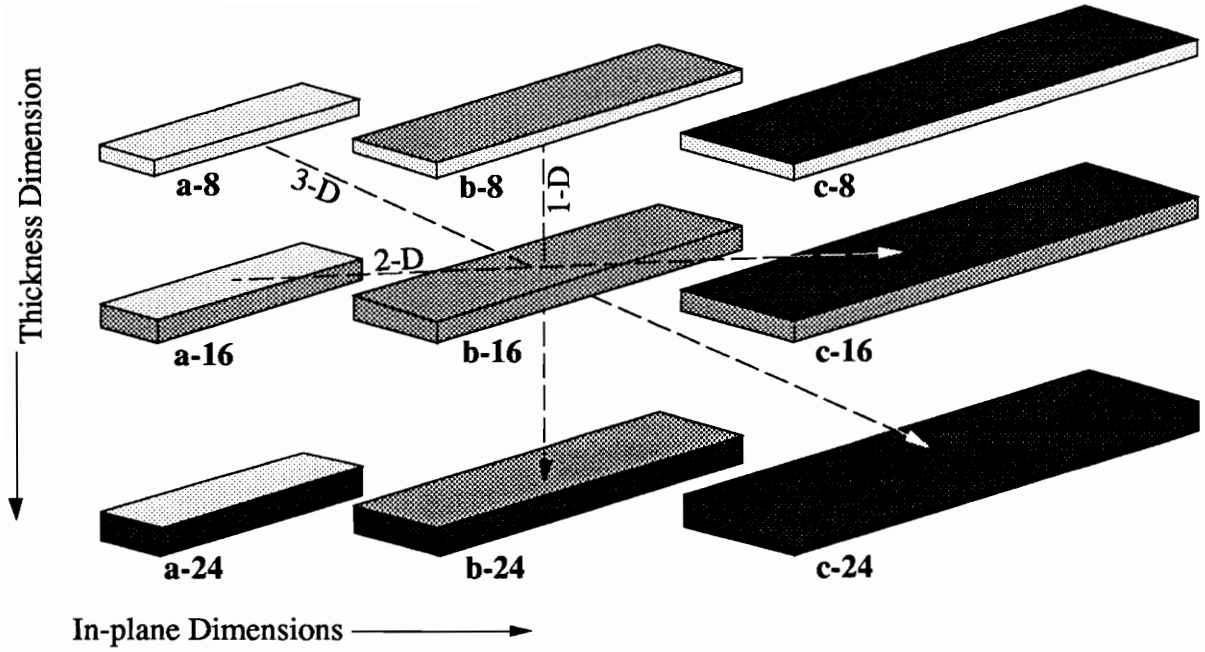

Figure 2.1 1-D, 2-D and 3-D scaling, where the letter represents the specimen's in-plane dimensions, and the number represents the number of plies.

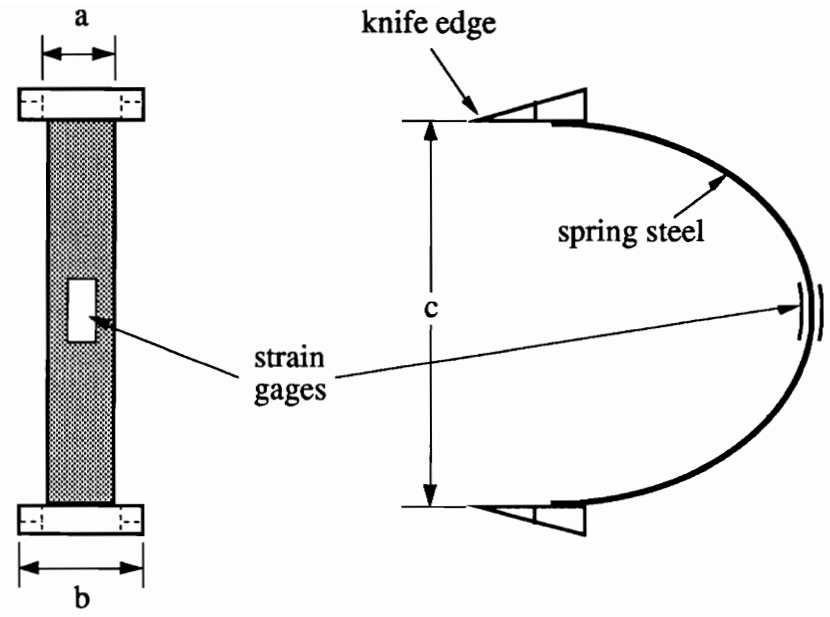

Figure 2.2 Schematic of custom extensometers.

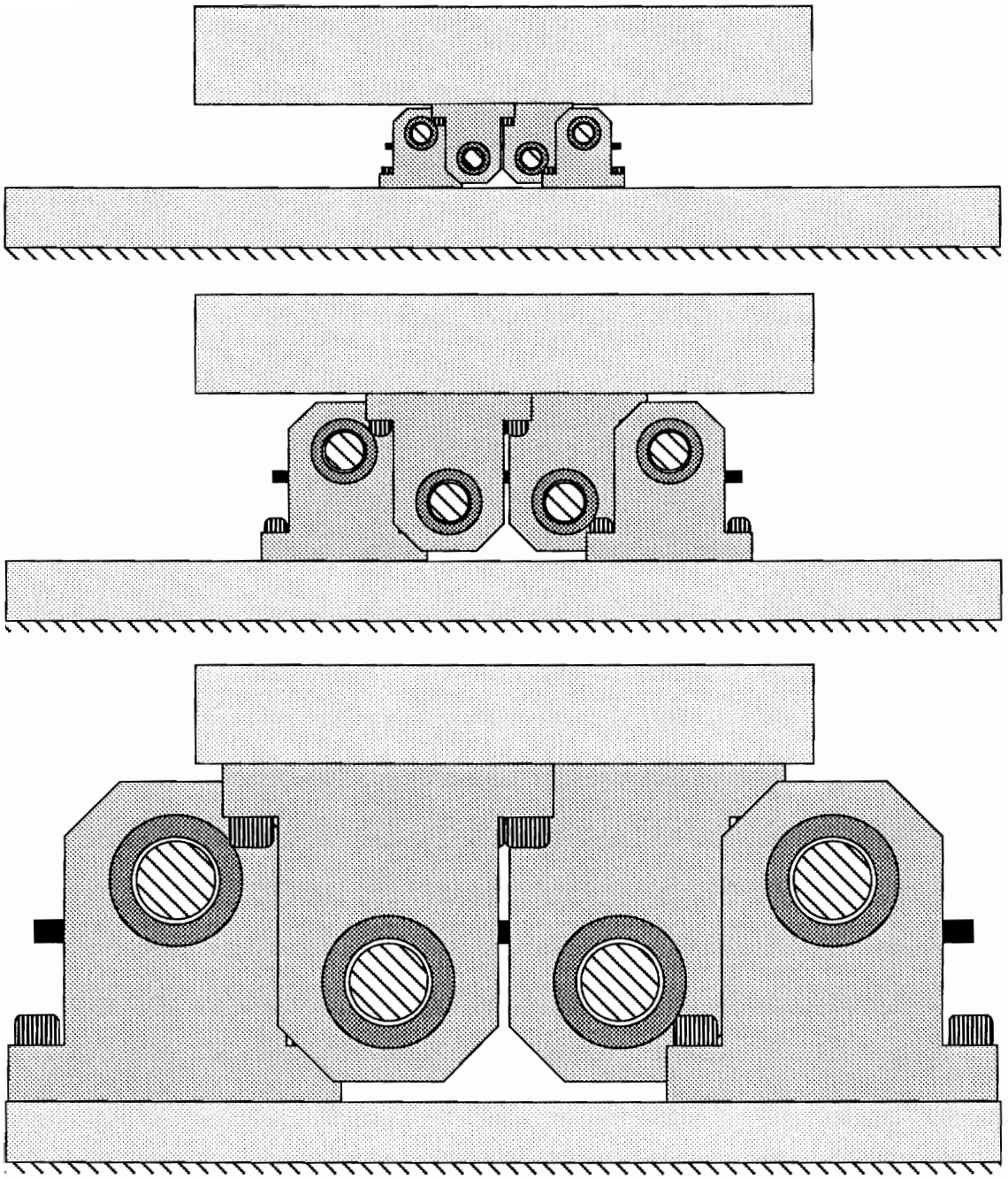

Figure 2.3 Schematic of four-point flexure fixture.

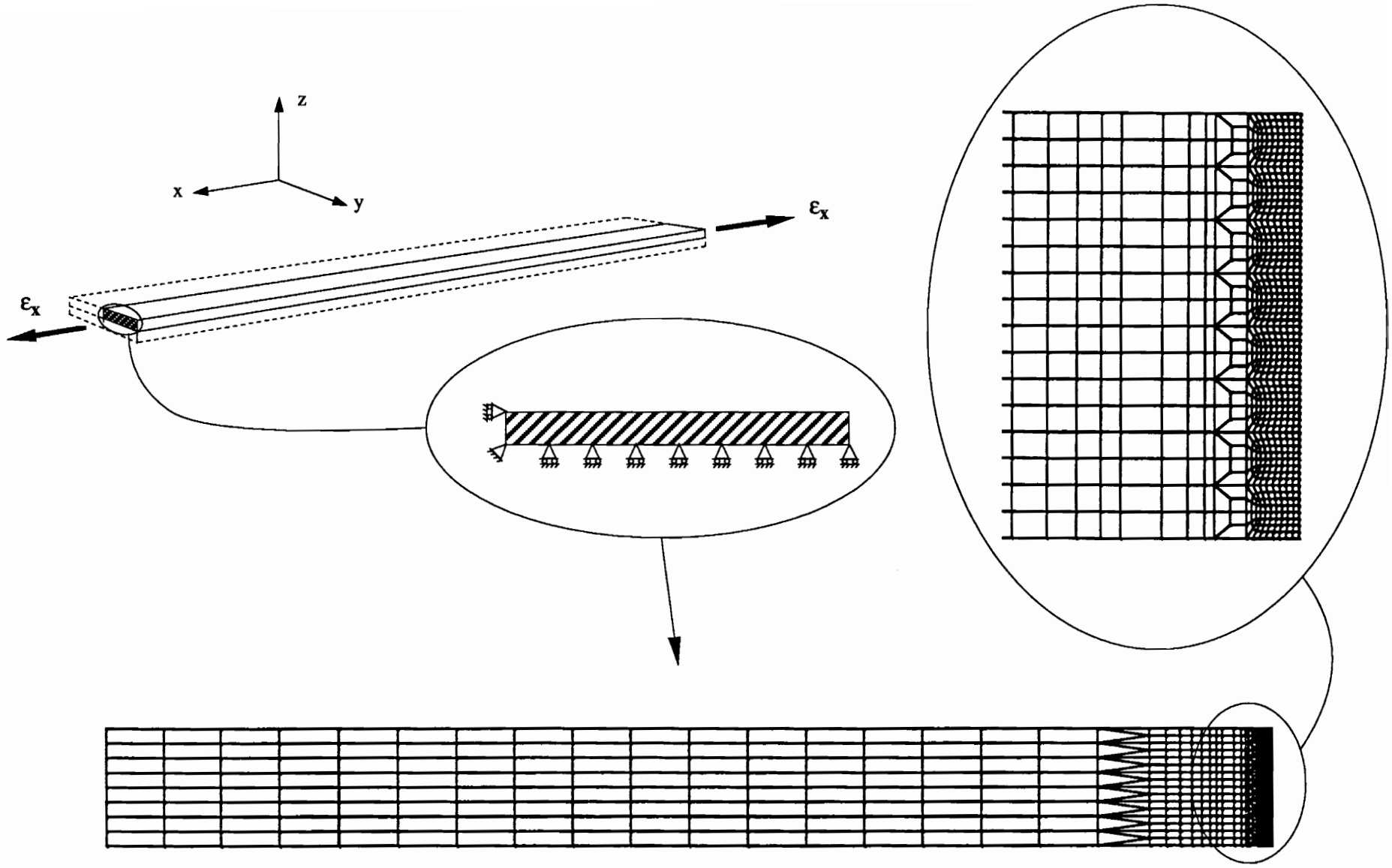

Figure 3.1 2-D finite element mesh and boundary conditions.

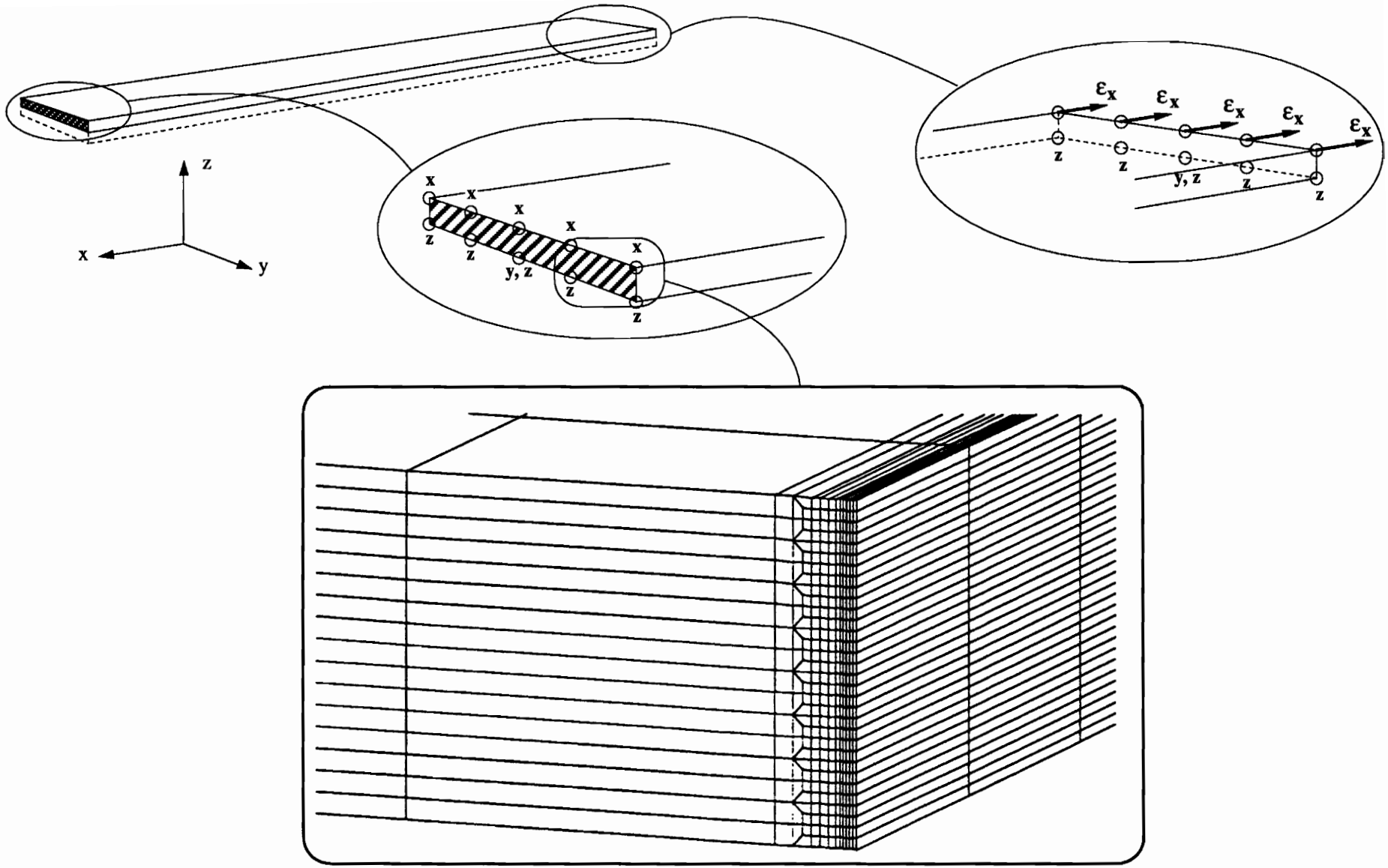

Figure 3.2 3-D finite element mesh and boundary conditions.

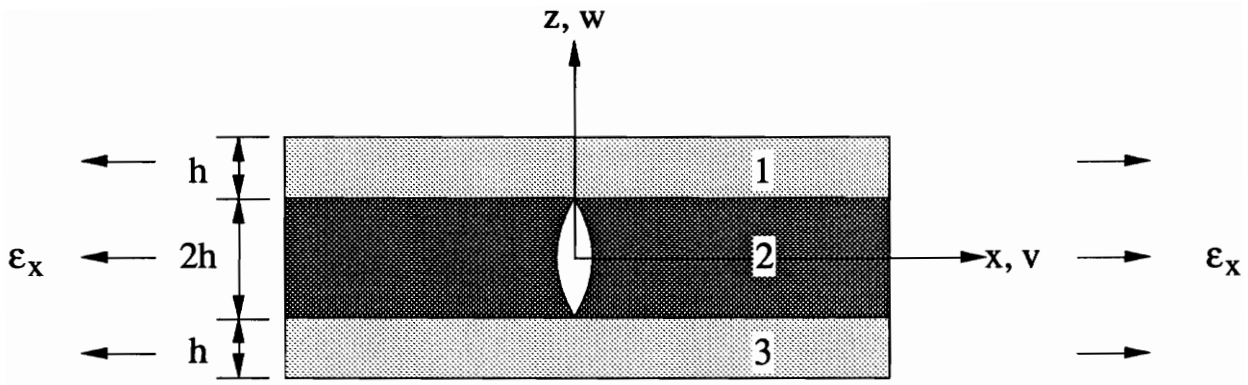

Figure 3.3 Vasiliev's [11] symmetric cracked laminate model.

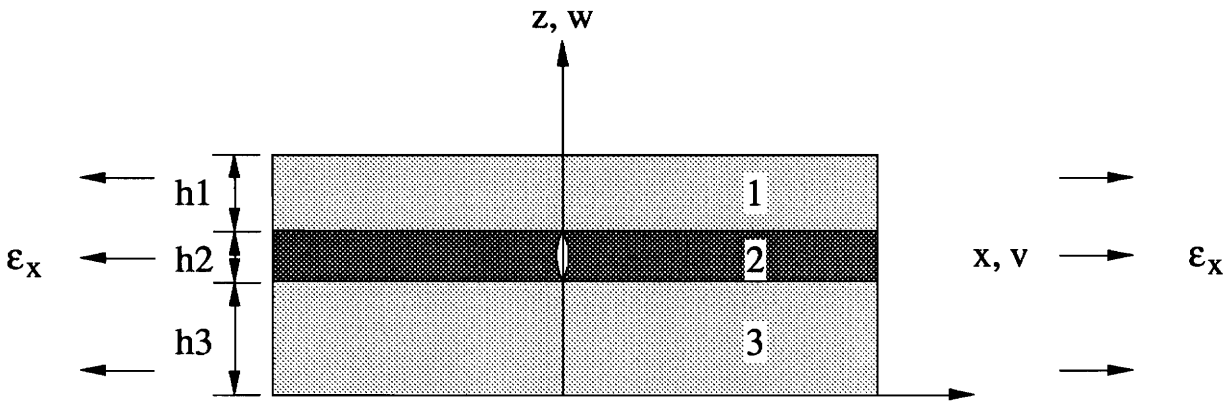

Figure 3.4 More general laminate with crack in 90° ply.

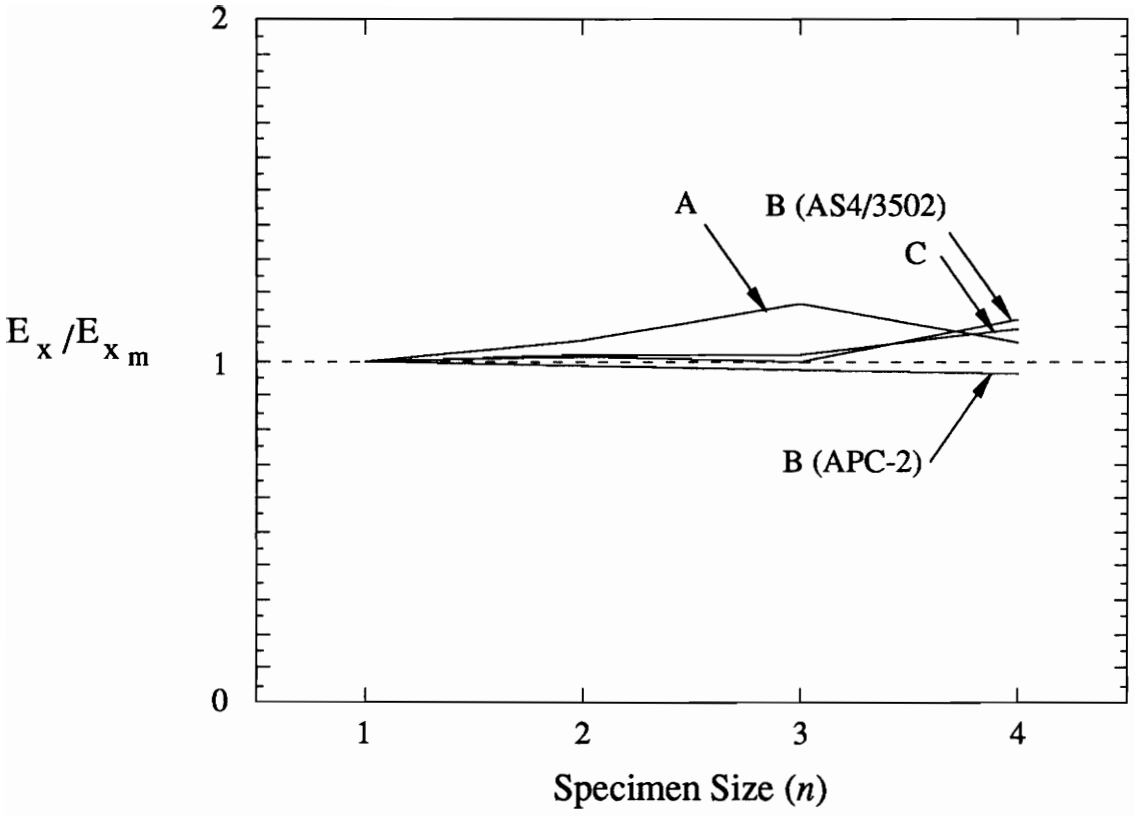

Figure 4.1 Normalized initial modulus for 3-D scaled specimens. When the actual thickness of the specimen was used (as above), variations in stiffness reflect differences in volume fraction.

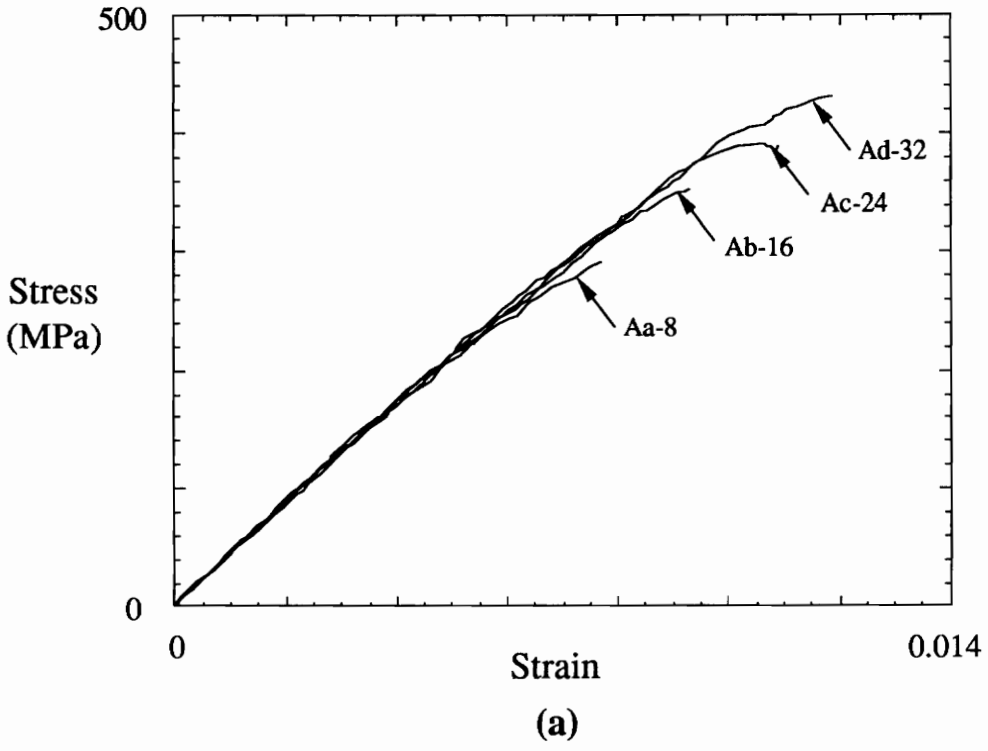

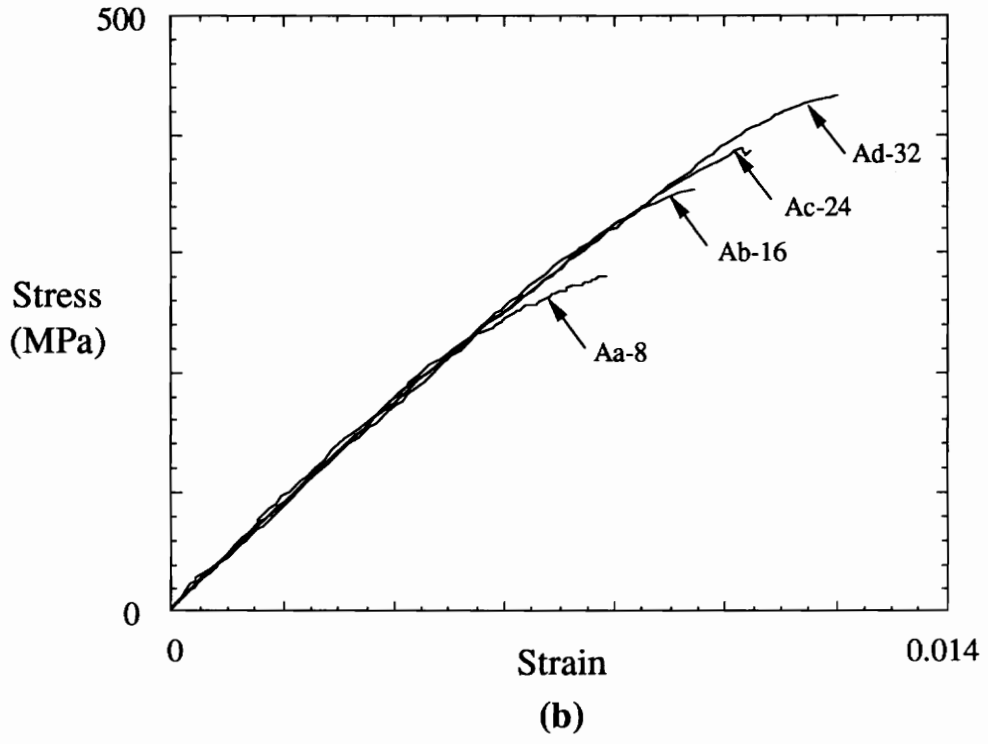

Figure 4.2 Typical stress/strain response of Lay-up *A* 3-D scaled specimens, measured with MTS (a) and custom (b) extensometers.

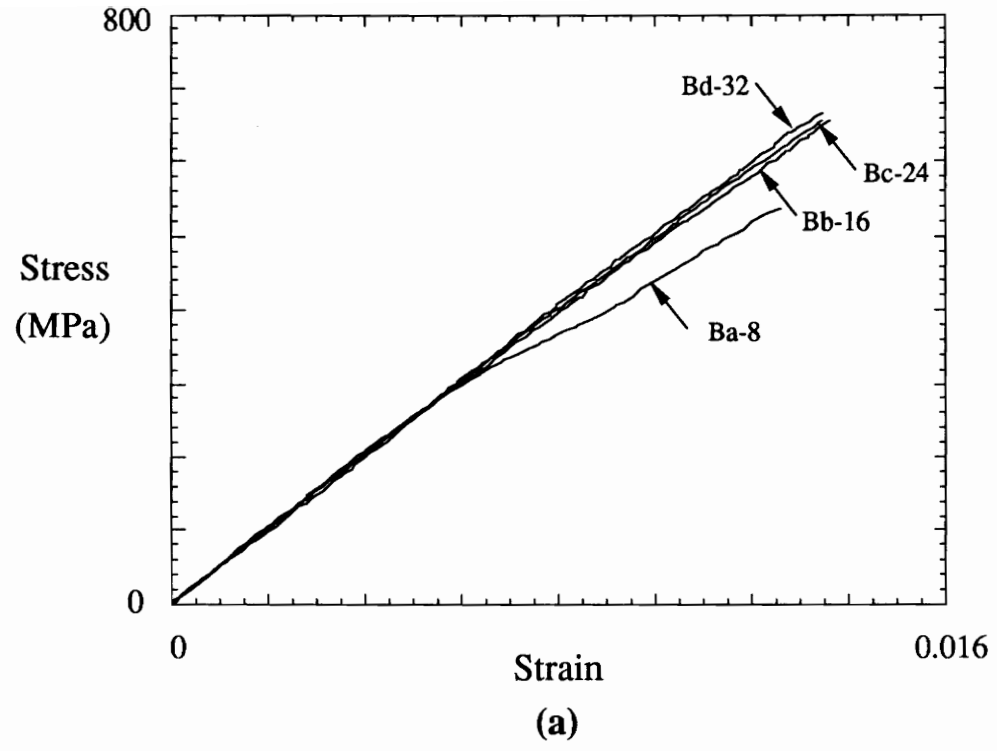

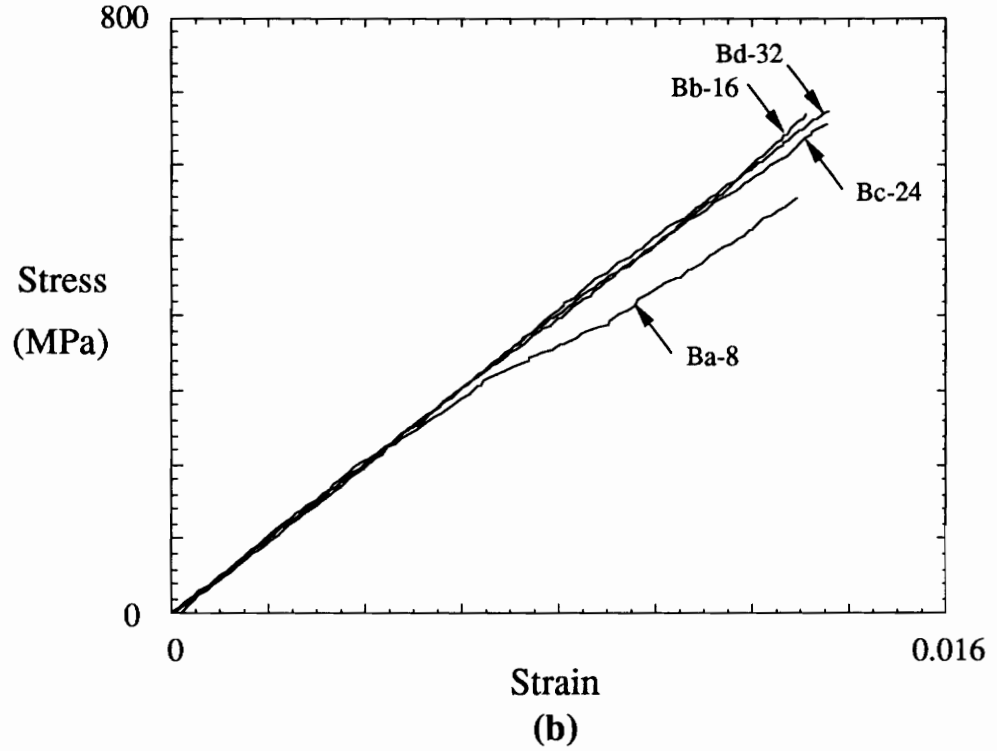

Figure 4.3 Typical stress/strain response of AS4/3502 Lay-up *B* 3-D scaled specimens, measured with MTS (a) and custom (b) extensometers.

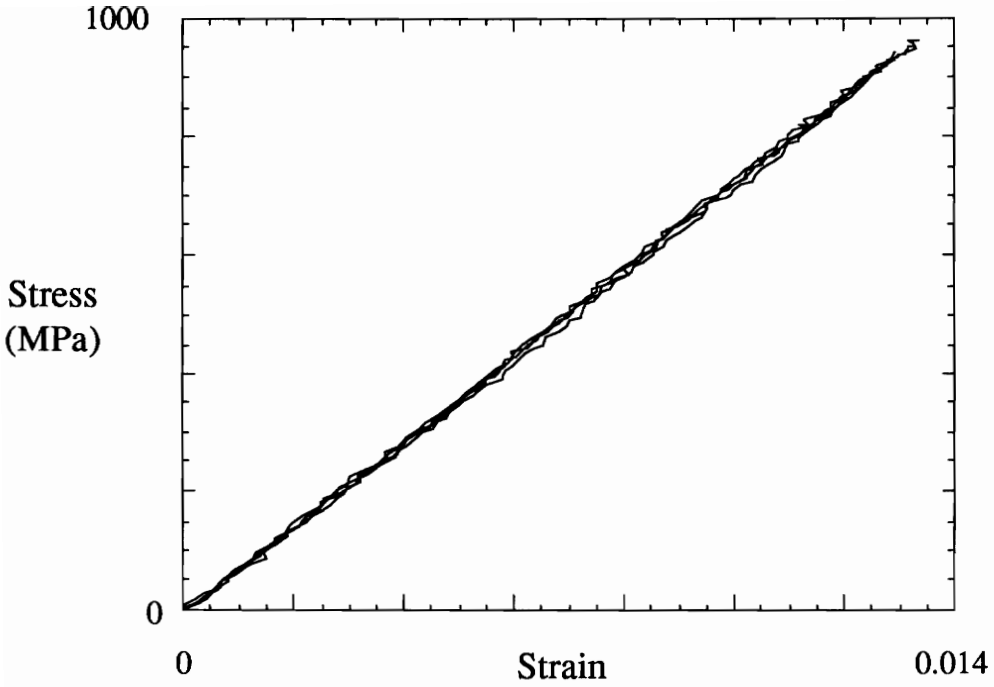

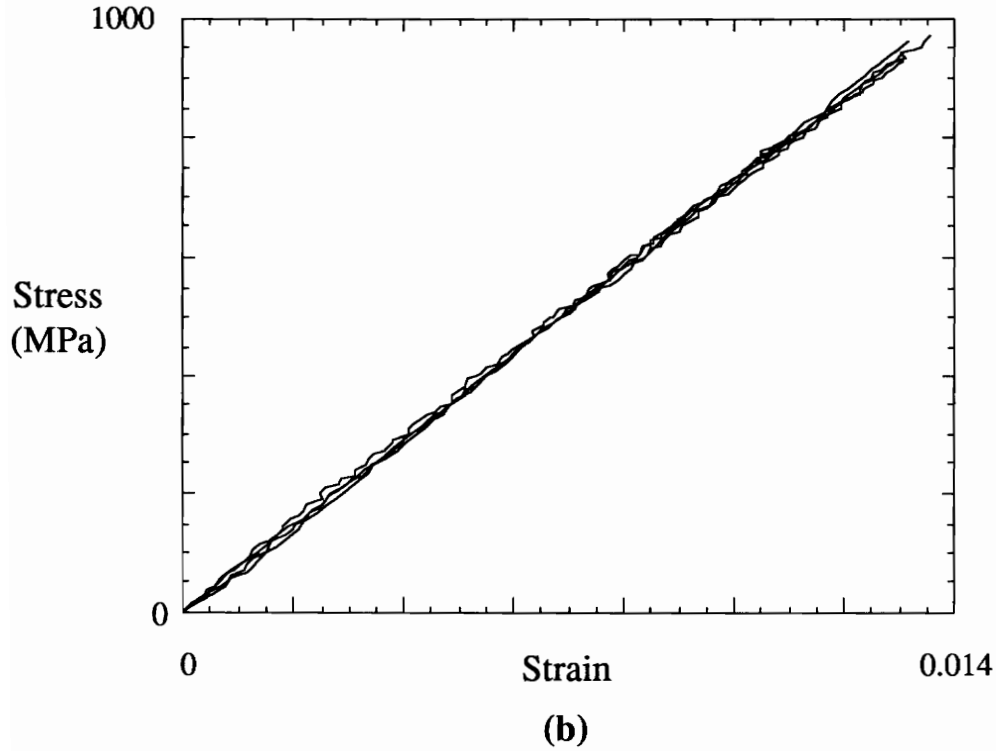

Figure 4.4 Typical stress/strain response of Lay-up *C* 3-D scaled specimens, measured with MTS (a) and custom (b) extensometers.

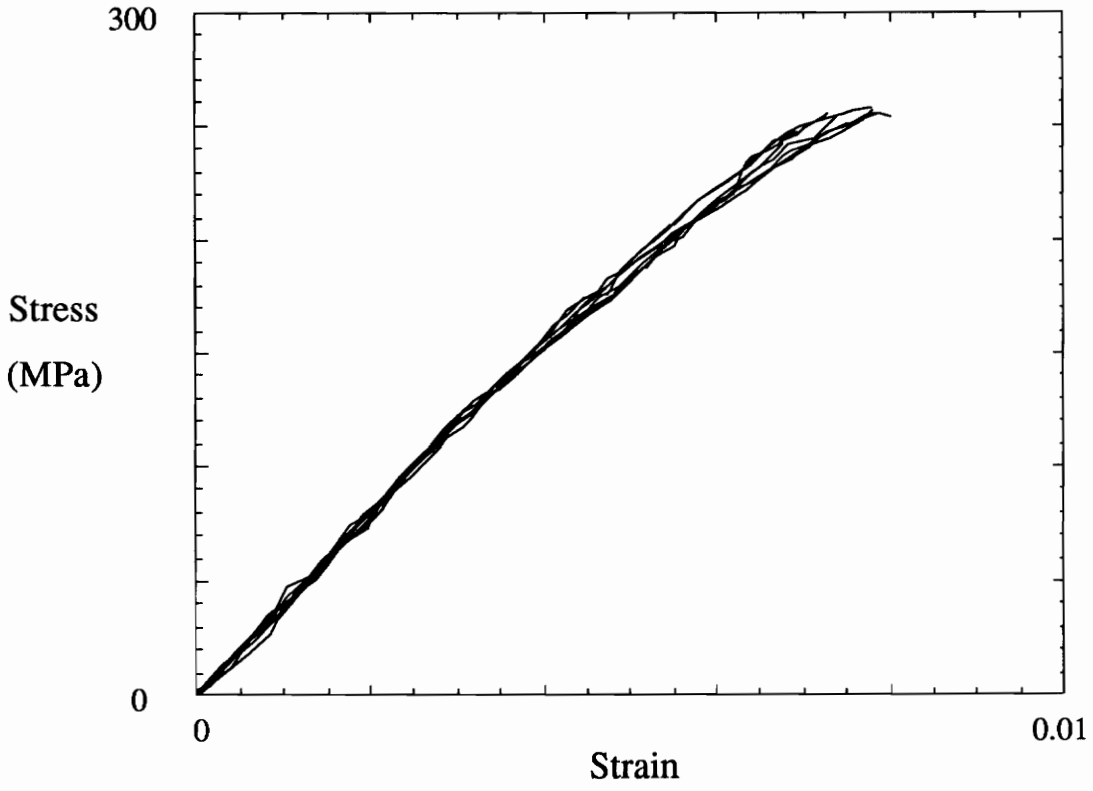

Figure 4.5 Stress/strain plots of all eight *Aa-8* specimens that were tested to failure, showing repeatability of response.

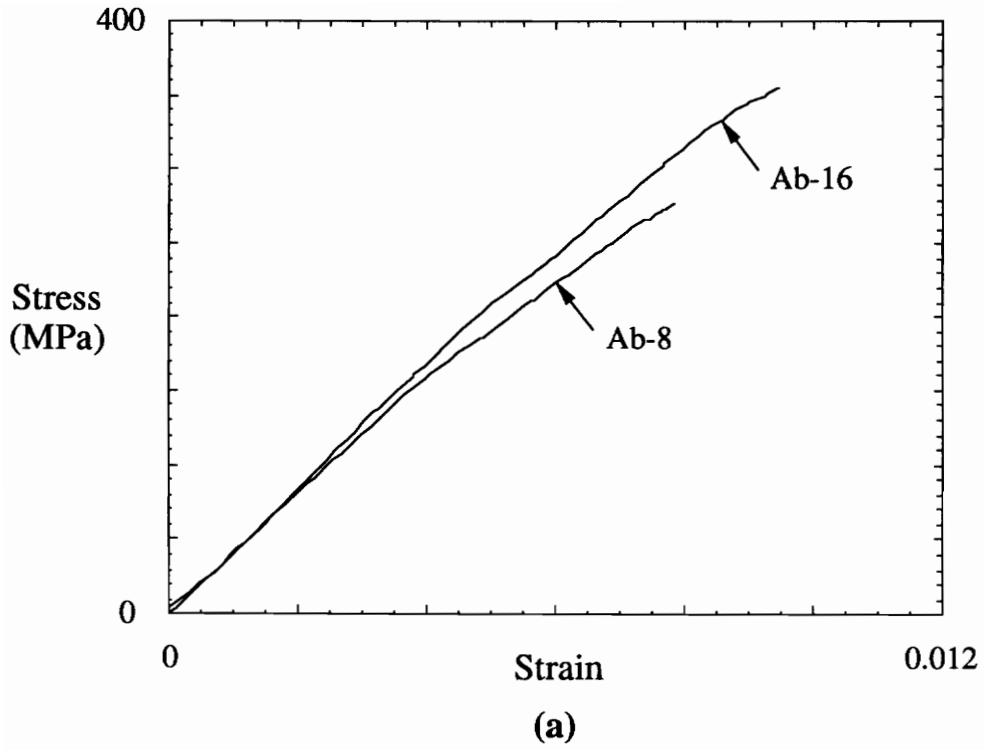

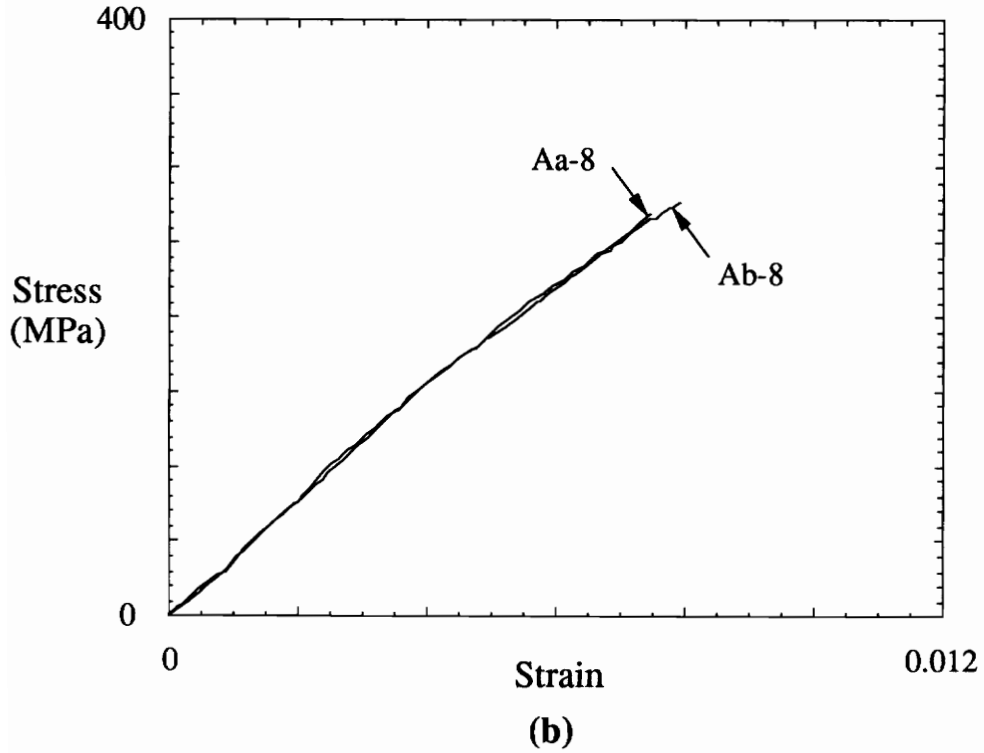

Figure 4.6 1-D (a) and 2-D (b) scaling of Lay-up *A* specimens.

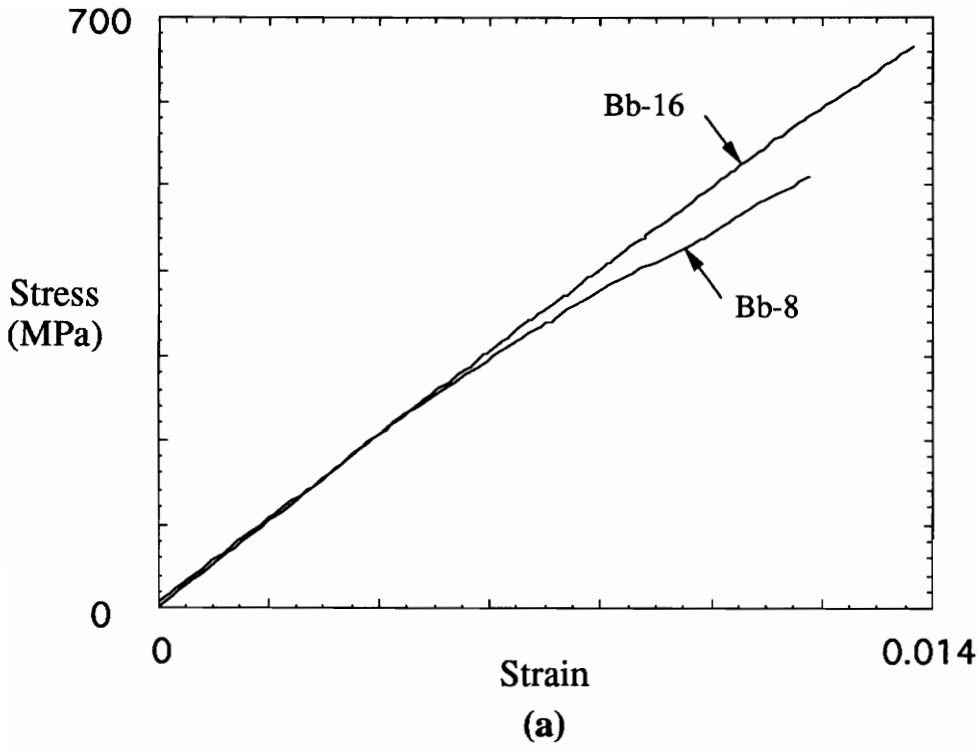

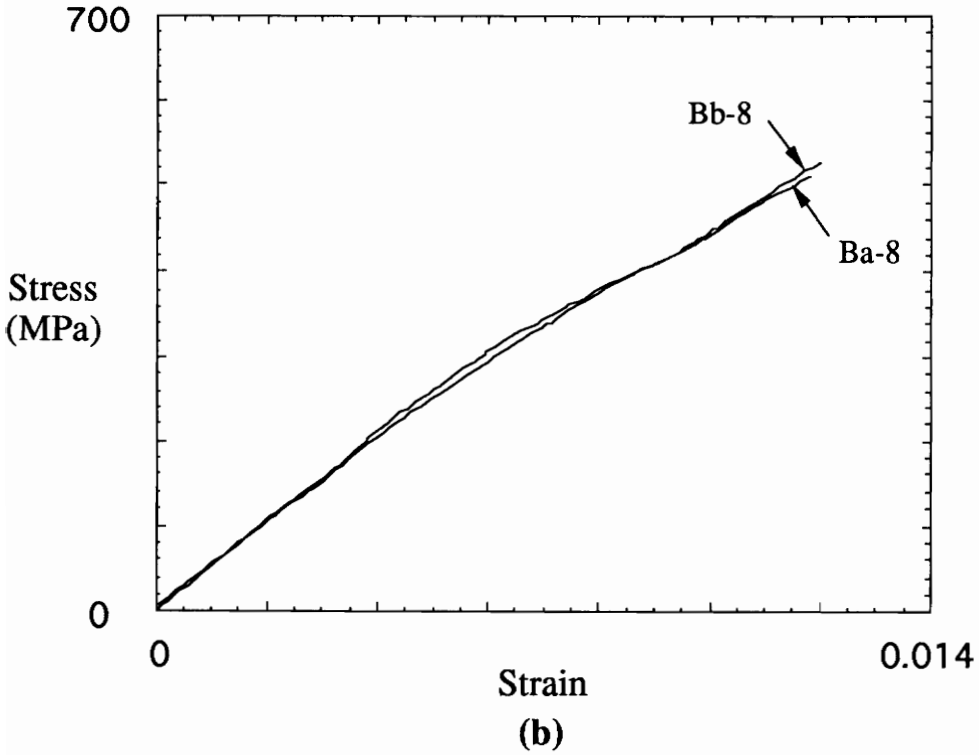

Figure 4.7 1-D (a) and 2-D (b) scaling of AS4/3502 Lay-up *B* specimens.

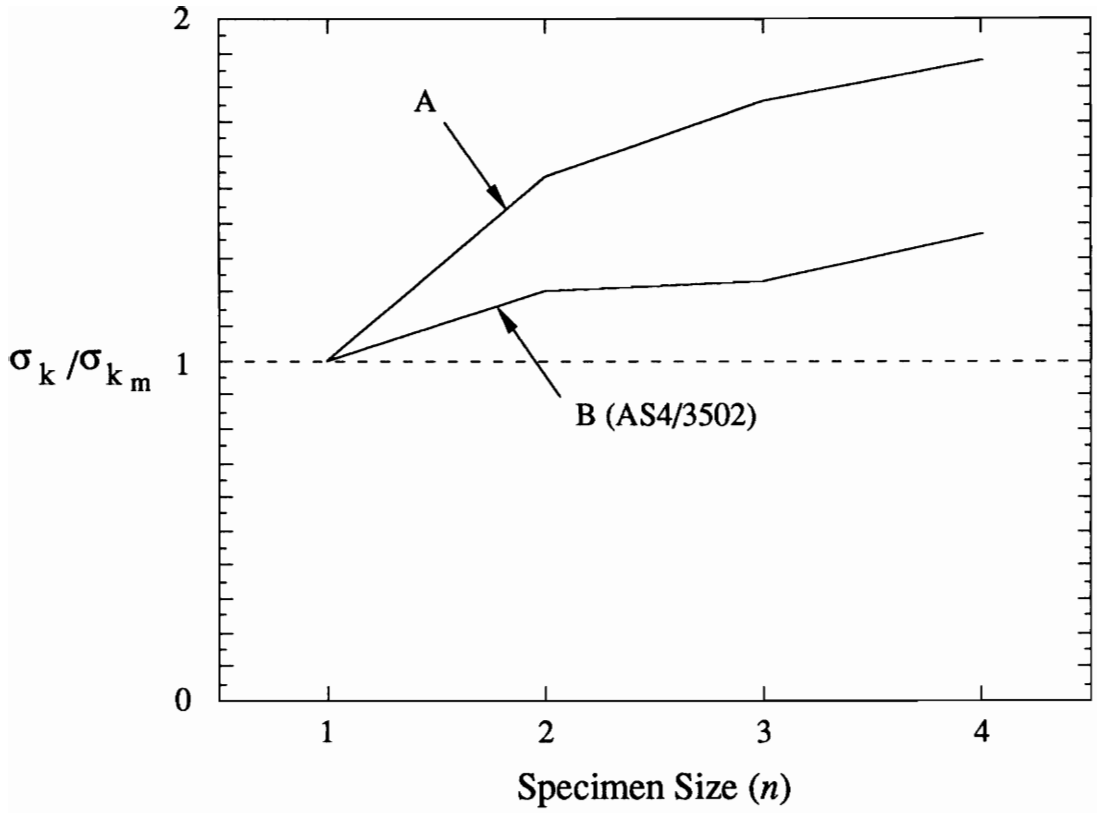

Figure 4.8 Normalized non-linear knee stress for 3-D scaled specimens.

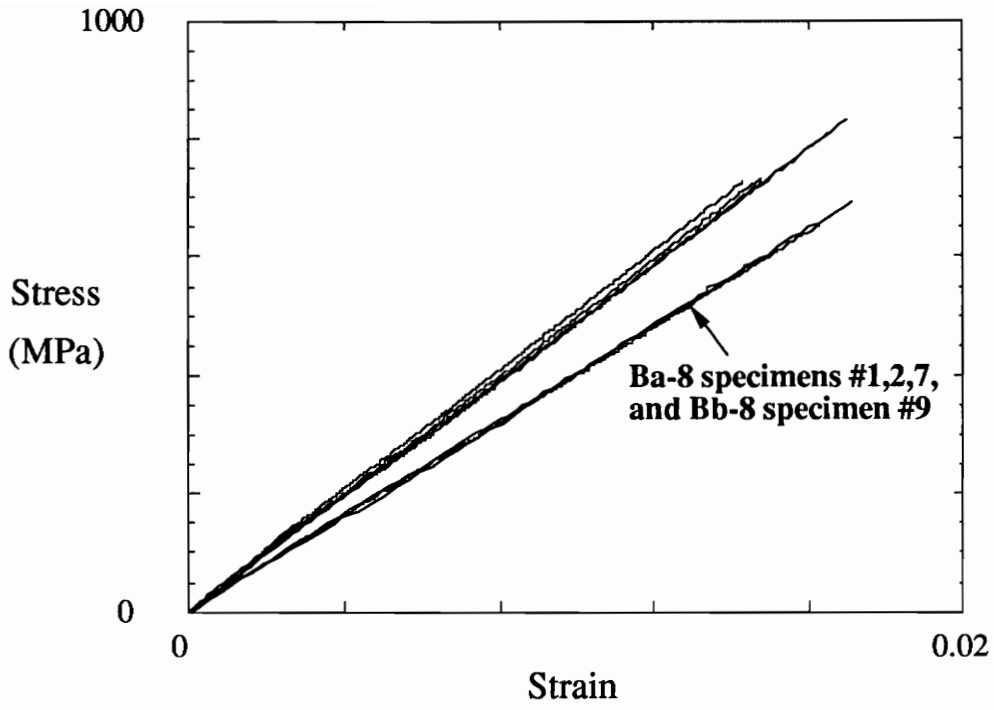

Figure 4.9 APC-2 stress/strain plots showing variability of response. All specimens were cut from the [±45/0/90]s panel.

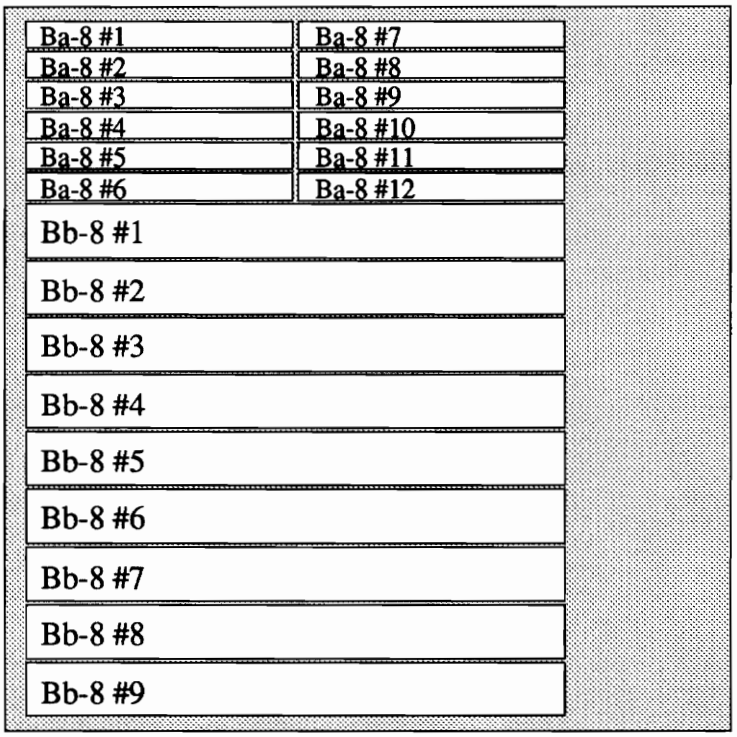

Figure 4.10 APC-2 [±45/0/90]s panel showing position of specimens.

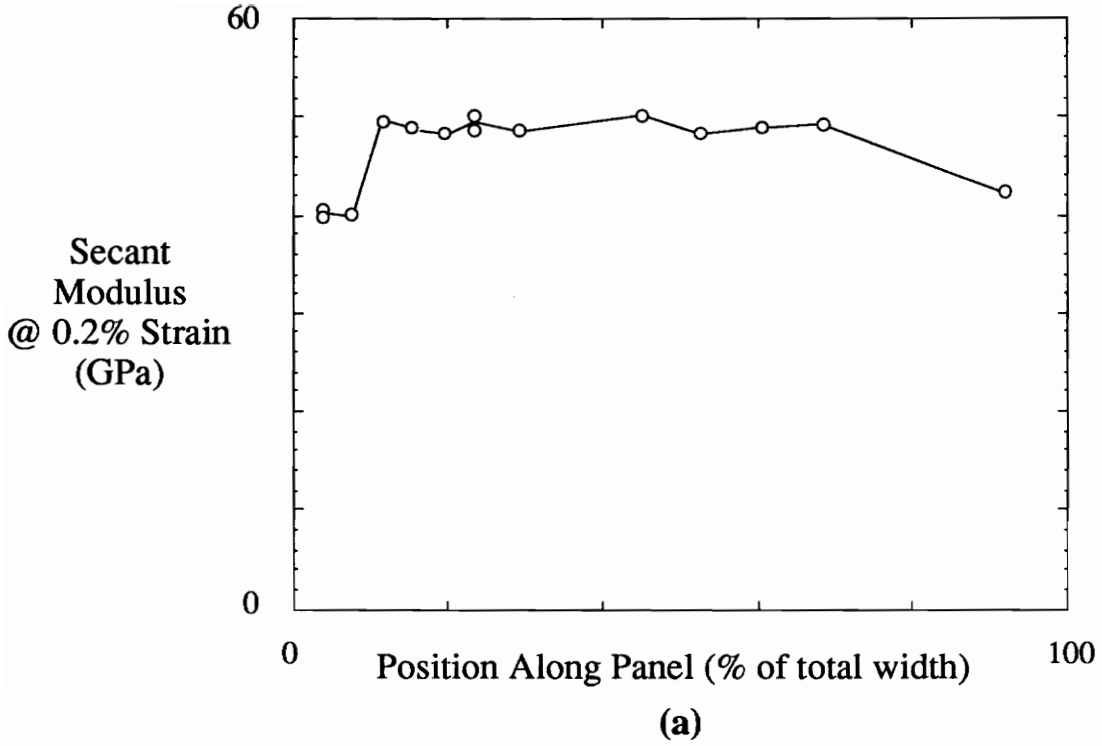

(a)

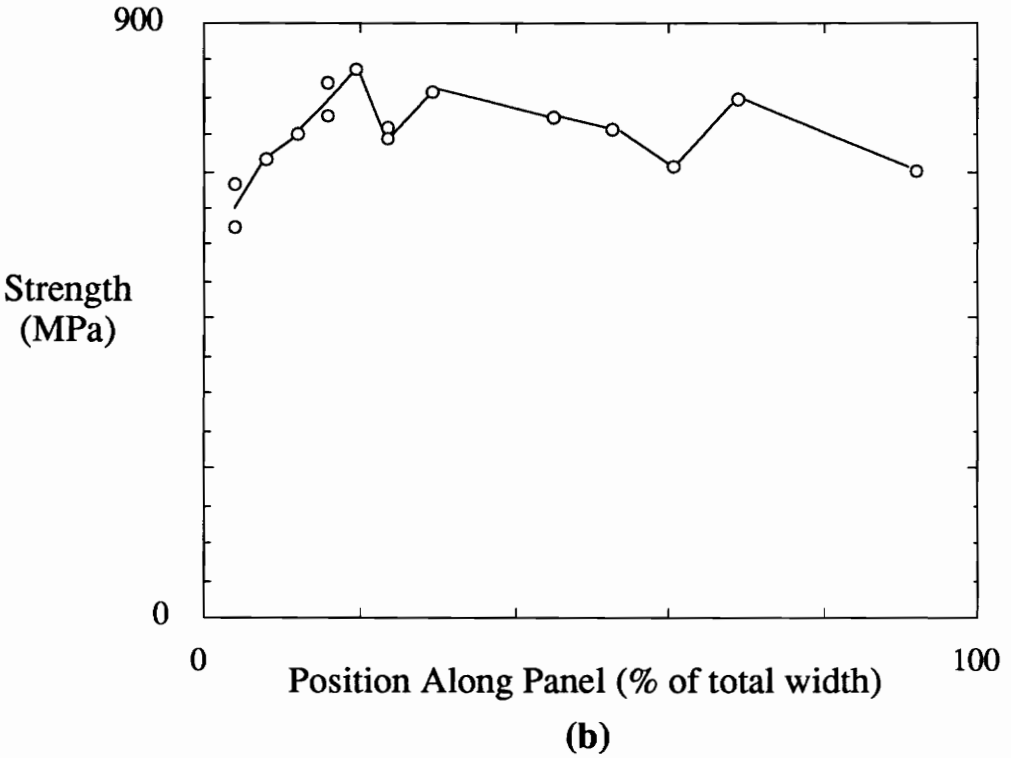

(b)

Figure 4.11 Initial modulus (a) and ultimate stress (b) of APC-2 specimens vs. position in panel.

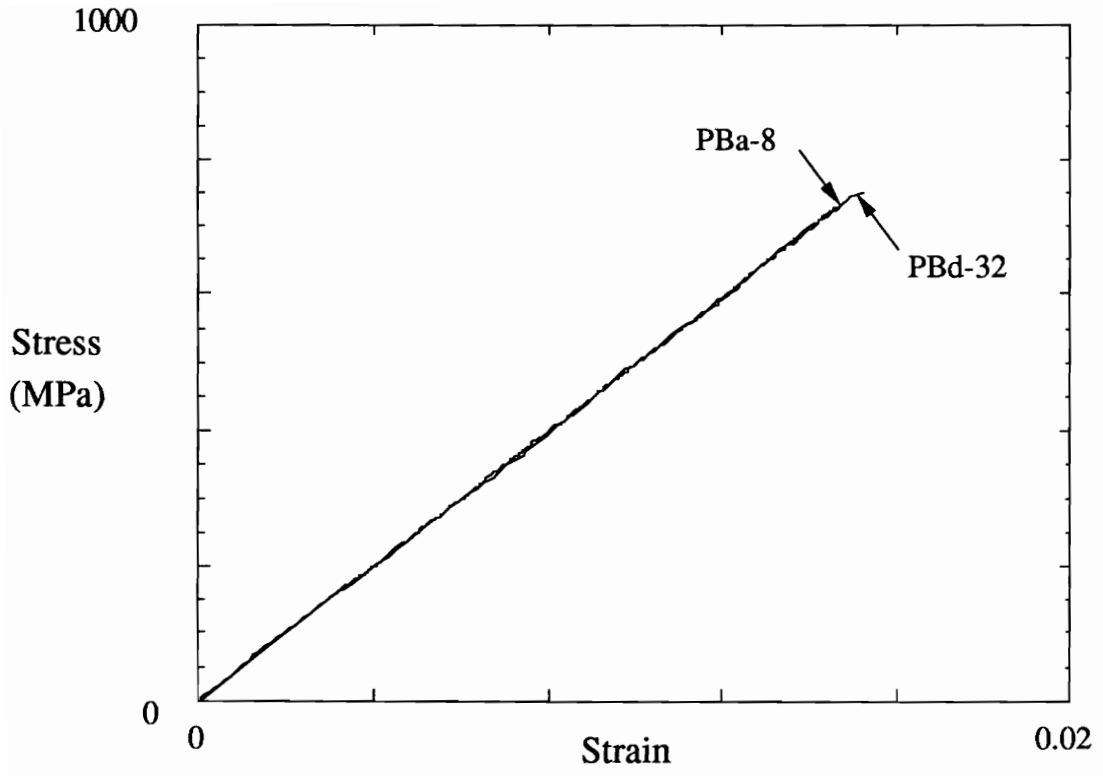

Figure 4.12 Typical stress/strain response of APC-2 3-D scaled specimens showing identical response of *Ba-8* and *Bd-32* specimens.

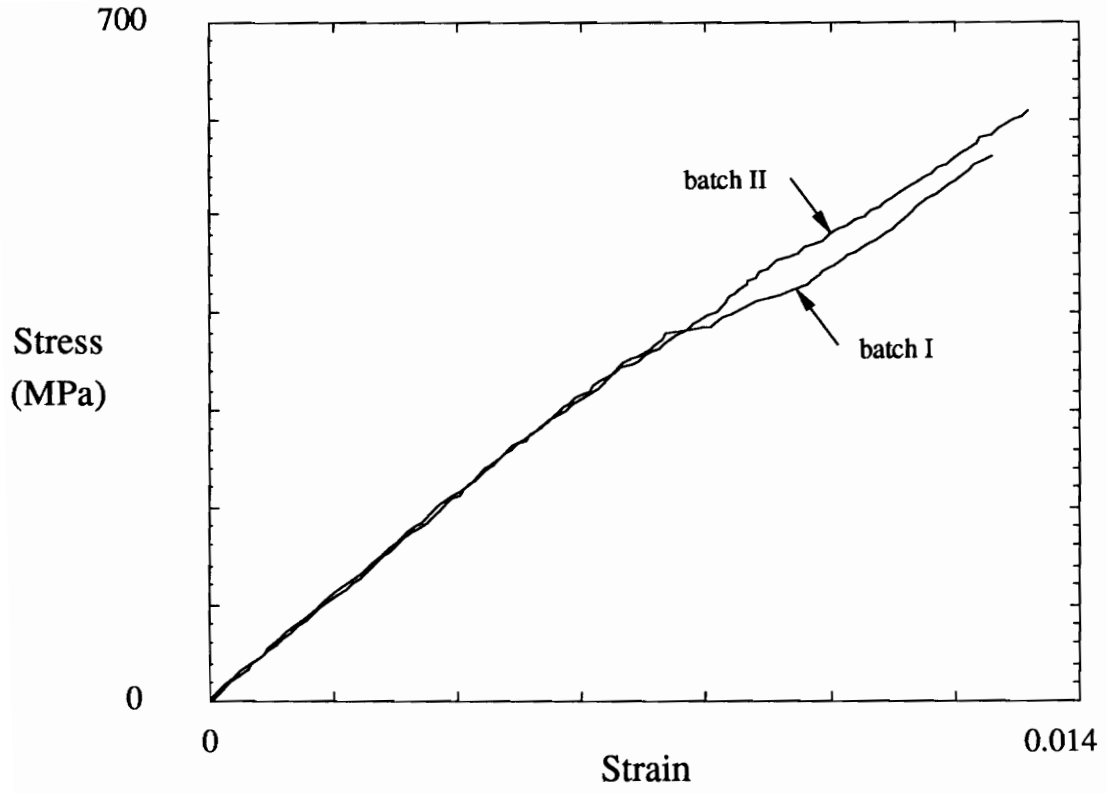

Figure 4.13 Batch *I* and batch *II* stress/strain response of two AS4/3502 *Ba-8* specimens.

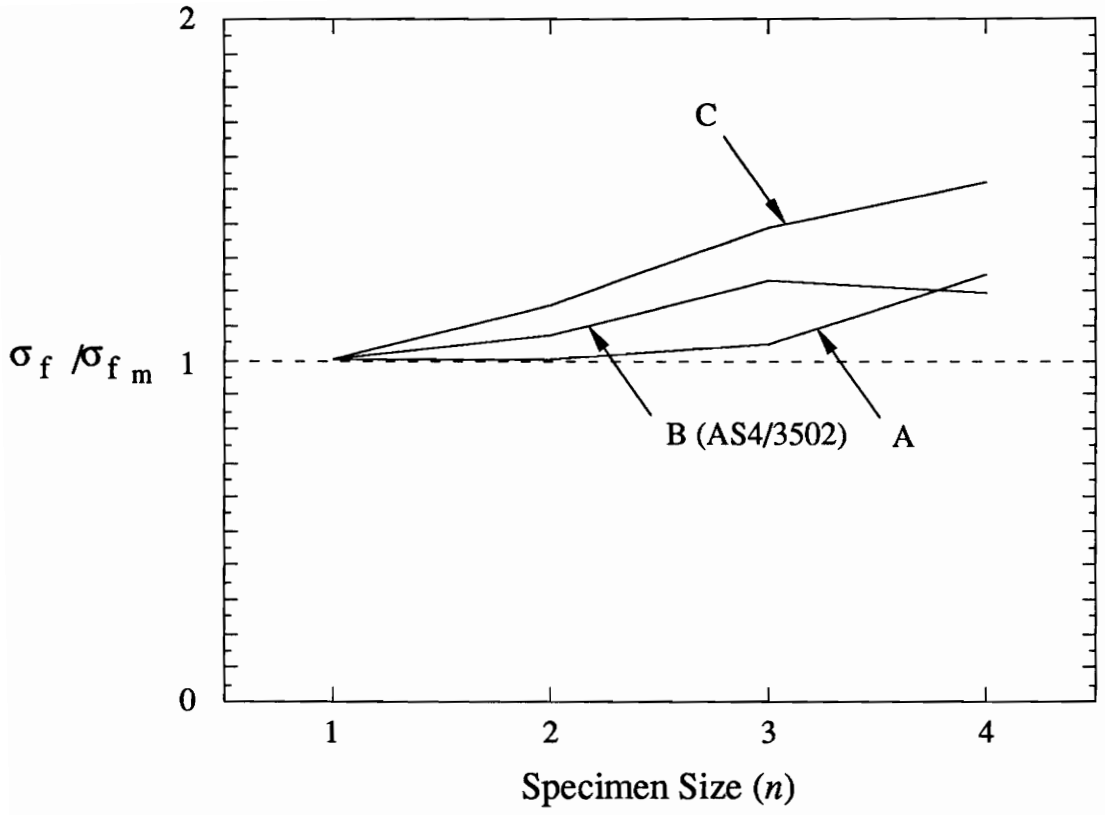

Figure 4.14 Normalized first ply failure for 3-D scaled specimens.

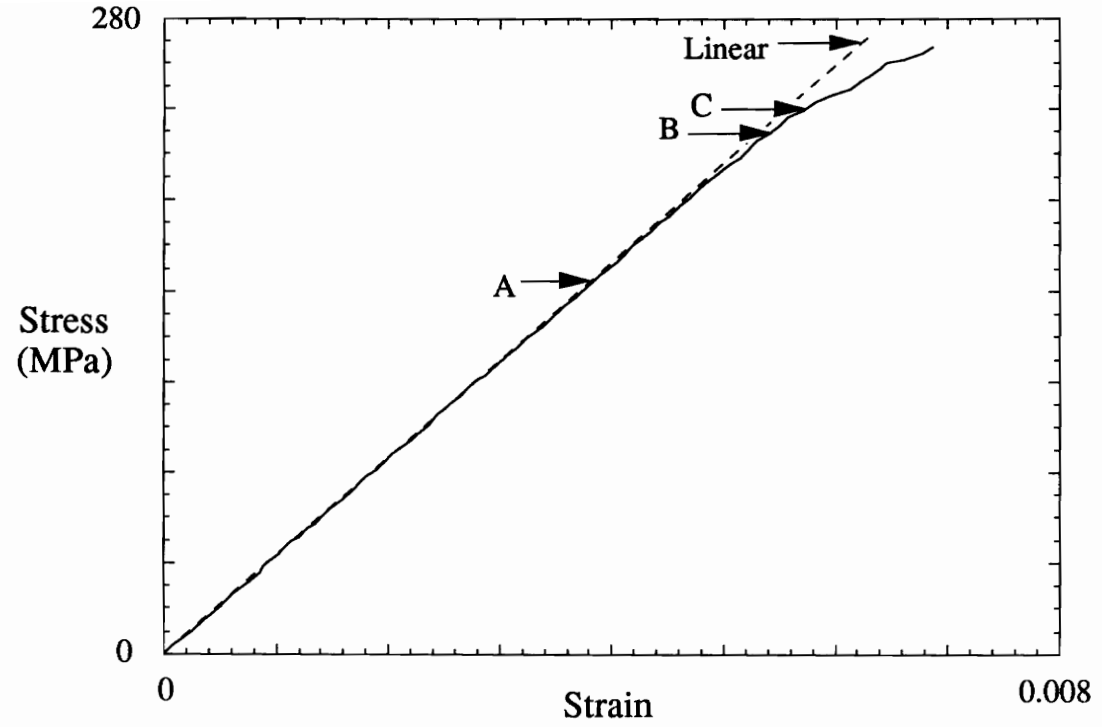

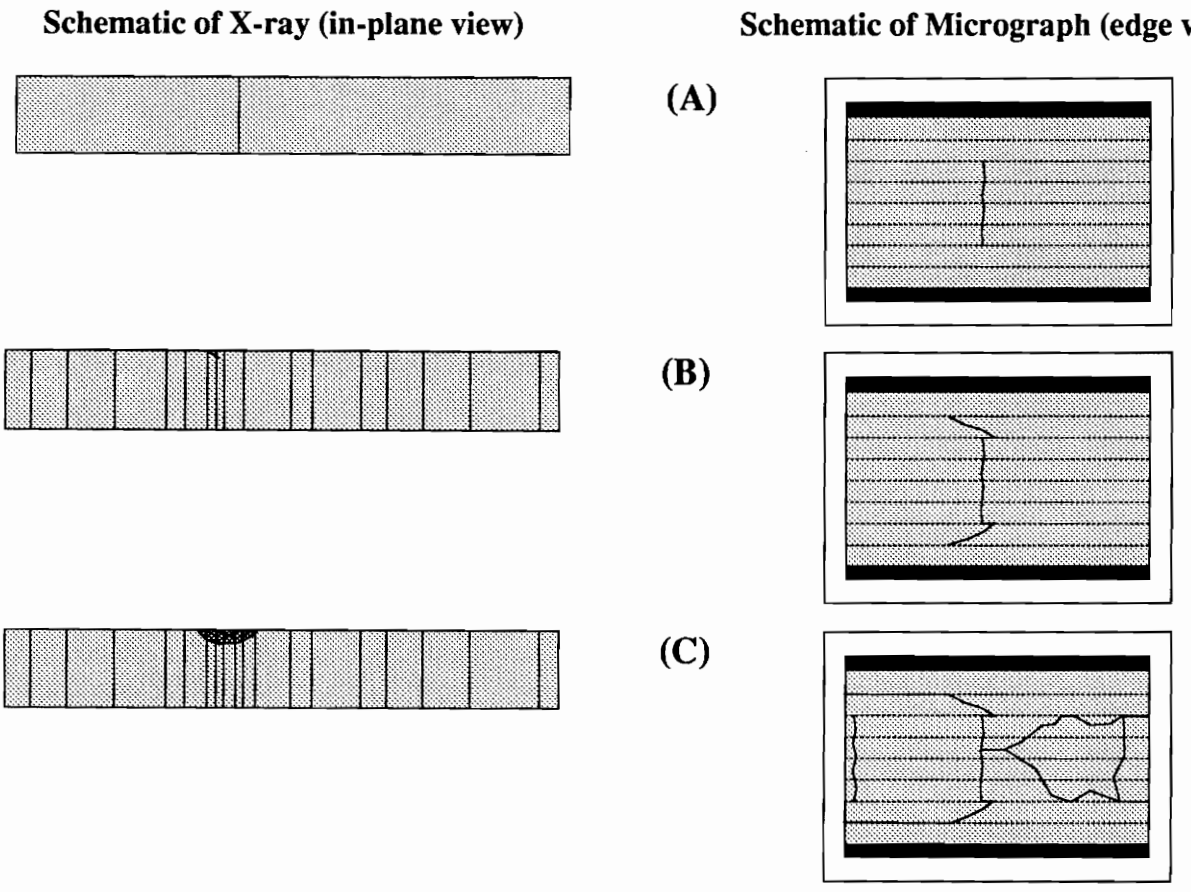

Figure 4.15 Stress/strain response of *Aa-8* specimen with damage modes indicated.

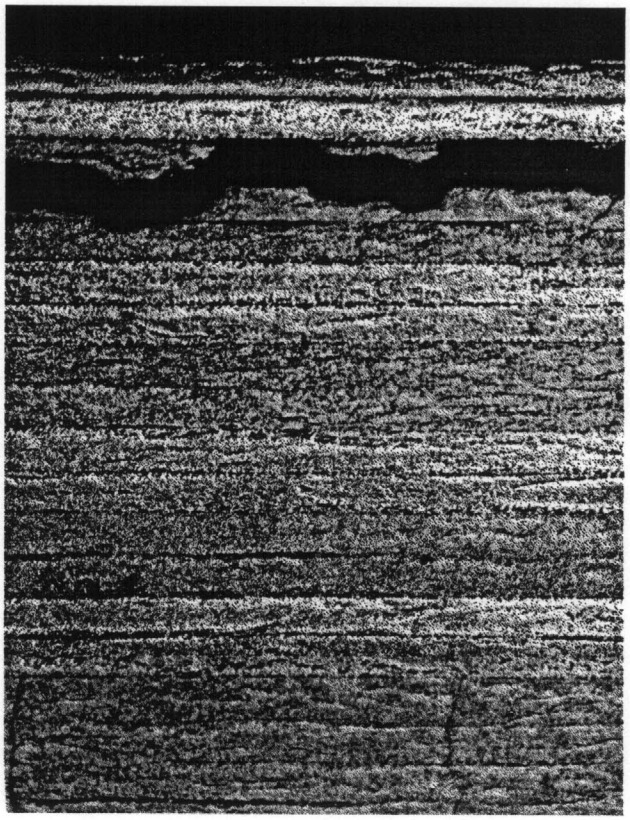

Figure 4.16 Micrograph of outer 90° delamination in an *Ad-32* specimen.

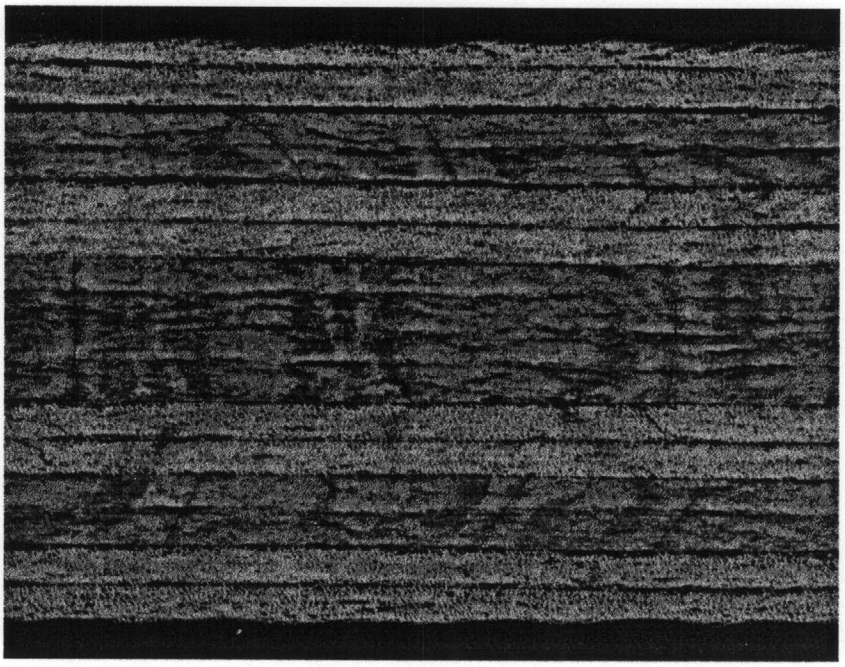

Figure 4.17 Cracks in outermost 90° ply in an *Ad-32* specimen, showing characteristic oblique angle.

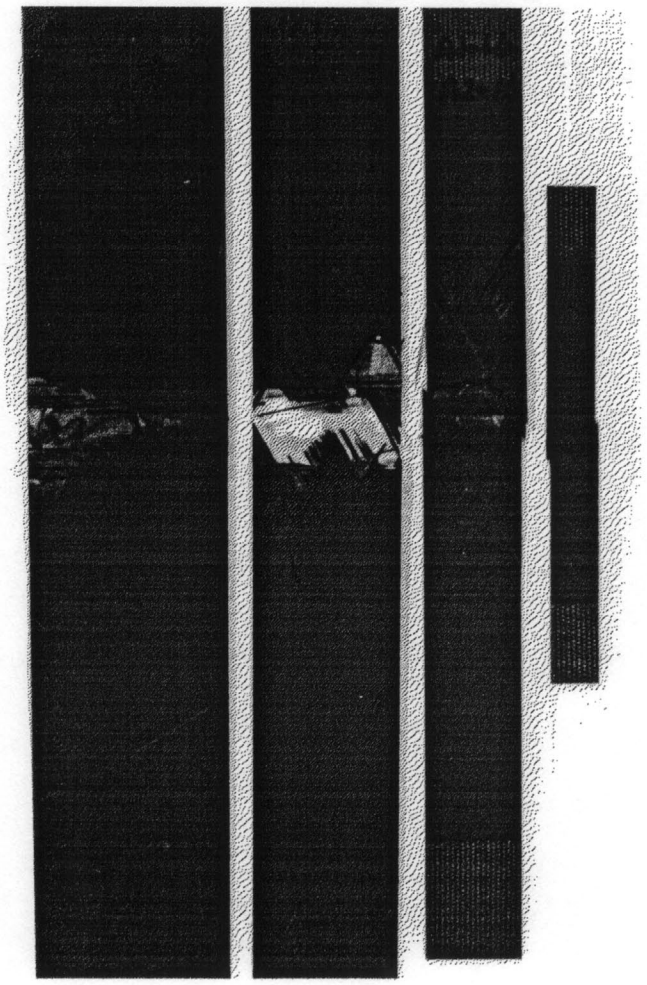

Figure 4.18 Lay-up *A* specimens showing final failure modes.

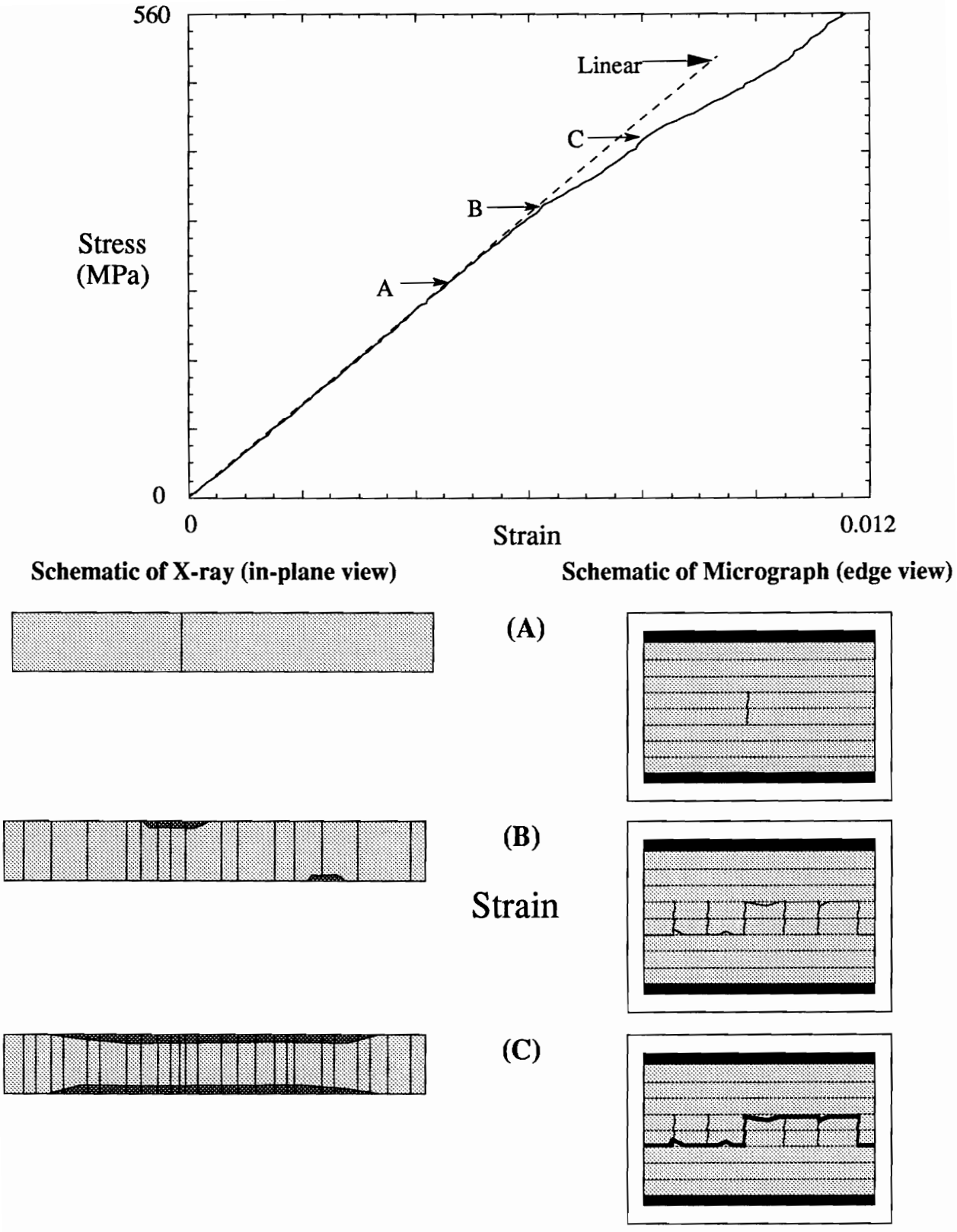

Figure 4.19 Stress/strain response of AS4/3502 *Ba-8* specimen with damage modes indicated.

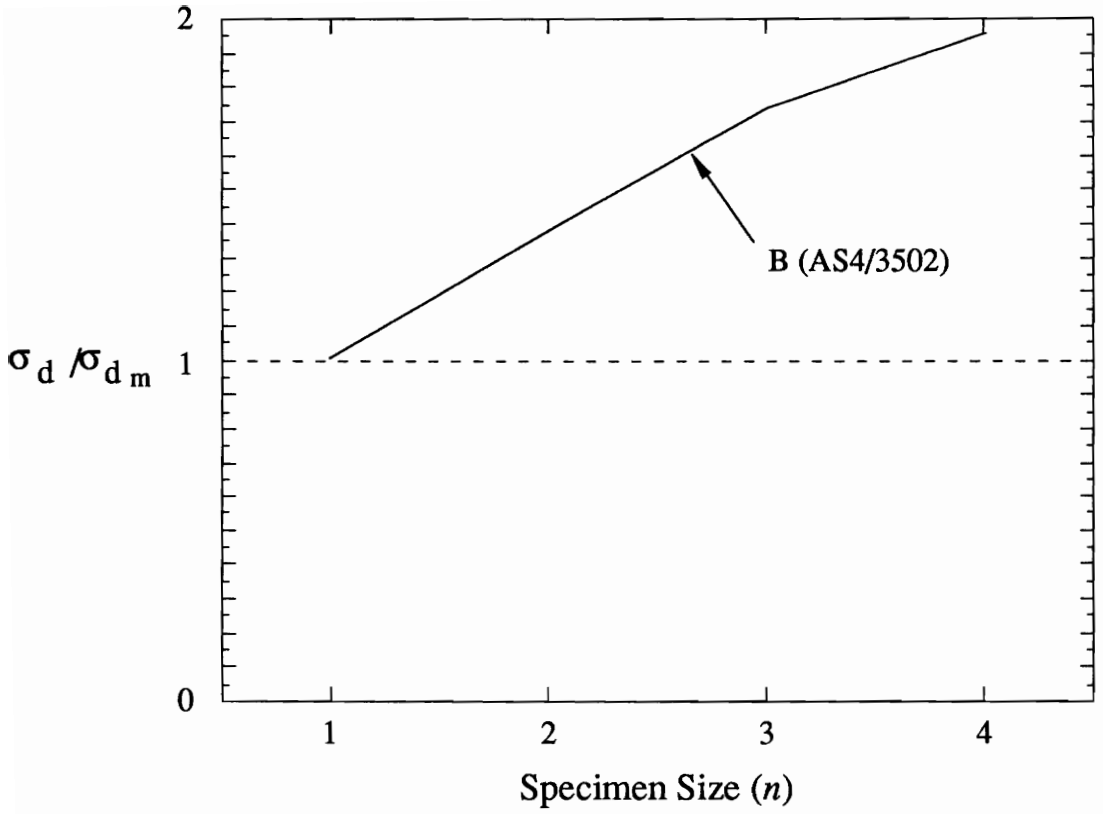

Figure 4.20 Normalized delamination knee stress for 3-D scaled AS4/3502 Lay-up *B* specimens.

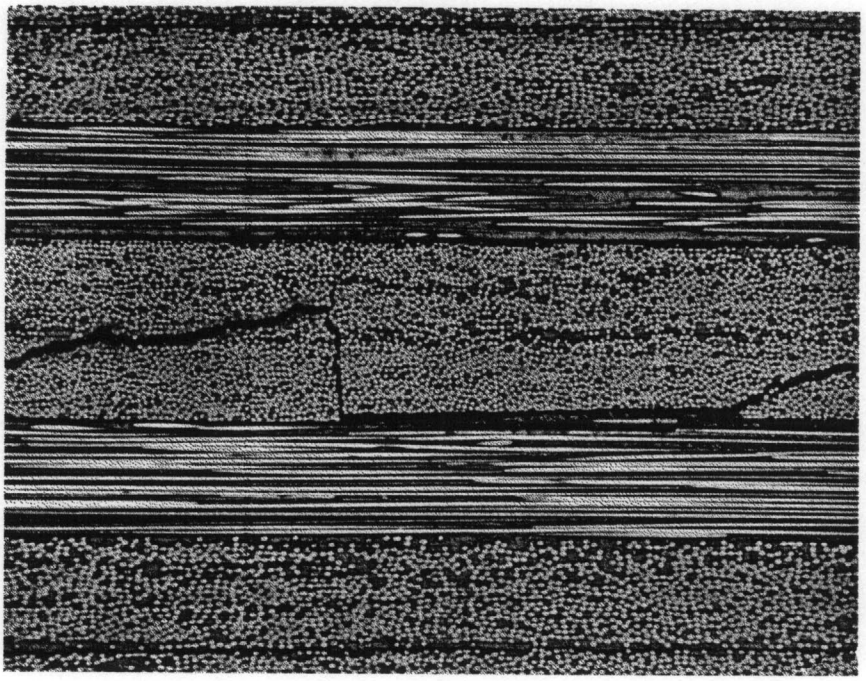

Figure 4.21 Micrograph of central 90° delamination in a Bd-32 specimen

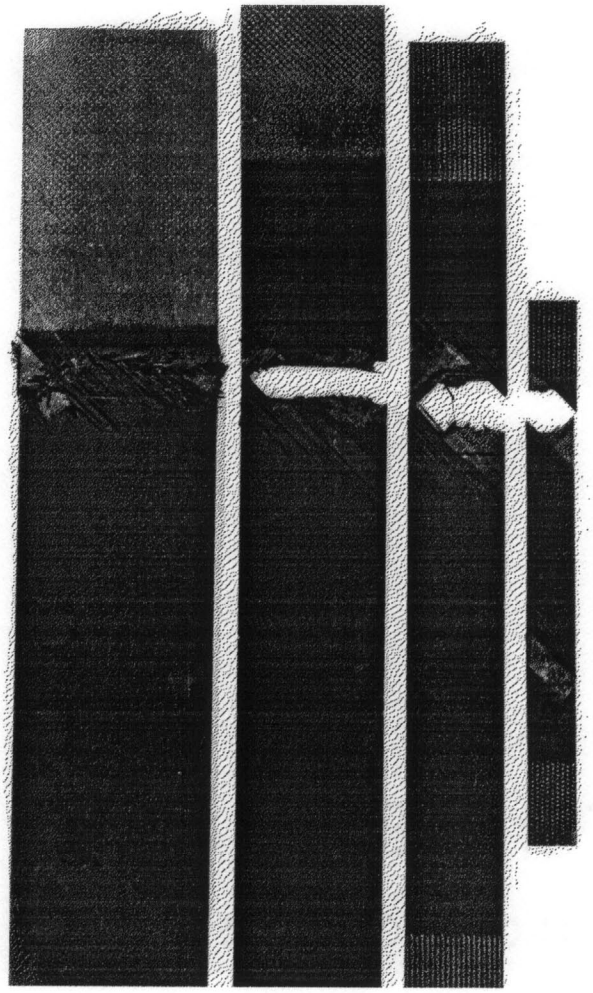

Figure 4.22 Lay-up *B* specimens showing final failure modes.

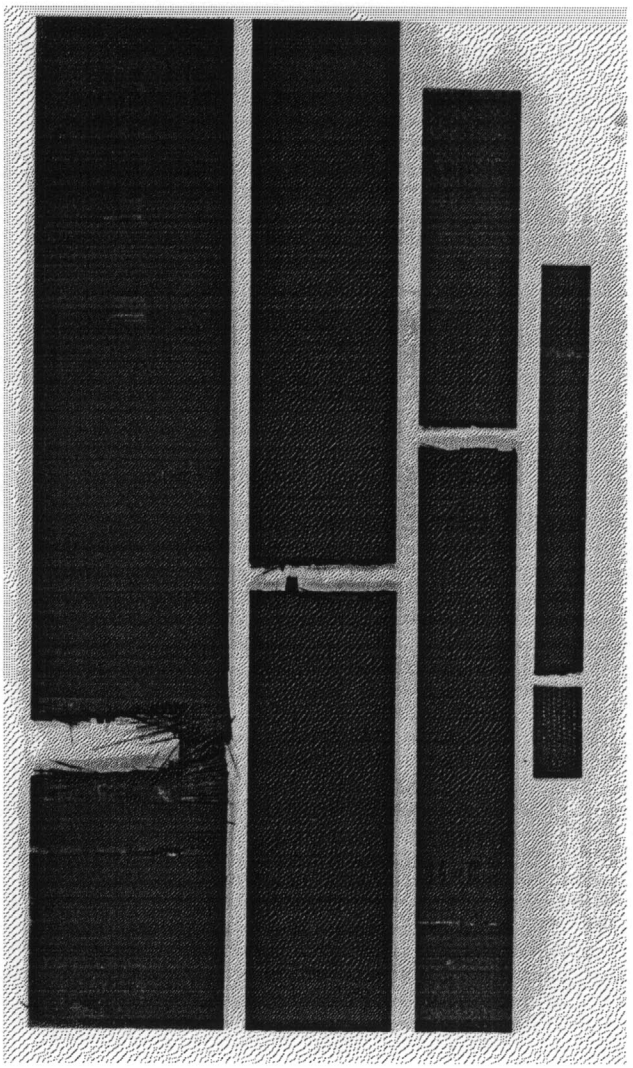

Figure 4.23 Lay-up *C* specimens showing final failure modes.

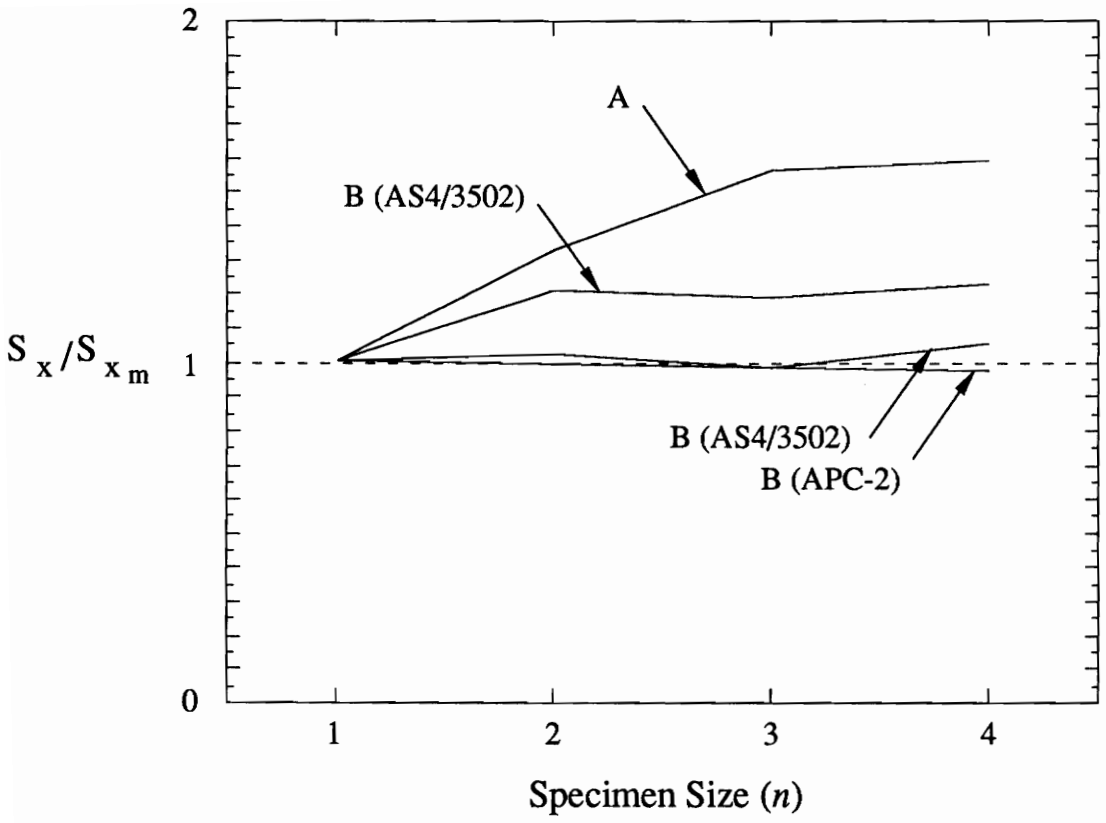

Figure 4.25 Normalized strength for 3-D scaled specimens.

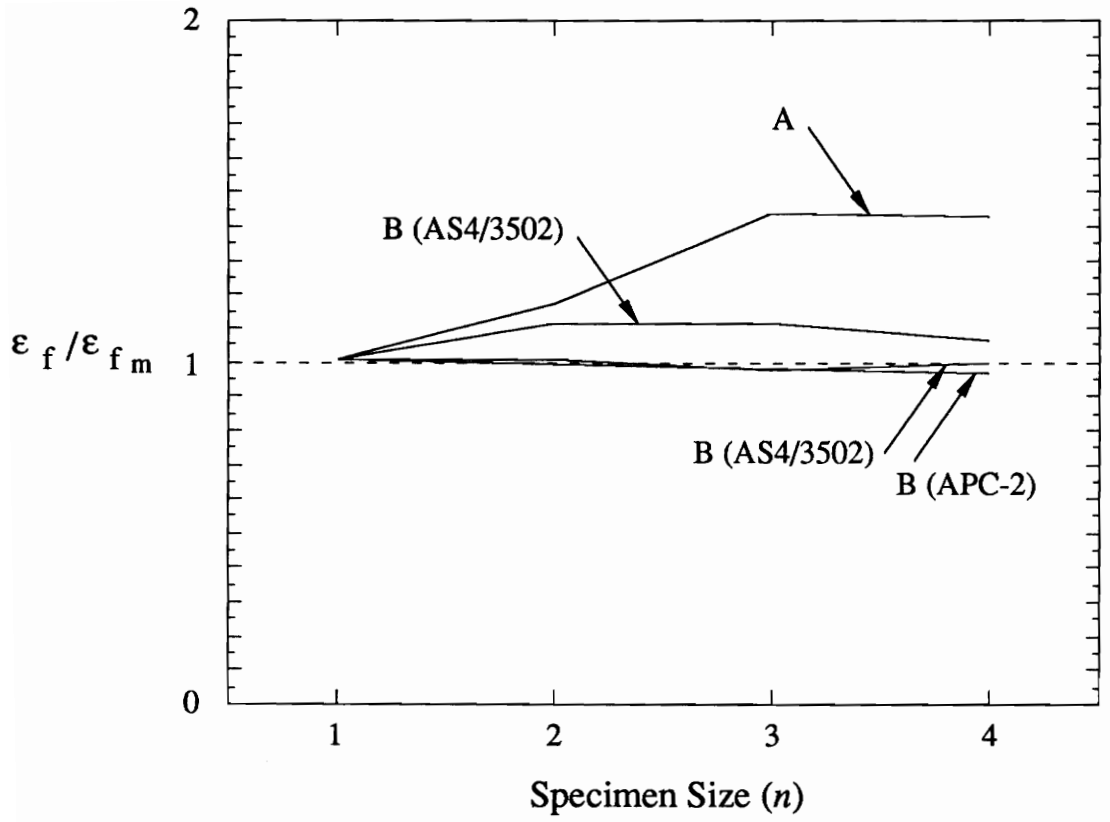

Figure 4.26 Normalized strain to failure for 3-D scaled specimens.

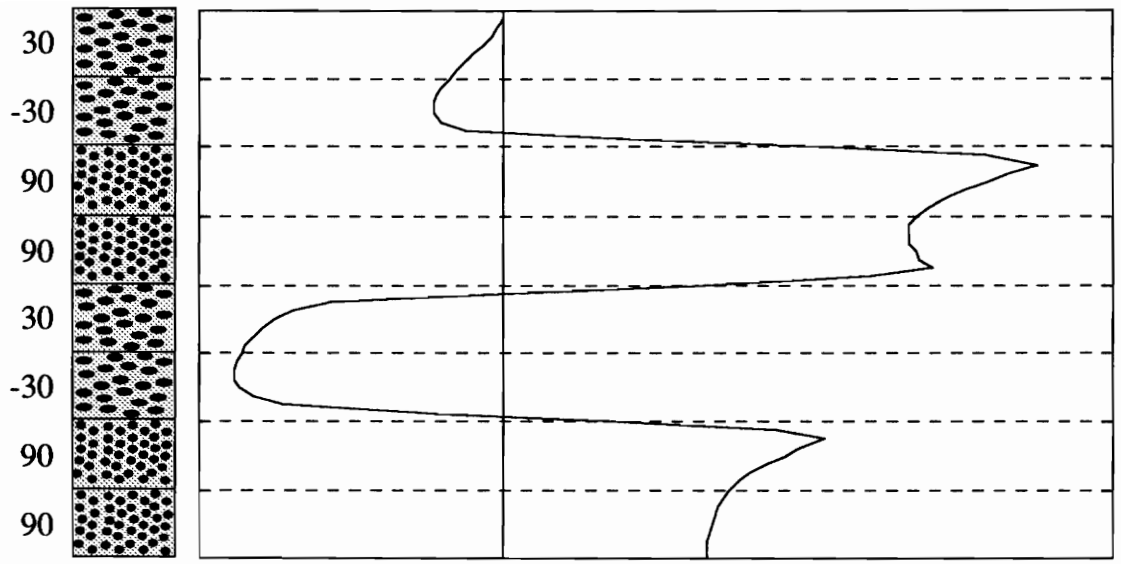

(a)

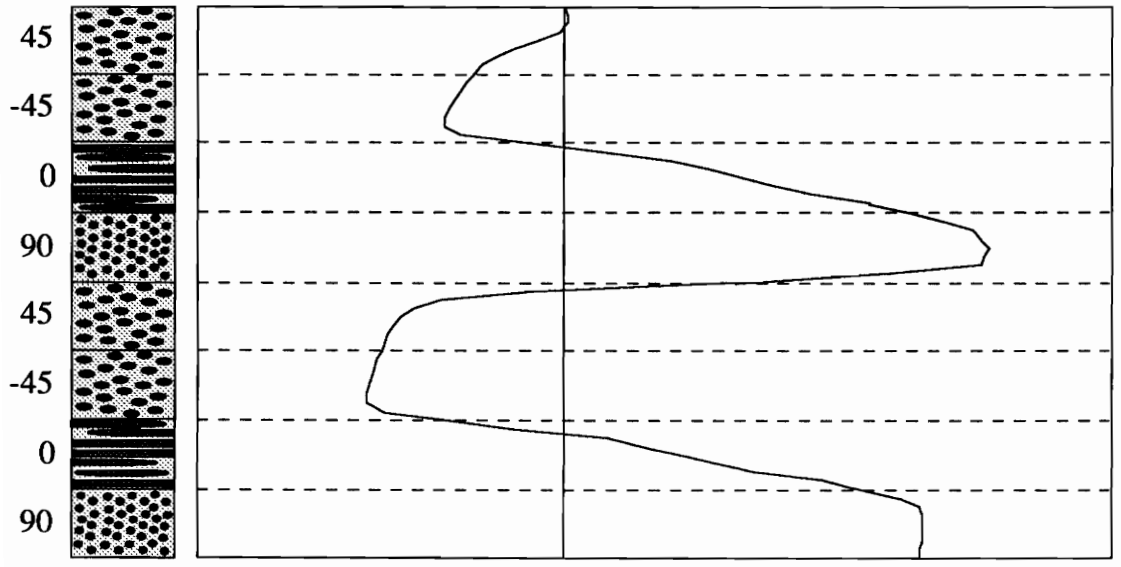

(b)

Figure 4.27 Finite element results showing through-the-thickness stress σ_z for Lay-up *A* (a) and *B* (b).

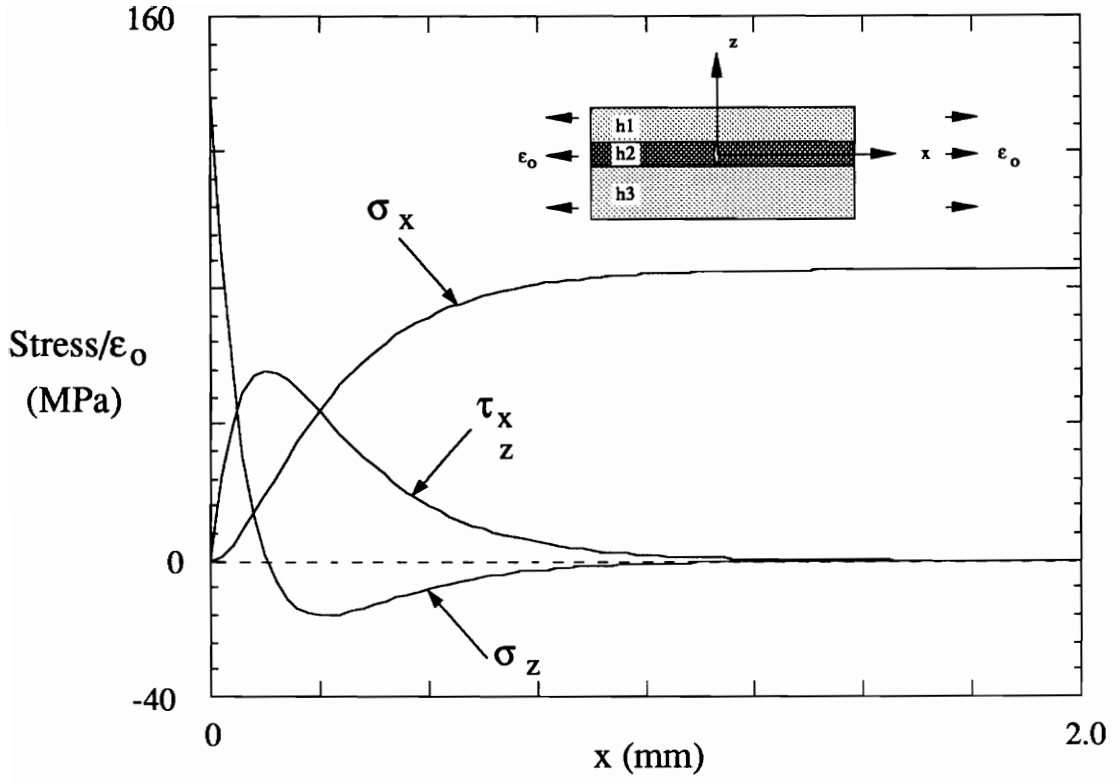

Figure 4.28 Analytical model results showing normal and shear stresses in 90° ply near crack.

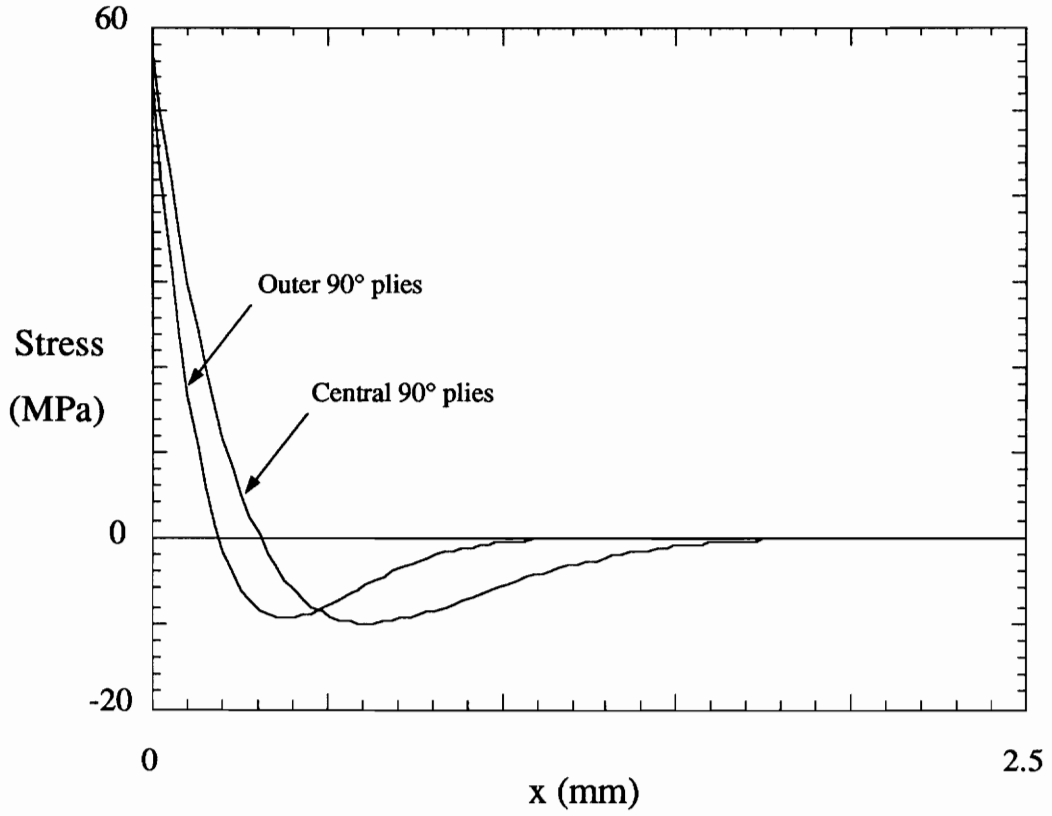

Figure 4.29 Analytical model results showing σ_z in a *Bb-16* specimen due to cracks in the central and outer 90° plies

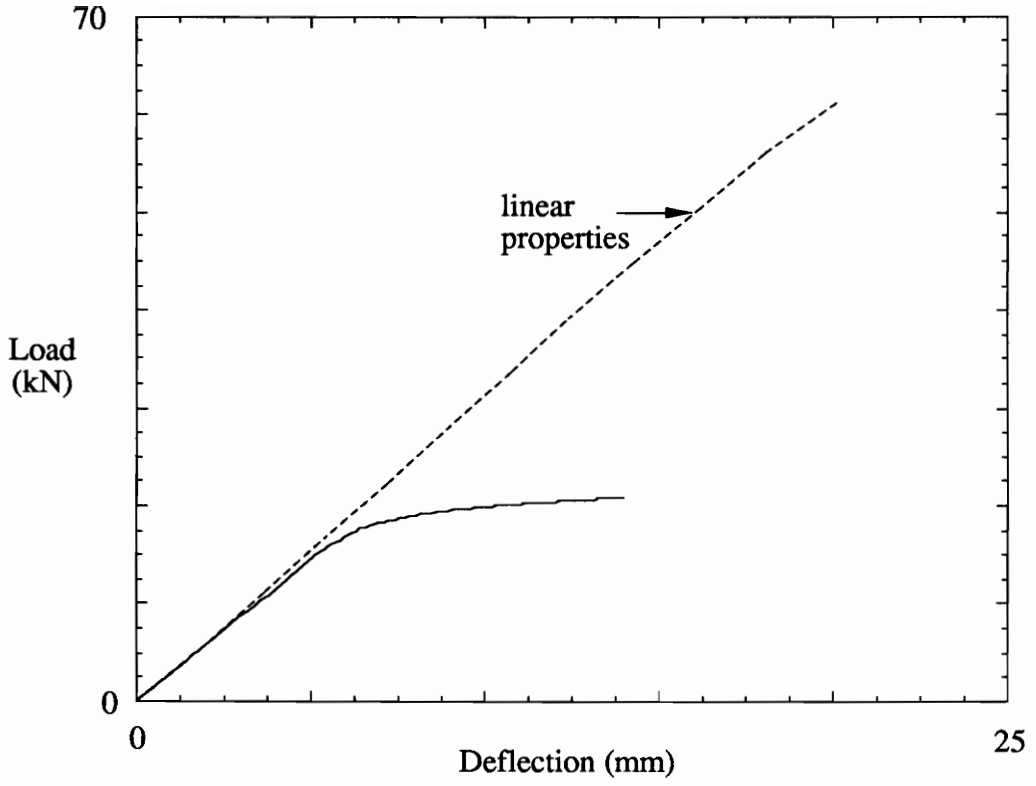

Figure 5.1 Load/deflection response of steel specimen vs. prediction.

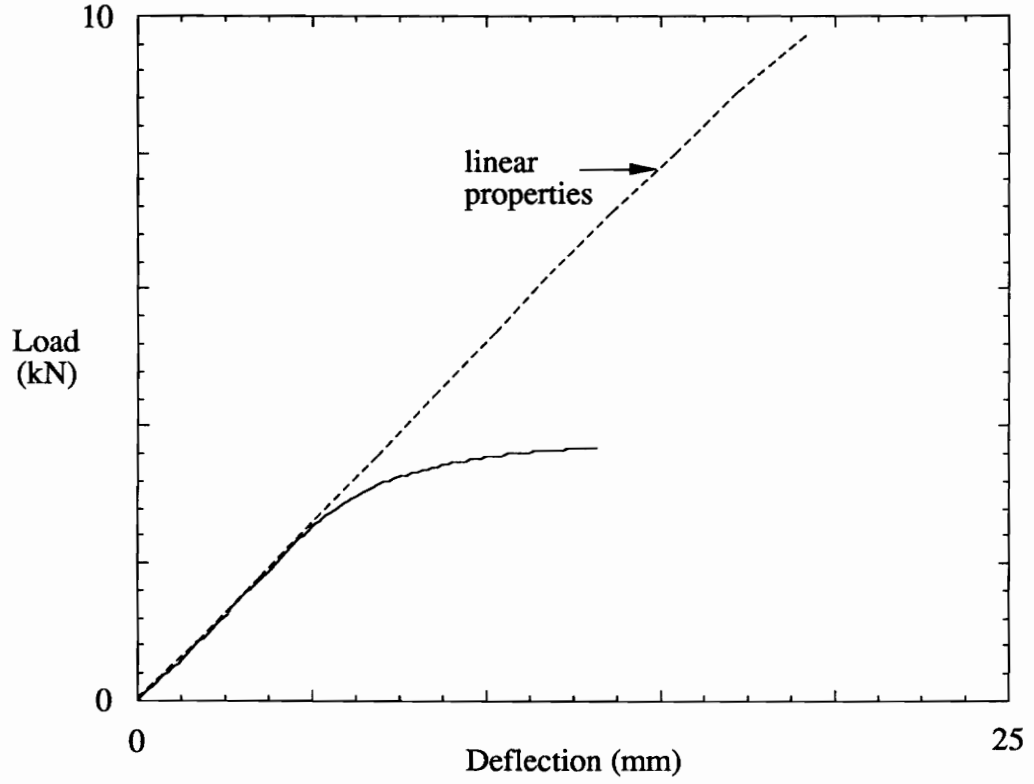

Figure 5.2 Load/deflection response of aluminum specimen vs. prediction.

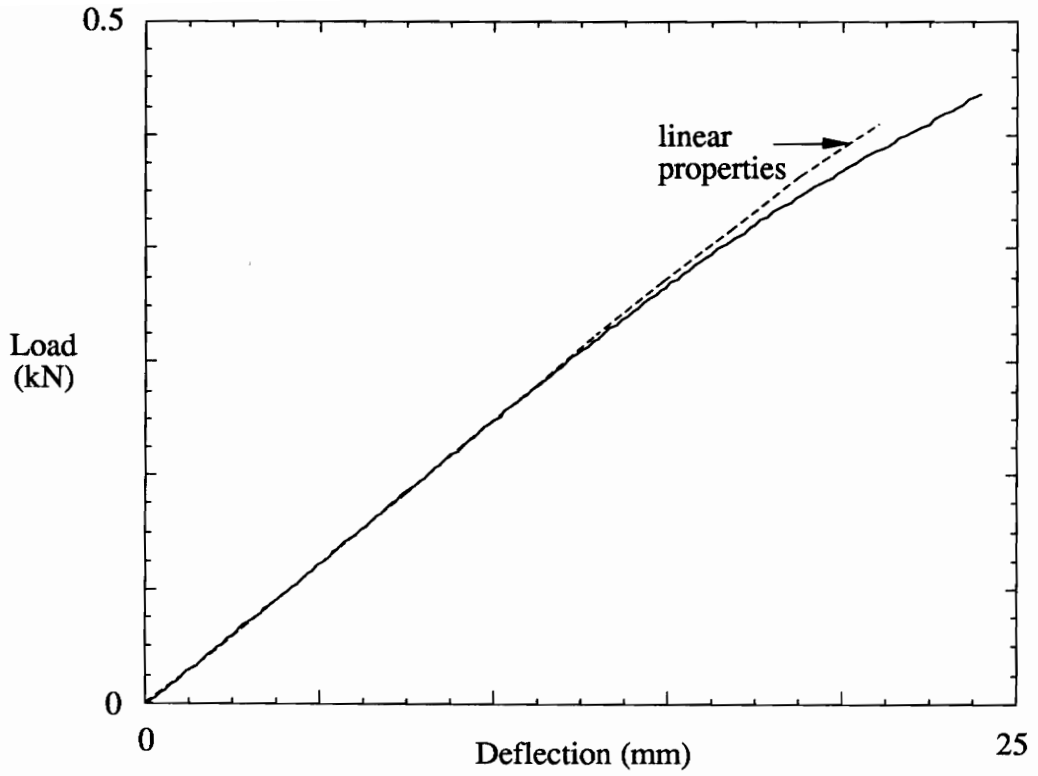

Figure 5.3 Load/deflection response of PMMA specimen vs. prediction.

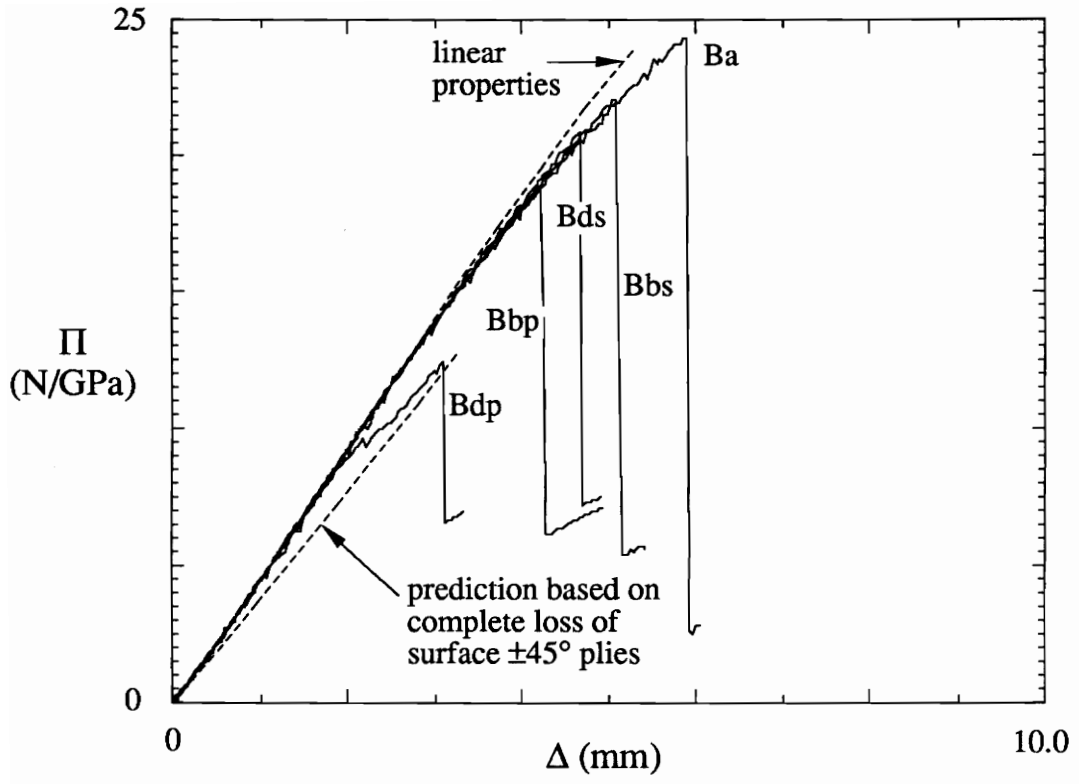

Figure 5.4 Normalized load/deflection response of Lay-up *B* specimens (ply- and sublaminate-level scaling).

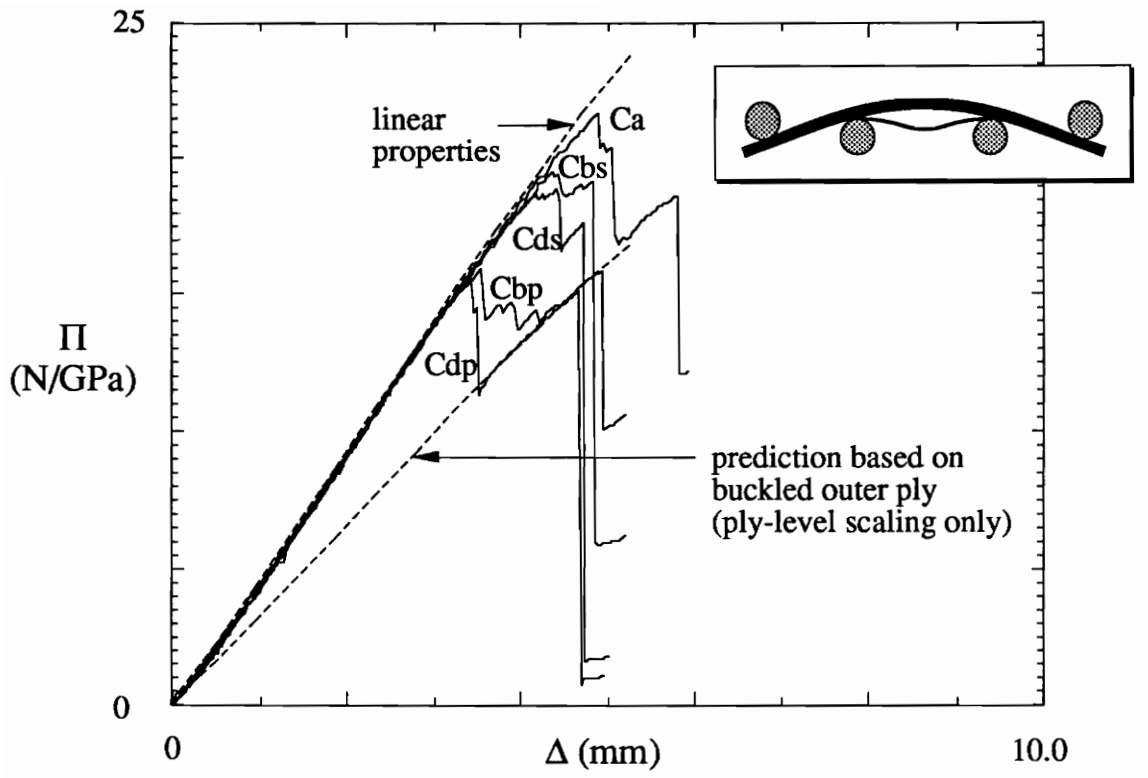

Figure 5.5 Normalized load/deflection response of Lay-up *C* specimens (ply- and sublaminate-level scaling).

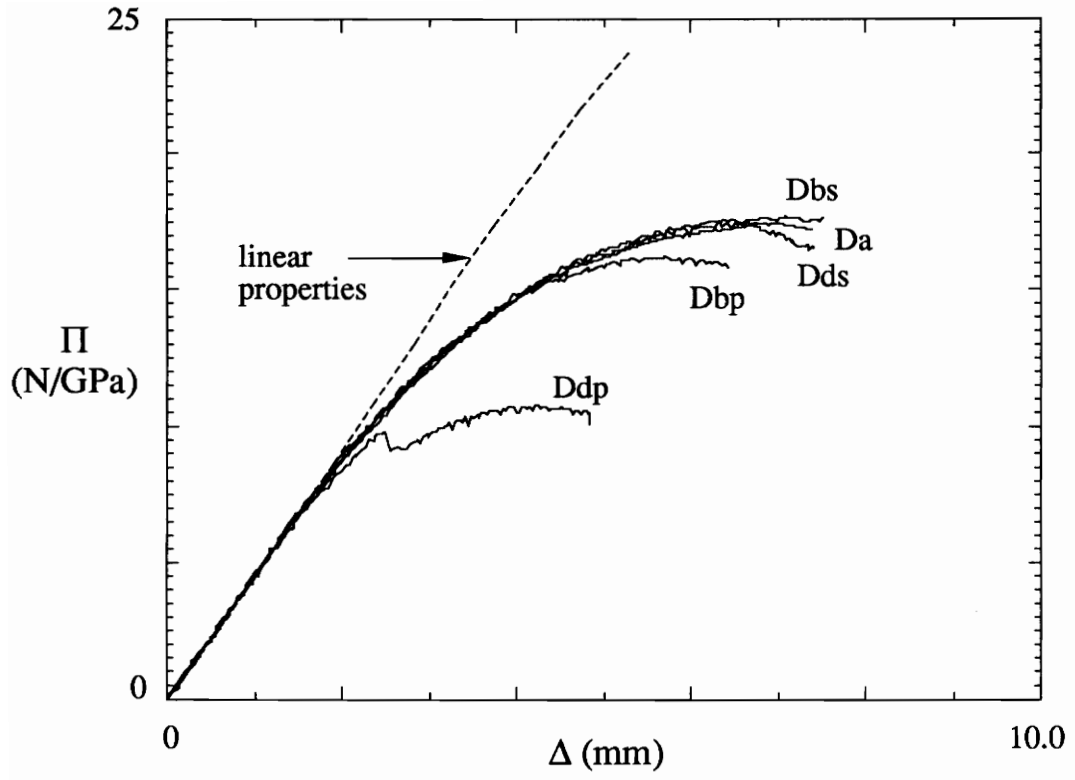

Figure 5.6 Normalized load/deflection response of Lay-up *A* specimens (ply- and sublaminate-level scaling).

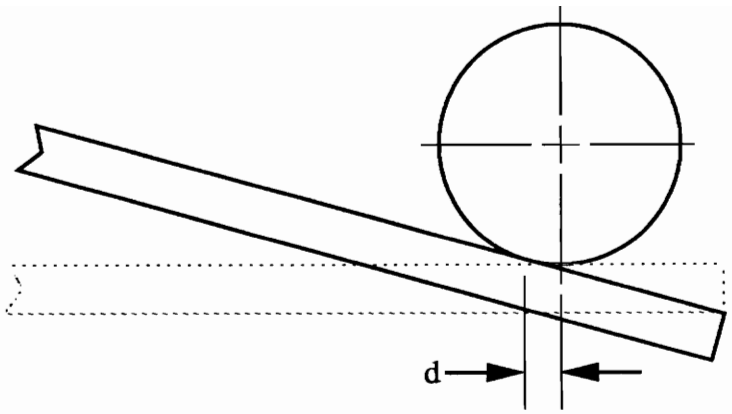

Figure 5.7 Schematic of specimen and roller showing inward movement of contact point as specimen deflects.

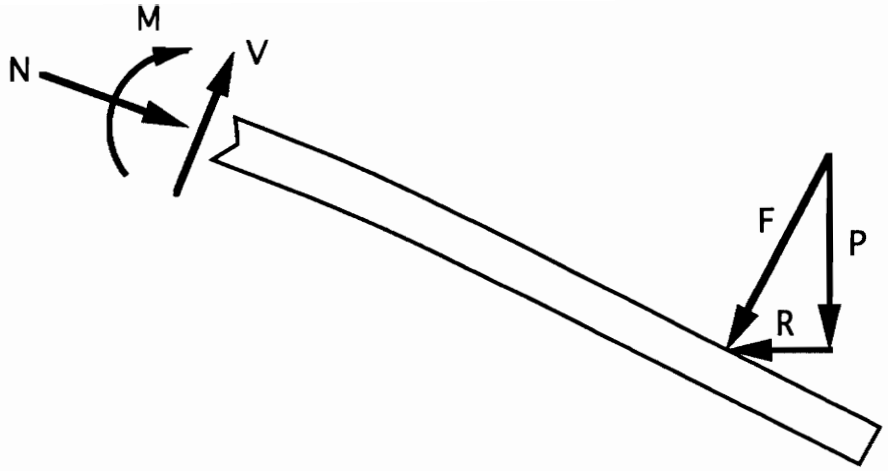

Figure 5.8 Schematic of specimen showing the load P read by the testing machine, and the actual load F that applies load to the specimen.

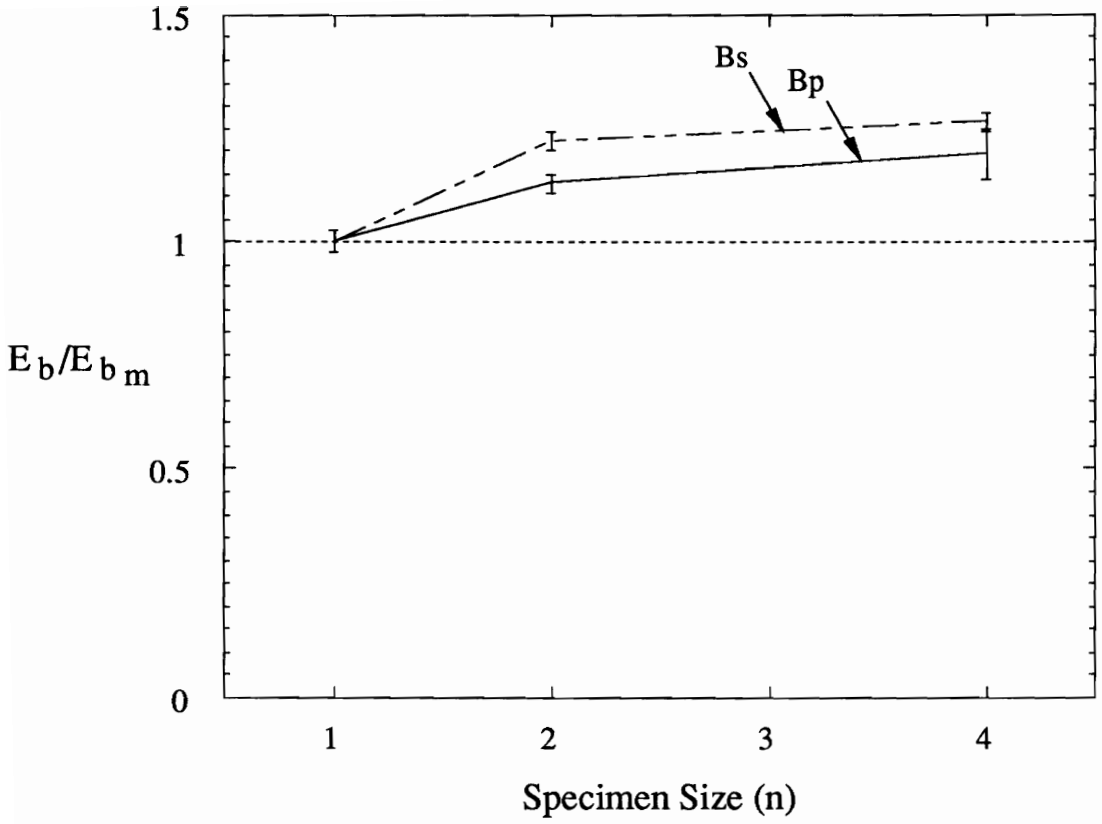

Figure 5.9 Normalized Lay-up *B* experimental bending stiffness plotted with respect to specimen size. Bars indicate standard deviation.

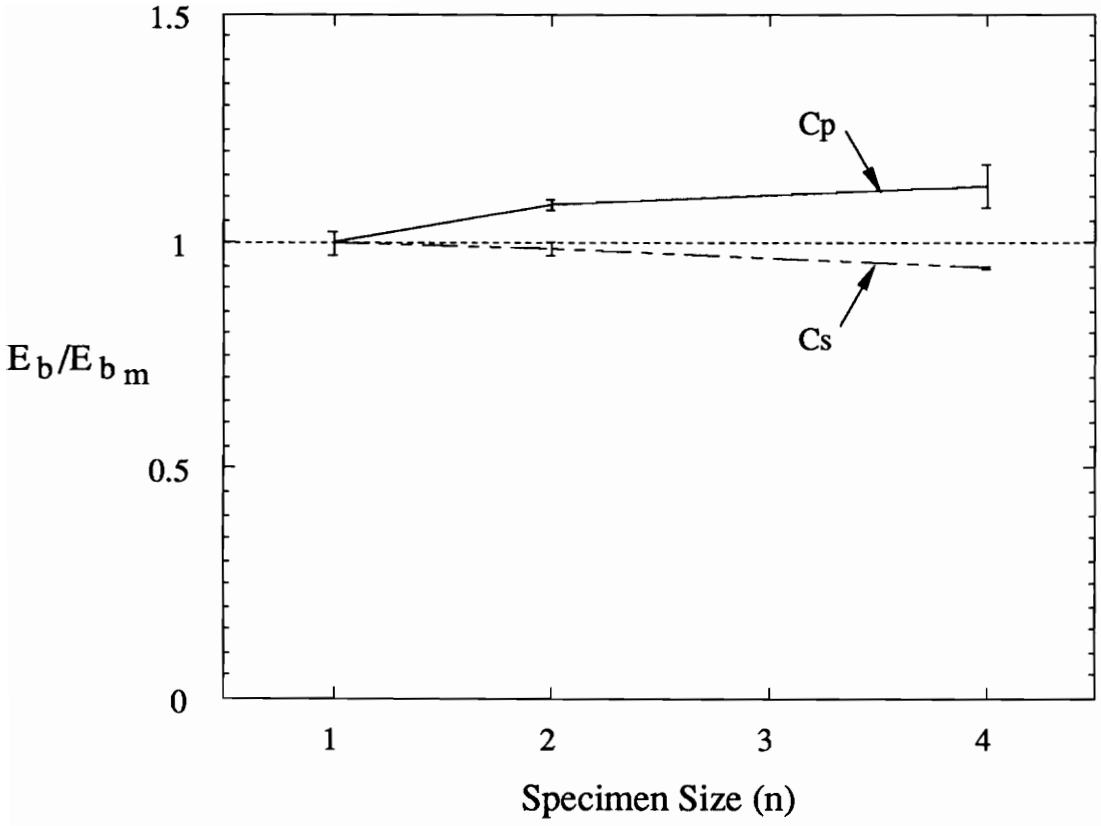

Figure 5.10 Normalized Lay-up *C* experimental bending stiffness plotted with respect to specimen size. Bars indicate standard deviation.

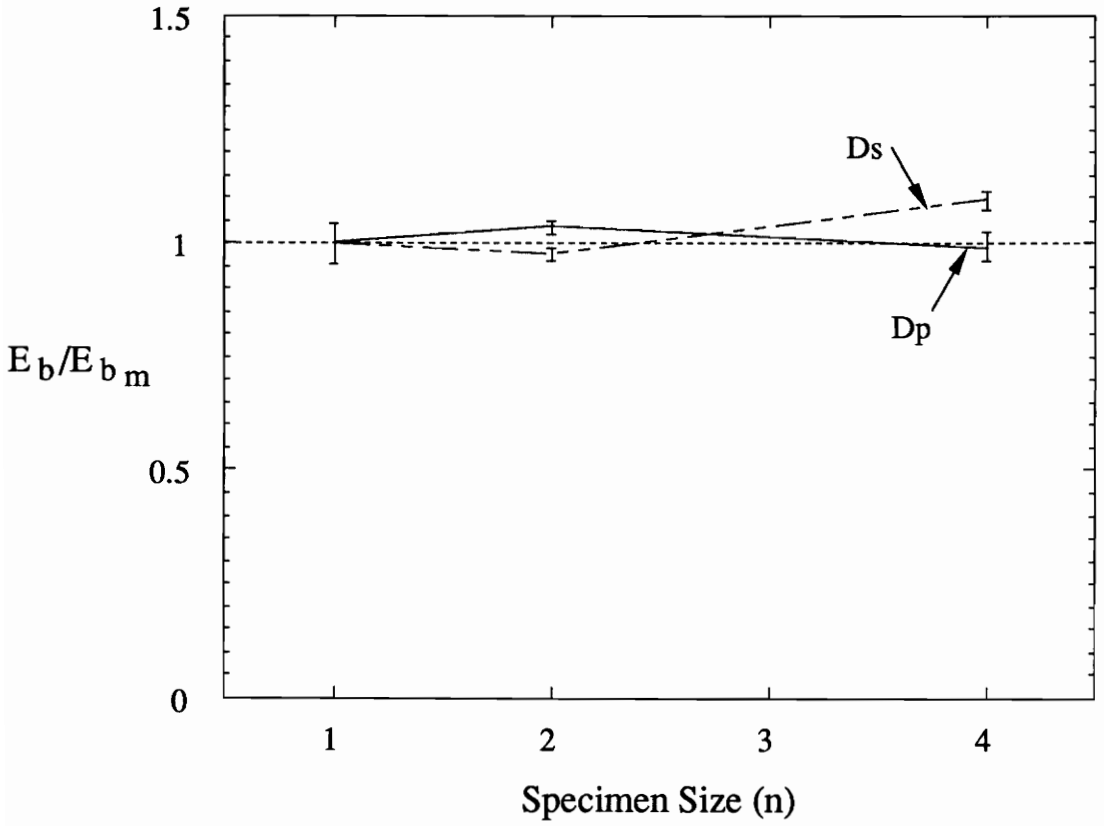

Figure 5.11 Normalized Lay-up *D* experimental bending stiffness plotted with respect to specimen size. Bars indicate standard deviation.

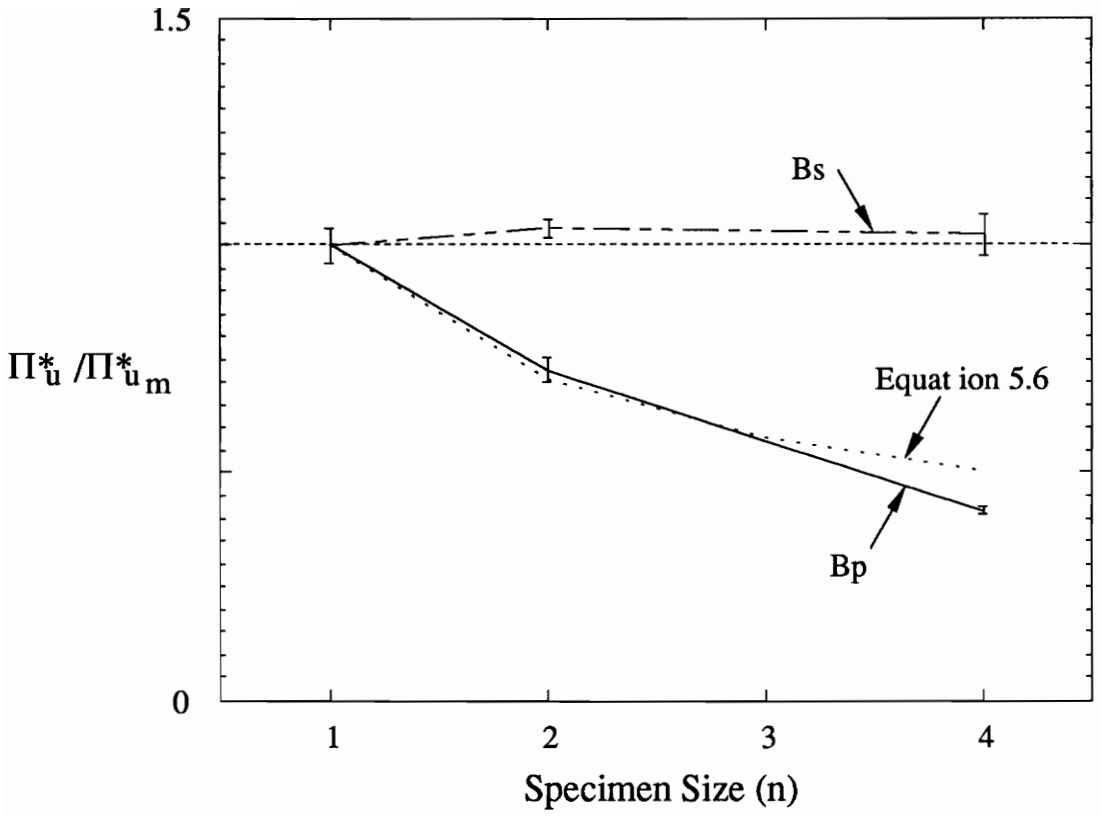

Figure 5.12 Normalized failure load of Lay-up *B* specimens. Sublaminate-level scaled values are adjusted to account for the strain in the outermost 0° fibers. Bars indicate standard deviations.

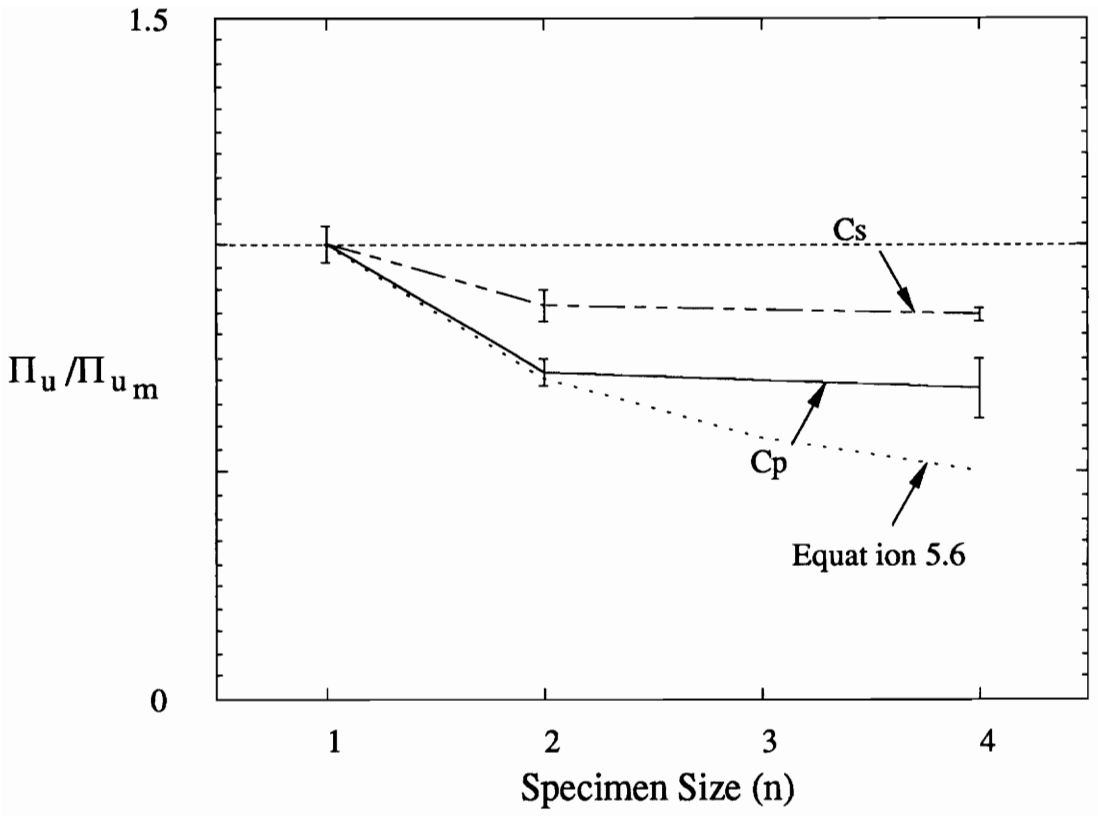

Figure 5.13 Normalized failure load of Lay-up *C* specimens. Bars indicate standard deviations. Compare with Figure 5.38.

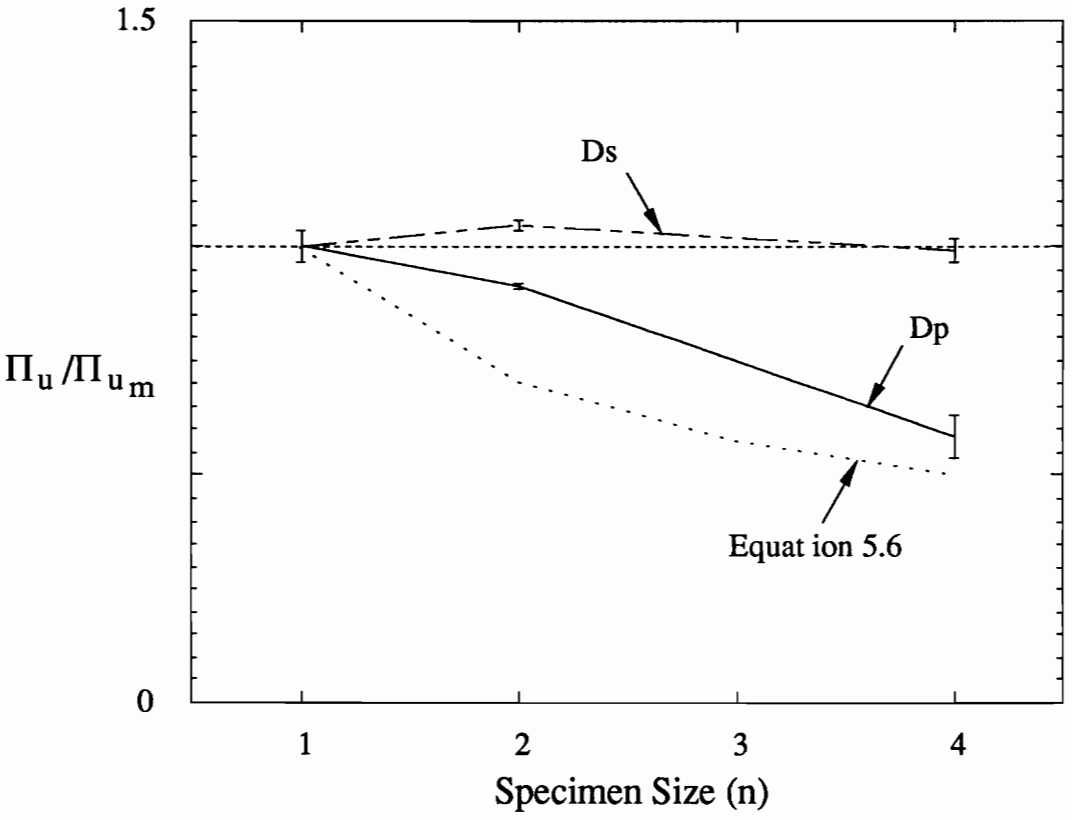

Figure 5.14 Normalized maximum load of Lay-up *D* specimens. Bars indicate standard deviations.

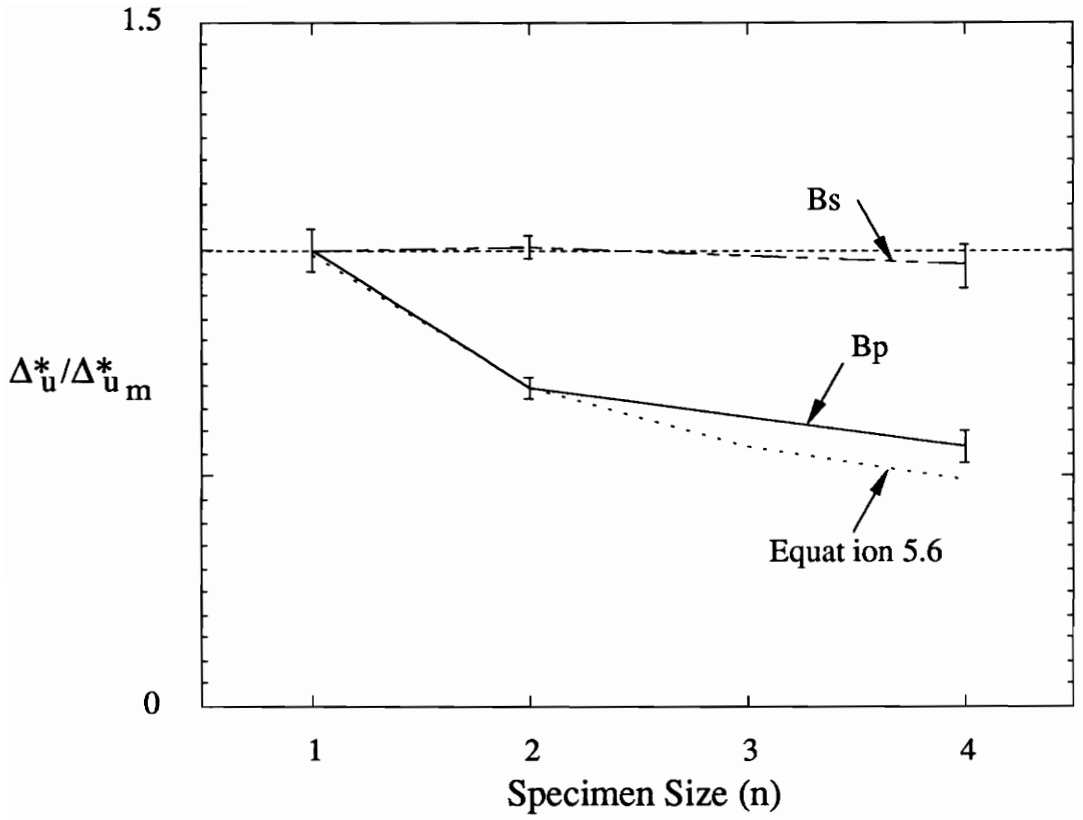

Figure 5.15 Normalized failure displacement of Lay-up *B* specimens. Sublaminate-level scaled values are adjusted to account for the strain in the outermost 0° fibers. Bars indicate standard deviations.

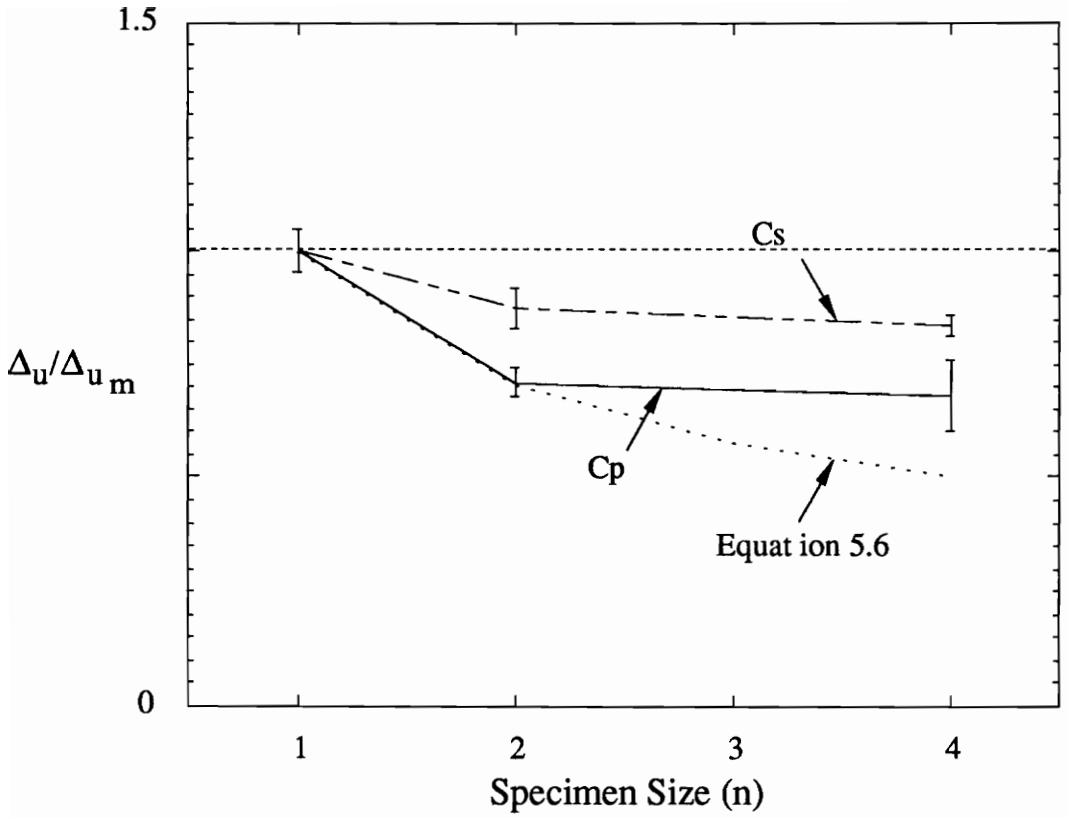

Figure 5.16 Normalized failure displacement of Lay-up *C* specimens.

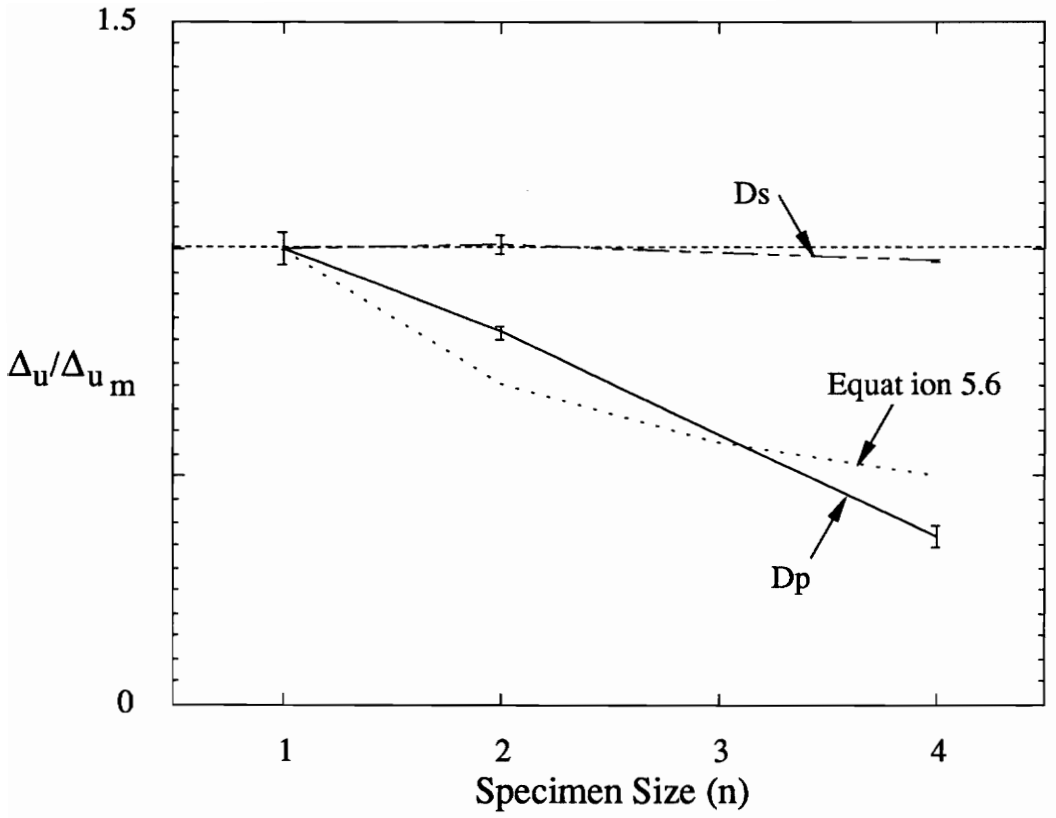

Figure 5.17 Normalized displacement corresponding to maximum load of Lay-up *D* specimens.

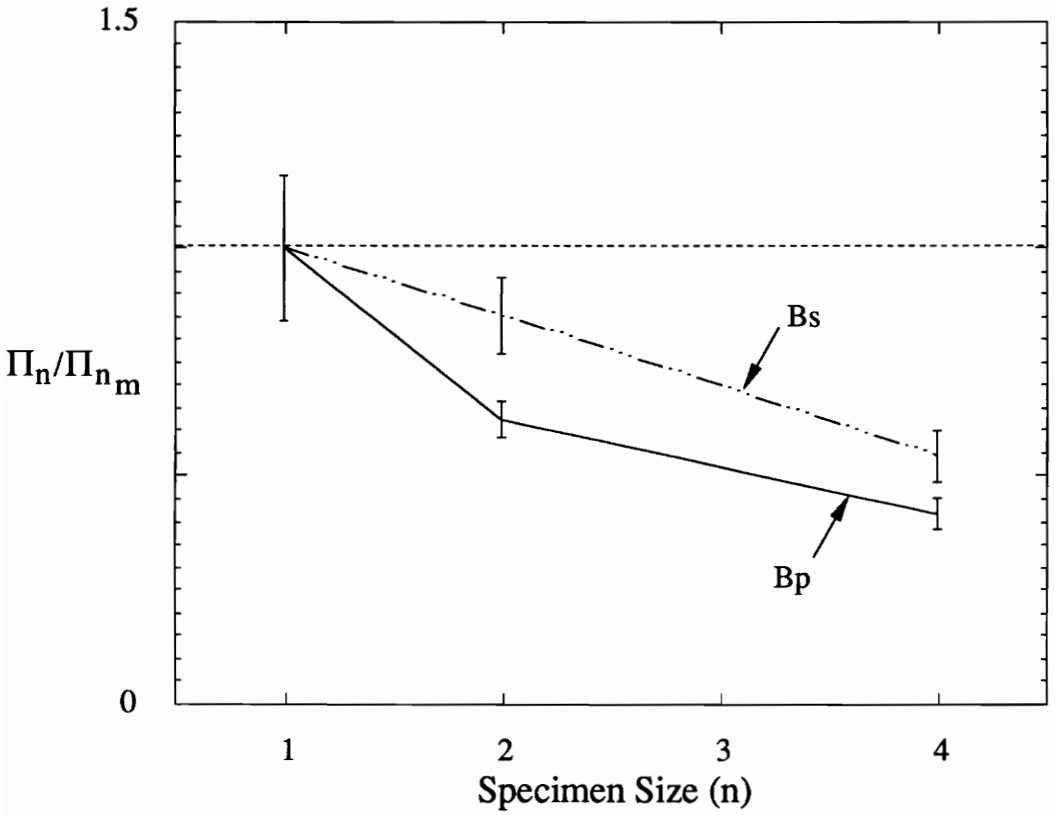

Figure 5.18 Normalized load corresponding to deviation from linear material properties. Lay-up *B* specimens.

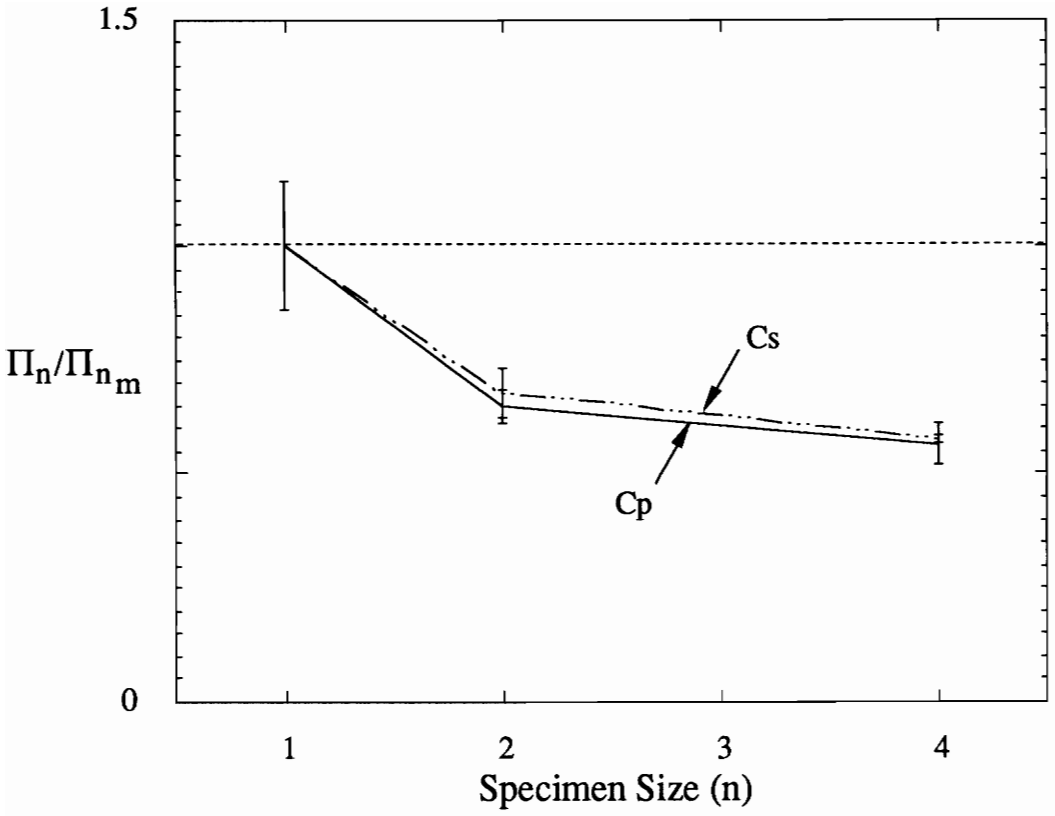

Figure 5.19 Normalized load corresponding to deviation from linear material properties. Lay-up *C* specimens.

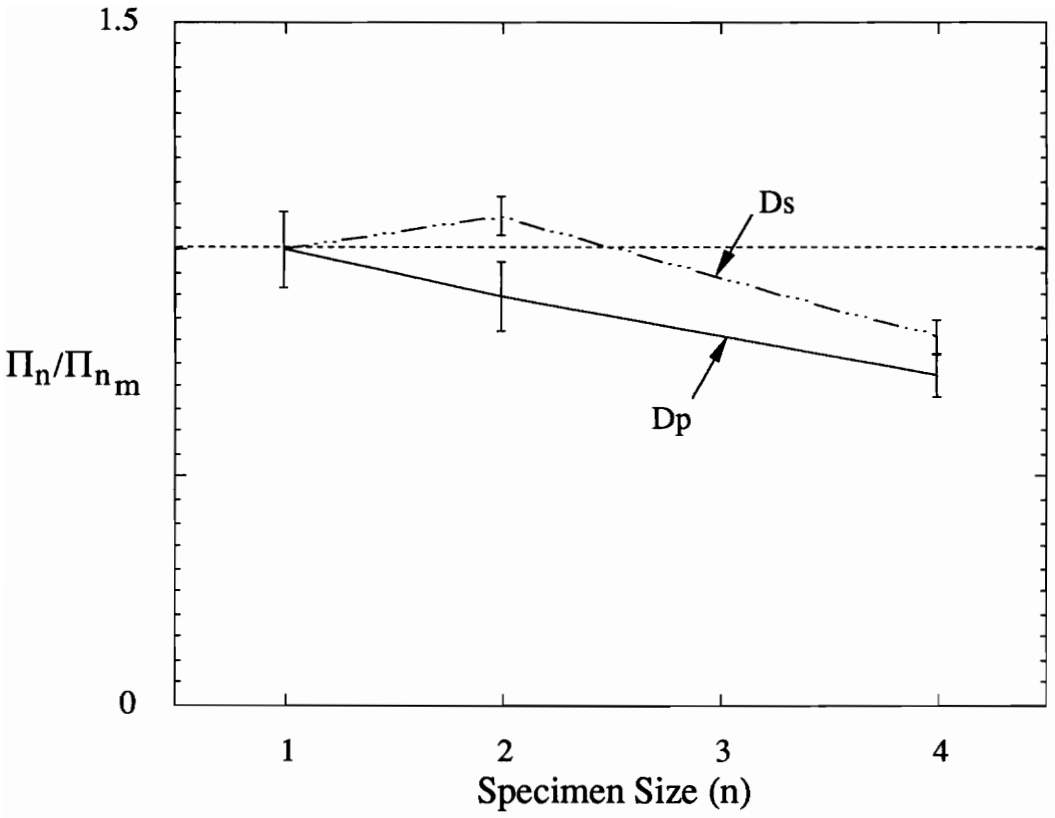

Figure 5.20 Normalized load corresponding to deviation from linear material properties. Lay-up *D* specimens.

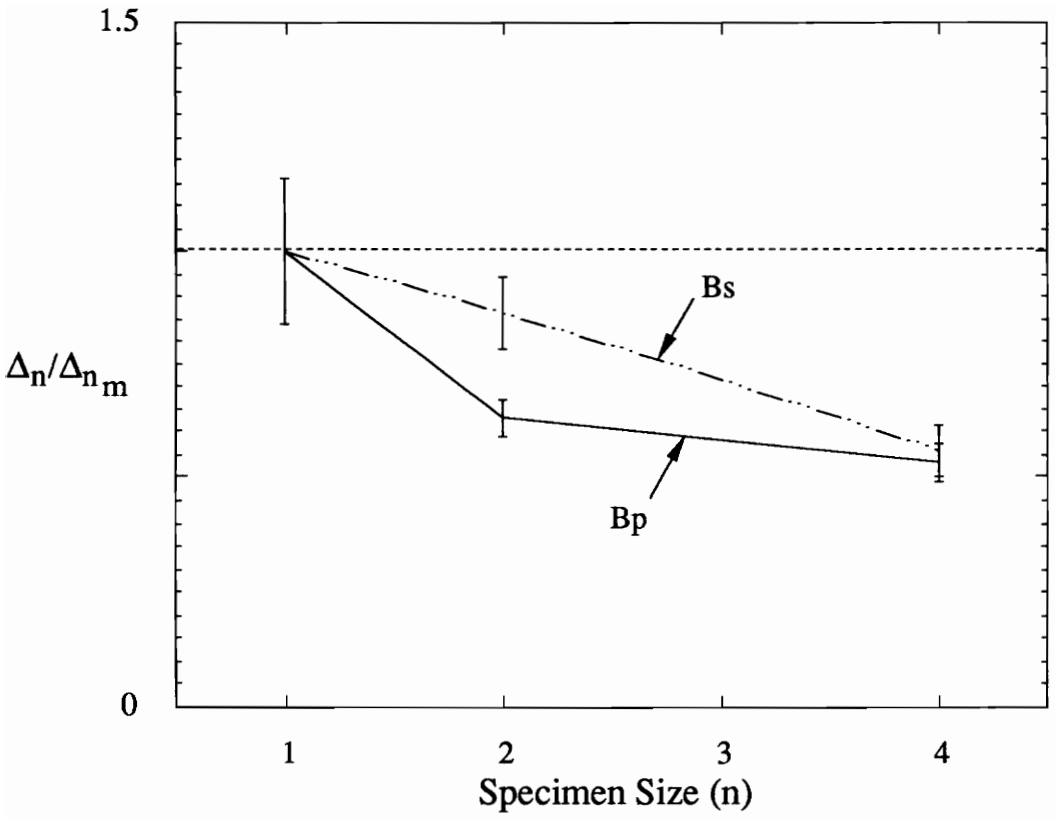

Figure 5.21 Normalized deflection corresponding to deviation from linear material properties. Lay-up *B* specimens.

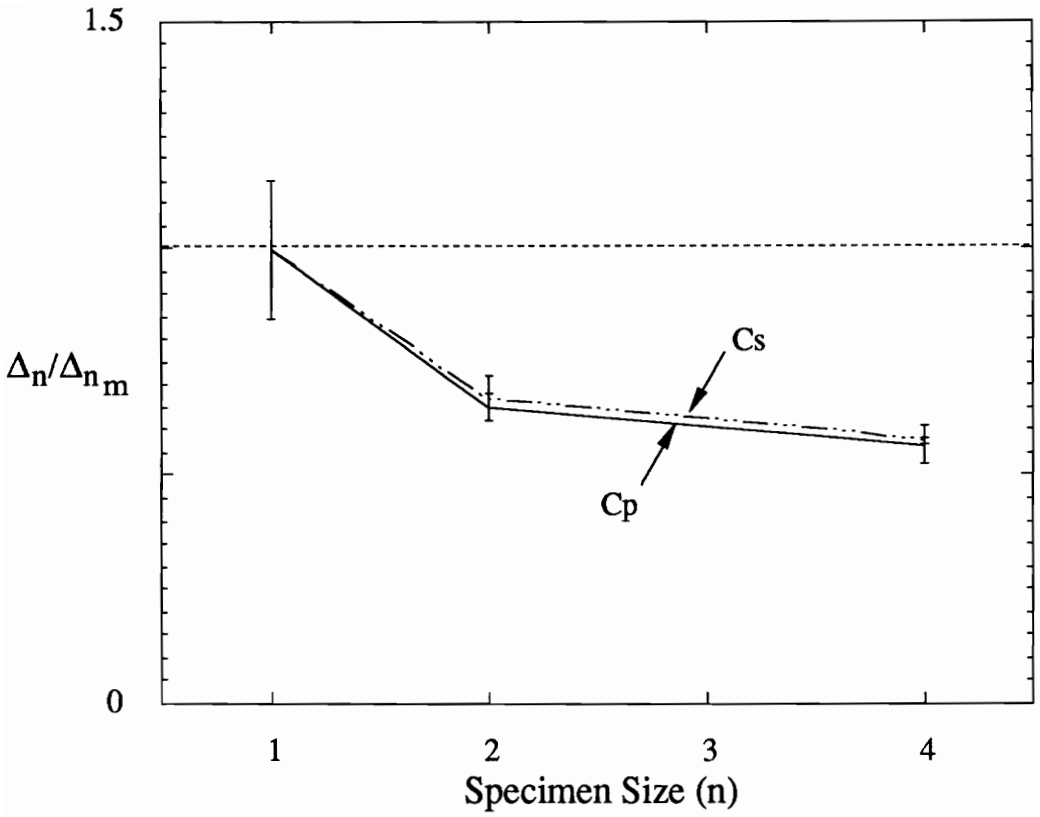

Figure 5.22 Normalized deflection corresponding to deviation from linear material properties. Lay-up *C* specimens.

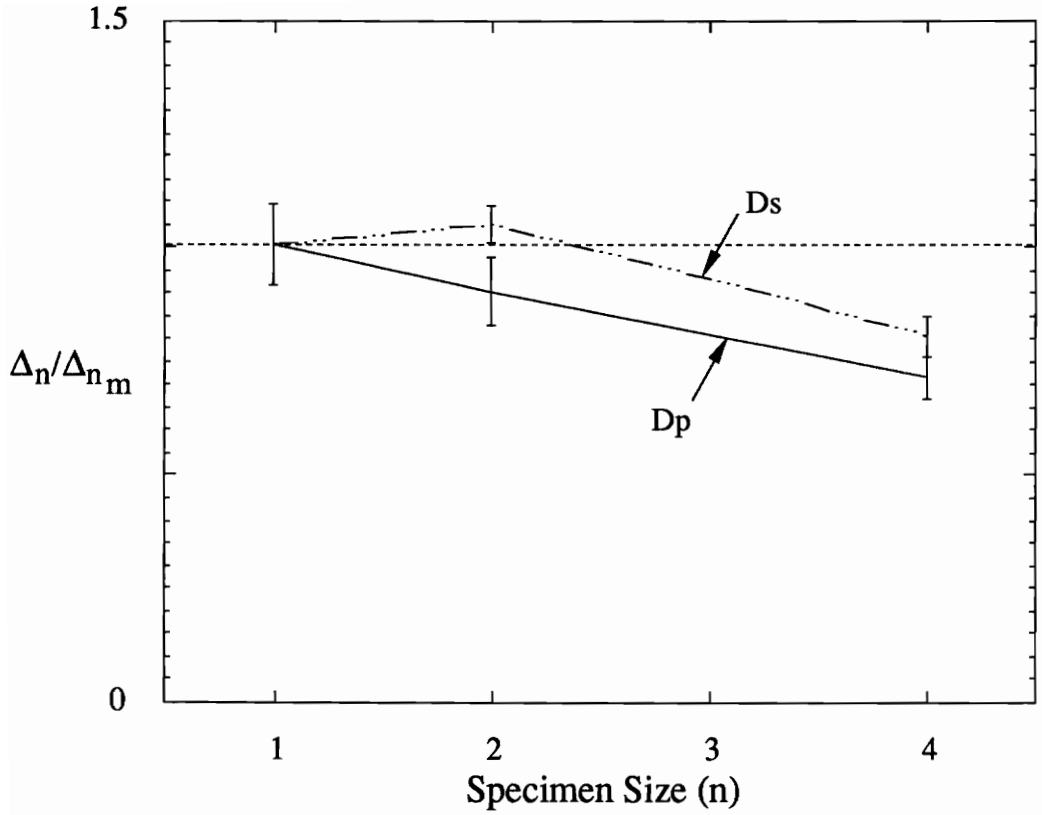

Figure 5.23 Normalized deflection corresponding to deviation from linear material properties. Lay-up *D* specimens.

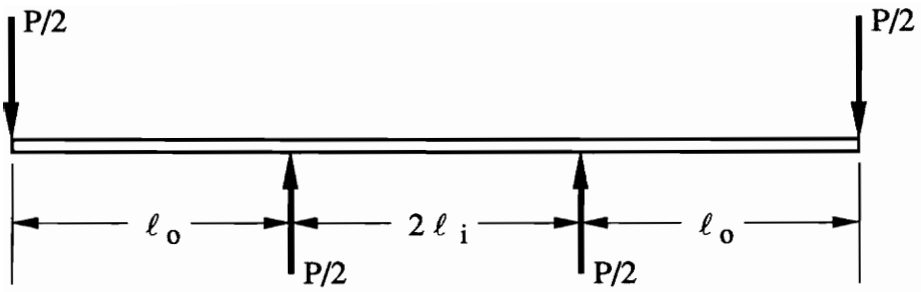

Figure 5.24 Inner and outer roller spans

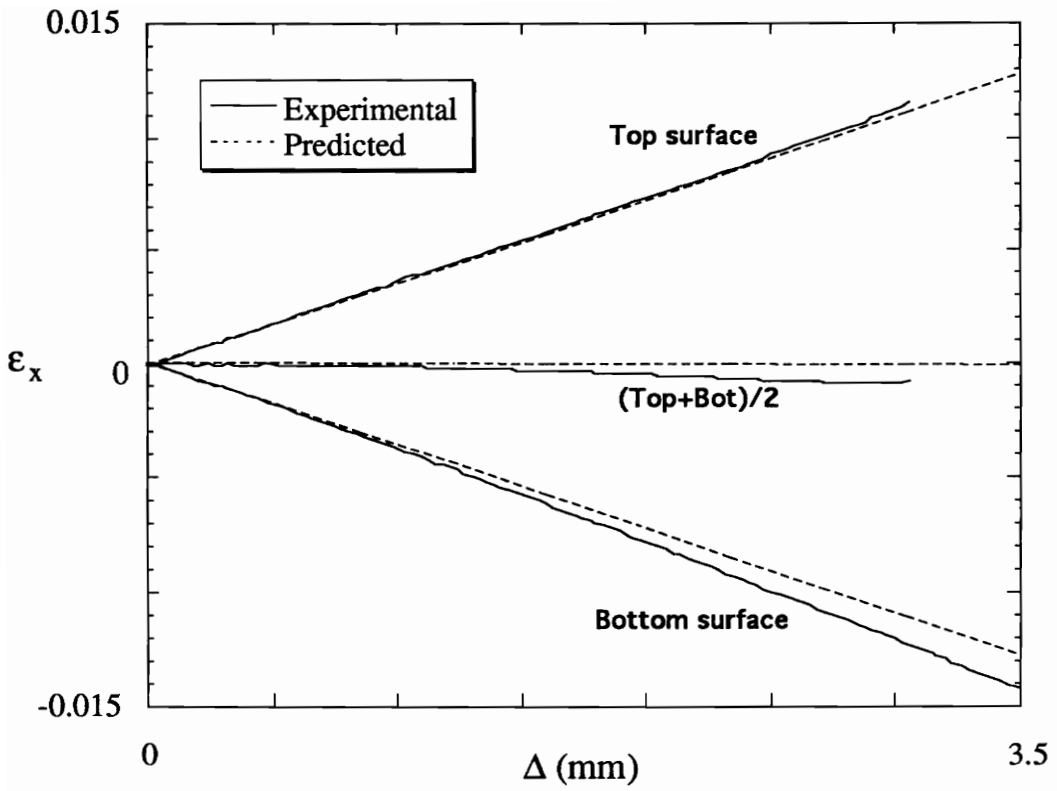

Figure 5.25 Typical strain vs. roller displacement curves showing shift of neutral axis due to unsymmetric local strain softening in the specimen gage section.

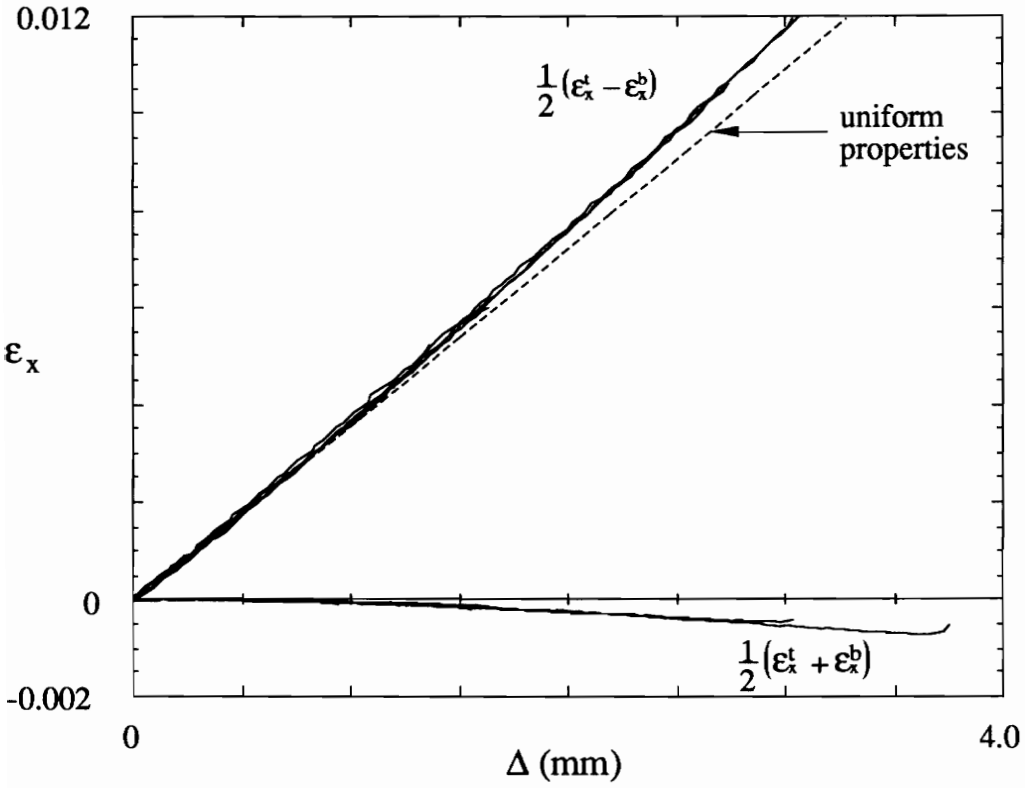

Figure 5.26 Lay-up *B* scaled surface strains vs. roller deflection.

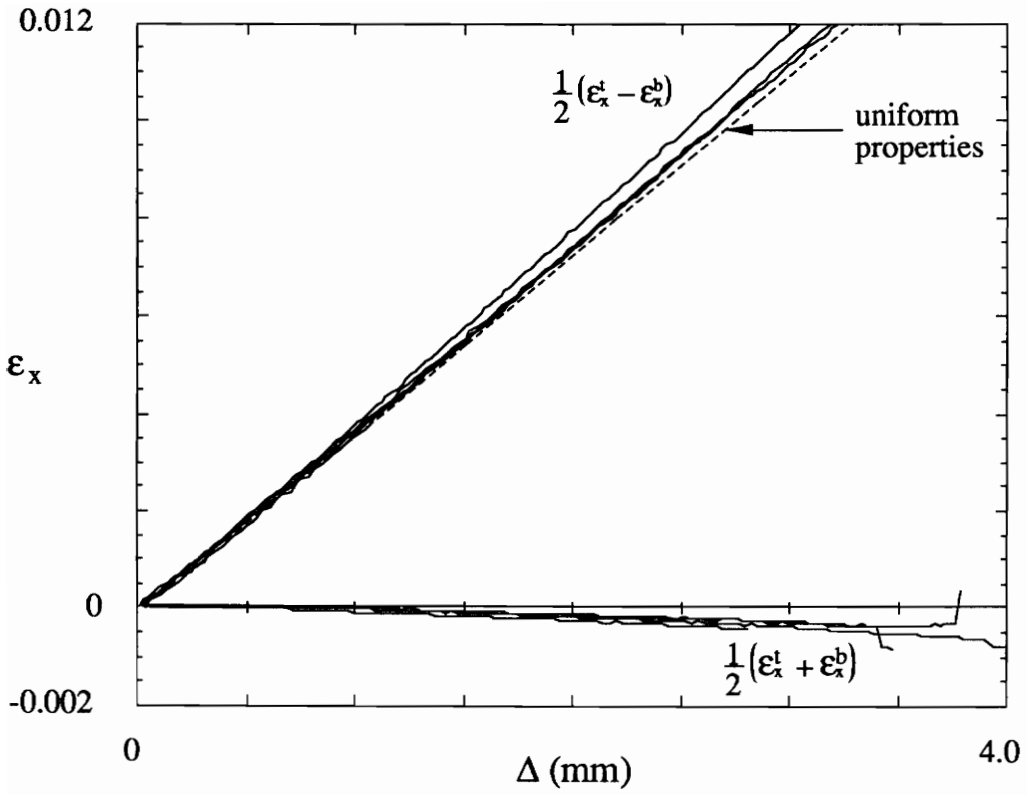

Figure 5.27 Lay-up *C* scaled surface strains vs. roller deflection.

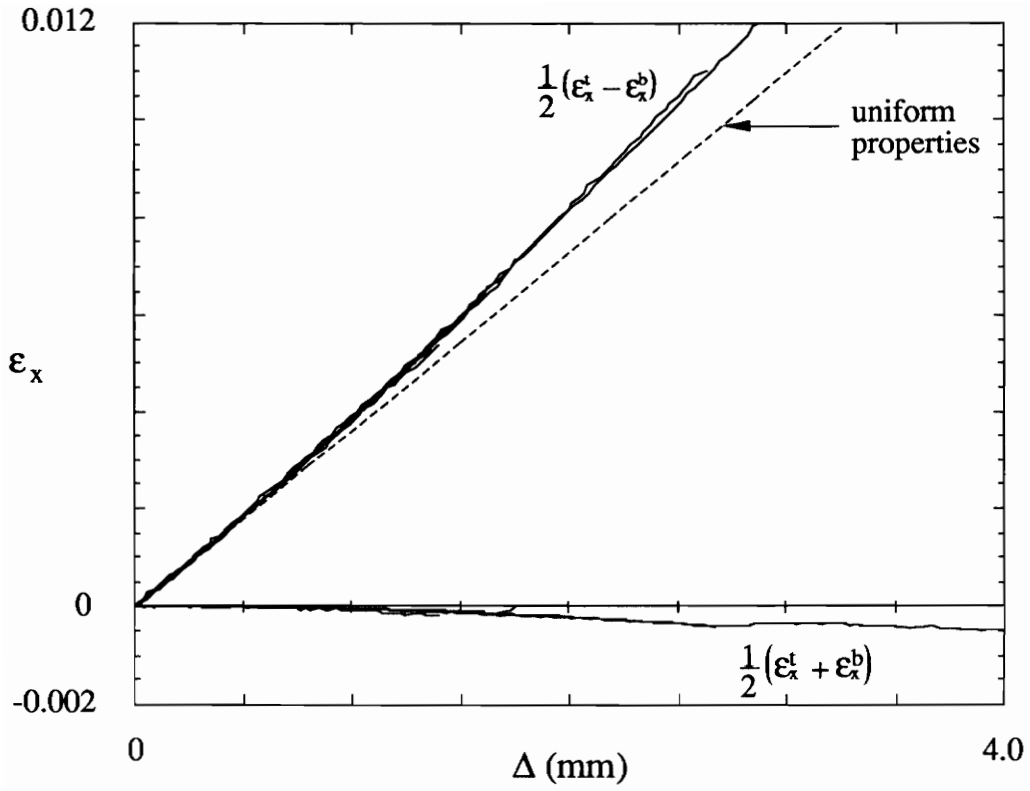

Figure 5.28 Lay-up *D* scaled surface strains vs. roller deflection.

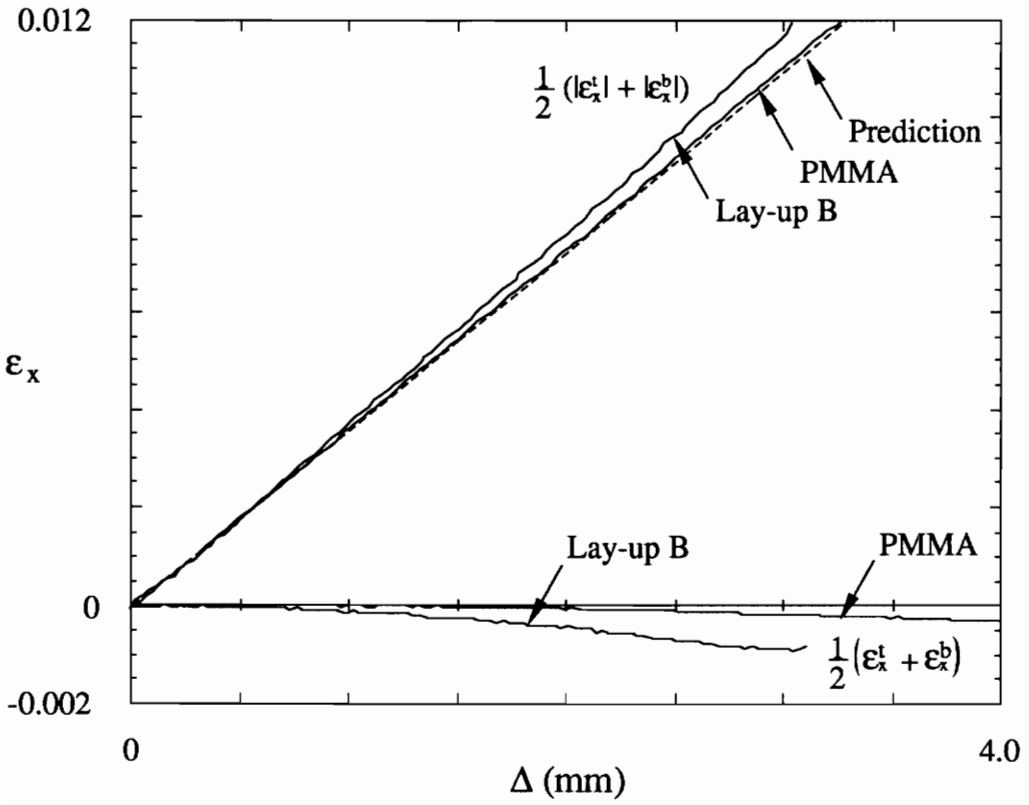

Figure 5.29 Strain/displacement plots of a typical Lay-up B specimen, and a PMMA specimen.

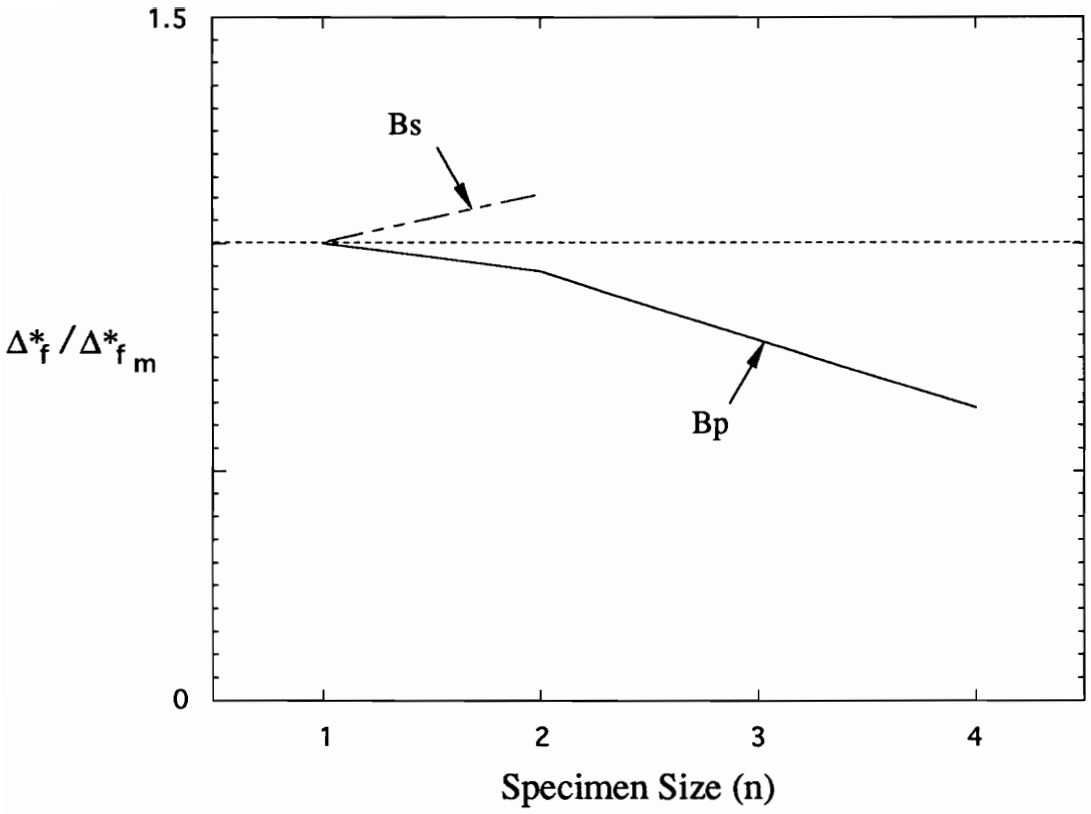

Figure 5.30 Normalized deflection of Lay-up *B* specimens at failure of the outermost 90° ply. Sublaminate-level scaled values are adjusted to account for the strain in the outermost 90° fibers.

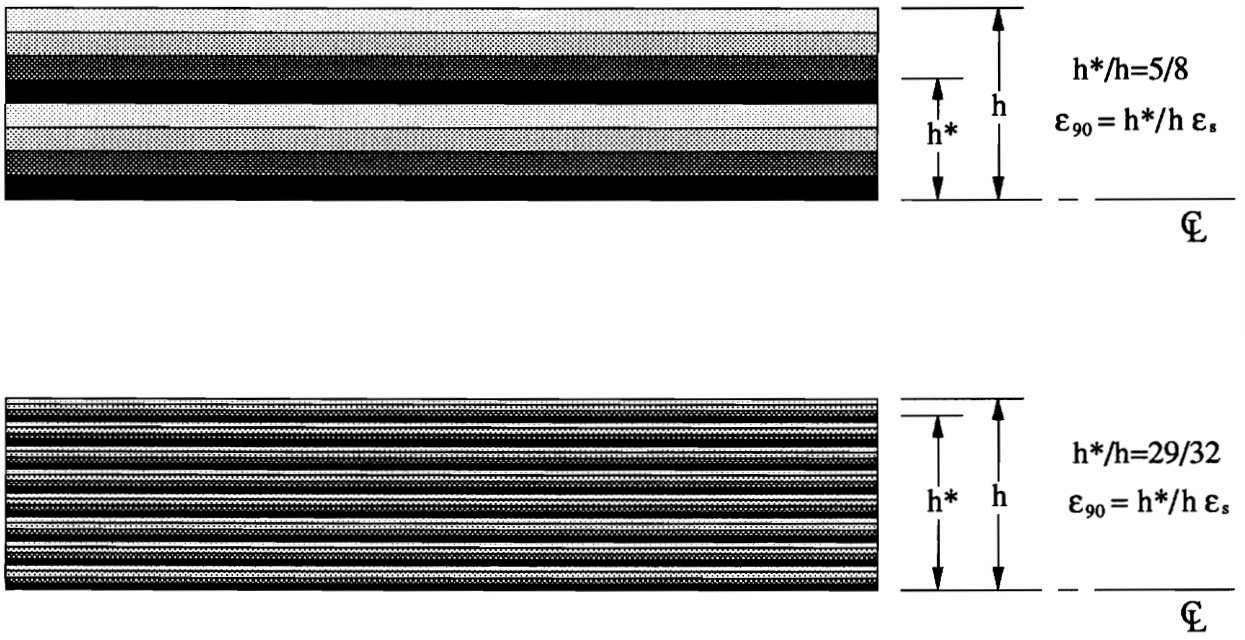

Figure 5.31 Difference in strain in outermost 90° fibers in Lay-up *B* when sublaminate-level scaling is used. For a given surface strain, the strain in the outer 90° fibers will be different in sublaminate-level scaled specimens than in ply-level scaled specimens. ε_{90} is the strain of the outermost 90° fibers and ε_s is the surface strain.

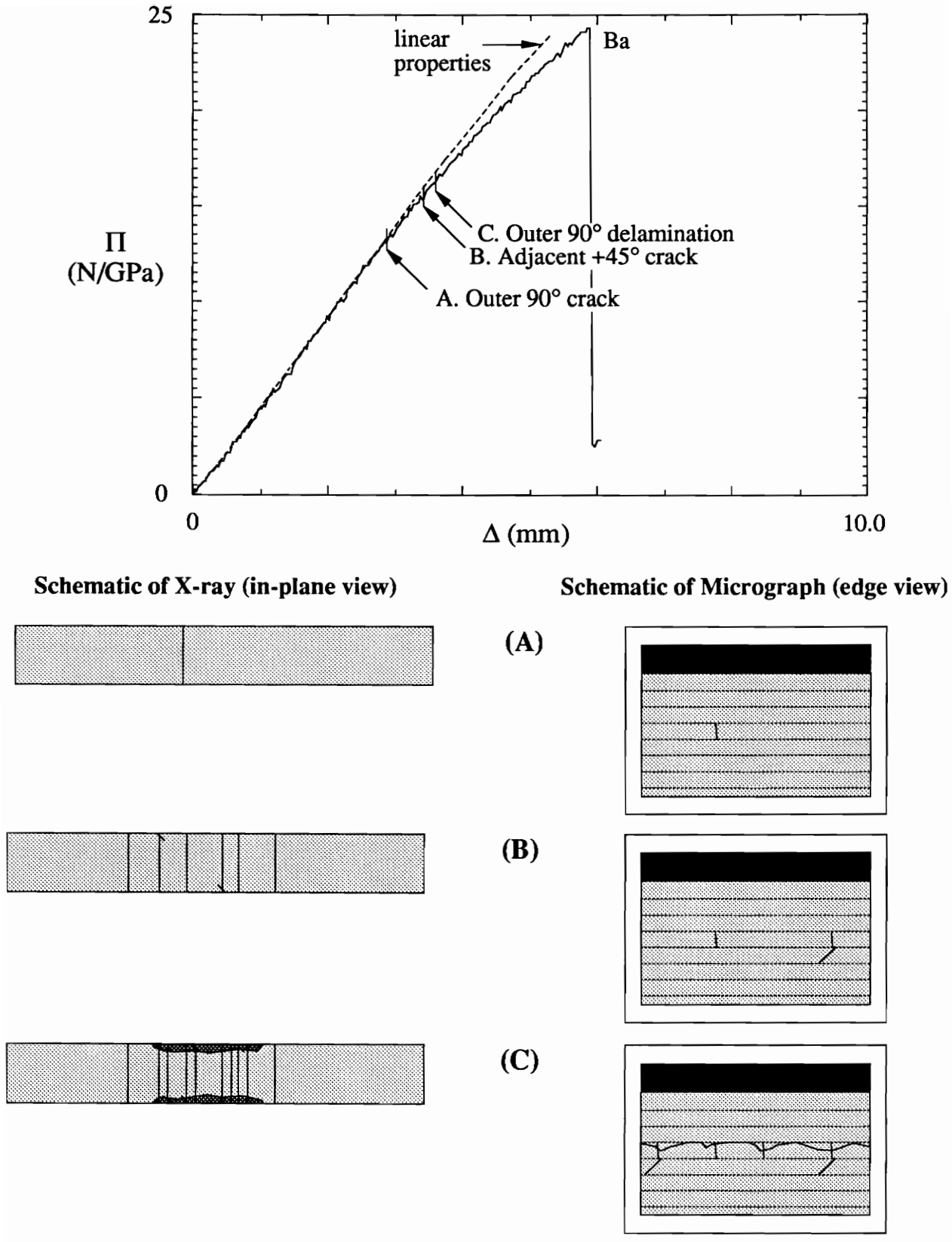

Figure 5.32 damage in Ba specimens

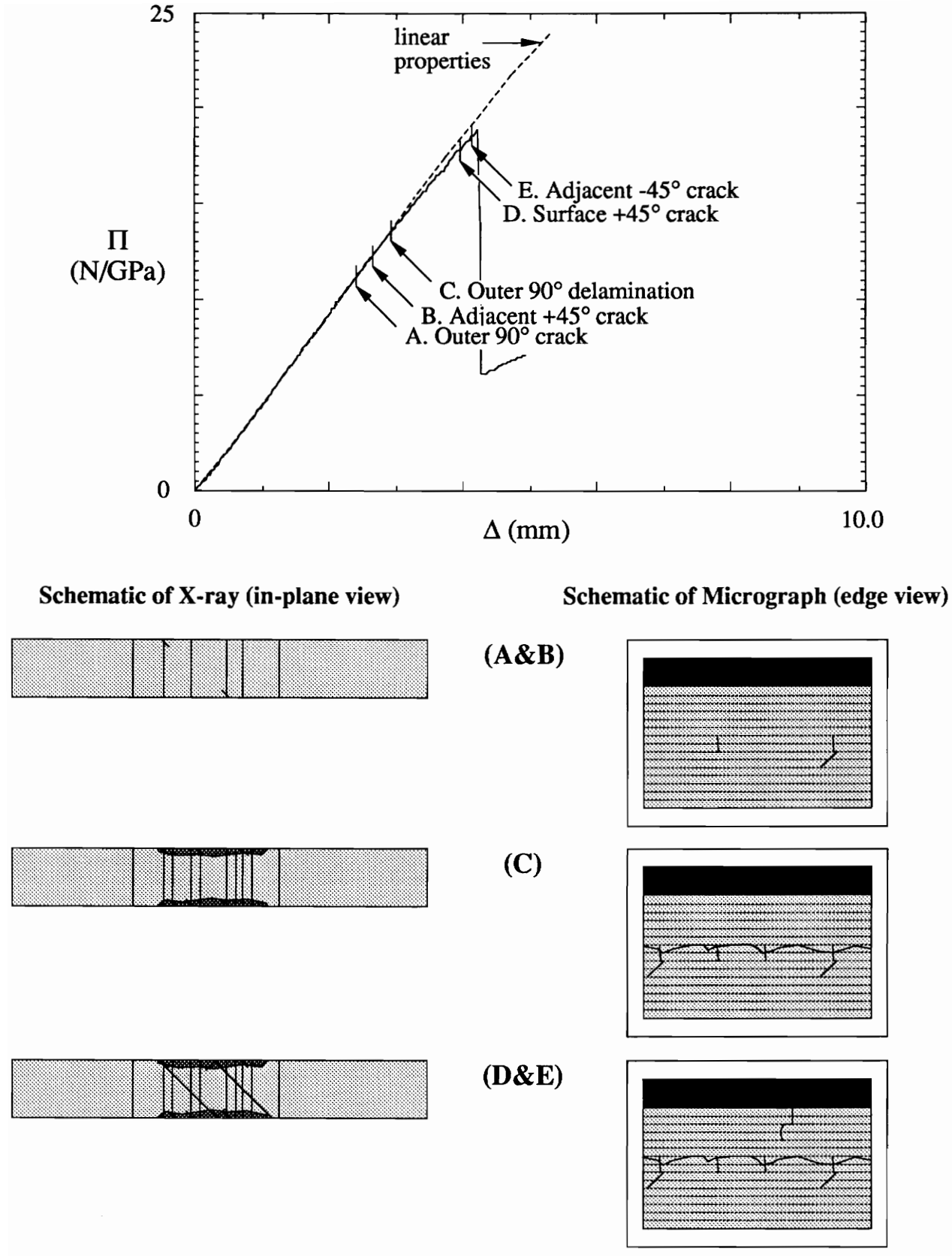

Figure 5.33 damage in Bbp specimens

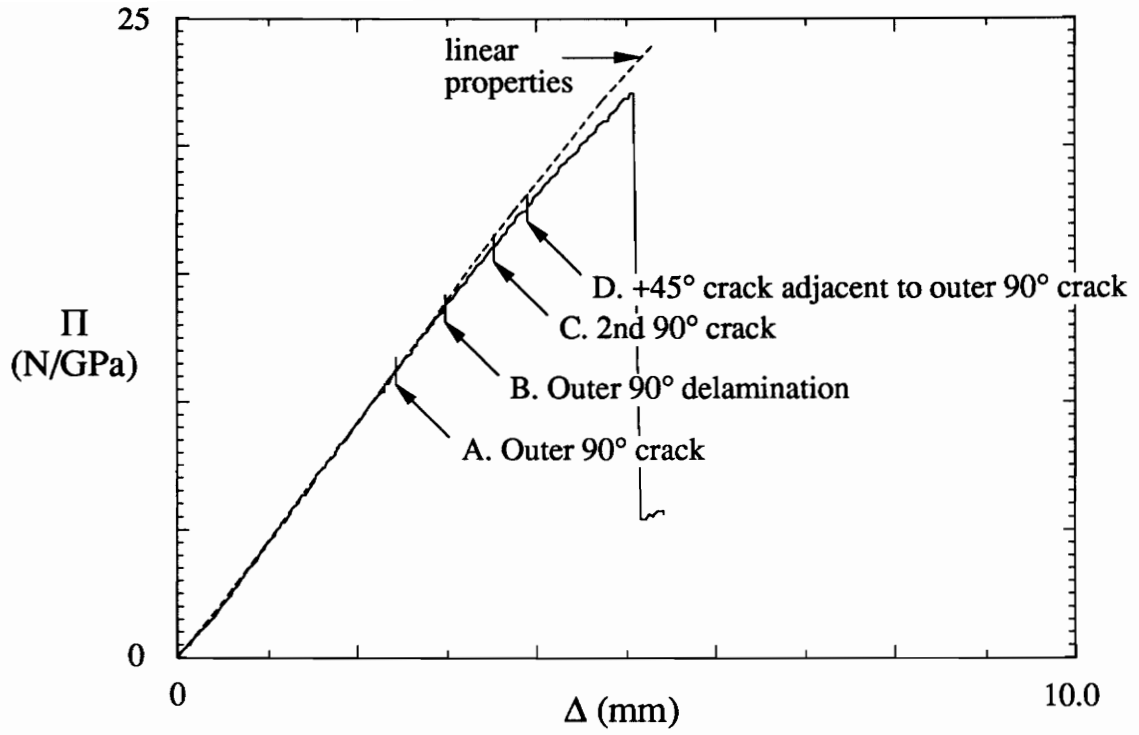

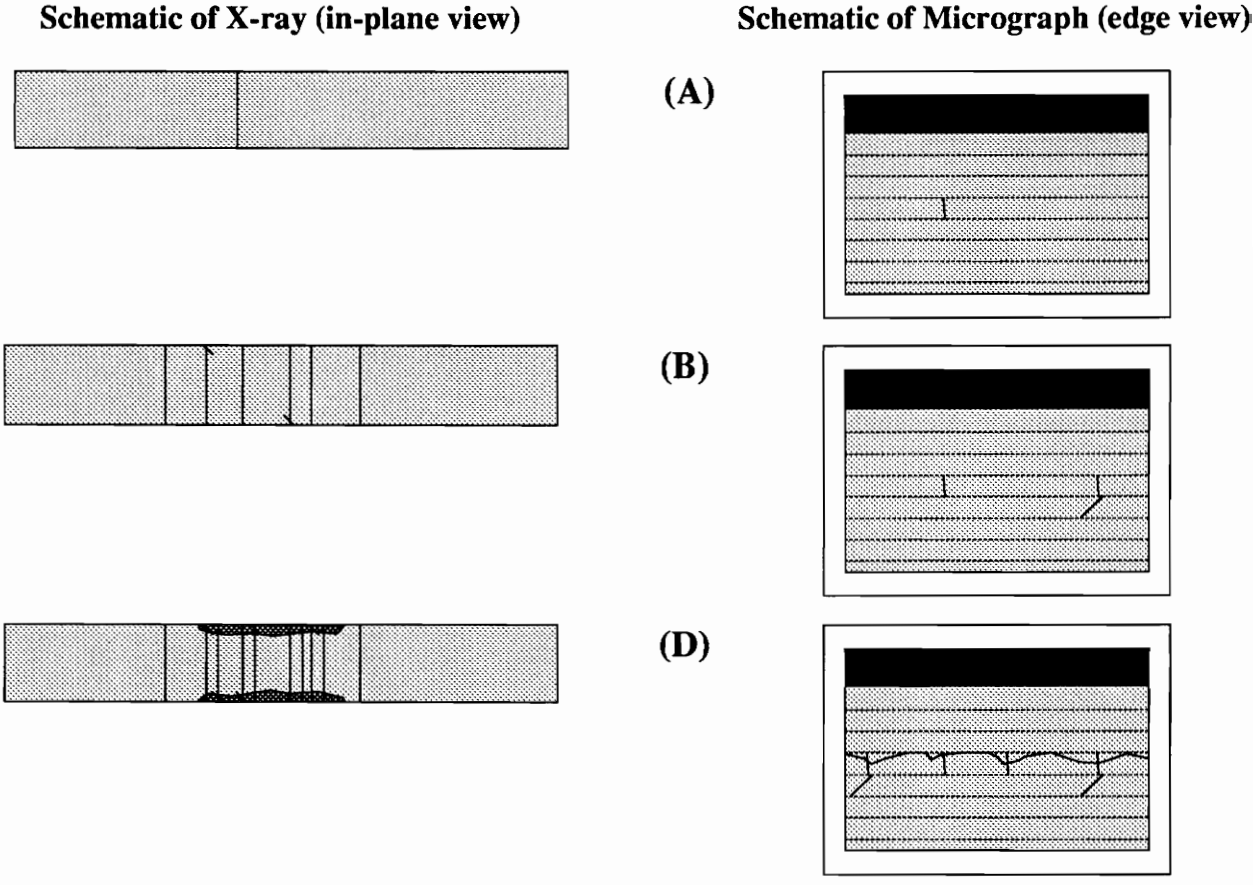

Figure 5.34 damage in Bbs specimens

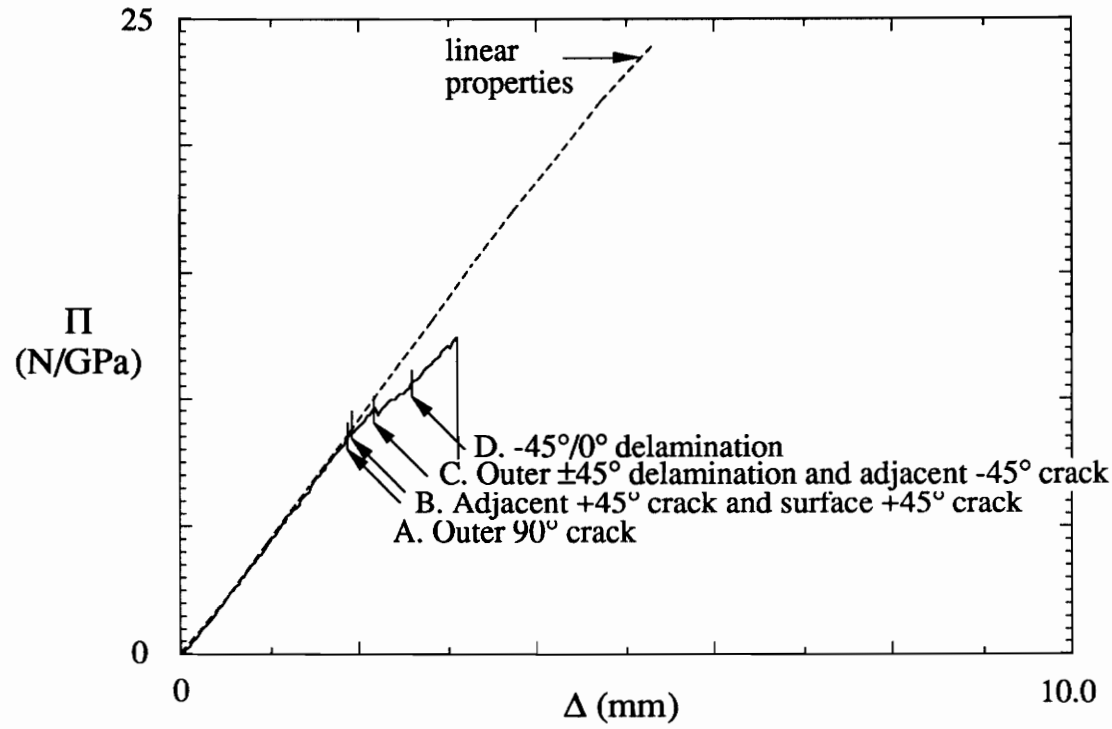

Schematic of X-ray (in-plane view)

Schematic of Micrograph (edge view)

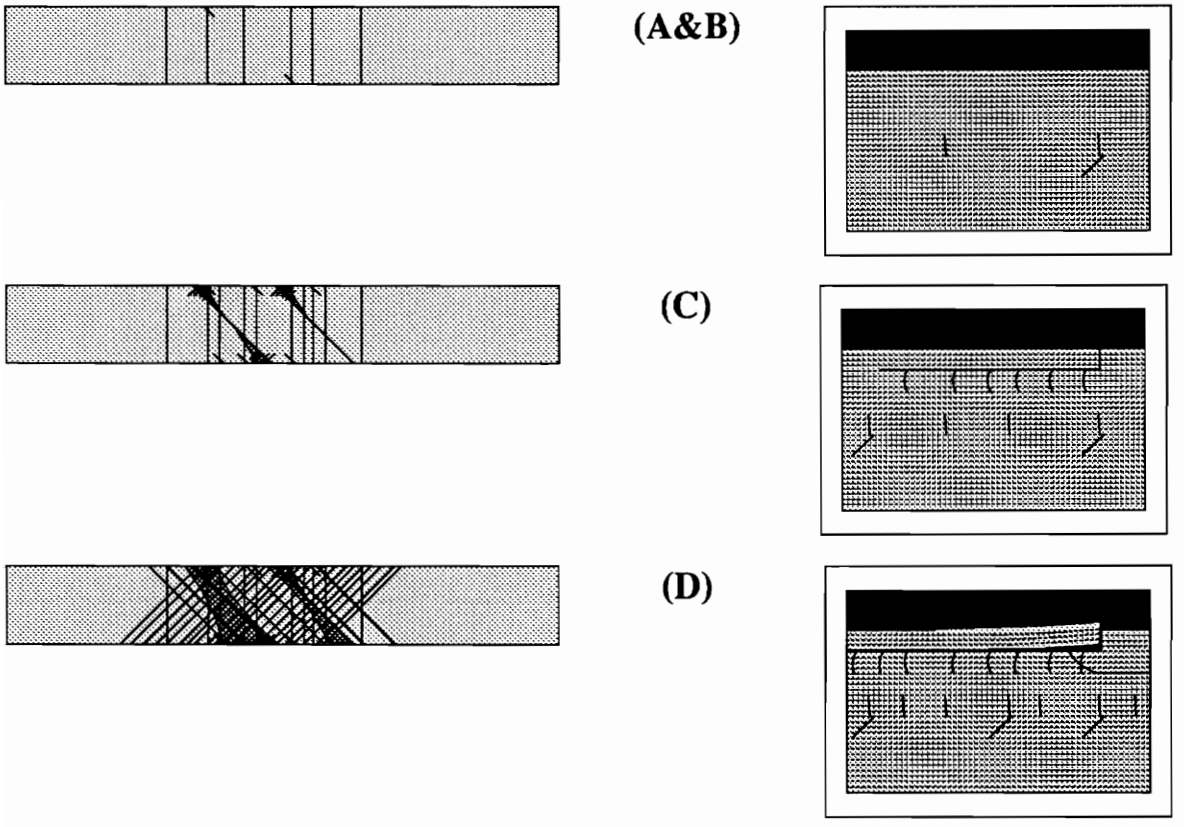

Figure 5.35 damage in Bdp specimens

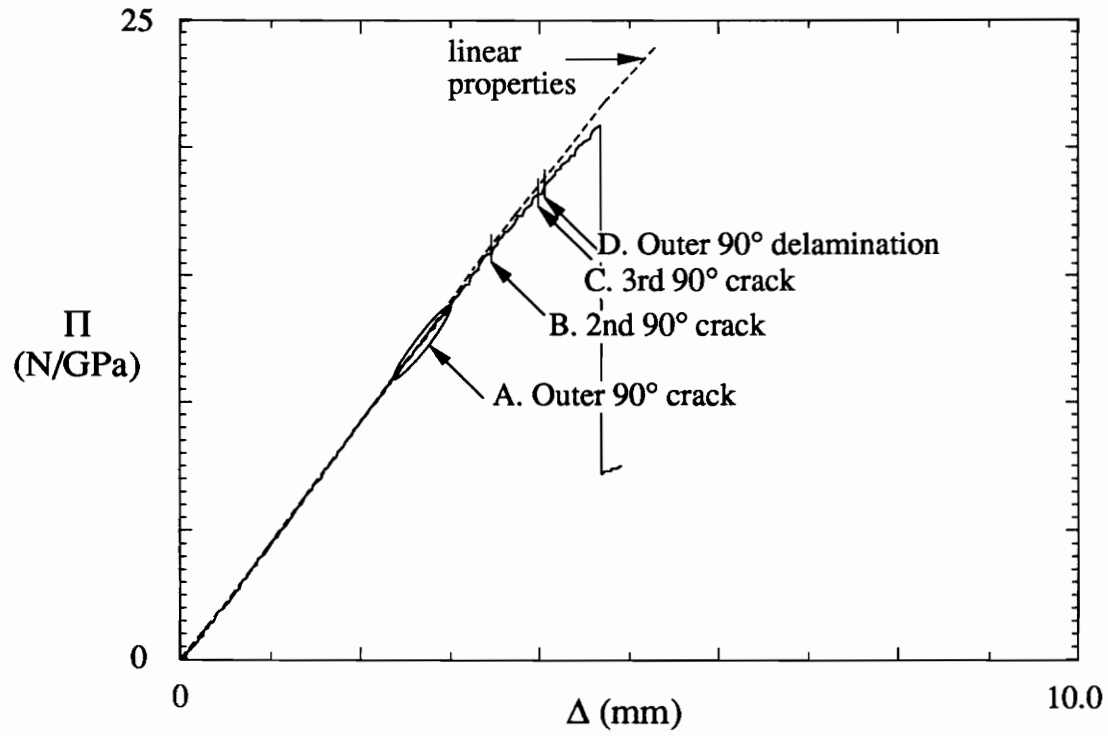

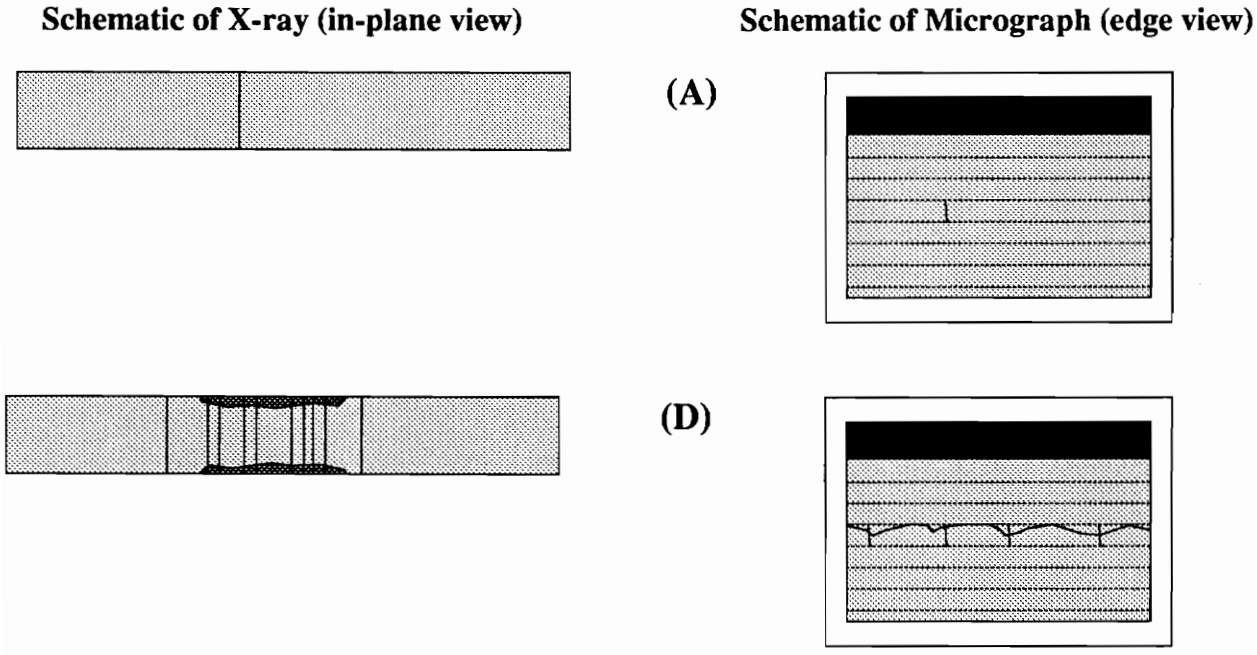

Figure 5.36 damage in Bds specimens

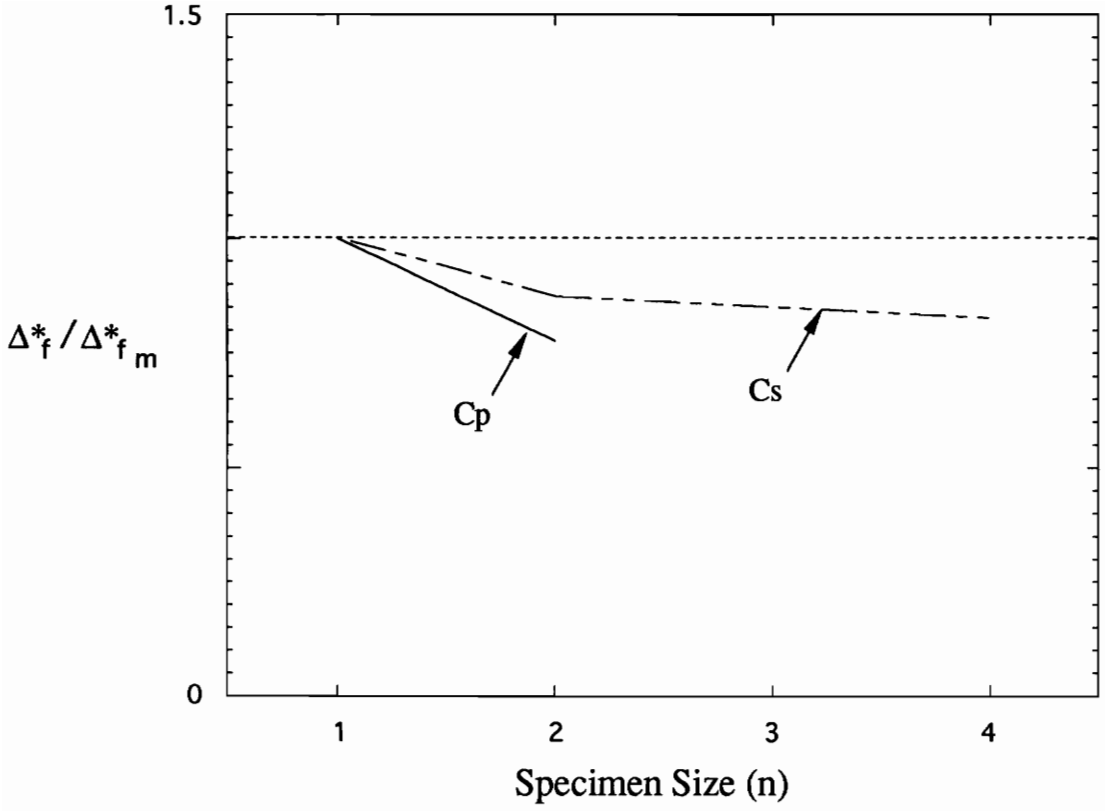

Figure 5.37 Normalized deflection of Lay-up *C* specimens at failure of the outermost 90° ply. Sublaminate-level scaled values are adjusted to account for the strain in the outermost 90° fibers.

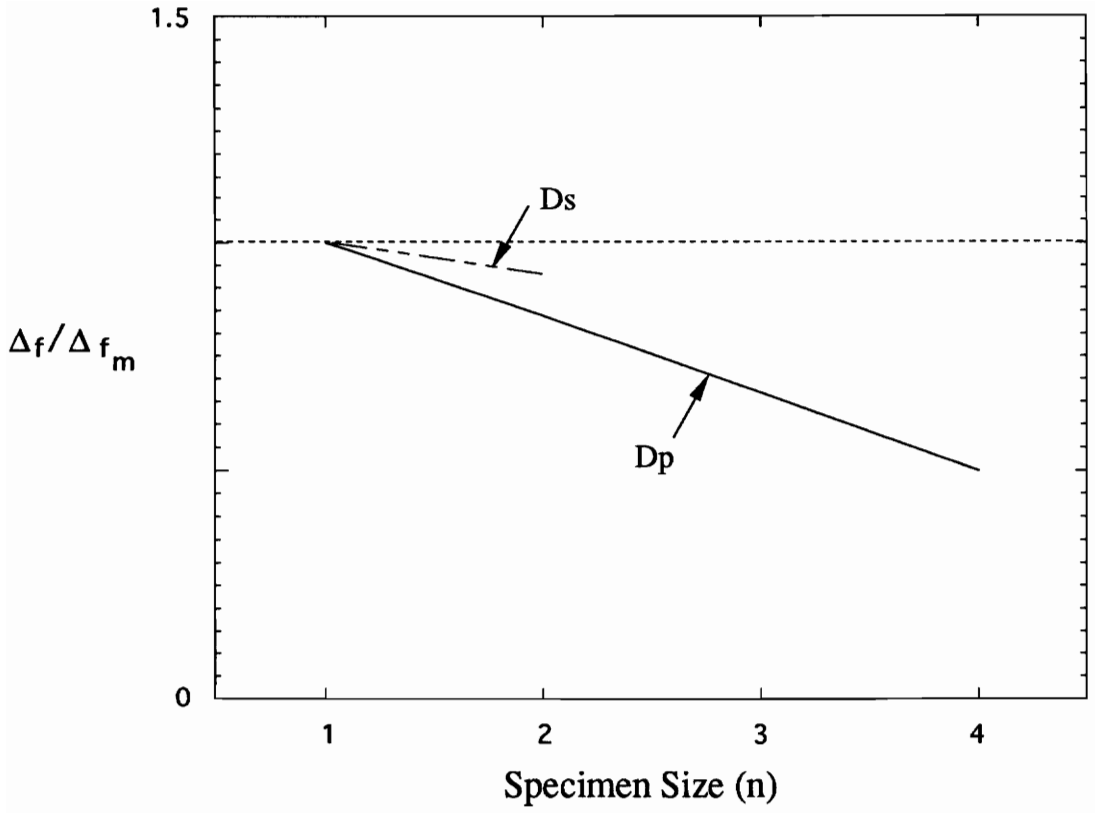

Figure 5.38 Normalized deflection of Lay-up *D* specimens at failure of the surface 45° ply.

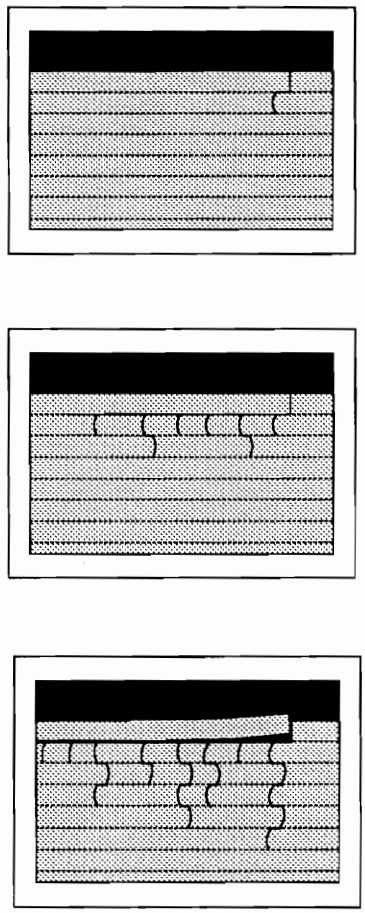

Figure 5.39 Damage in Lay-up *D* specimens

Schematic of X-ray (in-plane view)

Ddp specimen

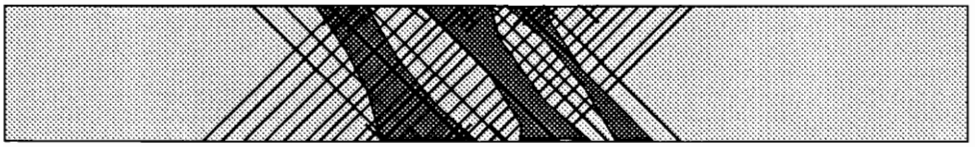

Dds specimen

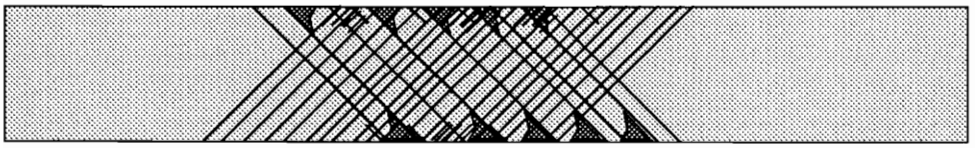

Figure 5.40 Damage in *Ddp* and *Dds* specimens

Figure 5.41 Shims placed between rollers and specimen in order prevent crushing of surface plies that causes delamination and buckling.

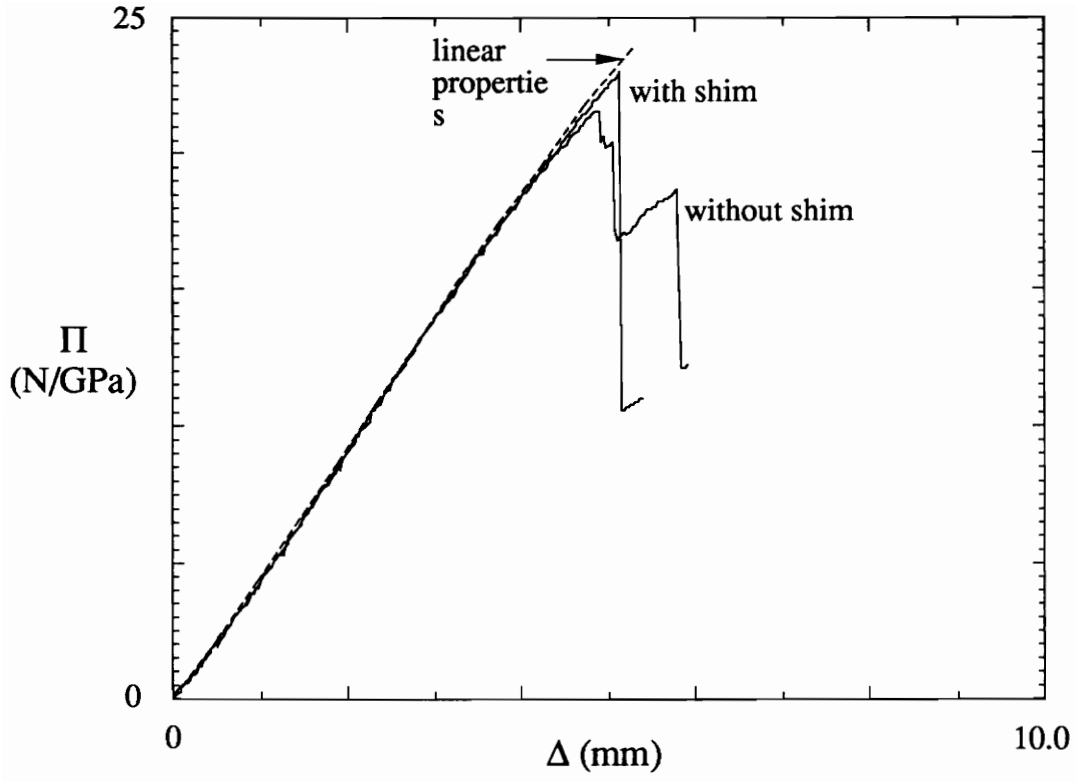

Figure 5.42 Response of *Ca* specimens with and without shims.

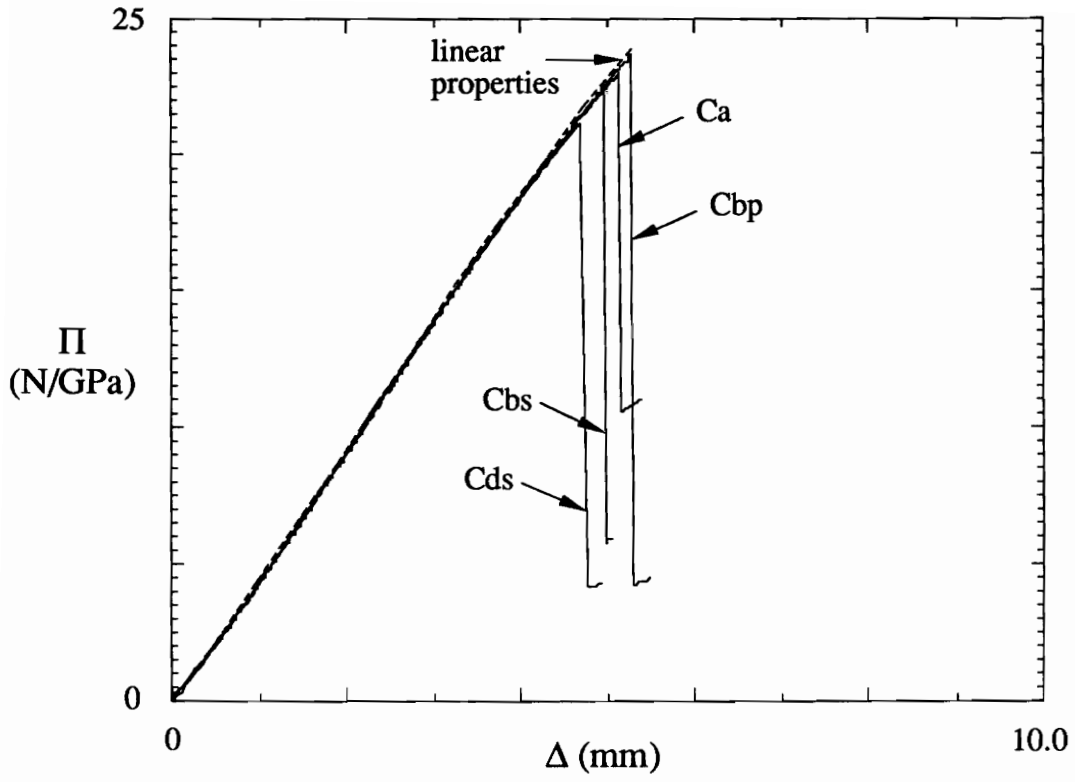

Figure 5.43 Scaled response of Lay-up *C* specimens with shims between rollers and specimens.

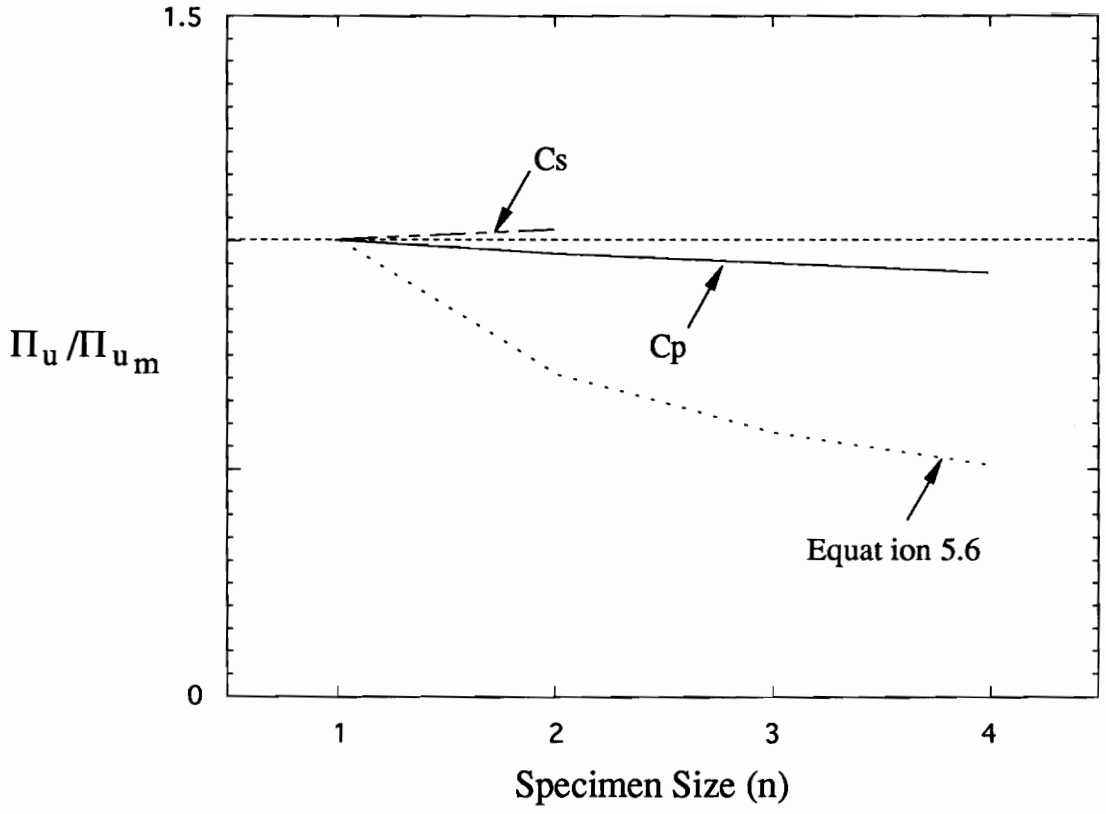

Figure 5.44 Normalized failure load of Lay-up *C* specimens with shims between rollers and specimens.

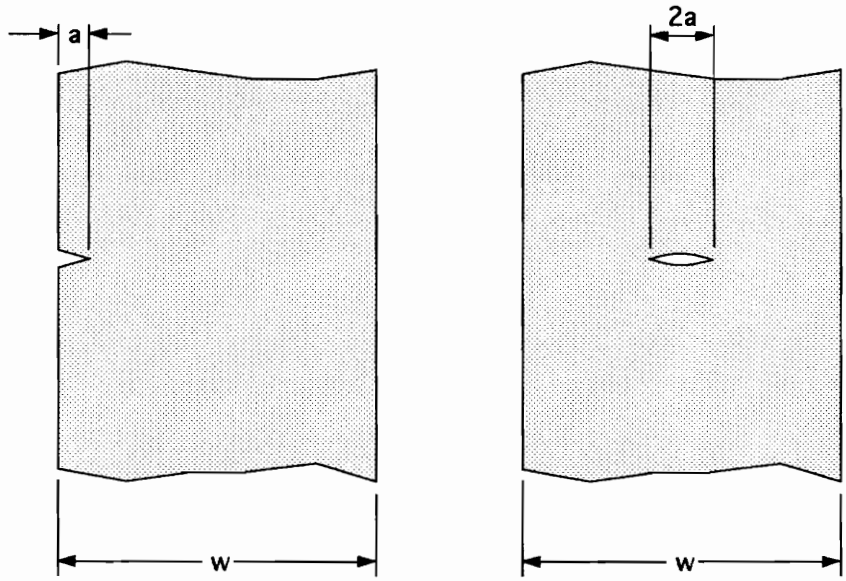

Figure 6.1 Schematic of cracks in a homogeneous, isotropic plates.

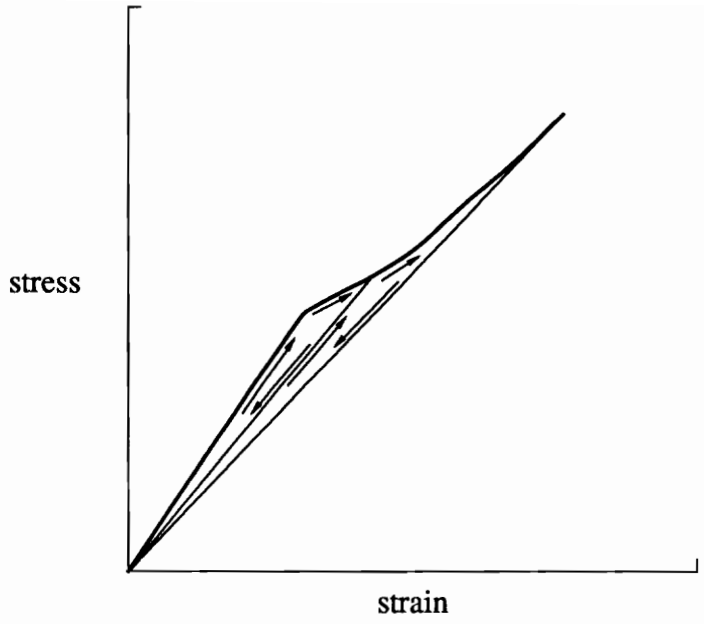

Figure 6.2 Schematic stress/strain response of a delaminating specimen showing possible loading/unloading paths.

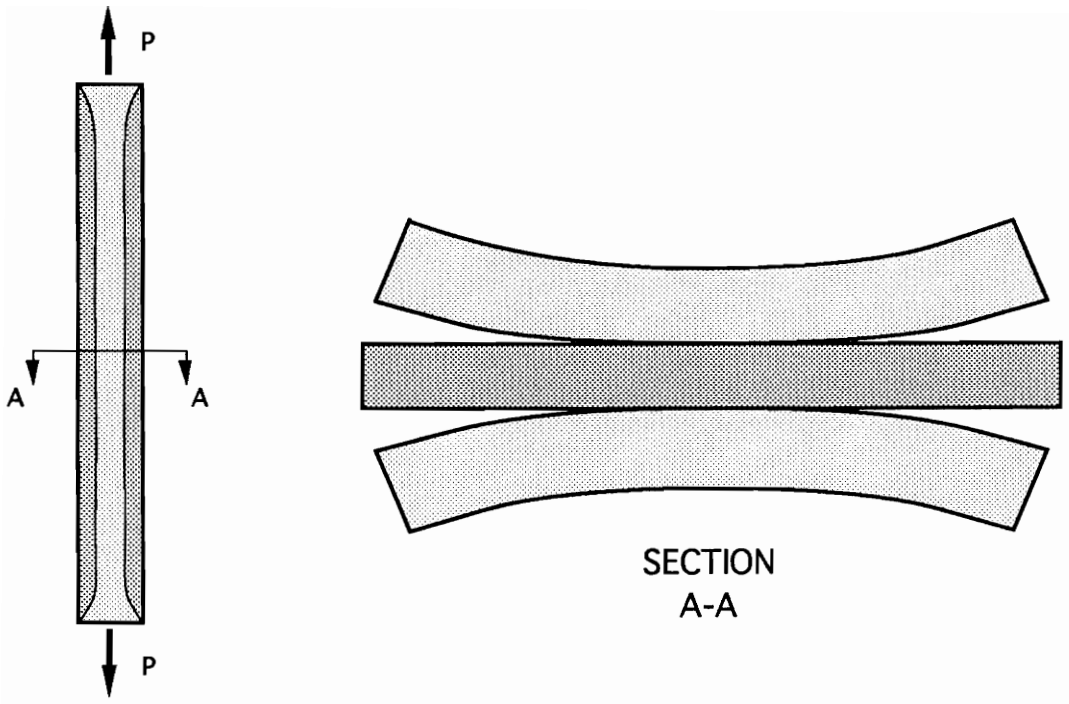

Figure 6.3 Schematic of sublaminates formed by delamination

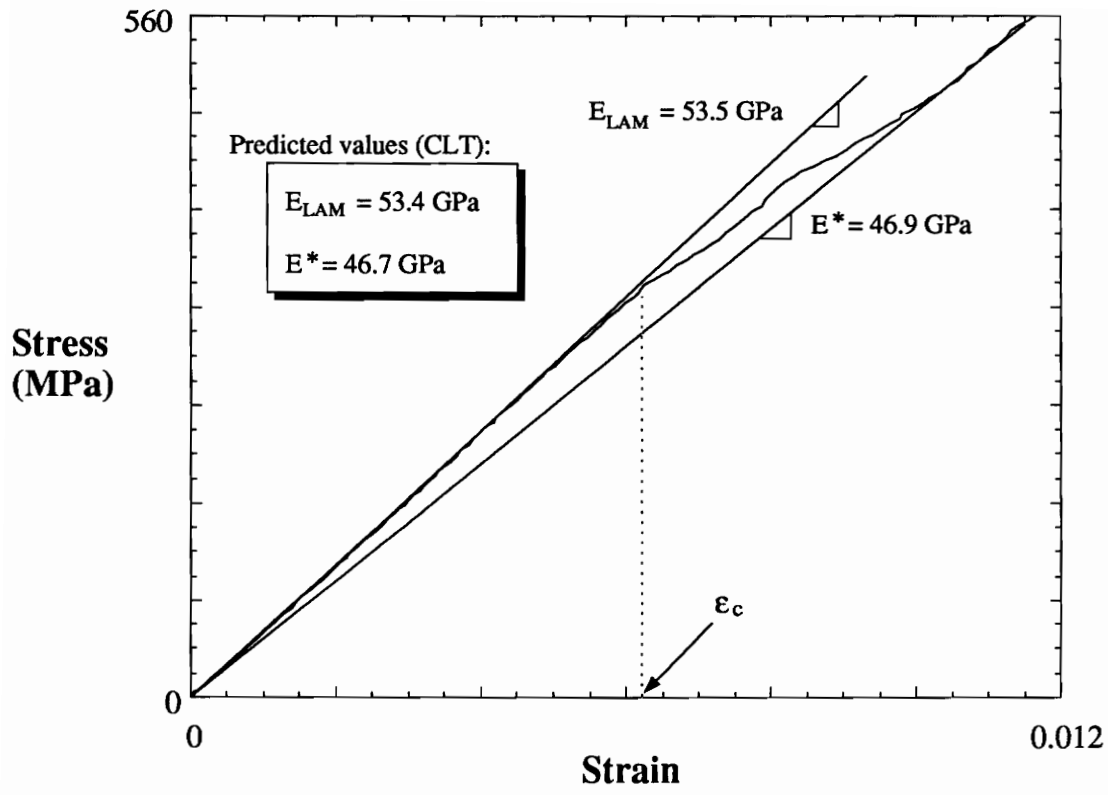

Figure 6.4 Stress/strain response of a AS4/3502 *Ba-8* specimen showing average experimental values of E_{LAM} and E^*, as well as values calculated with CLT.

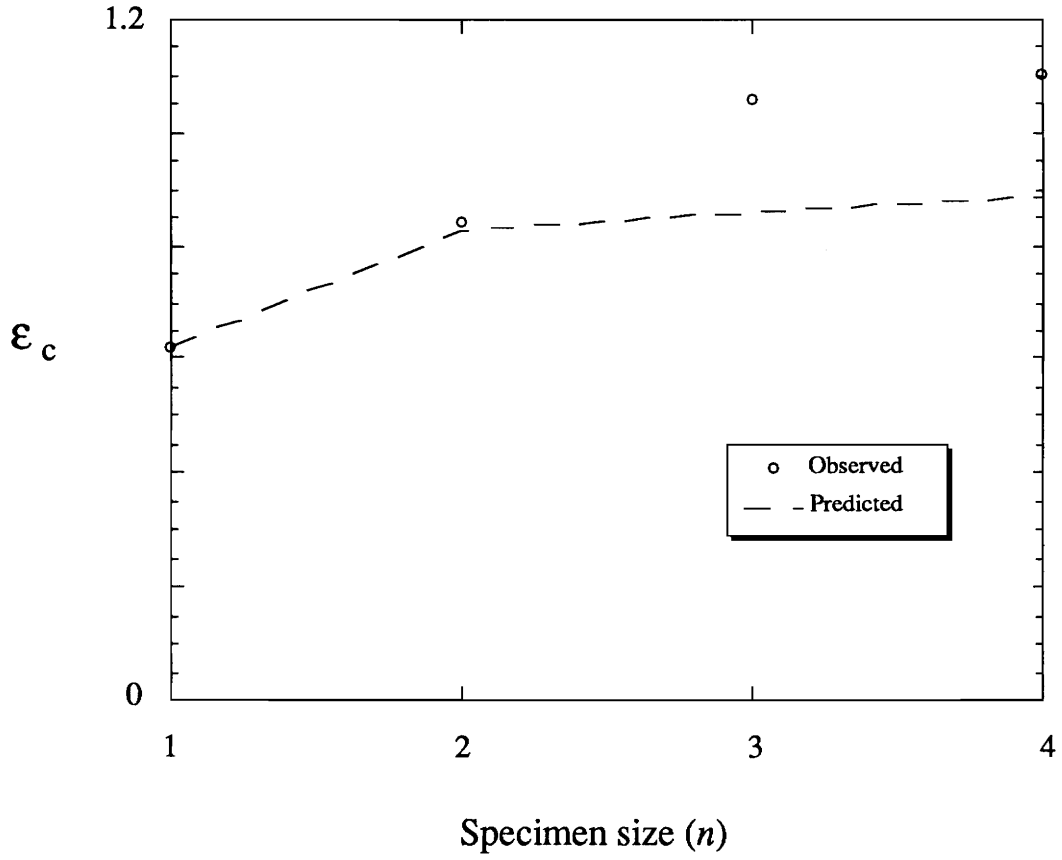

Figure 6.5 Predicted vs. observed delamination strain for AS4/3502 Lay-up *B*.

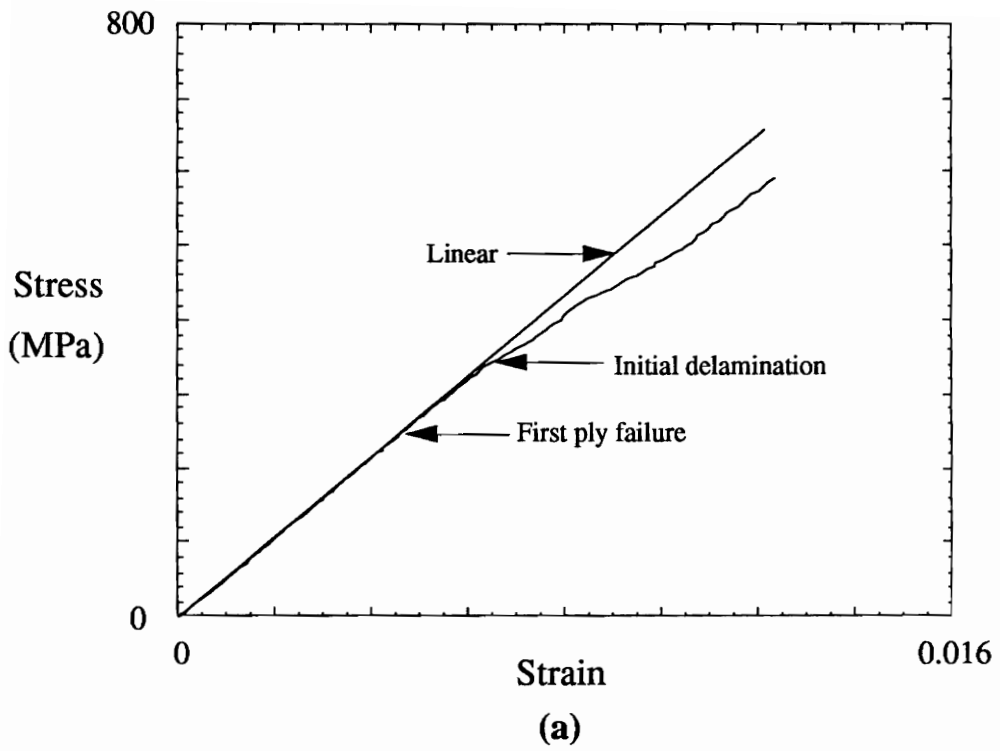

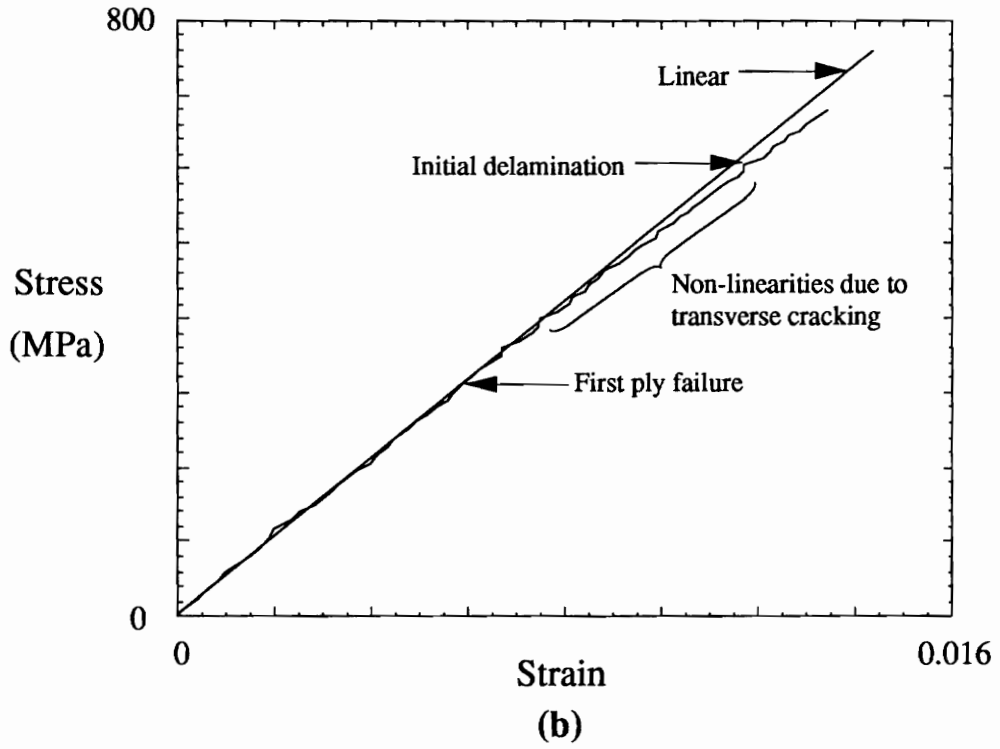

Figure 6.6 ***Ba-8*** **(a) and** ***Bd-32*** **(b) stress/strain plots showing differences in response.**

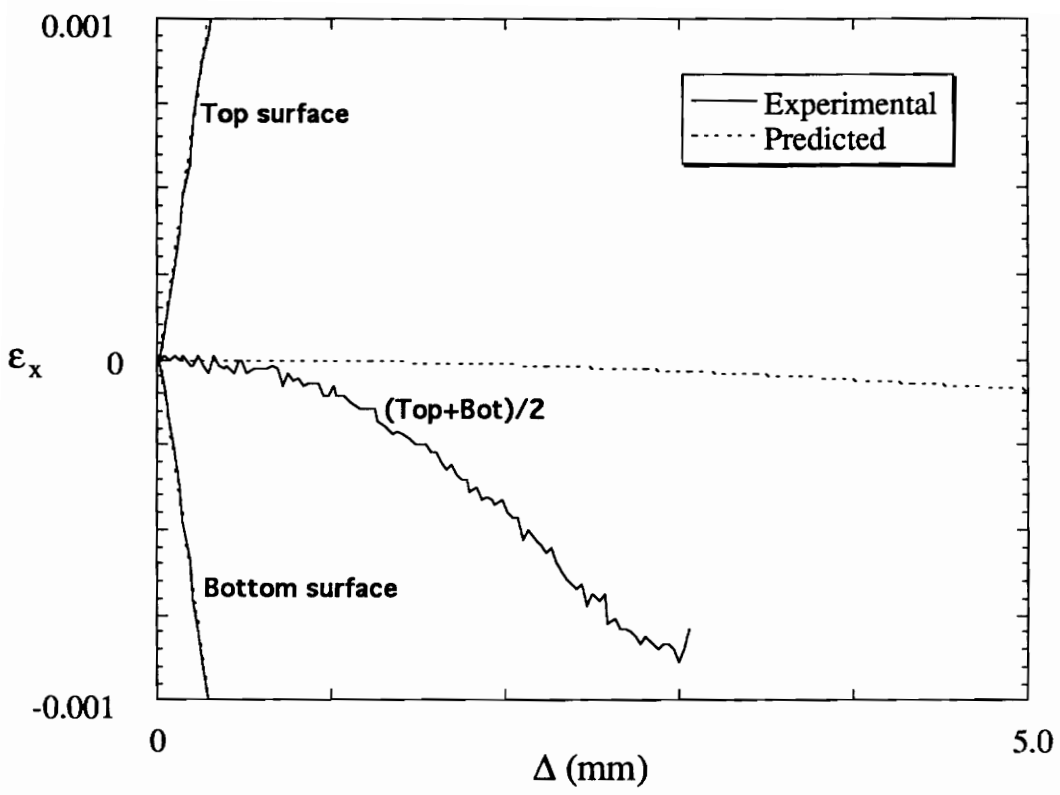

Figure 7.1 Figure 5.20 rescaled to show actual shift in neutral axis compared to shift predicted based solely on the axial loads induced in the specimen by the fixture.

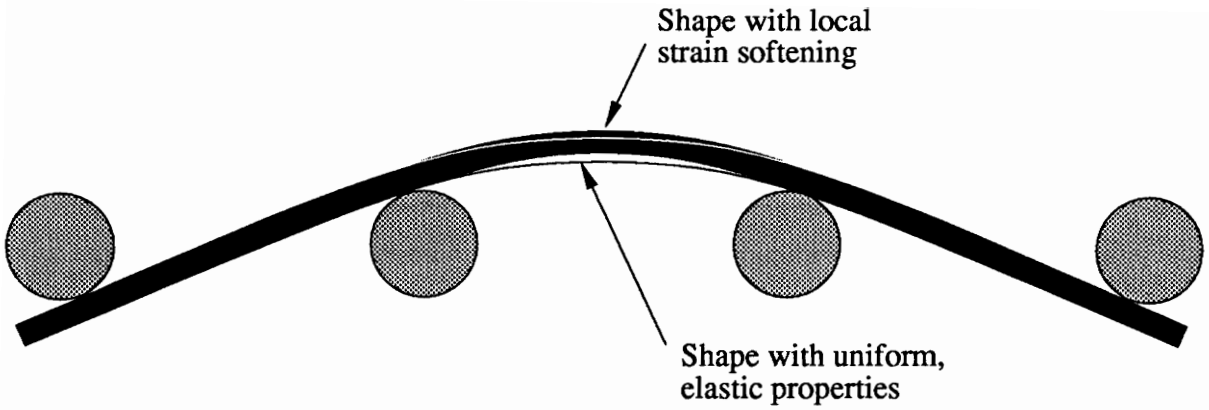

Figure 7.2 Local softening in gage section leads to greater longitudinal strain for a given deflection.

APPENDIX

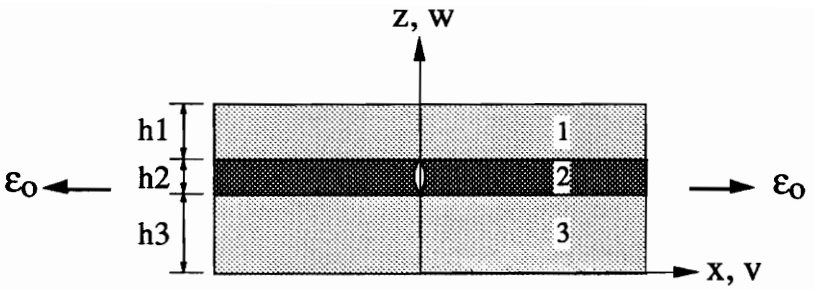

Equlibrium equations:

$$\frac{\partial \sigma_x}{\partial x} + \frac{\partial \tau_{xz}}{\partial z} = 0\,,$$

$$\frac{\partial \sigma_z}{\partial z} + \frac{\partial \tau_{xz}}{\partial x} = 0\,, \tag{A.1}$$

where

$$\sigma_x = E_x \frac{\partial u}{\partial x}\,,\quad \sigma_z = E_x \frac{\partial w}{\partial z}\,,\quad \tau_{xz} = G_{xz}\left(\frac{\partial u}{\partial z} + \frac{\partial w}{\partial x}\right). \tag{A.2}$$

Assume:

$$\sigma_x^{(1)} = \sigma_o^{(1)} + \sigma_1(x)\,,$$

$$\sigma_x^{(2)} = \sigma_o^{(2)} + \sigma_2(x)\,, \tag{A.3}$$

$$\sigma_x^{(3)} = \sigma_o^{(3)} + \sigma_3(x)\,,$$

where $\sigma_i(x)$ are functions of x only,

$$\sigma_o^{(1)} = E_1\,\varepsilon_o\,,\quad \sigma_o^{(2)} = E_2\,\varepsilon_o\,,\quad \sigma_o^{(3)} = E_3\,\varepsilon_o\,, \tag{A.4}$$

and

$$\varepsilon_o = P\,/\,(h_1E_1 + h_2E_2 + h_3E_3)\,. \tag{A.5}$$

Consider the first of Equations A.1 in conjunction with layer (1):

$$\frac{\partial \tau_{xz}^{(1)}}{\partial z} = -\frac{\partial \sigma_x^{(1)}}{\partial x}\,. \tag{A.6}$$

Substituting from Equations A.3:

$$\frac{\partial \tau_{xz}^{(1)}}{\partial z} = -\sigma_1'(x), \tag{A.7}$$

where (') indicates differentiation with respect to x. Integrating with respect to z:

$$\tau_{xz}^{(1)} = -z\,\sigma_1'(x) + f_1(x)\,. \tag{A.8}$$

But the shear boundary condition at the top surface is

$$\tau_{xz}^{(1)}(x,\, z=h_1+h_2+h_3) = 0\,, \tag{A.9}$$

so

$$f_1(x) = (h_1+h_2+h_3)\,\sigma_1'(x)\,. \tag{A.10}$$

$\therefore$

$$\boxed{\tau_{xz}^{(1)} = (h_1+h_2+h_3-z)\,\sigma_1'(x)}\,. \tag{A.11}$$

Consider the second of Equations A.1 in conjunction with layer (1):

$$\frac{\partial \sigma_z^{(1)}}{\partial z} = -\frac{\partial \tau_{xz}^{(1)}}{\partial x}\,. \tag{A.12}$$

Substituting from Equation A.11:

$$\frac{\partial \sigma_z^{(1)}}{\partial z} = -(h_1+h_2+h_3-z)\,\sigma_1''(x). \tag{A.13}$$

Integrating with respect to z:

$$\sigma_z^{(1)} = -z\,(h_1+h_2+h_3-\frac{1}{2}z)\,\sigma_1''(x) + f_2(x)\,. \tag{A.14}$$

But the normal stress boundary condition at the top surface is

$$\sigma_z^{(1)}(x,\, z=h_1+h_2+h_3) = 0\,, \tag{A.15}$$

so

$$f_2(x) = \frac{1}{2}(h_1+h_2+h_3)^2\ \sigma_1''(x)\ . \tag{A.16}$$

$\therefore$

$$\boxed{\sigma_z^{(1)} = \frac{1}{2}(z-h_1-h_2-h_3)^2\ \sigma_1''(x)}\ . \tag{A.17}$$

Consider the first of Equations A.1 in conjunction with layer (3):

$$\frac{\partial \tau_{xz}^{(3)}}{\partial z} = -\frac{\partial \sigma_x^{(3)}}{\partial x}\ . \tag{A.18}$$

Substituting from Equations A.3:

$$\frac{\partial \tau_{xz}^{(3)}}{\partial z} = -\sigma_3'(x)\ . \tag{A.19}$$

Integrating with respect to z:

$$\tau_{xz}^{(3)} = -z\ \sigma_3'(x) + f_3(x)\ . \tag{A.20}$$

But the shear boundary condition at the bottom surface is

$$\tau_{xz}^{(3)}(x,\ z=0) = 0\ , \tag{A.21}$$

so

$$f_3(x) = 0\ . \tag{A.22}$$

$\therefore$

$$\boxed{\tau_{xz}^{(3)} = -z\ \sigma_3'(x)}\ . \tag{A.23}$$

Consider the second of Equations A.1 in conjunction with layer (3):

$$\frac{\partial \sigma_z^{(3)}}{\partial z} = -\frac{\partial \tau_{xz}^{(3)}}{\partial x}\ . \tag{A.24}$$

Substituting from Equation A.23:

$$\frac{\partial \sigma_z^{(3)}}{\partial z} = z\, \sigma_3''(x). \tag{A.25}$$

Integrating with respect to z:

$$\sigma_z^{(3)} = \frac{1}{2} z^2\, \sigma_3''(x) + f_4(x)\,. \tag{A.26}$$

But the normal stress boundary condition at the bottom surface is

$$\sigma_z^{(3)}(x,\, z{=}0) = 0\,, \tag{A.27}$$

so

$$f_4(x) = 0\,. \tag{A.28}$$

$\therefore$

$$\boxed{\sigma_z^{(3)} = \frac{1}{2} z^2\, \sigma_3''(x)}\,. \tag{A.29}$$

Consider the first of Equations A.1 in conjunction with layer (2):

$$\frac{\partial \tau_{xz}^{(2)}}{\partial z} = -\frac{\partial \sigma_x^{(2)}}{\partial x}\,. \tag{A.30}$$

Substituting from Equations A.3:

$$\frac{\partial \tau_{xz}^{(2)}}{\partial z} = -\sigma_2'(x). \tag{A.31}$$

Integrating with respect to z:

$$\tau_{xz}^{(2)} = -z\, \sigma_2'(x) + f_5(x)\,. \tag{A.32}$$

But the shear boundary condition at the layer 2/layer 3 interface is

$$\tau_{xz}^{(2)}(x,\, z{=}h_3) = \tau_{xz}^{(3)}(x,\, z{=}h_3)\,, \tag{A.33}$$

so substituting from Equation A.23:

$$f_5(x) = h_3[\sigma_2'(x) - \sigma_3'(x)] \quad . \tag{A.34}$$

Also, the shear boundary condition at the layer 1/layer 2 interface is

$$\tau_{xz}^{(2)}(x,\, z=h_2+h_3) = \tau_{xz}^{(1)}(x,\, z=h_2+h_3) \;, \tag{A.35}$$

so substituting from Equation A.11:

$$f_5(x) = h_1\, \sigma_1'(x) + (h_2+h_3)\, \sigma_2'(x) \quad . \tag{A.36}$$

Equating Equations A.34 and A.36:

$$\sigma_2'(x) = -\frac{h_1}{h_2}\, \sigma_1'(x) - \frac{h_3}{h_2}\, \sigma_3'(x). \tag{A.37}$$

Integrating with respect to x, and recognizing that horizontal equilibrium must be maintained:

$$\boxed{\sigma_2(x) = -\frac{h_1}{h_2}\, \sigma_1(x) - \frac{h_3}{h_2}\, \sigma_3'(x)}. \tag{A.38}$$

Consider the second of Equations A.1 in conjunction with layer (2):

$$\frac{\partial \sigma_z^{(2)}}{\partial z} = -\frac{\partial \tau_{xz}^{(2)}}{\partial x} \;. \tag{A.39}$$

Substituting from Equation A.32:

$$\frac{\partial \sigma_z^{(2)}}{\partial z} = -\, z\, \sigma_2''(x) + f_5'(x). \tag{A.40}$$

Substituting from either Equation A.34 or A.36:

$$\begin{aligned} \frac{\partial \sigma_z^{(2)}}{\partial z} &= -\, z\, \sigma_2''(x) + h_3\, \sigma_2''(x) - h_3\, \sigma_3''(x), \quad \text{or} \\ \frac{\partial \sigma_z^{(2)}}{\partial z} &= -\, z\, \sigma_2''(x) + h_1\, \sigma_1''(x) + (h_2+h_3)\, \sigma_3''(x). \end{aligned} \tag{A.41}$$

Integrating the first of Equations A.41 with respect to z:

$$\sigma_z^{(2)} = -\frac{1}{2} z^2 \sigma_2''(x) + z\, h_3\, \sigma_2''(x) - z\, h_3\, \sigma_3''(x) + f_6(x) . \tag{A.42}$$

But the normal stress boundary condition at the layer 2/layer 3 interface is

$$\sigma_z^{(2)}(x, z=h_3) = \sigma_z^{(3)}(x, z=h_3) , \tag{A.43}$$

so substituting from Equation A.29:

$$f_6(x) = -\frac{1}{2} h_3^2 [\sigma_2''(x) - 3\, \sigma_3''(x)] . \tag{A.44}$$

Also, the normal stress boundary condition at the layer 1/layer 2 interface is

$$\sigma_z^{(2)}(x, z=h_2+h_3) = \sigma_z^{(1)}(x, z=h_2+h_3) , \tag{A.45}$$

so substituting from Equation A.17:

$$f_6(x) = \frac{1}{2} h_1^2 \sigma_1''(x) + \frac{1}{2} (h_2 - h_3) \sigma_2''(x) + h_3 (h_2+h_3) \sigma_3'' . \tag{A.46}$$

Equating Equations A.44 and A.46:

$$\sigma_2''(x) = -\frac{h_1^2}{h_2^2} \sigma_1''(x) + \frac{h_3}{h_2}\left(\frac{h_3}{h_2} - 2\right) \sigma_3''(x) . \tag{A.47}$$

Integrating with respect to x, and recognizing that $\sigma_2(x)$ must decay to zero as $x \to \infty$:

$$\boxed{\sigma_2(x) = -\frac{h_1^2}{h_2^2} \sigma_1(x) + \frac{h_3}{h_2}\left(\frac{h_3}{h_2} - 2\right) \sigma_3(x)} . \tag{A.48}$$

Integrating the second of Equations A.41 with respect to z:

$$\sigma_z^{(2)} = -\frac{1}{2} z^2 \sigma_2''(x) + z\, h_1\, \sigma_1''(x) + z\, (h_2+h_3)\, {}_2''(x) + f_7(x) . \tag{A.49}$$

But the normal stress boundary condition at the layer 2/layer 3 interface is

$$\sigma_z^{(2)}(x, z=h_3) = \sigma_z^{(3)}(x, z=h_3) , \tag{A.50}$$

so substituting from Equation A.29:

$$f_7(x) = -h_1\, h_3\, \sigma_1''(x) - h_3(h_2 + \frac{1}{2} h_3)\, \sigma_2''(x) + \frac{1}{2} h_3^2\, \sigma_3''(x). \tag{A.51}$$

Also, the normal stress boundary condition at the layer 1/layer 2 interface is

$$\sigma_z^{(2)}(x, z=h_2+h_3) = \sigma_z^{(1)}(x, z=h_2+h_3)\ , \tag{A.52}$$

so substituting from Equation A.17:

$$f_7(x) = [-h_1(h_2+h_3) + \frac{1}{2} h_1^2]\, \sigma_1''(x) - \frac{1}{2}(h_2+h_3)^2\, \sigma_2''(x). \tag{A.53}$$

Equating Equations A.51 and A.53

$$\sigma_2''(x) = \frac{h_1}{h_2}\left(\frac{h_1}{h_2} - 2\right) \sigma_1''(x) - \frac{h_3^2}{h_2^2}\, \sigma_3''(x). \tag{A.54}$$

Integrating with respect to x, and recognizing that $\sigma_2(x)$ must decay to zero as $x \to \infty$:

$$\sigma_2(x) = \frac{h_1}{h_2}\left(\frac{h_1}{h_2} - 2\right) \sigma_1(x) - \frac{h_3^2}{h_2^2}\, \sigma_3(x)\ . \tag{A.55}$$

Substituting from Equation A.48:

$$\boxed{\sigma_1(x) = \frac{h_3}{h_1}\left(\frac{h_3 - h_2}{h_1 - h_2}\right) \sigma_3(x)}\ . \tag{A.56}$$

Substituting back into Equation A.48:

$$\boxed{\sigma_1(x) = H_1\, \sigma_2(x)},\ \text{or}$$
$$\boxed{\sigma_3(x) = H_2\, \sigma_2(x)}, \tag{A.57}$$

where

$$H_1 = \frac{h_2}{h_1} \frac{(h_2 - h_3)}{(h_1 - 2h_2 + h_3)}\ ,\ \text{and}$$
$$H_2 = \frac{h_2}{h_3} \frac{(h_2 - h_1)}{(h_1 - 2h_2 + h_3)}\ . \tag{A.58}$$

From Equations A.3, A.11, A.17, A.23, A.29, A.32, A.34, A.42 A.44 and A.57, the stresses in all layers can finally be written, in terms of stresses in layer 2, as:

$$\sigma_x^{(1)} = \sigma_o^{(1)} + H_1\, \sigma_2(x)\,,$$

$$\tau_{xz}^{(1)} = H_1\,(h_1 + h_2 + h_3 - z)\, \sigma_2'(x)\,, \tag{A.59}$$

$$\sigma_z^{(1)} = \frac{1}{2} H_1\,(z - h_1 - h_2 - h_3)^2\, \sigma_2''(x)\,,$$

$$\sigma_x^{(2)} = \sigma_o^{(2)} + \sigma_2(x)\,,$$

$$\tau_{xz}^{(2)} = [h_3\,(1 - H_2) - z]\, \sigma_2'(x)\,, \tag{A.60}$$

$$\sigma_z^{(2)} = [-\frac{1}{2} z^2 + h_3\,(1 - H_2)\, z + \frac{1}{2} h_3^2\,(3H_2 - 1)]\, \sigma_2''(x)\,,$$

$$\sigma_x^{(3)} = \sigma_o^{(3)} + H_2\, \sigma_2(x)\,,$$

$$\tau_{xz}^{(3)} = -H_2\, z\, \sigma_2'(x)\,, \tag{A.61}$$

$$\sigma_z^{(3)} = \frac{1}{2} H_2\, z^2\, \sigma_2''(x)\,.$$

VITA

David Page Johnson was born in Evanston, Illinois in June 1963, and lived with his family in Wilmette, Illinois. He attended Logan Elementary School and Howard Junior Highschool in Wilmette. In June 1981 he graduated from New Trier East Highschool in Winnetka, Illinois. David then attended Fall 1981 and Winter 1982 classes at Brigham Young University. Following this, he served an eighteen month mission for the Church of Jesus Christ of Latter-day Saints in the Arizona Tempe Mission in their Spanish-speaking program. David resumed his studies at Brigham Young University, and graduated with a B.S. in Mechanical Engineering in April 1989. He then began attending Virginia Polytechnic Institute and State University, where he received an M.S. in Engineering Mechanics in May 1991 and a Ph.D. in Engineering Mechanics in May 1994.